-

ASHRAE RP-870

Develop Data Base for Determining Optimum Compressor Rating Points for Residential Refrigerator and Freezer Compressors

Principal Investigators:

S.A. Klein
Mechanical Engineering Dept.
University of Wisconsin
Madison, WI 53706
klein@engr.wisc.edu

D.T. Reindl
Engineering Professional Development
University of Wisconsin
Madison, WI 53706
dreindl@facstaff.wisc.edu

The following report is the M.S. thesis entitled 'A Semi-Empirical Method for Modeling Reciprocating Compressors in Residential Refrigerators and Freezers' by Ms. Dagmar Jähnig. Ms. Jähnig was supervised by S.A. Klein and D.T. Reindl.

May 1999

-

-

Abstract

Calorimeter testing data for domestic refrigerator/freezer compressors have been collected. The current method to represent compressor performance data recommended by the Air-Conditioning and Refrigeration Institute (ARI) has been applied to all experimental data. It has been found that the model does not reliably interpolate and extrapolate.

A semi-empirical model to represent compressor performance has been developed. The model is based on the concept of volumetric efficiency and assumes a polytropic compression process. The model contains 5 curve fit parameters that have to be determined with non-linear regression. A minimum of 4 measurements of mass flow rate and electrical power are necessary to generate accurate compressor maps with this model. The model has been shown to extrapolate within 5% error to 10°C higher and lower condensing and evaporating temperatures than represented in the measured data.

The effect of a change in ambient temperature has been compared with data available in the literature and seems well represented in the model as a change in the suction temperature.

-

Acknowledgements

I would like to thank my advisors Sandy Klein and Doug Reindl for giving me the chance to further pursue my education and for their guidance throughout my thesis project. They were always available to talk to. A special thanks to Sandy for providing a few new features in EES that made it easier to do the calculations needed for this project.

I very much enjoyed working in the Solar Energy Lab and would like to thank all the other graduate students for creating a very productive and fun working atmosphere. I enjoyed the discussions about various topics over lunch and also the activities outside the lab.

The project was sponsored by the American Society of Heating, Refrigerating and Air-Conditioning Engineers (ASHRAE) Technical committee 7.1. I would like to thank the committee for their financial support throughout my graduate program.

-

Table of Contents

-

-

-

List of Tables

-

List of Figures

-

-

-

Nomenclature

A1a…D1	Compressor model numbers
a,b,d,e,f	Curve fit coefficients
AHAM	Association of Home Appliance Manufacturers
ARI	Air-Conditioning and Refrigeration Institute
$C_1…C_{10}$	ARI Curve fit coefficients
C	Clearance volume ratio
c_p	Specific heat at constant pressure, kJ/kg K
CR	Compression ratio
c_v	Specific heat at constant volume, kJ/kg K
D_h	Hydraulic diameter
f	Friction factor
h	Enthalpy, kJ/kg
k	Isentropic exponent
k	Curve Fitting Parameter
L	Duct length
$\dot{m}$	Mass flow rate, kg/s
n	Polytropic exponent
N	Number of data points
OF	Objective function
p	Pressure, kPa
Q	Heat transfer rate, W (Btu/hr)

-

RPM	Motor speed
T	Temperature
V	Volume, m^3
v	Specific volume, m^3/kg
v	Velocity
W	Work, kJ/kg

Greek Symbols

Δ	Difference
η	Efficiency
ρ	Density

Subscripts

calc	Calculated
comb	Combined
cond	Condenser
discharge	Conditions at the discharge of the cylinder
evap	Evaporator
mean	Average
meas	Measured
rel	Relative
shell	Averaged over the compressor shell
suction	Conditions at the suction of the cylinder

Chapter 1

Introduction

1.1 Background

Preserving food has always been a necessity of mankind. Keeping food fresh by cooling it, i.e. by slowing down the growth of bacteria is a fairly difficult task. Until the invention of refrigeration the only means of lowering the temperature was by harvesting and storing blocks of 'natural' ice grown during the winter or by evaporative cooling. Nowadays most domestic refrigerators use vapor-compression refrigeration cycles.

1.1.1 Refrigerators

A refrigerator is designed to cool an enclosed space to a set temperature. Many refrigerators consist of two compartments that are maintained at different temperatures. The freezer compartment is usually kept at a temperature of about -15°C (5°F), the fresh food compartment at 5-10°C (36-50°F). Most refrigerators have only one refrigeration cycle and therefore only one compressor. This cycle operates at the conditions of the lower temperature compartment, the freezer compartment. To cool the fresh food compartment, cold air is circulated from the freezer to the fresh food compartment.

1.1.2 Refrigeration Cycles

A vapor-compression refrigeration cycle typically consists of a compressor, a condenser, an expansion valve and an evaporator. Such a system is shown in figure 1-1.

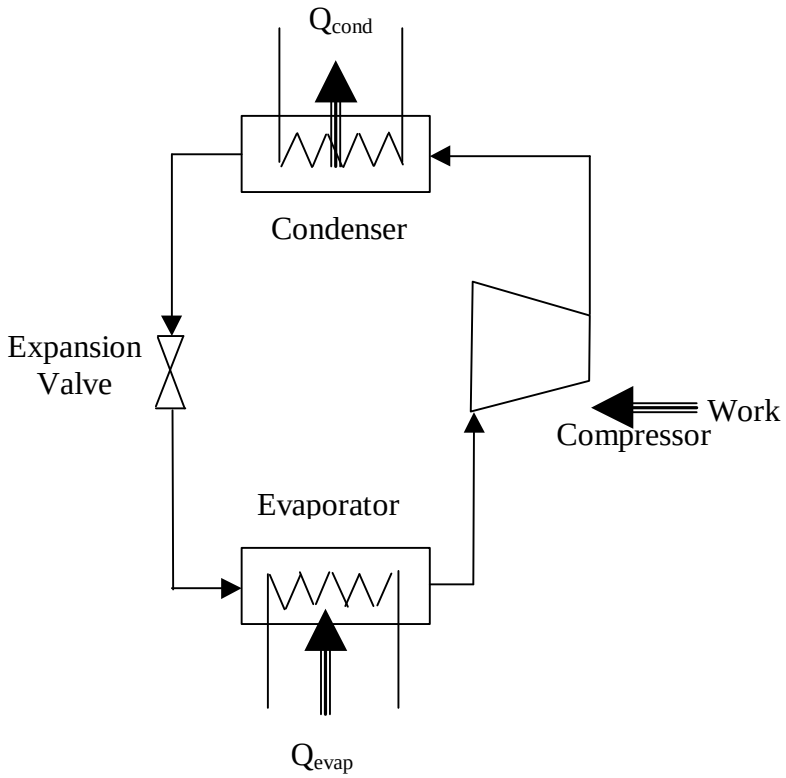

Figure 1-1: Schematic of a typical vapor-compression refrigeration cycle

The refrigerant is compressed to a higher pressure. This process requires mechanical work. In the condenser the refrigerant is cooled and then liquified. The condenser is a heat exchanger behind or underneath the refrigerator that rejects heat to the ambient. The refrigerant then passes through an expansion device (usually a capillary tube) where the pressure is reduced. The evaporator is located inside the freezer and/or fresh food compartment. The energy needed to evaporate the refrigerant is drawn from inside the refrigerator that is thereby cooled.

The compressor is a central component of every refrigerator or freezer. It is the compressor that has to be supplied with electrical energy to produce refrigerant mass flow to generate the desired cooling effect. An electrical motor converts the electrical energy into mechanical energy that is needed to operate the compressor. Most refrigerators use fixed speed compressors. These compressors do not operate at steady-state but are started when the temperature in the freezer compartment rises above a setpoint. When the temperature in the freezer compartment reaches the low setpoint, the compressor shuts off and the refrigerant pressures in the system equalize. During the off-cycle heat transfer occurs from the refrigerant to the surroundings and to the air inside the refrigerator. The temperatures and pressures under which the compressor operates vary considerably during this process.

1.1.3 Energy Efficiency

Electrical power generation still relies widely on fossil fuels that are known to generate CO_2, which contributes to global warming. The impact of power generation on the environment has been of concern for years and most industrialized countries have agreed to reduce their CO_2 production in the near future. The most promising measure to achieve that goal is to develop technologies that consume less energy.

In an effort to reduce energy consumption in households the U.S. Department of Energy has set a limit on the amount of energy consumption for refrigerators. The current standard has been in effect since 1993. It limits the energy use, for example, of a 1000-liter-refrigerator with manual defrost to 779 kWh/yr. A new standard is going to be effective July 1, 2001 that will require the same refrigerator to consume less than

558 kWh/yr [AHAM(1993)]. Refrigerator manufacturers are working on different methods to meet these deadlines. The goal is to develop a refrigerator that consumes as little energy as possible but the first costs still have to be reasonable to be able to sell the new refrigerators. In addition, the refrigerated space should not become too small, for example by using very thick insulation to reduce energy consumption.

In addition to the environmental concerns, more energy efficient appliances also save the consumer money on utility bills. Developing energy efficient refrigerators is therefore a sales advantage for the manufacturer.

For the above mentioned reasons, refrigerator manufacturers have to select a compressor that can operate under the desired operating conditions and consumes as little energy as possible. To do this they have to know, as accurately as possible, how a specific compressor model performs at different evaporating, condensing and ambient temperatures. As explained in section 1.1.2 the compressor does not operate under steady-state conditions but over a wide range of different conditions. This kind of information is not always readily available from the manufacturer.

1.1.4 Compressor Maps

Compressor manufacturers usually provide information on how the compressor operates at a standard rating point. The current rating point conditions are –23.3°C (-10°F) evaporating temperature, 54.4°C (130°F) condensing temperature and 32.2°C (90°F) ambient, suction and liquid line temperature. These conditions do not well represent the actual operating conditions of a domestic refrigerator/freezer.

Manufacturers also provide maps that show the performance of a compressor for a range of evaporating and condensing temperatures. These maps are generated using a curve fit that does not contain any physics and therefore cannot be confidently extrapolated. At least 10 measurements of mass flow rate and power at different operating conditions have to be taken to be able to generate these maps.

All of this information is provided for an ambient temperature of 32.2°C (90°F) although the compressor in a domestic refrigerator is very likely to operate under much lower ambient temperatures.

A method to generate accurate compressor maps that contain information on the performance of a compressor under a wide range of evaporating, condensing and ambient temperatures is needed. This method should allow to take a small number of measurements and to interpolate and to extrapolate to other operating conditions.

1.2 Goals of the Project

The goals of this project involve seven steps that are listed below.

1) Collect compressor performance data

Collect calorimeter testing data for as many different compressor models and manufacturers as possible. Data should include mass flow rate and power for as many different operating conditions as possible to allow extrapolations. Data including shell and discharge temperatures and data at different ambient temperatures would also be useful.

2) Literature Review

Search the literature for existing models that can be used or modified to generate compressor performance maps.

3) Examine current method to present compressor performance data (ARI)

The current method is based on a purely empirical curve fit. It is to be investigated how accurate the method is and how well it interpolates and extrapolates.

4) Develop a semi-empirical model to generate compressor performance maps

A semi-empirical model should be developed that is at least partly based on physics and therefore extrapolates more reliably than the current method (ARI). The data collected in part 1 will be used to validate the model.

5) Determine the number of data points needed to generate accurate compressor maps

It needs to be determined how many measurements have to be taken to be able to generate accurate compressor maps with the model developed in part 4. The current method requires a minimum of 10 measurements. The new model should require significantly less.

6) Test extrapolation capabilities of the model

It should be investigated how well the model is able to predict the compressor performance at operating conditions that are not in the range of the data used to fit the model. The data collected in part 1 should be used for this analysis.

7) Investigate the effect of the ambient temperature

The performance of a compressor depends also on the ambient temperature. Using experimental data from the literature this effect should be quantified and compared to the response of the model to a change in ambient temperature.

Chapter 2

Refrigeration Compressors

2.1 Compressor Components

The compressors studied in this project are reciprocating compressors directly coupled to an AC electric motor in a hermetic unit. Principle components of a reciprocating compressor include a piston, cylinder, intake and discharge valves. The compressor shell also contains lubricant oil. A schematic of such a compressor is shown in figure 2-1.

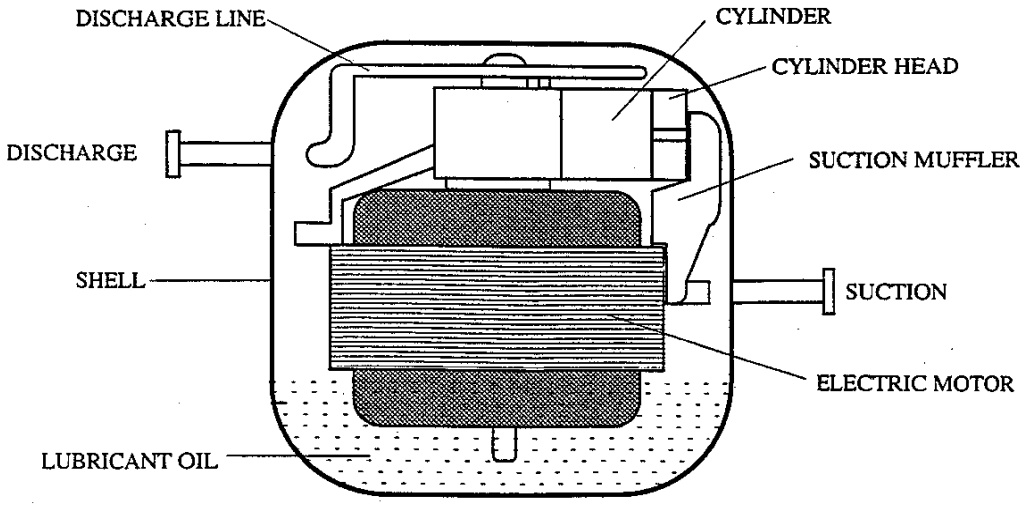

Figure 2-1: Schematic of a hermetic reciprocating compressor [Cavallini et al., 1996]

Low temperature low pressure refrigerant vapor enters the compressor shell through the suction line. Upon entering the compressor shell, a portion of the vapor directly enters the suction muffler and, eventually, enters the cylinder through the suction valve. The remaining refrigerant bypasses the suction muffler by the gap between the

suction line and the suction muffler. The bypassed refrigerant travels throughout the compressor shell where it mixes with the lubricant oil and absorbs heat from the electric motor. This process serves to cool the motor windings. After the compression process, the refrigerant leaves the cylinder through the discharge valve and then through a discharge line. The discharge line does not directly lead out of the compressor shell but is instead routed around the cylinder and motor inside the shell before it actually exits. This routing provides noise reduction. Since the refrigerant exits the cylinder at high temperature, heat transfer takes place between the refrigerant in the discharge line and the refrigerant and oil in the shell so that the refrigerant leaves the compressor shell at a temperature lower than at the cylinder outlet.

The pressure drop that occurs in the discharge line has been estimated using an equation for pressure drop in a straight pipe with smooth walls [Fox and McDonald (1992)].The discharge line is typically about 50cm long and has an inner diameter of 2mm. An equivalent length for nine 90-degree bends has been added. Pressure drops for mass flow rates that appear in compressor maps range from about 8 to 30kPa which is about 1 to 3% of the discharge pressure.

2.2 Compressor Cycle

The process occurring in a reciprocating compressor can be divided into four parts: the intake, the compression process itself, the discharge, and the re-expansion of the refrigerant vapor that remains in the clearance volume [Fröhlich (1961), Chlumský (1965), Threlkeld (1962)]. Figure 2-2 shows the piston of a compressor as well as a

diagram that indicates the pressure for the different positions of the piston during a stroke.

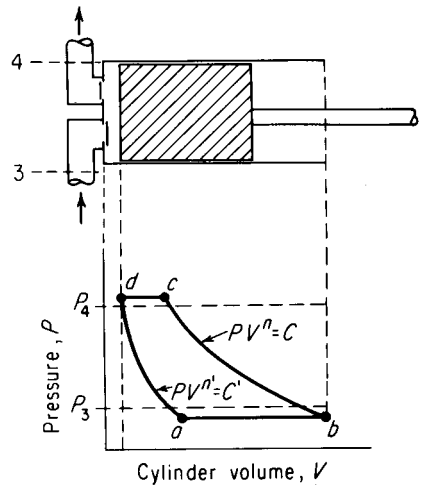

Figure 2-2: Schematic indicator diagram for a reciprocating compressor [Threlkeld, 1962]

The horizontal dashed lines in figure 2-2 indicate the suction and discharge pressures p_3 and p_4 respectively. The actual pressures inside the cylinder differ from these values because of pressure drops in the suction muffler, discharge line and the suction and discharge valves. Every compressor has a clearance volume that is the volume that is left in the cylinder when the piston rests at top dead center. At the end of the intake stroke (position b) the piston is at bottom dead center. As the piston moves upward from bottom dead center, the volume of refrigerant decreases and the pressure increases. At point c, the pressure in the cylinder is sufficient to open the discharge valve. The refrigerant is pushed out of the cylinder from position c to d. The vertical dashed line by position d represents the clearance volume. As the piston begins to move down, the refrigerant that is left in the clearance volume re-expands to the lower suction pressure at position a.

Therefore only the difference between the volume at position b and position a is available for drawing in refrigerant during the next intake stroke. The ratio between the volume that is actually taken in the cylinder and the total displacement volume of the cylinder is called the volumetric efficiency. See chapter 3 for more details.

2.3 Measured Performance of Compressors (Calorimeter Testing)

Calorimeters are being used to measure the steady state performance of a compressor. The evaporating and condensing conditions can be specified in a calorimeter test. The calorimeter operates in an environmental chamber with a specified temperature. For standard tests, this is 32.2°C (90°F).

A schematic of a calorimeter system is shown in figure 2-3 [Haider et al. (1997)]. The refrigerant leaves the compressor at the set pressure and is condensed in the condenser using a separate chiller system. The refrigerant leaves the condenser at the ambient temperature and then it passes through a flow meter and is expanded to the set lower pressure. The expansion valve pneumatically controlled the pressure in the evaporator. The evaporator is heated with an electrical heater in a secondary liquid bath. This electrical heater also controls the amount of superheat. In standard testing the refrigerant is heated to the ambient temperature.

The electrical power input is measured and the input to the electrical heater is equal to the refrigeration capacity defined as the mass flow rate multiplied by the enthalpy difference between evaporator inlet and compressor inlet. Therefore measuring the input to the electrical heater is another way of determining the mass flow rate.

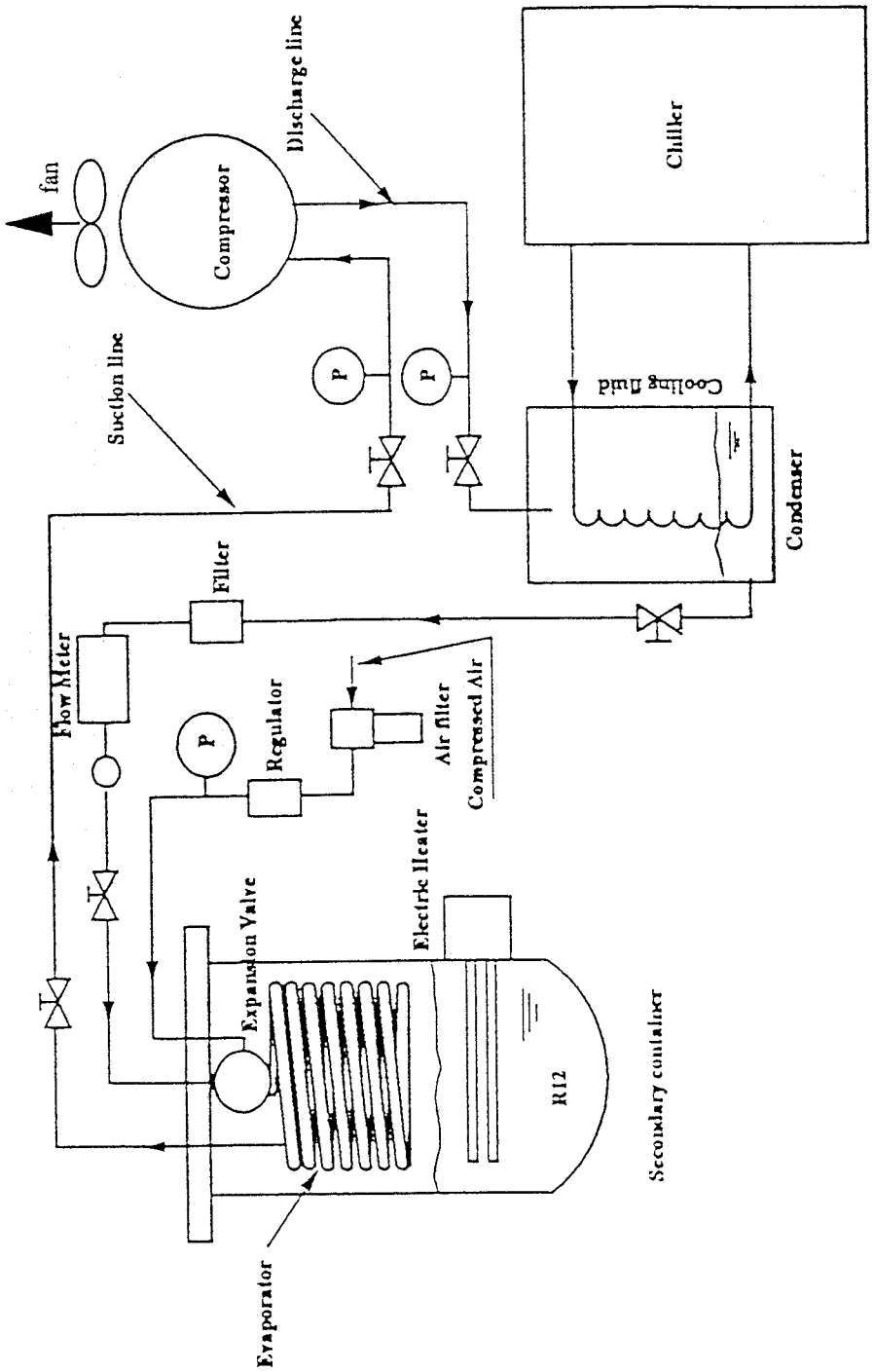

Figure 2-3: Schematic diagram of a calorimeter system [Haider et al. (1997)]

Other configurations of calorimeters exist. Marriott (1973) describes a system with only one heat exchanger and a series of control valves to maintain the desired temperatures. This system was developed to reduce the time that it takes for each test to reach steady-state, to 15 minutes.

2.4 Compressor Maps

The performance of a particular compressor is often illustrated by the use of compressor maps. These maps show the mass flow rate and/or refrigeration capacity, the input power and/or input current as a function of evaporating temperature. The maps include curves for different condensing temperatures. The following figure shows examples of compressor maps furnished by the manufacturer.

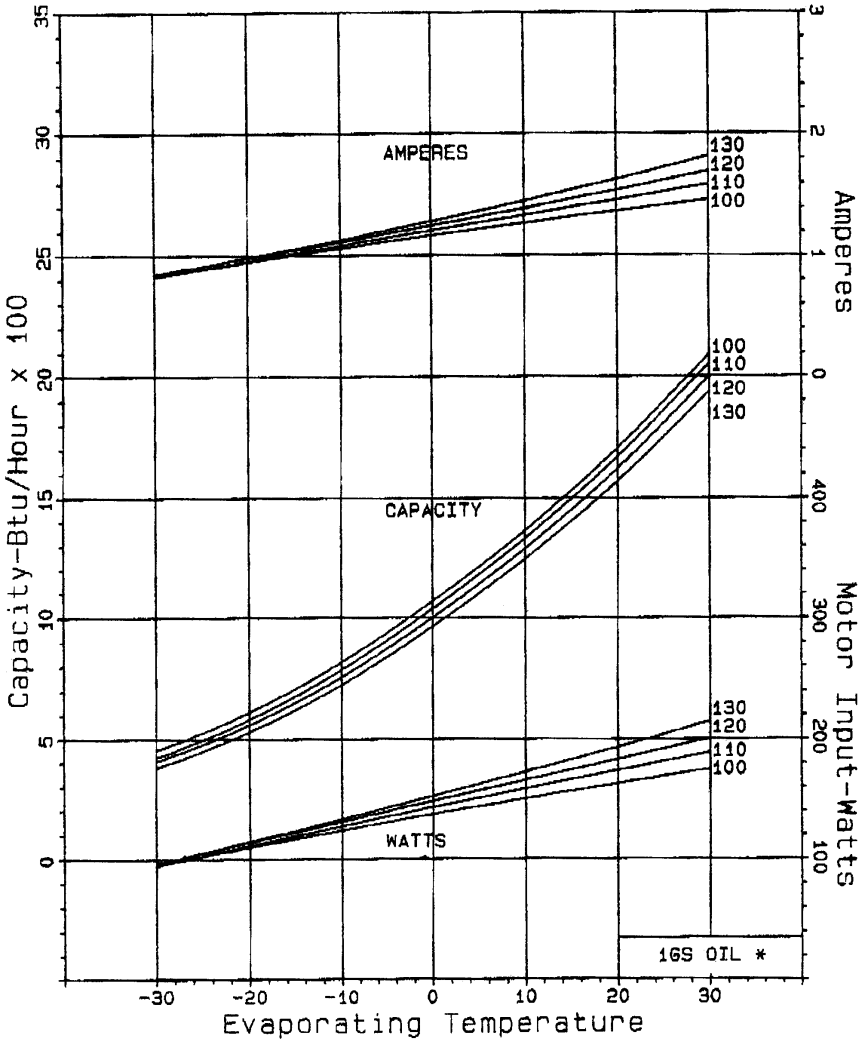

Figure 2-4: Example of a compressor map

2.5 Compressor Testing Data

Compressor performance data for a series of hermetic reciprocating compressors that are used in domestic refrigerators and freezers have been collected from both compressor and refrigerator/freezer manufacturers. For the purpose of this project, it was

necessary to obtain raw experimental data rather than smooth data that have been calculated using methods such as ARI curve fits (see section 2.6 for more details). The raw data are not readily available to the general public. It has been obtained directly from manufacturers for use in this project. The names of the manufacturers and compressor models are confidential.

The following table (2-1) summarizes all of the data sets that have been used for this project. A data set number has been assigned to uniquely identify the different data sets. Different manufacturers are identified with different upper case letters. Compressors from three different manufacturers have been used (A, B, and C). The different compressor models for each manufacturer are indicated using different numbers. There are a few models that have been tested by different organizations. These data sets are distinguished with lower case letters (e.g. B9a, B9b, and B9c). Figure 2-5 shows the data set numbering scheme.

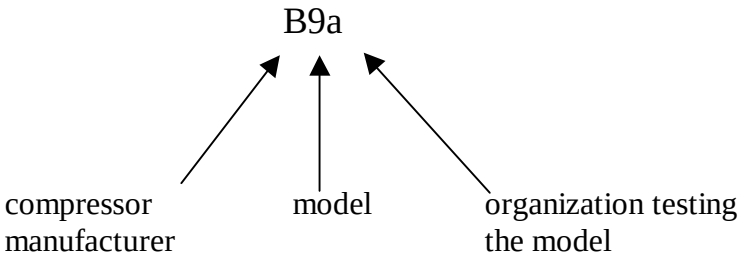

Figure 2-5: Data set numbering scheme

Some data sets contain either the mass flow rate of the refrigerant or the refrigeration capacity and some include both values. If both values were given, the mass flow rate value was used for fitting the different models. If only the refrigeration capacity was given, the mass flow rate was calculated using the fact that in standard calorimeter

testing the refrigerant is both superheated and subcooled to 32.2°C (90°F). The majority of tests has been performed at an ambient temperature of 32.2°C (90°F). Data on a few tests at different ambient temperatures has been used for investigation the effect of ambient temperature in chapter 6.2.

The following parameters, at different condensing and evaporating temperatures, were available for all compressor models:

Power input

Mass flow rate and/or refrigeration capacity

Displacement volume

Motor speed

For some models the discharge temperature and shell temperature were also available. Table 2-1 also indicates the refrigerant used for each compressor model and the refrigeration capacity at the standard rating point conditions of –23.3°C/-10°F evaporating temperature and 54.4°C/130°F condensing temperature. The table does not include the data at different ambient temperatures that has been used in chapter 6.2. See chapter 6.2 for more details.

Data Set Number	Number of Data Points	Capacity at Standard Rating Point [Btu/hr]	COP [-]/ EER [Btu/W-hr]	Mass Flow Rate	Capacity	Power	ARI Coefficients	Maps	Refrigerant	Additional Information	
										Shell Temp.	Discharge Temp.
A1a	16	689	1.6/5.3	x	x	x			R134a	x	x
A1b	14	681	1.5/5.2		x	x			R134a		
A2	14	863	1.4/4.7		x	x			R134a		
A3	14	not available	-		x	x			R134a		
A4	14	839	1.5/5.2		x	x			R134a		
A5	11	861	1.4/4.8		x	x			R134a		
A6a	9	878	1.5/5.1	x		x	n/a		R12	x	x
A6b	9	763	1.3/4.6	x		x	n/a		R12	x	x
B1	15	735	1.6/5.6	x	x	x	x	x	R134a	x	x
B2	16	1012	1.6/5.6	x	x	x	x	x	R134a	x	x
B3	15	1115	1.6/5.6	x	x	x	x	x	R134a	x	x
B4	10	763	1.2/4.1	x	x	x	x	x	R134a	x	x
B5	16	991	1.2/4.2	x	x	x	x	x	R134a	x	x
B6	15	503	1.1/3.6	x	x	x	x	x	R134a	x	x
B7	16	371	1.1/3.6	x	x	x	x	x	R134a	x	x
B8	17	251	1.0/3.3	x		x			R134a	x	x
B9a	9	842	1.2/4.0	x		x	n/a		R12	x	x
B9b	9	917	1.3/4.3	x		x	n/a		R12	x	x
B9c	9	902	1.3/4.5	x		x	n/a		R12	x	x
C1	12	not available	-	x		x	x		R134a		
C2	12	not available	-	x		x	x		R134a		

Table 2-1: Summary of calorimeter testing data used in the project

The following figures (2-6 through 2-8) show data for compressor A1a. Plots of mass flow rate and power versus evaporating temperature as well as power per unit mass flow rate versus evaporating temperature are shown.

Plotting power per unit mass flow rate helps to identify measurement errors as it shows whether or not the data makes physical sense. The power per unit mass flow rate should decrease with increasing evaporating temperature and increase with increasing condensing temperature. Plots of all of the data sets are attached in appendix A.

The data set shown in figure 2-1 does not contain any obvious errors. However, there are a few data sets that include data points that appear to contain suspicious data. Data sets B5, B6, B7 and B8 contain at least one or two suspicious points. The suspicious data is especially obvious in the power per unit mass flow rate plots.

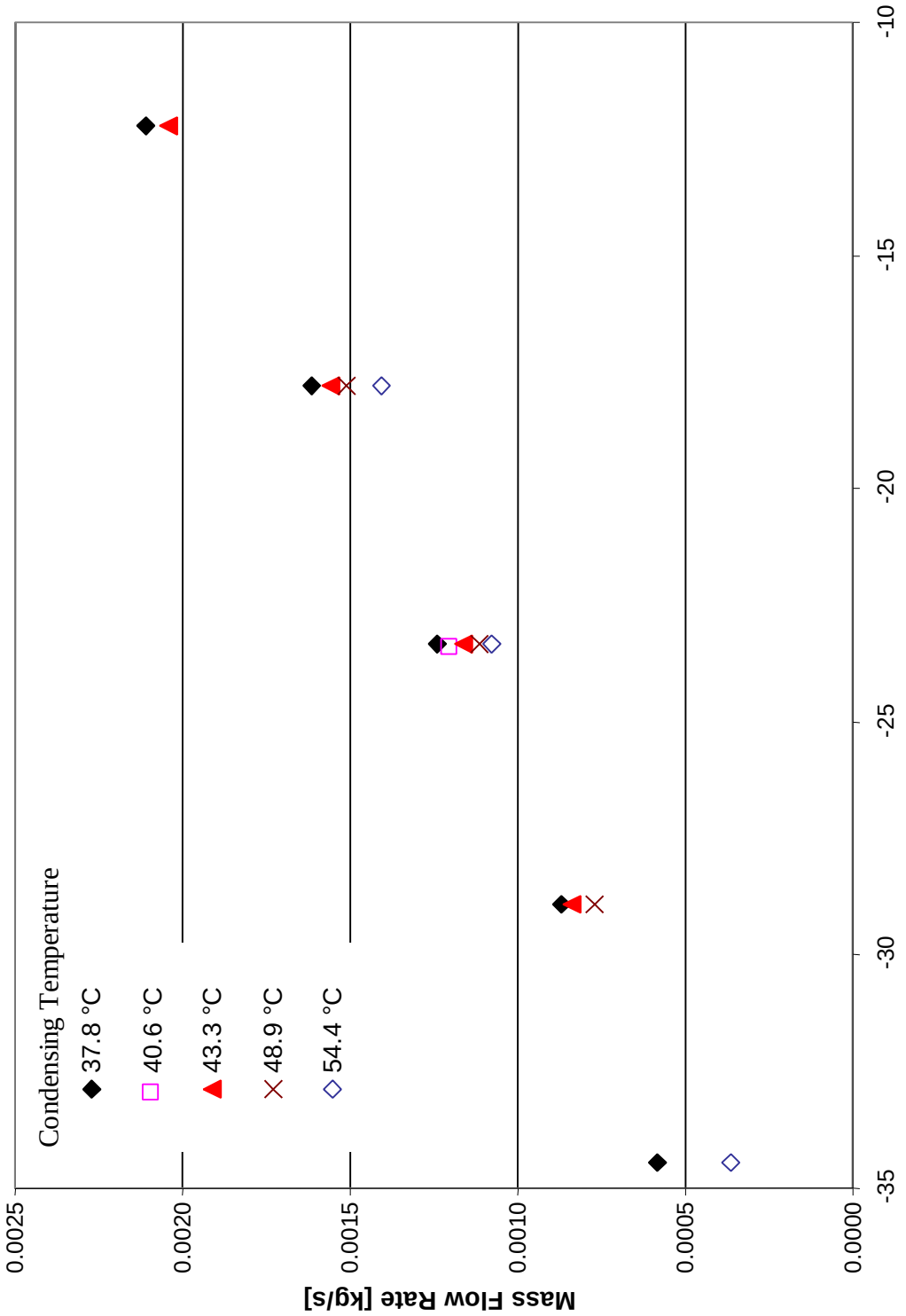

Figure 2-6: Measured mass flow rate data (data set A1a)

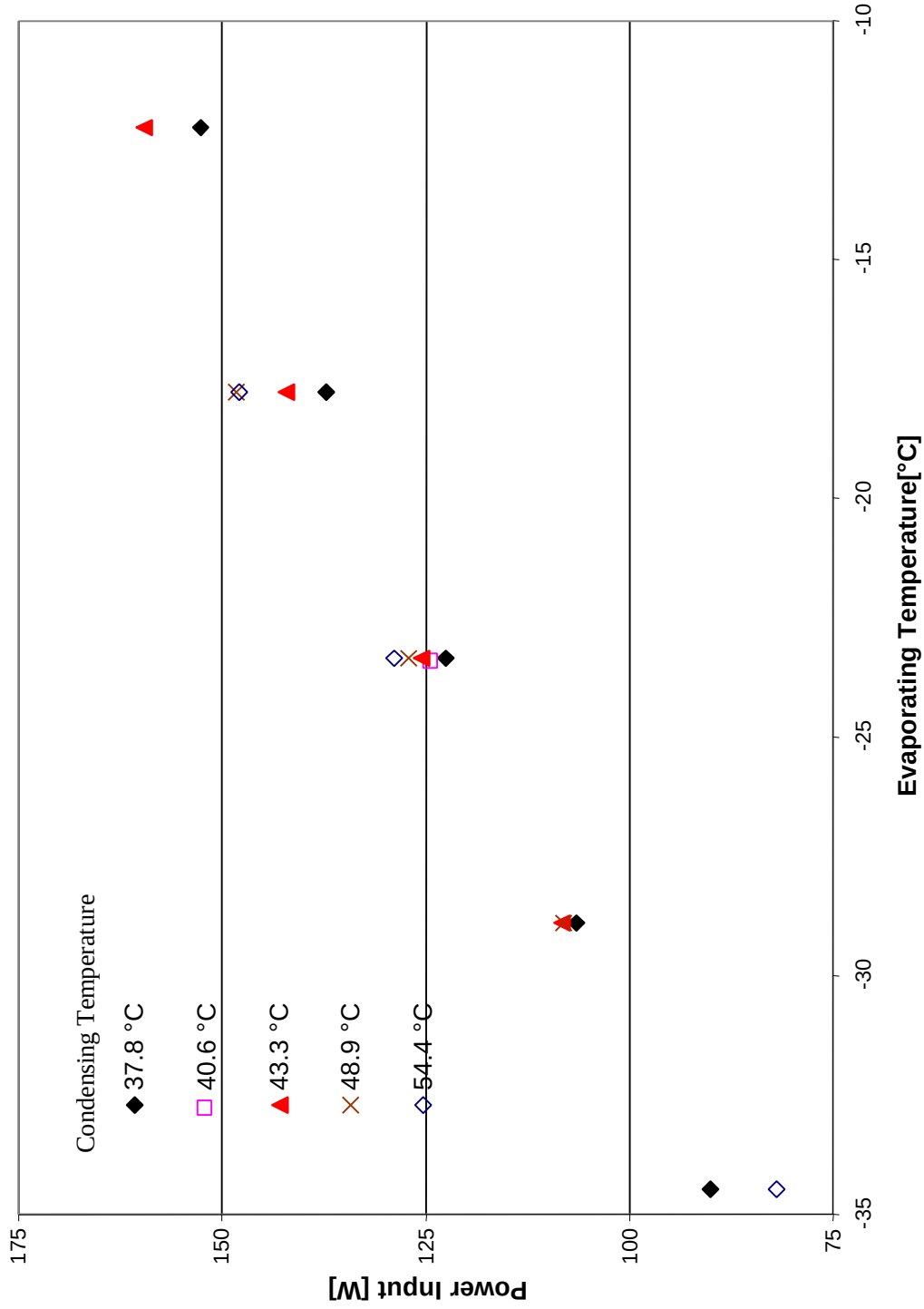

Figure 2-7: measured power input data (data set A1a)

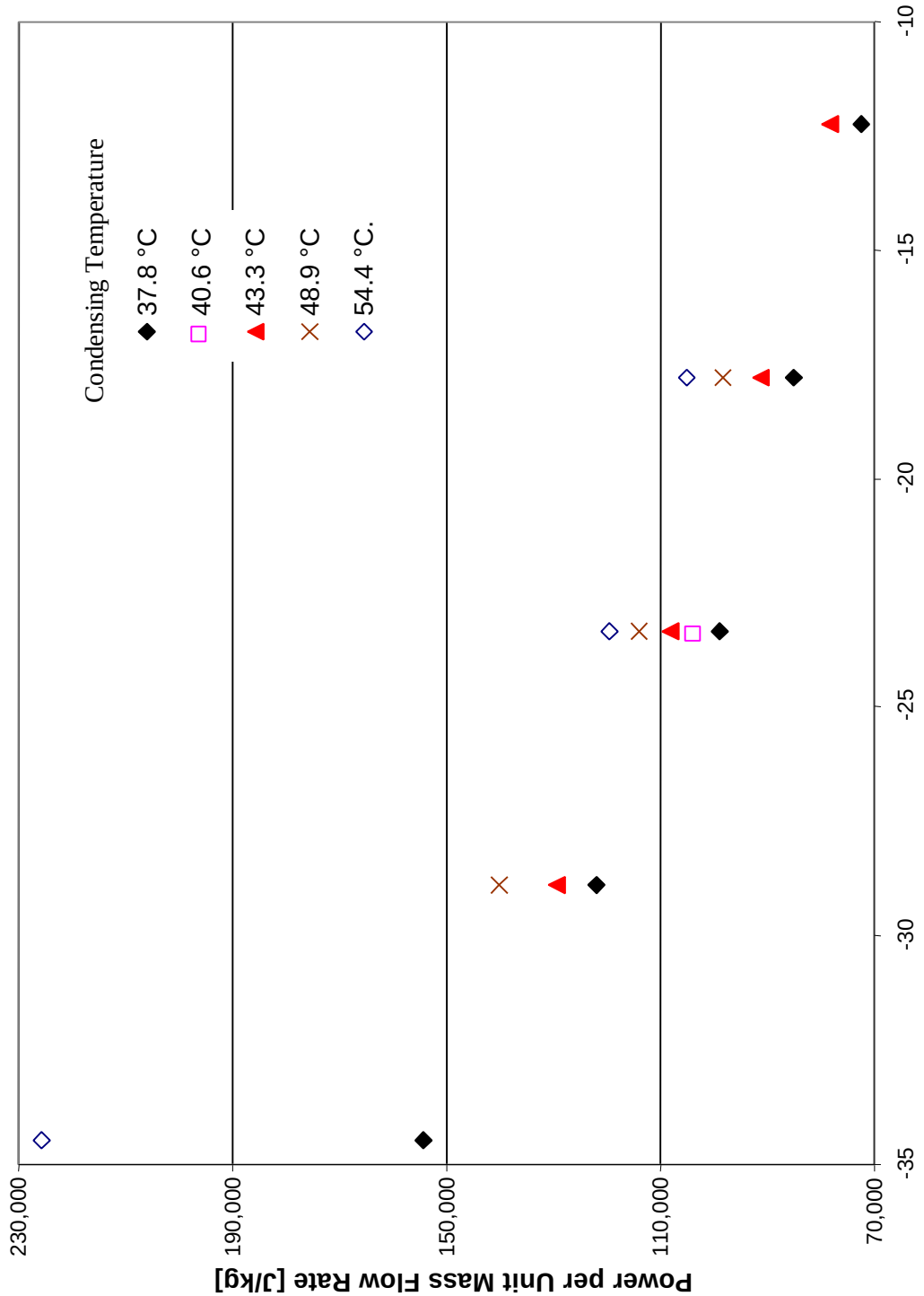

Figure 2-8: Measured power per unit mass flow rate data (data set A1a)

2.6 ARI Method for Presenting Compressor Performance Data

2.6.1 Curve Fit Method

The Air-Conditioning and Refrigeration Institute's (ARI) standard 540-91 provides a method on how to present compressor performance data for "all positive displacement refrigerant compressors and compressor units" [ARI, 1991]. This method uses compressor performance data to curve fit coefficients of polynomial equations.

The equations are of the form

$$X = C_1 + C_2 \cdot T_{evap} + C_3 \cdot T_{cond} + C_4 \cdot T_{evap}^2 + C_5 \cdot T_{evap} \cdot T_{cond} + C_6 \cdot T_{cond}^2 + C_7 \cdot T_{evap}^3 + C_8 \cdot T_{cond} \cdot T_{evap}^2 + C_9 \cdot T_{evap} \cdot T_{cond}^2 + C_{10} \cdot T_{cond}^3 \quad (2\text{-}1)$$

where X can represent refrigeration capacity, power input, mass flow rate or motor current.

T_{evap} – saturated evaporating temperature

T_{cond} – saturated condensing temperature

C_1 to C_{10} - curve fit parameters.

To determine the 10 coefficients in each equation at least 10 measurements of the entity represented by X have to be made.

There are recommendations for ranges of both condensing and evaporating conditions that should be covered with the tests. There are different ranges for high and low temperature applications.

A computer program written by ARI called SURFACEC determines the 10 coefficients. The program reads an input file containing the refrigerant evaporating and

condensing temperatures as well as the corresponding measured value of X and creates an output file with the 10 coefficients and the relative error for each measured data point. This error is determined using the following equation:

$$\Delta X = \frac{X_{meas} - X_{calc}}{X_{meas}} \cdot 100 \qquad (2\text{-}2)$$

where ΔX - error in %

X_{meas} - measured value for the variable X

X_{calc} - value for the variable X calculated with the ARI SURFACEC program

The program uses a least squares curve fit to determine the 10 coefficients. The ARI standard 540-91 allows the values calculated using the curve fit to differ by plus or minus 1 percent from the measured values. In the case that certain data points differ by more than 1 percent, these data points should be indicated by the manufacturer.

2.6.2 ARI Curve Fits of Calorimeter Testing Data

The ARI SURFACEC program was run for all sets of calorimeter testing data provided by compressor manufacturers. In some cases, the errors between curve fit and measured data are very small and the compressor maps obtained look reasonable, at least in the range of operating temperatures where measured data were provided. Figures 2-8 and 2-9 show such maps for mass flow rate and input power. Performance curves have been extrapolated using the curve fit at higher and lower evaporation temperatures than were represented in the experimental data. Additional curves for both a higher and a lower condensing temperature are also shown in figures 2-9 and 2-10. Examination of

figure 2-9 shows that extrapolating to a condensing temperature of 60°C leads to values of the mass flow rate that are almost the same as for a condensing temperature of 54.4°C at evaporating temperature of -30°C and lower. The same behavior is seen for extrapolation to lower condensing temperatures, as evident in the 32.2°C curve.

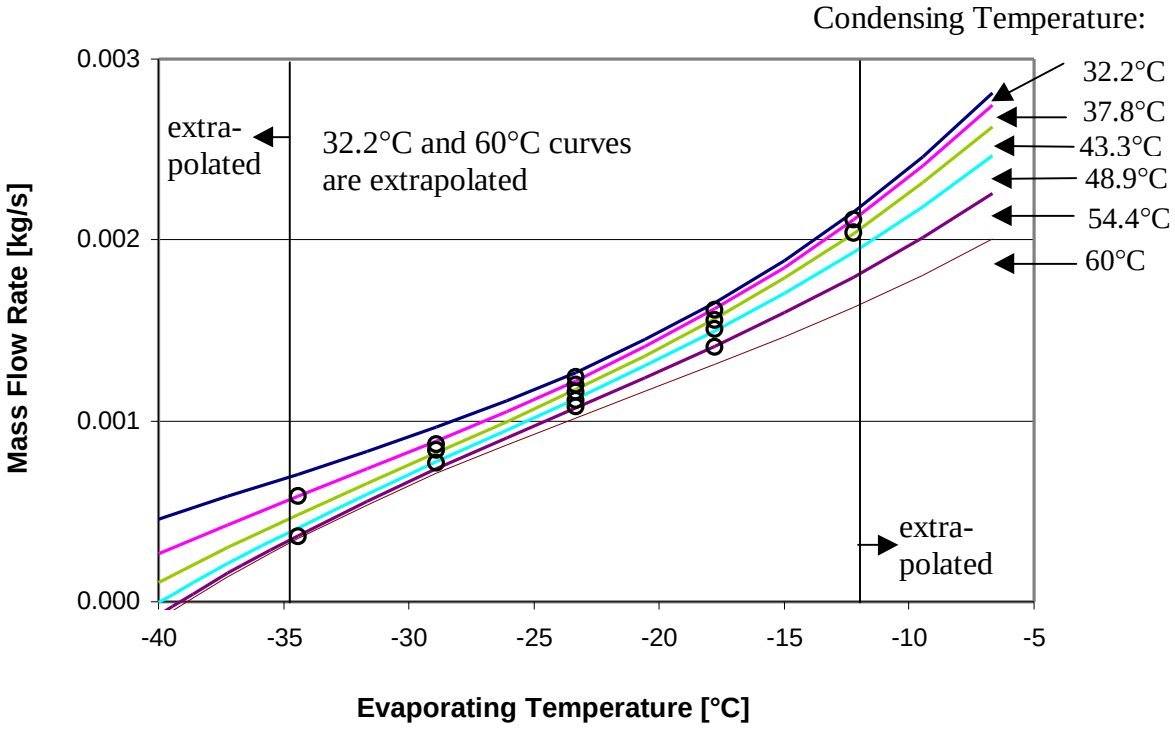

Figure 2-9: ARI mass flow rate map (data set A1a)

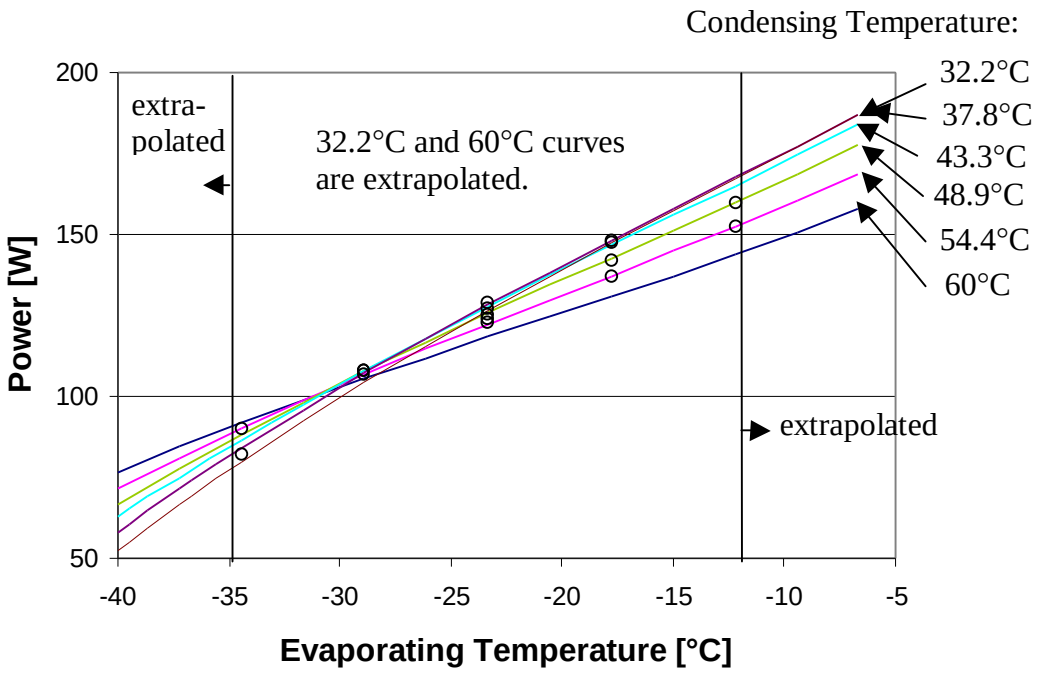

Figure 2-10: ARI power map (data set A1a)

The mass flow rate and power maps seem to fit the data reasonably well for some data sets, as seen in figures 2-11 and 2-12. But plotting the power input per unit mass flow rate as a function of evaporating and condensing temperature (Figure 2-13) shows that the curve fit does not necessarily make physical sense, as seen in figure 2-13.

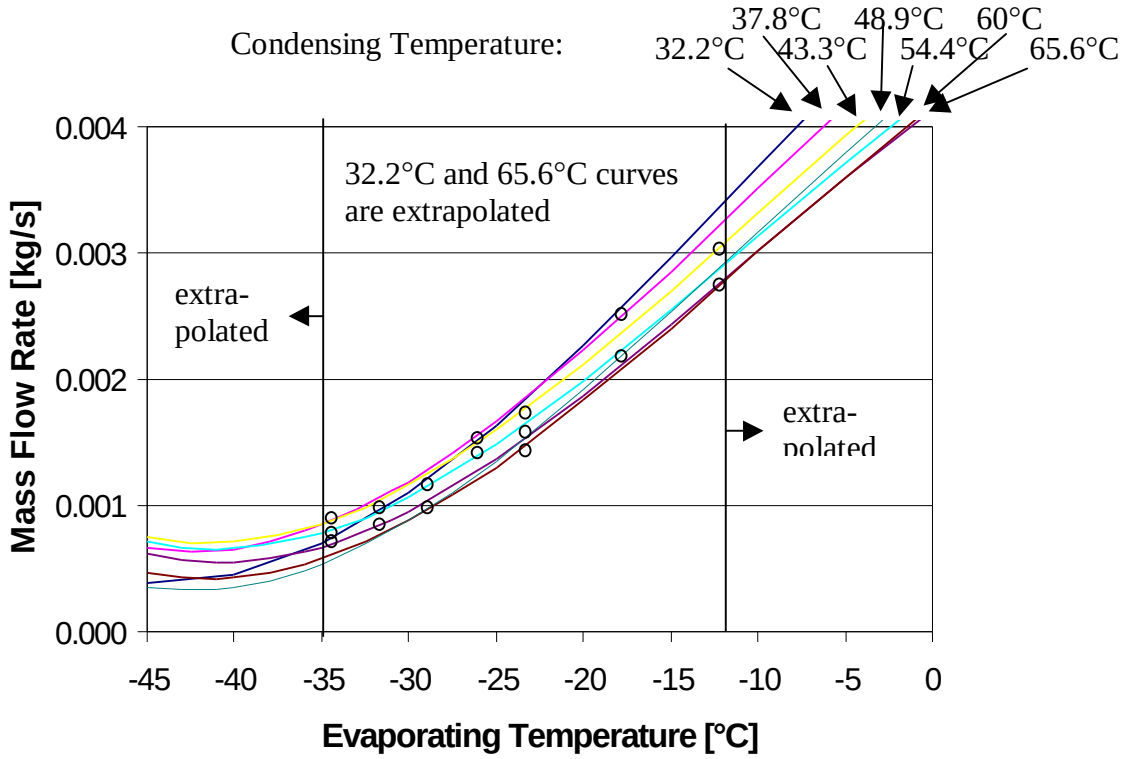

Figure 2-11: ARI mass flow rate map (data set B5)

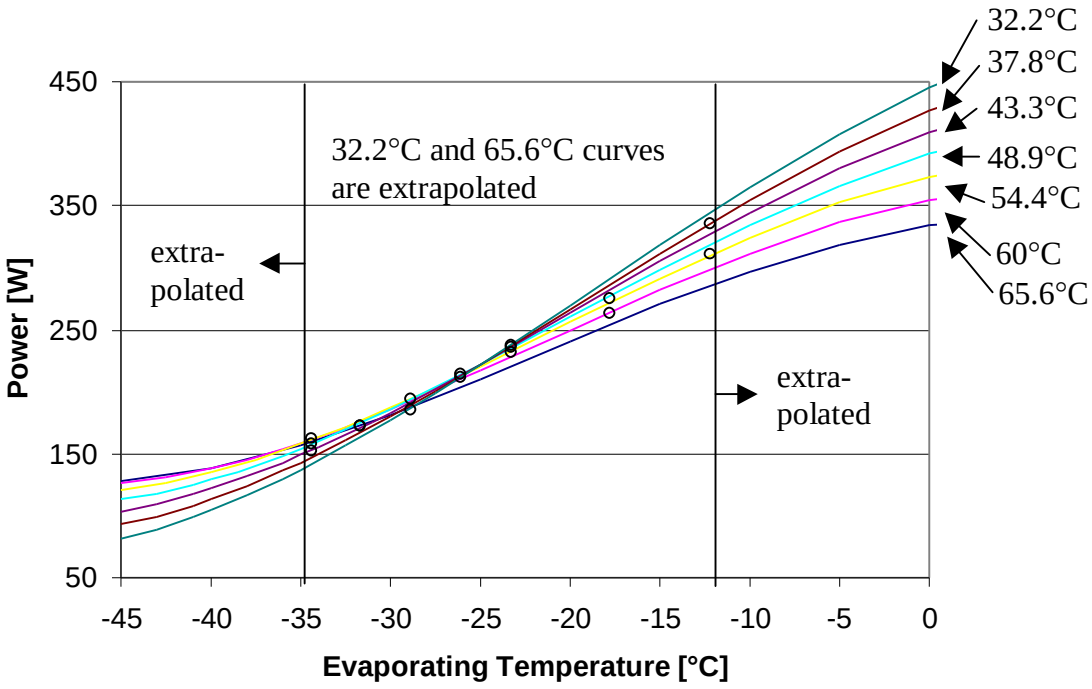

Figure 2-12: ARI power map (data set B5)

When extrapolating to lower evaporating temperatures, the input power per unit mass flow rate in figure 2-13 starts to decrease instead of increase with decreasing evaporating temperature. The extrapolated curve for a condensing temperature of 65.5°C lies lower than the curve for 60°C for most evaporating temperatures.

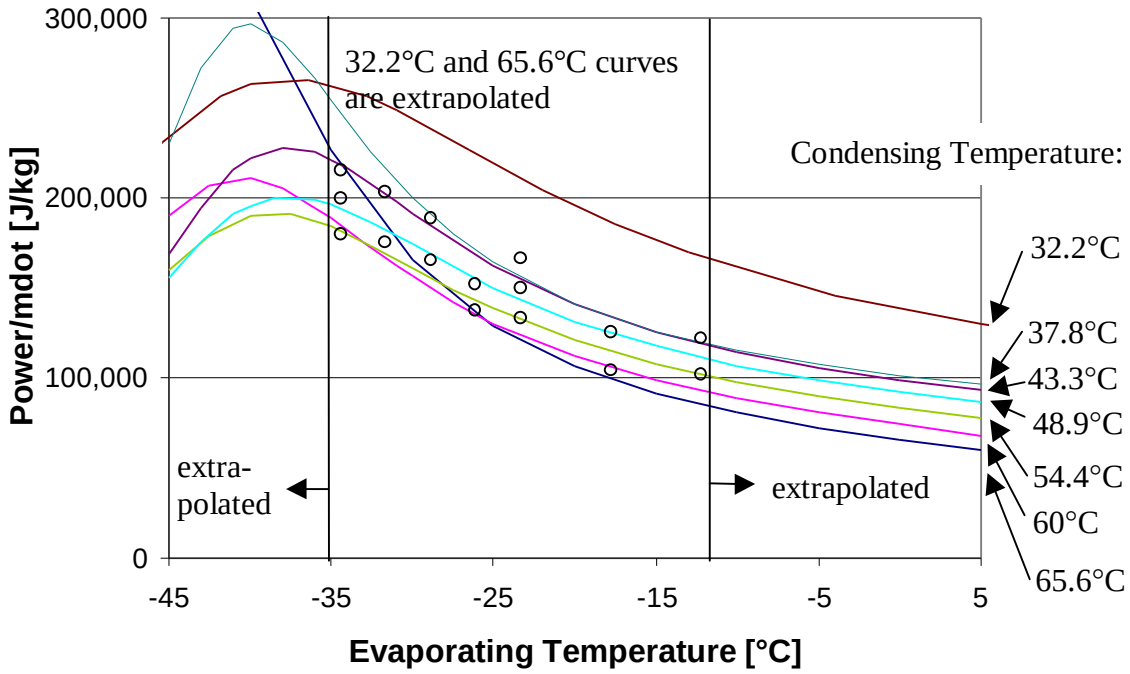

Figure 2-13: ARI power per unit mass flow rate map (data set B5)

In other cases, the curves represent the measured data points well but their shape between the data points and beyond the measured values are physically not possible. The most extreme example found among the 21 data sets examined in this research is shown in figures 2-14 and 2-15.

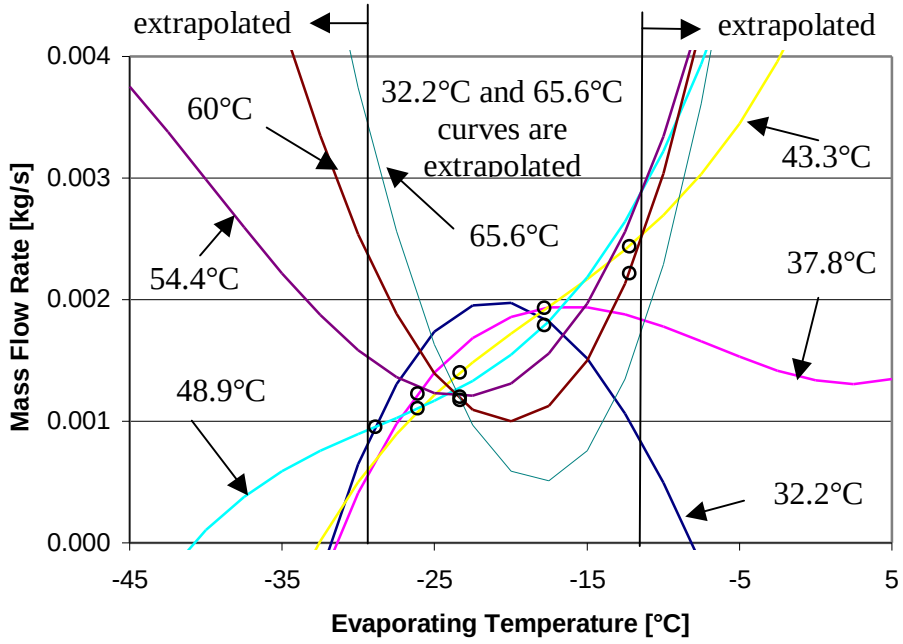

Figure 2-14: ARI mass flow rate map (data set B4)

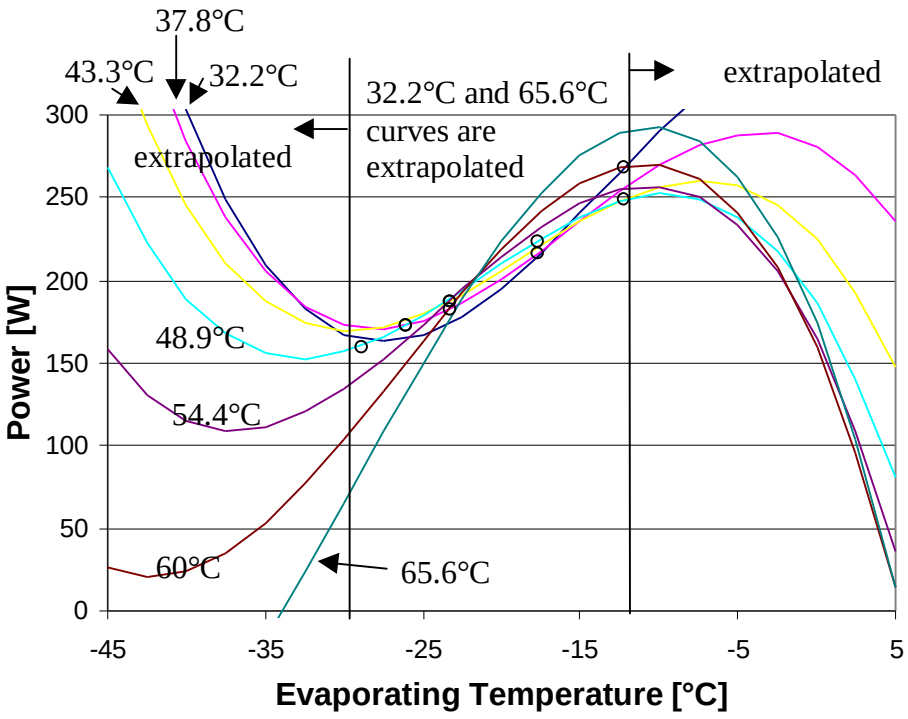

Figure 2-15: ARI power map (data set B4)

The data set used to generate figures 2-14 and 2-15 has only 10 measured data points. The least squares curve fit leads to very small errors. The largest error for mass flow rate is 0.41% and 0.24% for input power. In theory, it should be possible to fit a polynomial with 10 coefficients perfectly to 10 data points. However, the compressor maps generated with the ARI curve fit show that extrapolation and even interpolation can lead to very inaccurate predictions.

There are also some cases where the errors of the ARI curve fit are very high. Some are as high as 70%. There may be grounds for assuming that, in these cases measurement errors are responsible. This would, for example, explain why the errors are considerably greater for mass flow rate than for power as mass flow rate measurements are more likely to be inaccurate than electrical power measurements. These data sets are B2, B6, B7 and B8. Virtually every data set contains one or more data points that differ more than the 1 percent that is required by the ARI standard from the ARI curve fit. Plots of ARI curve fits for all data sets are attached in appendix B.

Interestingly enough, it is also possible to use the ARI program with less than 10 measured data points. In fact the program still determines 10 coefficients when there are as few as 3 measured data points. For one of the data sets that contains only 9 measured points the program was run and a mass flow rate map generated with the obtained coefficients is shown in figure 2-16 as well as the measured data. The map contains only the curve for 37.8°C condensing temperature. Curves for other condensing temperatures fall more or less directly on top of the one shown. The fact that the ARI program will allow the user to fit 10 coefficients with fewer than 10 data points is clearly a flaw in the program.

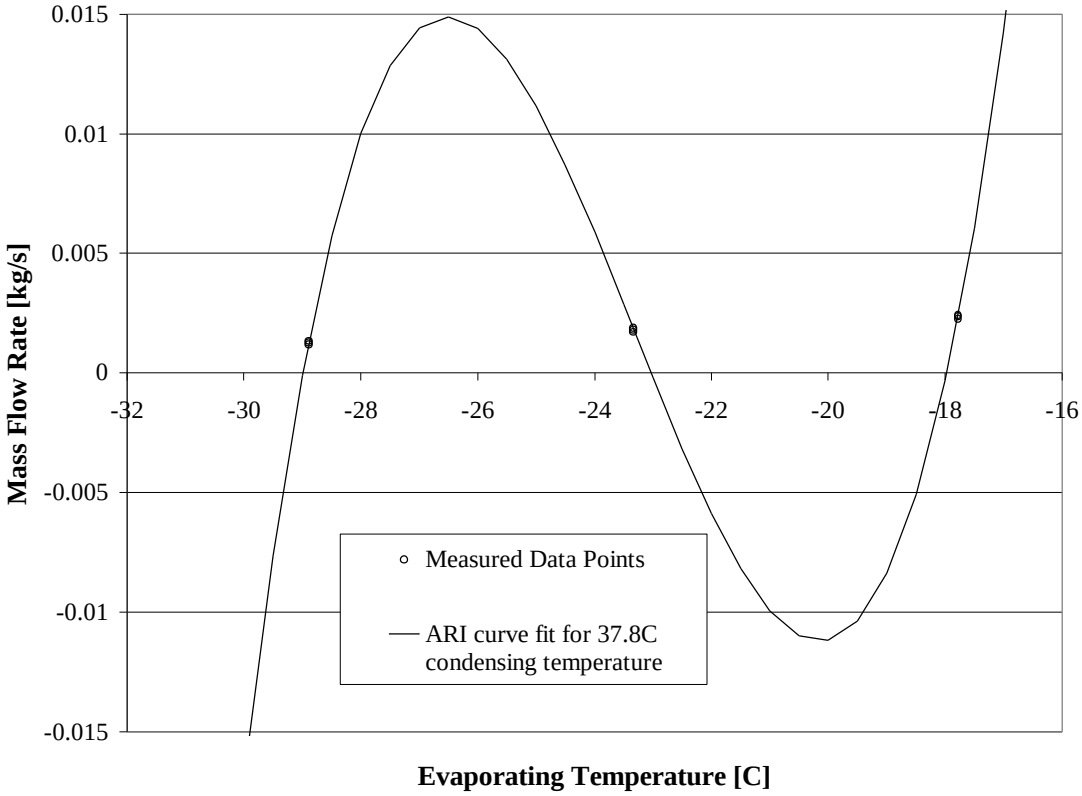

Figure 2-16: ARI mass flow rate map (data set B9a)

There seem to be several factors that affect the quality of curve fits obtained with the ARI method.

1) More measured data leads to a curve fit that is more likely to accurately interpolate and extrapolate.
2) If the measured data are distributed uniformly over the range of condensing and evaporating temperatures, the curve fit is more likely to be useful for interpolation and maybe even for extrapolation to slightly higher or lower evaporating or condensing temperatures. If there is, for example, only one measured data point at one particular condensing temperature, this curve is fixed only at one point and can have a physically impossible shape for all other condensing temperatures.

Some manufacturers supplied us with measured data as well as the 10 coefficients of the ARI curve fit. It has to be noted that the coefficients do not always match the coefficients obtained using the ARI program with the given data. It seems that manufacturers remove suspicious data points or adjust the data in a way so that the compressor maps make physical sense if the coefficients calculated by the ARI program do not give reasonable looking maps.

Chapter 3

Compressor Modeling

3.1 Literature Review

Several different approaches to modeling refrigeration compressors exist in the literature. In thermodynamics textbooks [Moran and Shapiro (1993)] compressors are assumed to be adiabatic and an isentropic efficiency is used to account for inefficiencies. Motor inefficiencies and heat transfer from the compressor to its surroundings are not taken into account.

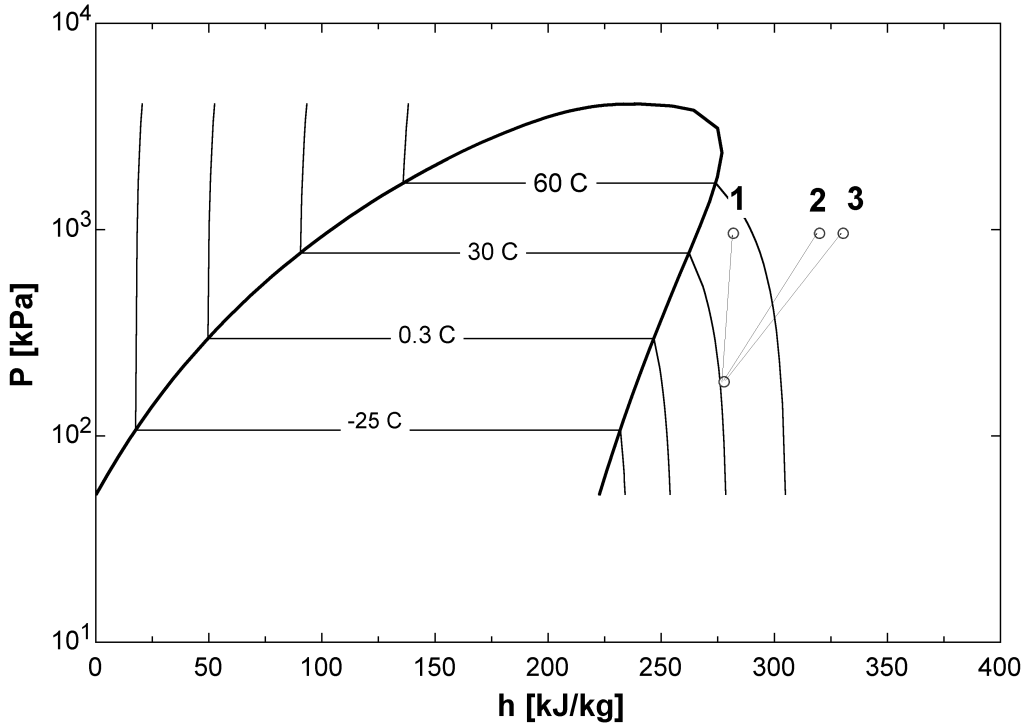

Figure 3-1: Pressure – enthalpy diagram showing a measured outlet state (1), isentropic compression (2) and adiabatic compression with an isentropic efficiency of 0.8

Figure 3-1 illustrates compression process endpoints for three different processes. Process 1 depicts actual suction and discharge conditions for a real compressor (model A1a). The inlet conditions for the data point shown are 183.3 kPa and 32.2°C. Process number 2 in the figure is an isentropic process (adiabatic and reversible). The isentropic efficiency is 1. Process number 3 is also adiabatic but not reversible. The process shown has an isentropic efficiency of 0.8; therefore the power needed for this process is larger than the power needed for the isentropic case. For the measured outlet state (point 1), the refrigerant exits the compressor significantly cooler than in the isentropic case which shows that the compressor is far from being adiabatic. The figure also shows that, when the compressor is not adiabatic, less power is necessary to achieve the same pressure rise [Baehr (1992), Çengel and Boles (1994)]. However, the power does not go to zero as suggested in figure 3-1 (enthalpy rise is close to zero) because not all the heat transfer takes place simultaneously but rather before and after the compression process. The power is approximately equal to the heat transfer off the compressor shell. In a domestic refrigerator or freezer the hermetic compressor shell is generally painted black and a fan blows over it to enhance heat transfer and thereby lower the power consumption.

3.1.1 Detailed Models

Hermetic refrigeration compressors are described in chapter 2. The state of the refrigerant depends not only on what happens in the actual compression cylinder but it is also changed as the refrigerant passes through the suction muffler, the valves and

discharge line. There is also interaction with the lubricant oil and the surroundings through the compressor shell.

Very detailed models have been developed that describe the heat transfer between the many components of a refrigeration compressor [Fagotti et al. (1994),Cavallini et al. (1996)]. These models use energy balances on every part inside the compressor (cylinder, suction muffler, discharge line, refrigerant, oil, etc.) to determine the refrigerant mass flow rate. Many tests would be required to determine and validate a large number of heat transfer coefficients. It would also be necessary to take measurements inside the compressor, for example at the inlet and outlet to the cylinder to determine conditions at these points and the amount of heat transfer into the refrigerant in the suction muffler. A detailed model approach will complicate not simplify measurements taken in standard testing procedures. Todescat et al. (1992) compare different approaches to model the heat transfer inside a compressor.

The goal of this project is to find a model that requires only very few tests to characterize compressor performance. Therefore the detailed modeling approach described above was not pursued any further.

Kent (1974) and Prakash and Singh (1974) use thermodynamics to describe the changes of the refrigerant state through out the suction, compression and discharge process. Brok et al. (1980) model the heat transfer in the cylinder as well as use an energy balance on the heating of the refrigerant during the suction process.

Other model combine modeling heat transfer with describing the fluid dynamic behavior of the refrigerant. Hiller and Glicksman (1976) use only approximate representation of the dynamics in valves and manifolds to limit the number of parameters

involved. Röttger and Kruse (1976) describe the instationary gas pulsations in the valve chambers as well as the cylinder heat transfer. Escanes et al (1996) and Pérez-Segarra et al. (1994) develop a very detailed model of the fluid dynamics inside a compressor including also thermal considerations. MacLaran et al. (1976) establish the boundary conditions in piping and valves in a reciprocating compressor. The influence of the geometry of suction and discharge valves on the volumetric efficiency, the mass flow rate and the coefficient of performance was investigated by Rigola et al. (1996). Like the type of models described earlier, these models contain many parameters including geometric parameters of, for example, the suction muffler or valves, that are not readily available. Therefore this approach will not be further investigated. Rasmussen (1997) describes a very detailed model including the mechanical system of a variable speed compressor trying to keep the number of parameters that are difficult to measure as small as possible.

Dabiri and Rice (1981) use an empirical approach similar to the ARI method and develop correction factors to account for different levels of suction gas superheat. Haberschill et al. (1994) combined a volumetric efficiency approach for modeling the mass flow rate (as discussed below) with energy balances. Empirical relations are used for some model parameters such as the polytropic coefficient.

Marriott (1973) uses a curve fit with 36 parameters to model the power input to the compressor. To represent the refrigerant mass flow rate a volumetric efficiency approach has been used similar to the one described in section 3.3.

3.1.2 ERA Model (REMAP)

EPA (U.S. Environmental Protection Agency) developed a computer program that models the performance of a domestic refrigerator called EPA Refrigerator analysis (ERA) [EPA, 1993]. It contains a subprogram that is used to smooth measured compressor performance data. This program relies on the fact that both the compressor's volumetric and the isentropic efficiency are strongly correlated with the compression ratio. The program uses linear relationships to correlate both efficiencies.

The program uses a measured compressor map to determine curve fit parameters of those linear relationships that can be used to generate smooth maps. These smooth maps are then used by the ERA program to predict the performance of the compressor at various operating conditions. However, extrapolation can result in large errors using this curve fit.

3.2 Useful Modeling Parameters

The goal of this project is to find a model that can predict the performance of a compressor (i.e. the mass flow rate or capacity and the electrical power input) for a range of operating conditions. This model should contain a small number of parameters that can be determined with measurements on the particular compressor model. It should be possible to predict the compressor performance at operating conditions other than those tested using these parameters.

The operating conditions are the evaporating and condensing pressures and the ambient temperature. Although it would be useful for modeling purposes to take

temperature and/or pressure measurements at several points inside the compressor this is not practically feasible in the compressor testing that is used to determine performance maps.

However, it is easily possible to measure the refrigerant temperature at the discharge of the compressor and the temperature of the compressor shell. This information would be useful to do an energy balance on the compressor and determine the amount of heat transfer from the shell to the surroundings. See chapter 7 for more details. Some of the experimental data sets contained measured discharge and shell temperatures. These data were plotted against evaporation and condensing pressure as well as compression ratio to see whether there is any significant trend that could be useful for modeling mass flow rate and power at different operating conditions. Figures 3-2 through 3-7 shows these plots for two of the data sets. The reported discharge temperature was measured 1 inch away from the compressor shell for data set B9a and 2 inches away for data set B5. The shell temperatures are averages from measurements taken at the top, middle and bottom of the compressor shell.

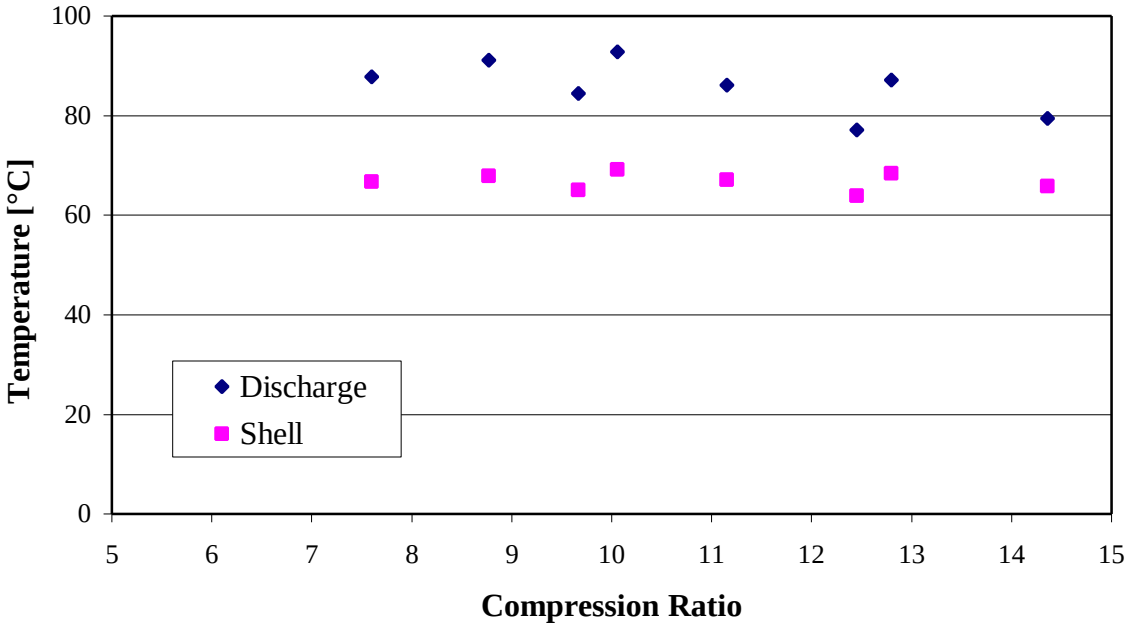

Figure 3-2: Shell and discharge temperature versus compression ratio (data set B9a)

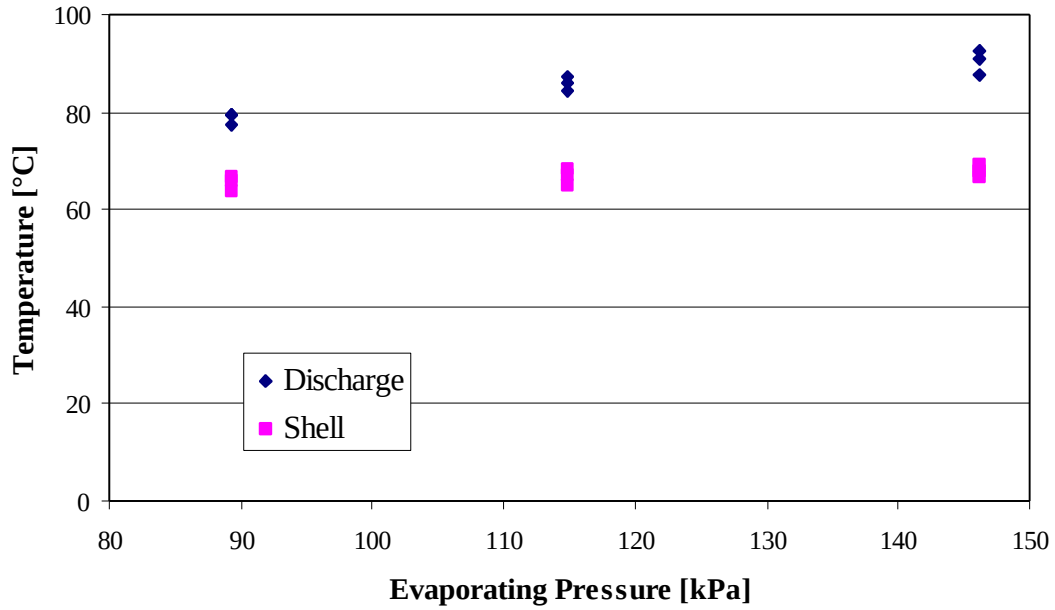

Figure 3-3: Shell and discharge temperature versus evaporating pressure (data set B9a)

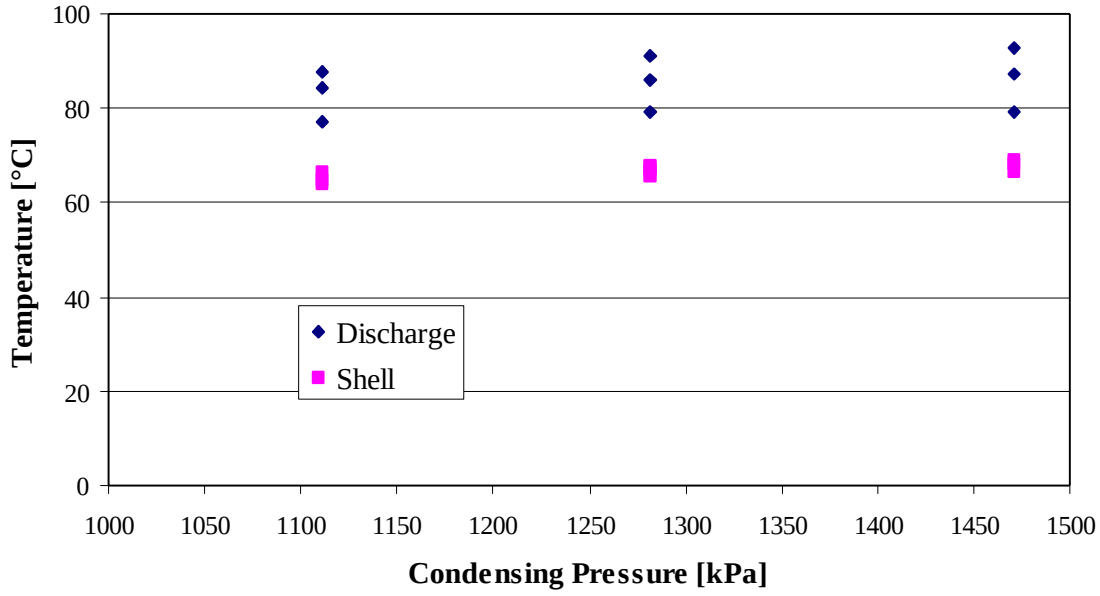

Figure 3-4: Shell and discharge temperature versus condensing pressure (data set B9a)

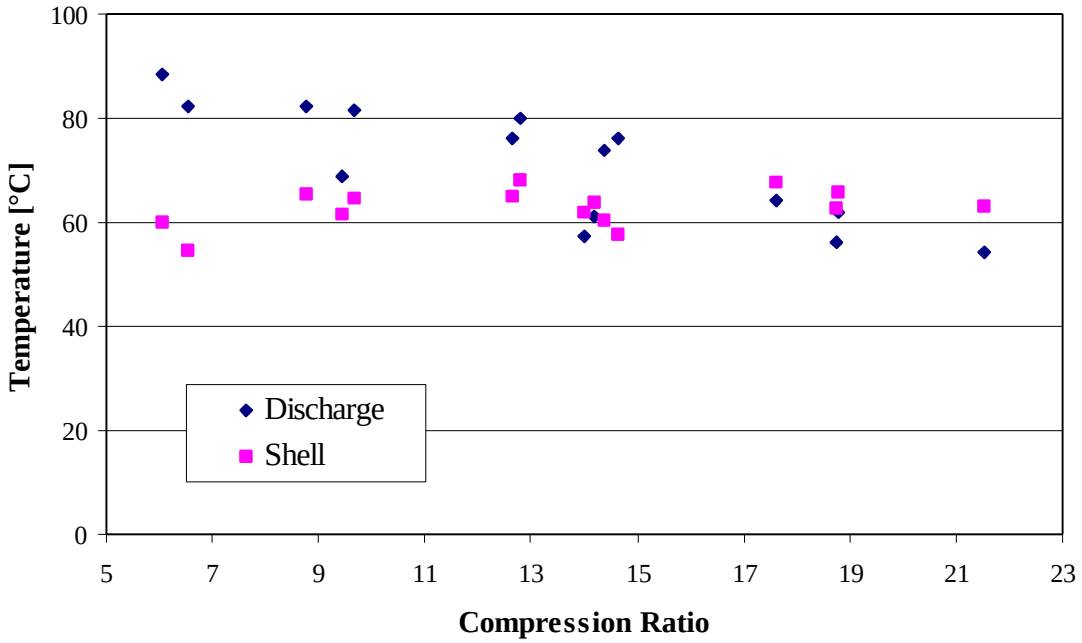

Figure 3-5: Shell and discharge temperatures versus compression ratio (data set B5)

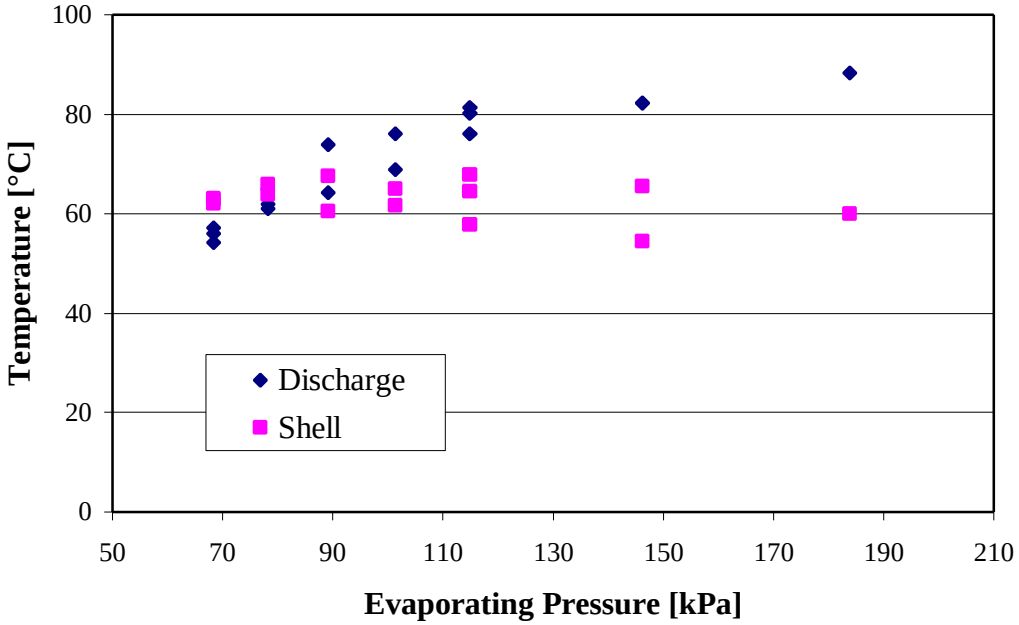

Figure 3-6: Shell and discharge temperatures versus evaporating pressure (data set B5)

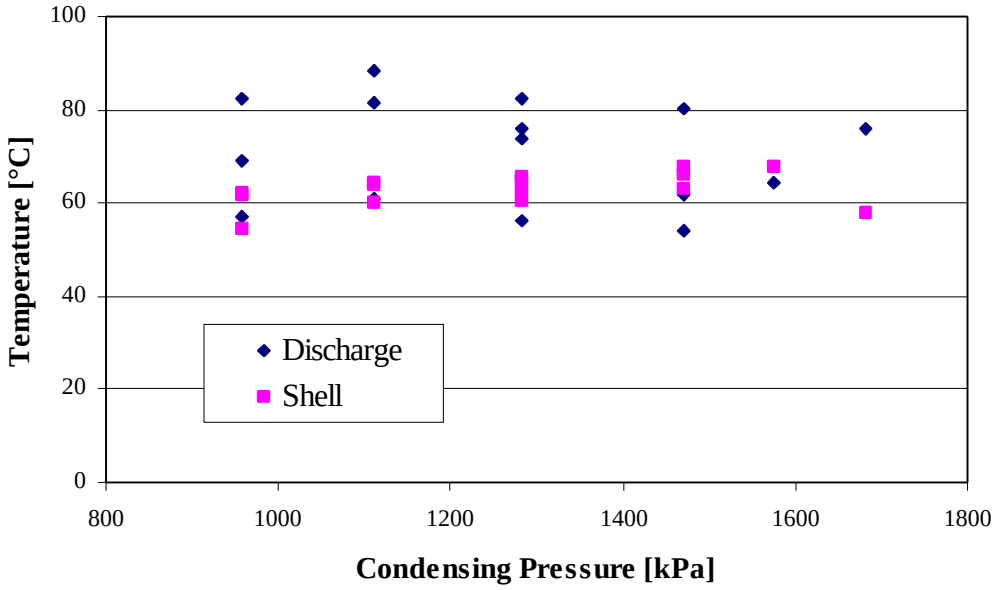

Figure 3-7: Shell and discharge temperatures versus condensing pressure (data set B5)

The measured shell temperatures do not vary much over the range of operating conditions tested. Therefore, it does not appear useful for modeling purposes. The

measured discharge temperature seems to decrease slightly with increasing compression ratio and increase with increasing evaporating pressure. The explanation for this is not clear. One would expect the discharge temperature to be higher for higher condensing temperatures and therefore higher compression ratios. Figure 3-8 shows the discharge temperature for data set B5 as a function of compression ratio indicating the evaporating temperature for each data point.

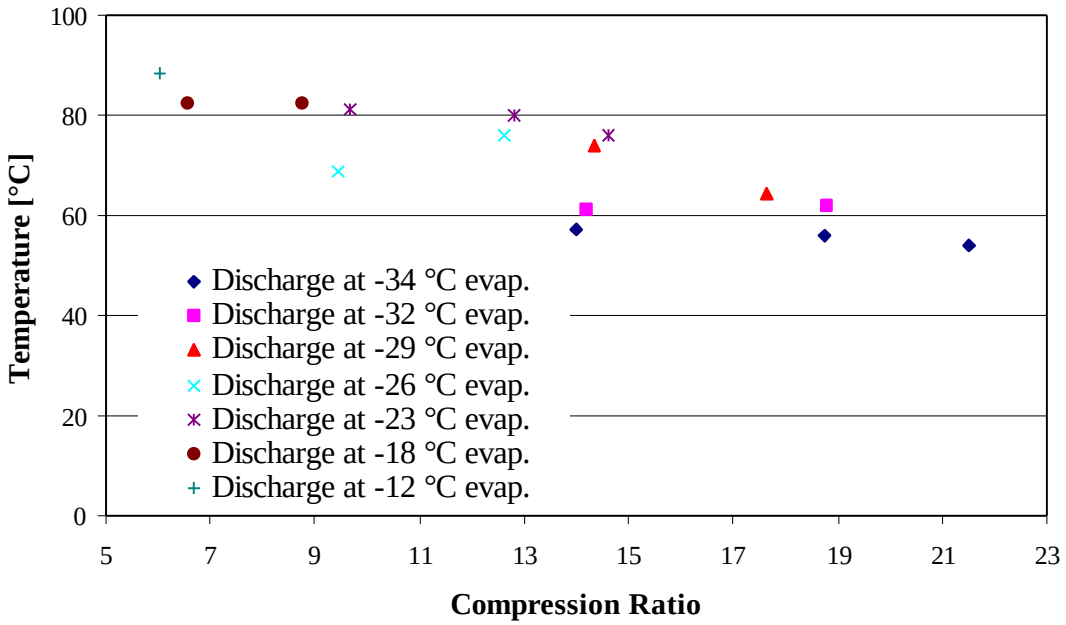

Figure 3-8: Discharge temperature versus compression ratio (data set B5)

One would expect the discharge temperature to increase with compression ratio for constant evaporating temperatures, but this in only the case for a few data points. These measured values seem to show that the temperature of the refrigerant one or two inches away from the shell is very different from the temperature of the refrigerant directly after the compression process. Although there is a distinct trend for the discharge temperature with compression ratio or evaporating temperature, the data scatter significantly and do not vary that much in value. It does not seem to contain much useful

information for correlating the mass flow rate or electrical power to the operating conditions.

In the literature it has been attempted to correlate the shell and discharge temperature to be able to model the heat transfer from the compressor shell [Cavallaro and Bullard (1995)]. The experimental data collected for this project has also been plotted in this way. Figures 3-9 and 3-10 show the average shell temperature plotted against the discharge temperature for data set B9a and B5.

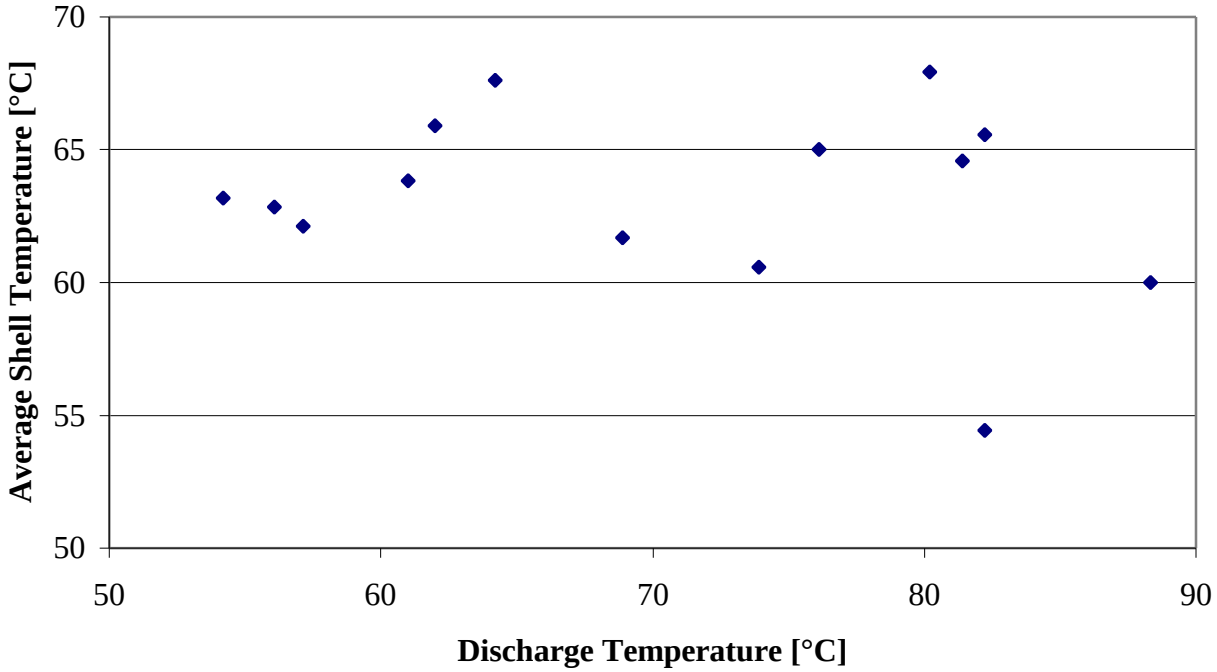

Figure 3-9: Average shell temperature versus discharge temperature (data set B5)

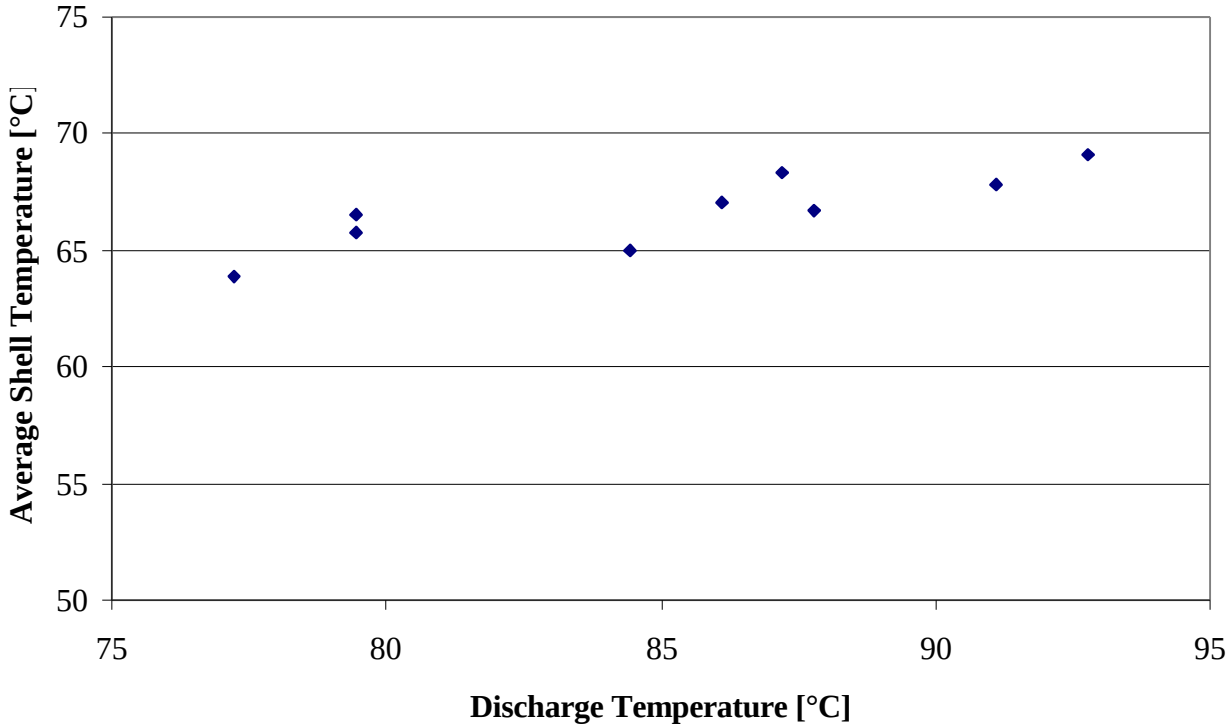

Figure 3-10: Average shell temperature versus discharge temperature (data set B9a)

The figures show that only data set B9a seems to show a trend of increasing shell temperature with discharge temperature. But the data still scatter significantly. In fact, the scatter is approximately 50% of the entire range of shell temperatures that were reported.

3.3 Volumetric Efficiency Model

The volumetric efficiency is defined as the mass of vapor that is actually pumped divided by the mass of vapor that the compressor could pump if it could handle the total piston displacement at the suction state. A model that is widely used [Threlkeld (1967), Browne et al. (1998), Popovic and Shapiro (1995)] uses the concept of volumetric efficiency to calculate the mass flow rate of a compressor. Popovic and Shappiro (1995) developed a semi-empirical model that included a polytropic exponent that varies with

compression ratio (see section 4.3.2 for more details). The model was developed for compressors much larger than the ones studied in this project.

The indicator diagram in figure 2-2 shows the refrigerant states that are being used in the following derivation. The volumetric efficiency can be represented by:

$$h_v = \frac{\frac{V_b - V_a}{v_b}}{\frac{V_b - V_d}{v_b}} = \frac{(V_b - V_a)\cdot v_{suction}}{(V_b - V_d)\cdot v_b} \qquad (3\text{-}1)$$

where η_v - volumetric efficiency

V_b - total displacement volume

V_a - volume of the re-expanded clearance vapor

V_d - clearance volume

v_b - specific volume of the refrigerant in the cylinder after the intake (re-expanded clearance vapor mixed with fresh intake)

$v_{suction}$ - specific volume of the refrigerant at suction line conditions

The compression and expansion process are described as polytropic processes. It is assumed that they have the same polytropic exponent n.

$$p_{suction}\cdot V_a^n = p_{discharge}\cdot V_d^n \qquad (3\text{-}2)$$

with $p_{suction}$ - suction pressure

$p_{discharge}$ - discharge pressure

n - polytropic exponent

Because the pressures at state c and d are equal and the pressures at state a and b are also equal, equation (3-2) can be transformed into:

$$\frac{V_a}{V_d} = \left(\frac{p_{discharge}}{p_{suction}} \right)^{\frac{1}{n}} \tag{3-3}$$

The clearance volume ratio C can be expressed as

$$C = \frac{V_d}{V_b - V_d} \tag{3-4}$$

From equation (3-1) the following can be derived:

$$h_v = \left[1 + \frac{V_d}{V_b - V_d} - \frac{V_d}{V_b - V_d} \cdot \frac{V_a}{V_d} \right] \cdot \frac{v_{suction}}{v_b} \tag{3-5}$$

Introducing equations (3-3) and (3-4) into equation (3-5) leads to

$$h_v = \left[1 + C - C \left(\frac{p_{discharge}}{p_{suction}} \right)^{\frac{1}{n}} \right] \cdot \frac{v_{suction}}{v_b} \tag{3-6}$$

The volumetric efficiency can also be expressed in terms of mass flow rate and piston displacement. It is the mass flow rate that is actually pumped divided by the mass of refrigerant if the entire piston displacement volume were filled with refrigerant at the suction conditions.

$$h_v = \frac{\dot{m} \cdot v_{suction}}{V \cdot RPM} \tag{3-7}$$

with V- displacement volume

Combining equations (3-6) and (3-7) leads to the following expression for the mass flow rate.

$$\dot{m} = \left[1 + C - C \left(\frac{p_{discharge}}{p_{suction}} \right)^{\frac{1}{n}} \right] \cdot \frac{V \cdot RPM}{v_b} \tag{3-8}$$

The work that is necessary can be calculated as the work necessary to do the compression process minus the work gained from the re-expansion of the clearance vapor [Kent (1974), Hahne (1993), Moran and Shapiro (1993)].

$$W = \int_b^c V dp - \int_a^d V dp \tag{3-9}$$

For polytropic processes with pv^n = const the work per compressor cycle is

$$W = \frac{n}{n-1} p_b (V_b - V_a) \left[\left(\frac{p_{discharge}}{p_{suction}} \right)^{\frac{n-1}{n}} - 1 \right] \tag{3-10}$$

Dividing equation (3-10) by the mass of the vapor that is taken in per cycle leads to an expression for the work per unit mass flow rate.

$$W = \frac{n}{n-1} p_{suction} v_b \left[\left(\frac{p_{discharge}}{p_{suction}} \right)^{\frac{n-1}{n}} - 1 \right] \tag{3-11}$$

3.4 Objective Function for Parameter Fitting Procedure

Each model presented in chapter 4 and 5 contains a number of curve fitting parameters that were determined using the method of least squares. The mass flow rate model and the power model were fitted separately because the power model contains the mass flow rate as a parameter. If mass flow rate and power were fitted at the same time, the mass flow rate model parameters could be used to help fit the power model but at the same time the mass flow rate model would fit worse. The errors between the measured and calculated value was normalized by dividing by the average of all measured values. This process ensures that errors of small values and big values are weighted equally.

The objective function for the least squares curve fit for mass flow rate is:

$$OF_{\dot{m}} = \sqrt{\frac{\sum_{i=1}^{N}\left(\frac{\dot{m}_{meas} - \dot{m}_{calc}}{\dot{m}_{mean}}\right)^2}{N}} \qquad (3\text{-}12)$$

with OF - objective function

N - number of data points

$\dot{m}_{meas}$ - measured mass flow rate

$\dot{m}_{calc}$ - calculated mass flow rate

$\dot{m}_{mean}$ - average of all measured mass flow rate data

The expression in parentheses in equation (3-12) is the error for each data points in percent of the average measured mass flow rate. It is going to be called the mean weighted error. To be able to compare the results with other curve fits like the ARI curve fit a relative error has been computed for each data point. This is the error in percent of the mass flow rate at that particular point. The relative error is defined as

$$Error_{rel} = \frac{\dot{m}_{meas} - \dot{m}_{calc}}{m_{meas}} \qquad (3\text{-}13)$$

The errors between measured and calculated power are defined similarly. Objective function for fitting the power model:

$$OF_{Power} = \sqrt{\frac{\sum_{i=1}^{N}\left(\frac{Power_{meas} - Power_{calc}}{Power_{mean}}\right)^2}{N}} \qquad (3\text{-}14)$$

which includes the mean weighted error in parentheses. The relative error in power is defined as

$$Error_{rel} = \frac{Power_{meas} - Power_{calc}}{Power_{meas}} \tag{3-15}$$

Chapter 4

Analysis of Mass Flow Rate Model

In this first analysis, a number of alternative models are developed to predict the mass flow rate produced by a compressor. Measured data points for each compressor model are used as a basis for fitting free parameters in the models.

4.1 The Volumetric Efficiency

The equation representing the volumetric efficiency of the compressor, shown in equation (4-1), was derived in chapter 3.

$$h_v = 1 + C - C \cdot \left(\frac{p_{discharge}}{p_{suction}} \right)^{\frac{1}{n}} \qquad (4\text{-}1)$$

where η_v - volumetric efficiency

C - clearance volume ratio

$p_{discharge}$ - discharge pressure

$p_{suction}$ - suction pressure

n - polytropic exponent

Equation (4-1) differs from equation (3-6). The specific volume after taking in fresh refrigerant has been assumed to be equal to the specific volume of the refrigerant in the suction line neglecting the fact that the state of the re-expanded clearance vapor is slightly different. In the final model, a pressure drop at the suction side has been introduced as an additional parameter. This will take the effect neglected here into account. See below for more details.

At a compression ratio of 1, i.e. the refrigerant leaves the compressor at the same pressure as it enters, the volumetric efficiency must be equal to 1. This behavior is correctly presented in equation (4-1) since η_v goes to 1 for every value of the clearance volume ratio and the polytropic exponent. The volumetric efficiency decreases with increasing compression ratio.

4.2 Factors Affecting the 'Measured' Volumetric Efficiency

An estimate of the volumetric efficiency can be determined from measured mass flow rate using the following equation.

$$h_{v,measured} = \frac{\dot{m}_{measured}}{\frac{V \cdot RPM}{v_{suction}}} \qquad (4\text{-}2)$$

where $\eta_{v,measured}$ 'measured' volumetric efficiency

$\dot{m}_{measured}$ -measured refrigerant mass flow rate [kg/s]

V - displacement of the piston [m^3/rev.]

RPM - motor speed [rpm]

$v_{suction}$ - specific volume of the refrigerant at the suction side of the compressor [m^3/kg]

The value of this 'measured' volumetric efficiency depends on what the suction conditions of the compressor are assumed to be. One could approximate the compressor inlet conditions with the conditions at the inlet to the compressor shell. For calorimeter testing, this is generally a temperature of 32.2°C (90°F) at the suction pressure. However, equation (4-1) was developed to describe only the compression process in the actual

cylinder. Compressor suction conditions differ from the cylinder inlet due to a pressure drop across both the suction muffler and the suction valve. In addition, a portion of the refrigerant entering the compressor inlet passes through the compressor shell before entering the cylinder causing the temperature of the refrigerant to rise as a result of heat transfer from the motor.

Figure 4-1 shows the 'measured' volumetric efficiency as a function of compression ratio for three assumed inlet conditions:

1) No pressure drop and no temperature rise
2) Pressure drop of 5% and no temperature rise
3) Temperature rise of 10°C and no pressure drop

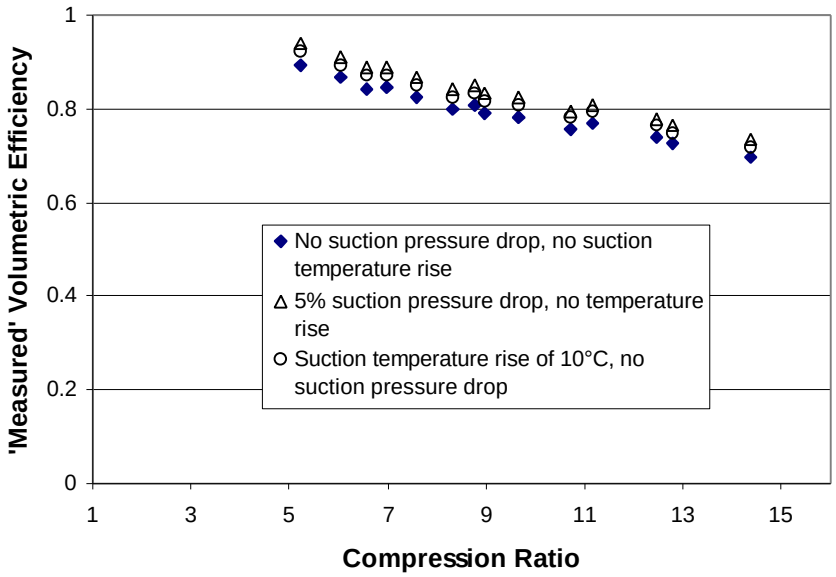

Figure 4-1: 'Measured' volumetric efficiency with and without suction pressure drop and temperature rise (data set A2)

The compression ratio takes the suction pressure drop into account. The assumed cylinder suction pressure is used to calculate the compression ratio instead of the evaporating pressure.

In general, the data scatters very little if it is plotted in this way. There are only three data sets in the 21 sets investigated where the data scatters significantly: These data sets are the ones that also show very big errors for the ARI curve fit method (B2 and B8). Therefore the accuracy of these measurements is questionable. The third data set that shows significant scatter in the 'measured' volumetric efficiency plot is B7 that has at least a few suspect data points as shown in chapter 2. There is one data set (B1) that shows two outliers and another one (B6) that shows one outlier in the 'measured' volumetric efficiency plot. These points have been shown to also have relatively large errors with the ARI curve fit. Interestingly enough, all data sets that appear to be inaccurate were measured by the same manufacturer. See appendix C for plots for all data sets.

Adding a pressure drop or temperature rise at the inlet increases the volumetric efficiency for all data points. It doesn't significantly increase or decrease the scatter in the data. A pressure drop and a temperature rise have very similar effects on the 'measured' volumetric efficiency. Both increase the value for the specific volume of the refrigerant at the inlet. Therefore, they are confounded and cannot be solved for separately.

4.3 Calculating the Volumetric Efficiency

Two parameters have to be determined to define the volumetric efficiency in equation (4-1): the clearance volume ratio C and the polytropic exponent n. In addition, pressure drops at the suction and discharge side of the compressor could be considered. The clearance volume ratio of the compressor is assumed to be a constant parameter for a

given compressor model. The polytropic exponent can be considered to be a constant or a variable.

4.3.1 Constant Polytropic Exponent and No Pressure Drops / Temperature Rise

In a first attempt to represent the mass flow rate, the suction and discharge pressures were assumed to be equal to the evaporation and condensing pressures. The suction temperature was assumed to be equal to 32°C (90°F). For this case, there are only two unknowns in equation 3-8: the clearance volume ratio C and the polytropic exponent n. Both were assumed to be constant. First, the clearance volume ratio was set to a reasonable value for the actual clearance volume ratio of a refrigerator or freezer compressor. A value of 0.015 was chosen. Using the method of least squares as described in chapter 3.4, the value for the polytropic exponent that best fit the data was determined for all sets of testing data.

Figure 4-2 shows the calculated as well as the ‘measured’ volumetric efficiency as a function of compression ratio for the assumed clearance volume ratio. The figure also shows the calculated volumetric efficiency for a series of other specified values of the clearance volume ratio C.

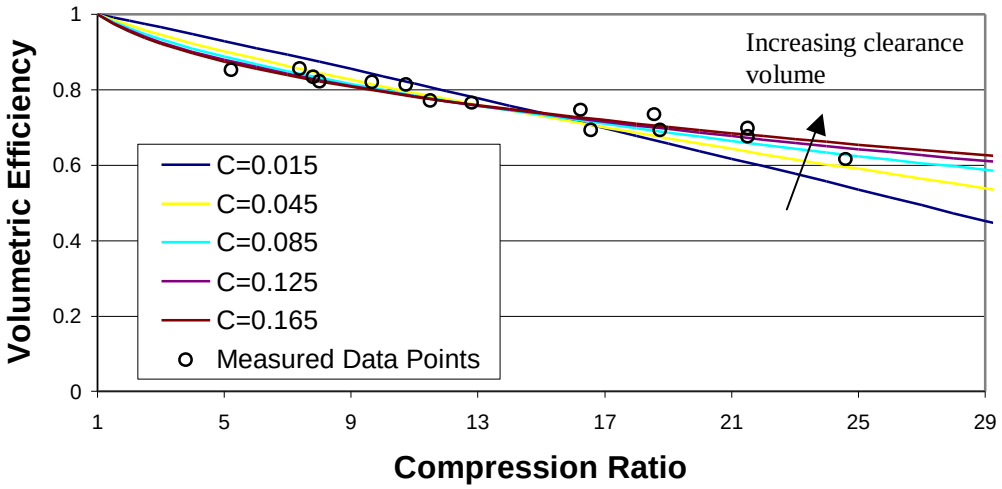

Figure 4-2: Volumetric efficiency for constant clearance volume ratio and constant polytropic exponent (data set B2)

The average errors as well as the corresponding values for the polytropic exponent n for this particular set of data are shown in table 4-1.

C	Average Relative Error [%]	n
0.015	7.52	0.9293
0.025	5.93	1.0971
0.045	4.19	1.3911
0.085	2.92	1.9059
0.125	2.76	2.3859
0.165	2.91	2.8515

Table 4-1: Average relative errors and values for the polytropic exponent for constant n and different values of the clearance volume ratio (data set B2)

The errors are very large for reasonable values of the clearance volume ratio C (<5%). The actual clearance volume ratio of domestic refrigerator/freezer compressors is about 0.015 according to compressor manufacturers. The errors are considerably smaller for higher values of C. For this particular data set, there is an optimum at a clearance volume ratio (one that minimizes mass flow rate errors) of around 0.12. At a certain level

of clearance volume ratio, raising it even further only leads to higher values for the polytropic exponent but does not change the shape of the curve significantly.

It is possible to solve for both the clearance volume ratio and the polytropic exponent at the same time using the least squares curve fit method. However, estimates of the two parameters that best fit the data typically do not make physical sense. The clearance volume ratio should not exceed 0.05. For an isentropic compression process, the polytropic exponent for both R134a and R12 is approximately 1.1. The least squares estimates for C and n, without considering pressure drops or an adjusted suction temperature, are much larger than expected for most of the data sets although the model fits the data reasonably well. There are 3 data sets where it was not possible to solve for C and n. Both parameters went to infinity. These data sets are B7 and B8 that have previously been suspected to contain measurement errors and data set B9b. Tables with the results for all data sets can be found in appendix C.

Another interesting finding showed that the values for C and n seem to be linked. The higher the value for clearance volume ratio is the higher is also the value for the polytropic exponent. See section 4.3.3 for more details on this behavior.

4.3.2 Polytropic Exponent as a Function of Compression Ratio

Models exist in the literature where the polytropic exponent is considered to be a function of compression ratio. Popovic and Shapiro [Popovic and Shapiro (1995)] suggested an equation of the form

$$n = a + \frac{b}{CR} + \frac{c}{CR^2} \tag{4-3}$$

$$\text{with } CR = \frac{p_{discharge}}{p_{suction}} \tag{4-4}$$

a,b,c - curve fit parameters

CR - compression ratio

This relationship was developed and validated for much larger compressors than the ones studied in this project.

To simplify calculations, only a first order equation was used for this considerations. It was shown that the same conclusions are true for a second order equation as shown in equation (4-3).

Introducing $n = a + \frac{b}{CR}$ into equation (4-1) leads to an expression for the volumetric efficiency that is highly nonlinear with compression ratio.

A least squares curve fit was performed for a fixed value of the clearance volume ratio to determine the values for the curve fit parameters a and b that best fit the data.

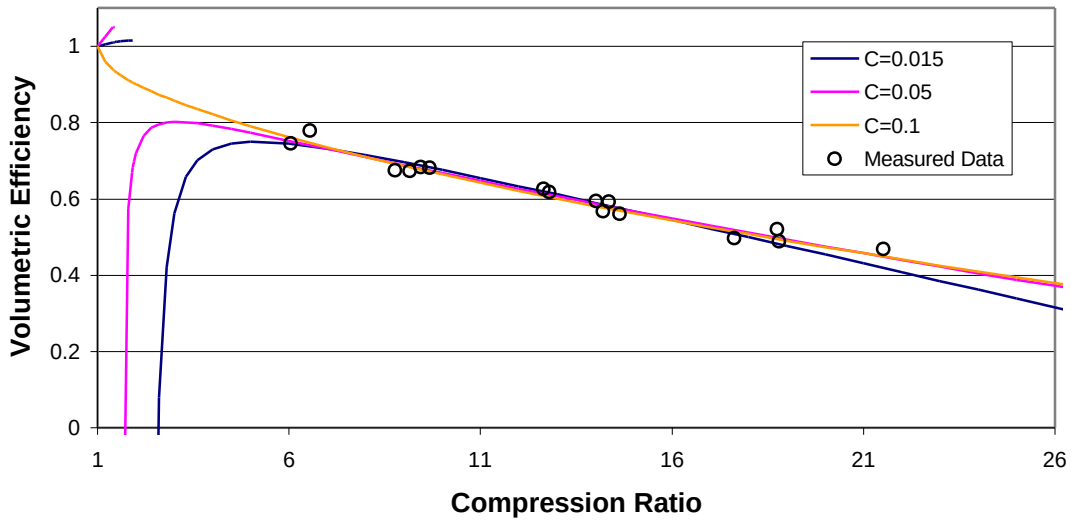

Figure 4-3: n = a + b/CR for different values of C (Data Set B3)

Figure 4-3 shows the curve fits for different values of the clearance volume ratio as well as the measured data.

The volumetric efficiency increases with decreasing compression ratio for compression ration s greater than 6. But at a certain point it starts to decrease rapidly and goes to negative infinity. At a compression ratio of –b/a the volumetric efficiency goes to a value of 1+C. From this value that is greater than 1 it decreases to reach a value of 1 at a compression ratio of 1. In some cases, there is a critical clearance volume above which the volumetric efficiency goes directly to one with decreasing compression ratio.

Fitting this model to the data shows that values for the curve fit parameters a and b and the clearance volume ration C exist that fit the experimental data very well. However, this type of equation would not be suitable for extrapolation. If only data at high compression ratios was used for the curve fit, the curve could start decreasing at even higher compression ratios and make predictions at lower compression ratios very inaccurate.

Other relationships for the polytropic exponent have been investigated but none of them fits the data as well as the models that are discussed in the following sections. Relationships that have been investigated include

$$n = a + b \cdot \frac{p_{discharge}}{p_{suction}} \tag{4-5}$$

$$n = a + b \cdot p_{discharge} \tag{4-6}$$

$$n = a + b \cdot p_{suction} \tag{4-7}$$

$$n = a + b \cdot p_{discharge} + c \cdot p_{suction} \tag{4-8}$$

4.3.3 Polytropic Exponent Equal to Isentropic Exponent

Choosing the polytropic exponent n to be a constant has several advantages. It forces the volumetric efficiency to consistently decrease with increasing compression ratio. This behavior makes physical sense and should be an advantage for extrapolation. It also makes the model mathematically much easier to solve.

The clearance volume ratio and the polytropic exponent were found to be highly correlated (see section 4.3.1). Figure 4-4 shows the optimal values for C and n found in section 4.3.1 for all data sets plotted against each other. It also shows the values found for n when C was held constant at different values for data set B9b.

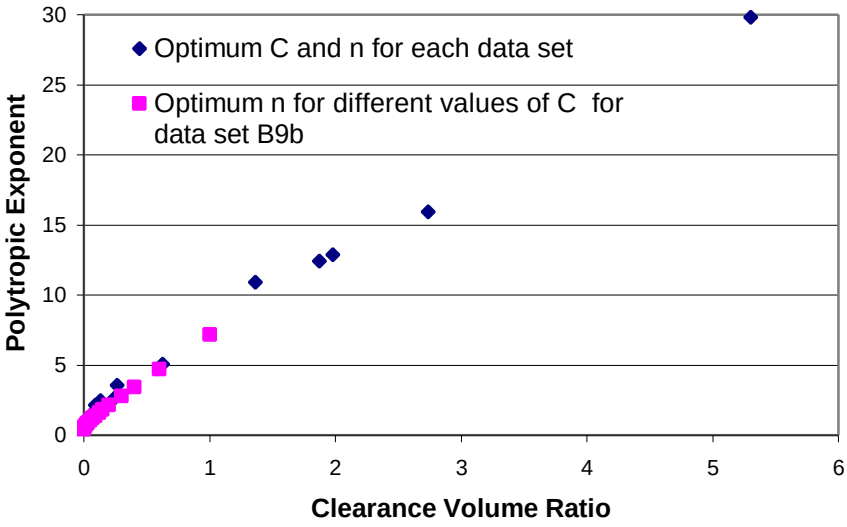

Figure 4-4: Polytropic exponent vs. clearance volume ratio for different data sets

Figure 4-4 shows that the polytropic exponent and the clearance volume ratio are strongly coupled. The higher the clearance volume ratio is the higher is also the polytropic exponent. Choosing a physically reasonable polytropic exponent results in much lower clearance volume ratios than the values found in section 4.3.1.

The polytropic exponent was set equal to the isentropic exponent k for the respective refrigerant. The compression process in the cylinder of the compressor itself can assumed to be close to adiabatic as most of the heat transfer takes place in the suction muffler and the discharge line. Therefore, assuming the polytropic exponent to be equal to the isentropic exponent seems reasonable. As shown in section 4.4, the value that is chosen for the polytropic exponent does not affect the calculated mass flow rate very much because the other model parameters compensate for the selected value of the polytropic index. For an ideal gas, the isentropic exponent can be calculated with:

$$k = \frac{c_p}{c_v} \tag{4-9}$$

where c_p - specific heat at constant pressure, f(T,p)

c_v - specific heat at constant volume, f(T,p)

The specific heat values at the cylinder suction conditions, i.e. including the suction pressure drop or temperature rise, were used.

For all following considerations, the polytropic exponent has been set equal to the isentropic exponent k at the suction conditions of the cylinder. If no pressure drops or a suction temperature rise are considered, this leaves only one unknown in equation 3-8: the clearance volume ratio. Solving for it directly by using the method of least squares leads to values that are between 2 and 6% for all data sets. However, the errors are very large. For some data sets the errors are as large as 25% in mass flow rate. An explanation of this might be that the suction conditions of the cylinder were assumed to be equal to those of the compressor shell. On the other hand, the compression was assumed to be adiabatic. The following section will deal with suction and discharge pressure drops that can be introduced into the model.

4.3.4 Pressure Drops

There is a pressure drop at the suction and at the discharge side of a hermetic reciprocating compressor. The pressure drop at the inlet that occurs before the refrigerant enters the cylinder causes the suction pressure of the cylinder to be lower than the evaporating pressure. At the discharge side of the cylinder, the refrigerant passes though a long narrow discharge line before it exits the compressor shell (see Figure 2-1). The compressors investigated here have fairly large pressure ratios, which means that the discharge pressure is much higher than the suction pressure. The effect of a pressure drop

is therefore much more significant at the suction side than at the discharge side. To simplify the model, the discharge pressure drop was therefore assumed to be zero. Any effects not taken into account by the model will be lumped together in the calculated model parameters.

Three different ways of calculating a suction pressure drop were considered: constant, percentage of the evaporating pressure and percentage of the evaporating pressure that is a function of the mass flow rate.

4.3.4.1 Constant or Percentage Suction Pressure Drop

A constant suction pressure drop can be calculated using the following equation:

$$\Delta p_{suction} = p_{evap} - p_{suction} \tag{4-10}$$

where p_{evap} is the evaporating temperature and $p_{suction}$ is the pressure at the inlet to the cylinder.

Instead of deducting a constant value from the evaporating pressure, one could also consider the pressure loss to be a certain constant percentage of the evaporating pressure:

$$p_{suction} = p_{evap}\left(1 - \Delta p_{suction}\right) \tag{4-11}$$

Equation (4-10) or (4-11) is added to the model and $p_{suction}$ is used to calculate the compression ratio and to calculate the specific volume at the inlet of the cylinder. There are now two parameters in the model that have to be solved for: the clearance volume ratio C and the pressure drop $\Delta p_{suction}$.

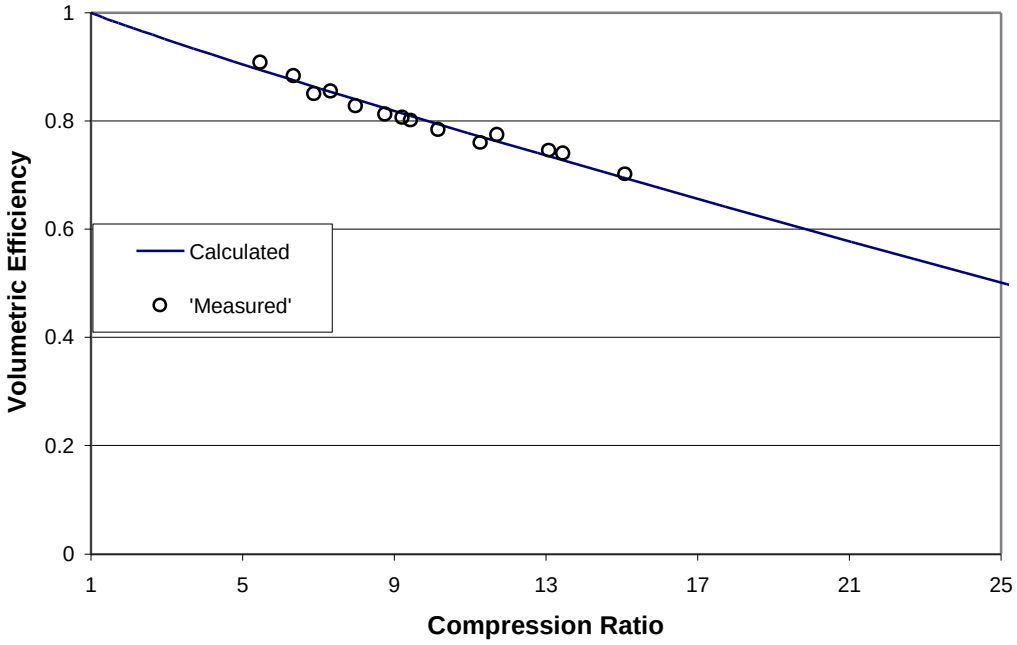

Figure 4-5: Volumetric efficiency for the percentage suction pressure drop model (data set A4)

It was found that the model fits the experimental data significantly better when a percentage is used for the pressure drop (equation 4-11) rather than a constant value (equation 4-10). Figure 4-5 shows a plot of the 'measured' volumetric efficiency for the case of a percentage suction pressure drop as well as the curve fit for data set A4.

The average relative error in mass flow rate for this data set is 1.3%. Figure 4-6 shows a compressor map for mass flow rate that has been calculated with the values for the clearance volume ratio and the pressure drop that have been determined (C = 0.02864, $\Delta p_{suction}$ = 4.746%). The experimental data points used to generate the fitted equation are also shown.

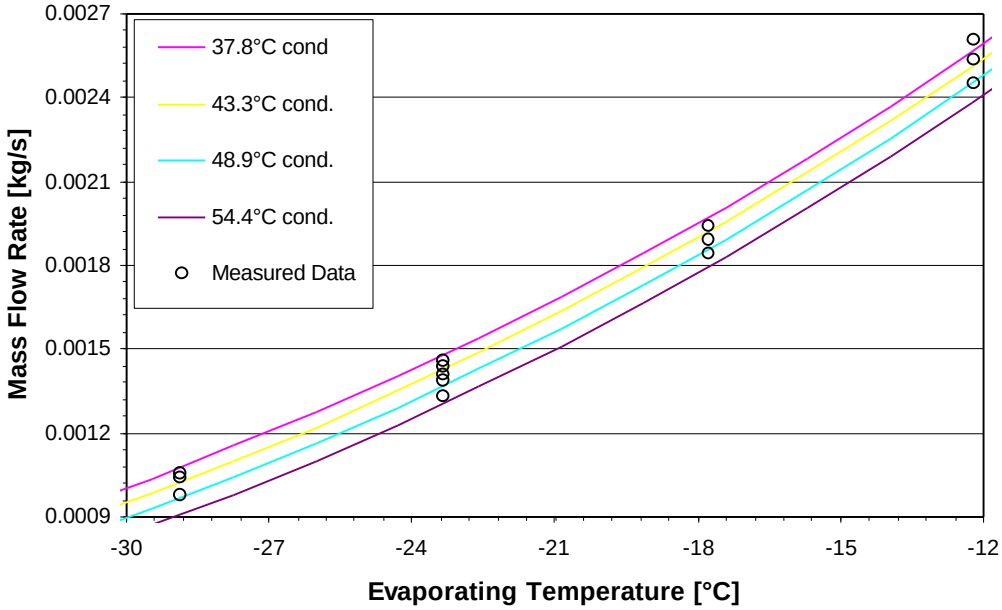

Figure 4-6: Mass flow rate map for the percentage pressure drop model (data set A4)

The differences between the model and the measured data for each data point are provided in table 4-2. As explained in chapter 3, there are two different error values, the mean weighted error and the relative error.

T_{evap} [°C]	T_{cond} [°C]	Mean Weighted Error	Relative Error
-12.2	37.8	-2.2%	-1.4%
-17.8	37.8	1.9%	1.6%
-23.3	37.8	1.3%	1.5%
-28.9	37.8	1.0%	1.6%
-23.3	40.6	0.9%	1.1%
-12.2	43.3	-1.4%	-1.0%
-17.8	43.3	1.7%	1.5%
-23.3	43.3	1.2%	1.4%
-28.9	43.3	-0.9%	-1.4%
-12.2	48.9	-0.1%	-0.1%
-17.8	48.9	1.0%	0.9%
-23.3	48.9	-1.4%	-1.6%
-28.9	48.9	-0.6%	-1.1%
-23.3	54.4	-1.4%	-1.7%
	Average	1.3%	1.3%

Table 4-2: Errors for the percentage pressure drop model for data set A4

For data set A4, all the errors are relatively small. The average relative error is 1.3% with a maximum error of only 1.7%. The errors in the left hand column in table 4-2 show that for some data points the mean weighted errors are slightly smaller and for some data points slightly bigger than the relative errors reported in the column on the right hand side. Overall however, the errors are very similar for both ways of reporting them. This is not the case for all sets of testing data. If for example the largest error in a data set occurs at a very small mass flow rate, dividing it by the measured mass flow rate at this data point rather than by the average mass flow rate leads to a very big error in percent even though it might not be that much bigger than the others in terms of kg/s. See appendix C for the results for all data sets.

The mass flow rate map of figure 4-6 and table 4-2 looks very reasonable. However, it seems to slightly underpredict mass flow rates for high evaporating temperatures. The values of the clearance volume ratio C that were found using this model were below 3.5% for all sets of testing data. The values for the suction pressure drop vary from 1.3% to around 20% depending on the data set. Values as high as 20% are, of course, physically not reasonable. For data set A4, the parameters that best fit the measured data are 2.9% for the clearance volume ratio and 4.7% for the suction pressure drop.

The mass flow rate map in figure 4-7 has been extrapolated over a wider range of evaporating and condensing temperatures than the conditions where measurements were taken. The extrapolated map for this model looks also very reasonable. See chapter 6 for more details on extrapolation capabilities of the different models.

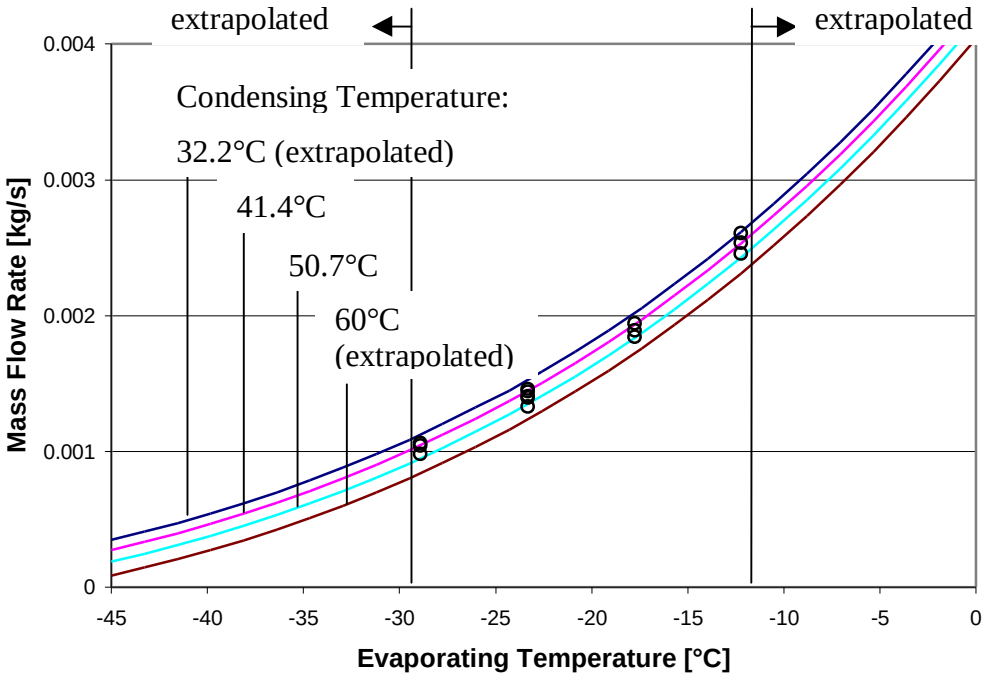

Figure 4-7: Extrapolated mass flow rate map for the percentage suction pressure drop model (data set A4)

4.3.4.2 Pressure Drop as a Function of Mass Flow Rate

Another way to model the suction pressure drop is to let it depend on the mass flow rate. For friction losses in a pipe the pressure drop is proportional to the fluid velocity to the second power as the Darcy equation (4-12) shows [Incropera, DeWitt (1996)]:

$$\Delta p_f = f \frac{L}{D_h} \cdot \frac{r \cdot v^2}{2} \qquad (4\text{-}12)$$

with Δp_f - friction losses in terms of total pressure

f - friction factor (dimensionless)

L - duct length

D_h - hydraulic diameter

ρ - fluid density

v - fluid velocity

In the case of a reciprocating compressor, the velocity of the refrigerant is not known because the pipe diameters are generally not published for the different compressor models. In addition, the geometry of the suction muffler and suction valve is much more complicated than that of a simple duct. It was therefore assumed that the refrigerant velocity is well enough represented by its mass flow rate and that all other phenomena occurring between the outlet of the evaporator and the suction of the compressor cylinder can be captured by a curve fit constant called k. Equations (4-13) through (4-15) show how the pressure drop has been modeled.

$$p_{suction} = p_{evap}\left(1 - \Delta p_{suction}\right) = p_{evap} - \Delta p_{suction} \cdot p_{evap} \tag{4-13}$$

$$p_{evap} - p_{suction} = \Delta p_{suction} \cdot p_{evap} = k \cdot \dot{m}^{2} \tag{4-14}$$

$$\Delta p_{suction} = \frac{k \cdot \dot{m}^{2}}{p_{evap}} \tag{4-15}$$

with k - curve fitting parameter

Δp - pressure drop in percent

By introducing equation (4-15) into the model as well as equation (4-11) another 2-parameter model is obtained. For this model the curve fitting parameters are the pressure drop constant k and the clearance volume ratio C.

Using a suction pressure drop that varies with mass flow rate for fitting the experimental data results in lower and therefore more reasonable numbers for the suction pressure drop than when using a constant percentage pressure drop. When using a suction pressure drop that varies with mass flow rate, the value for the clearance volume ratio is

slightly higher for all data sets but it is still below 5% for all sets of testing data. For some data sets the errors between measured and calculated mass flow rate are slightly higher than for the constant percentage pressure drop case, for some data sets they are slightly lower.

Table 4-3 shows the errors for each data point for data set A4 for this model. The average errors are slightly higher than for the constant pressure drop model. But all errors are still relatively small with the highest relative error at 2.8%.

T_{evap} [°C]	T_{cond} [°C]	Mean Weighted Error	Relative Error
-12.2	37.8	-1.8%	-1.1%
-17.8	37.8	2.8%	2.4%
-23.3	37.8	1.9%	2.2%
-28.9	37.8	1.2%	1.9%
-23.3	40.6	1.3%	1.6%
-12.2	43.3	-1.3%	-0.9%
-17.8	43.3	2.2%	1.9%
-23.3	43.3	1.4%	1.6%
-28.9	43.3	-1.2%	-2.0%
-12.2	48.9	-0.3%	-0.2%
-17.8	48.9	1.1%	1.0%
-23.3	48.9	-1.7%	-2.0%
-28.9	48.9	-1.4%	-2.4%
-23.3	54.4	-2.2%	-2.8%
	Average	1.7%	1.8%

Table 4-3: Errors for the percentage pressure drop model with pressure drop as a function of mass flow rate for data set A4

It seems that the two models (constant percentage pressure drop and varying with mass flow rate) are more or less equivalent in their ability to explain the experimental data. Both have two model parameters that have to be determined. But using a pressure drop that varies with mass flow rate makes the model mathematically far more complicated to solve.

4.3.5 Suction Temperature Rise

As mentioned earlier, before entering the cylinder the refrigerant passes through the suction muffler and a portion of it is circulated through the compressor shell and mixes with the oil. Instead or in addition to considering a suction pressure drop, one could also introduce a temperature rise between the inlet of the compressor shell and the suction valve of the cylinder. The following subsections investigate this possibility.

4.3.5.1 Constant Suction Temperature Rise

One way to model a temperature rise at the suction side of the compressor is by adding a constant value to the standard compressor inlet condition of 32°C / 90°F (equation 4-16). This would lead to a different value for the specific volume at the suction side of the compressor. However, the compression ratio does not change.

$$T_{suction} = 32°C + \Delta T_{suction} \tag{4-16}$$

This modification results in another model with two parameters: the clearance volume ratio C and the suction temperature rise $\Delta T_{suction}$. Fitting those two parameters to the measured data, leads to results that are almost identical to those if using the constant percentage pressure drop model.

4.3.5.2 Function of compression ratio/evaporating pressure

Several relationships that describe the suction temperature rise as a function of compression ratio or evaporating pressure have been investigated. Some of these relationships are shown in the following equations:

$$\Delta T = a + b \cdot CR \tag{4-17}$$

$$\Delta T = a + \frac{b}{CR} \tag{4-18}$$

$$\Delta T = a + b \cdot p_{evap} \tag{4-19}$$

$$\Delta T = a + b \cdot p_{evap} + c \cdot p_{evap}^{\,2} \tag{4-20}$$

In some cases the average relative error decreased but not significantly. The values for the suction temperature rise that were obtained varied only in a range of less than 1°C. Therefore, assuming a constant temperature rise is preferable. The model is mathematically less difficult to solve and the results are almost the same as with the more complicated models (equations 4-17 through 4-20).

Letting the suction temperature rise vary with another parameter introduces one or more additional parameter. This makes the minimization procedure much more complicated, as well as requiring more data.

4.4 Sensitivity Analysis

A sensitivity analysis has been performed to see which parameters in the model have the most influence on the calculated mass flow rate. The constant percentage suction pressure drop model as shown in the following equation has been analyzed.

$$\dot{m}_{calc} = \left(1 + C - C\left(\frac{p_{cond}}{p_{evap}(1-\Delta p)}\right)^{\frac{1}{n}}\right)\frac{V \cdot RPM}{v_{suction} \cdot 60} \qquad (4\text{-}21)$$

First, reasonable values have been used for all parameters that were then varied one by one by 1% leaving all other parameters constant. The following table shows the 'standard' values as well as how much the calculated mass flow rate varied in percent.

	Standard Value	Calculated Mass Flow Rate Variation [%]
C	0.03	0.19
Δp	0.05	0.065
n	1.1	0.43
p_{cond}	1100 kPa	0.21
p_{evap}	150 kPa	1.24
V	0.000006997 m^3	1
RPM	3500 rpm	1

Table 4-4: Sensitivity analysis: variation of the calculated mass flow rate with another parameter

The most important parameter seems to be the evaporating pressure. Errors in evaporating temperature measurements have the greatest influence on the calculated mass flow rate. The displacement volume and the motor speed also have a large influence on the mass flow rate, as they are directly proportional to the mass flow rate.

The next step is to determine whether or not choosing one parameter slightly higher or lower is being compensated by the model parameters. That means if for example the polytropic exponent n was chosen to be higher or lower than the isentropic exponent k, can the clearance volume ratio and/or the suction pressure drop adjust so that the errors are still approximately the same? The following table (4-5) contains the average relative errors for the case where n is equal to k at the suction conditions and for three constant values of n.

	Average Relative Error	C	$\Delta p_{suction}$
$n=k_{suction}$	1.28%	0.028	0.050
n=1	1.35%	0.021	0.062
n=1.1	1.28%	0.028	0.051
n=1.2	1.22%	0.036	0.041

Table 4-5: Average relative errors for different values of the polytropic exponent (data set A4)

The optimized values for C and $\Delta p_{suction}$ are also shown. For this particular data set, the values for $k_{suction}$ range from 1.102 to 1.104. Switching to a constant value of 1.1 does not change the average relative error very much. Even setting the value for n to the very low value of 1 or the very high value of 1.2 only changes the average relative error only by about 5%. Therefore it seems reasonable to choose a value for n that is easy to determine like the isentropic exponent that can be found tabulated for different refrigerants and temperatures.

4.5 Conclusion

In the previous sections of this chapter three models have been found to fit the test data about equally well. All of them use the volumetric efficiency equation derived in chapter 3 and a constant polytropic exponent. All three contain two model parameters:

1) Clearance volume ratio C and suction pressure drop $\Delta p_{suction}$
2) Clearance volume ratio C and suction pressure drop constant k
3) Clearance volume ratio C and constant suction temperature rise $\Delta T_{suction}$

The first and third model are very similar. The state change of the refrigerant between the inlet of the compressor shell and the inlet of the actual compression cylinder can be described in both a change in temperature and a change in pressure. In a real

compressor both effects take place but they are confounded in the model because physical processes affect the same parameter (the specific volume at the inlet). Therefore in the model, one parameter has to capture both effects.

Using a percentage pressure drop rather than a constant temperature rise as the second parameter seems to be preferable because its physically more realistic to assume that the suction pressure drop is a certain percentage of the evaporating pressure than to assume a temperature rise of a certain number of degrees for all operating conditions.

The second model that describes the suction pressure drop as a function of the mass flow rate, leads to values of the pressure drop that are physically realistic because they are lower than for the constant percentage pressure drop model. However, the model is mathematically more difficult to solve. The errors between measured and calculated mass flow rate are only for some data sets smaller than for the constant percentage pressure drop model. In general, the errors for all three model have the same order of magnitude.

Therefore it seems preferable to use the constant percentage pressure drop model (equation 3-8 and 4-11) knowing that both model parameters are actually curve fit coefficients rather than physical parameters. They do have some physical meaning but they also have to account for all physical phenomena that that take place in a refrigeration compressor but were not considered in the model.

Chapter 5

Analysis of Power Model

In chapter 4 a model for the refrigerant mass flow rate has been developed. This chapter deals with identifying a model to calculate the electrical power input necessary to pump this mass flow rate.

5.1 Combined Motor and Compressor Efficiency

An efficiency has been added to the expression for the compressor work (equation 3-11) to account for the fact that the measured power input is the compressor electrical input and not the power actually applied to the refrigerant. This combined efficiency accounts for electric motor inefficiencies as well as all other inefficiencies that occur inside the compressor such as frictional effects. The actual compression process has been assumed to be isentropic by using the isentropic exponent instead of the polytropic exponent. Therefore any heat loss from the compression cylinder has to be accounted for by the combined efficiency. Multiplying the compressor work by the mass flow rate leads to the following equation for calculating the electrical power input to the compressor.

$$Power \cdot h_{comb} = \dot{m} \cdot \frac{n}{n-1} \cdot p_{suction} \cdot v_{suction} \left[\left(\frac{p_{discharge}}{p_{suction}} \right)^{\frac{n-1}{n}} - 1 \right] \qquad (5\text{-}1)$$

with η_{comb} - combined motor and compressor efficiency

Power - compressor power input in W

The polytropic exponent n, the suction and discharge pressures and the specific volume at the suction side of the compressor are the same values as in the mass flow rate model discussed in chapter 4. Equation 5-1 requires estimates of the refrigerant mass flow rate itself to calculate compressor power input. Either the measured mass flow rate or the mass flow rate calculated with the model chosen in chapter 4 could be used in equation 5-1. There is only one additional parameter in equation 5-1 and that is the combined efficiency.

Because all other terms in equation (5-1) are known, the value for the combined efficiency that fits perfectly can be calculated for each data point. The combined efficiency has been plotted versus several parameters to determine what relationship can be used to describe its behavior. Results depend on whether the measured or the calculated mass flow rate is used and which model for the mass flow rate is chosen. Figure 5-1 shows the exact value of the combined efficiency for data set A4 plotted versus compression ratio, evaporating pressure and condensing pressure.

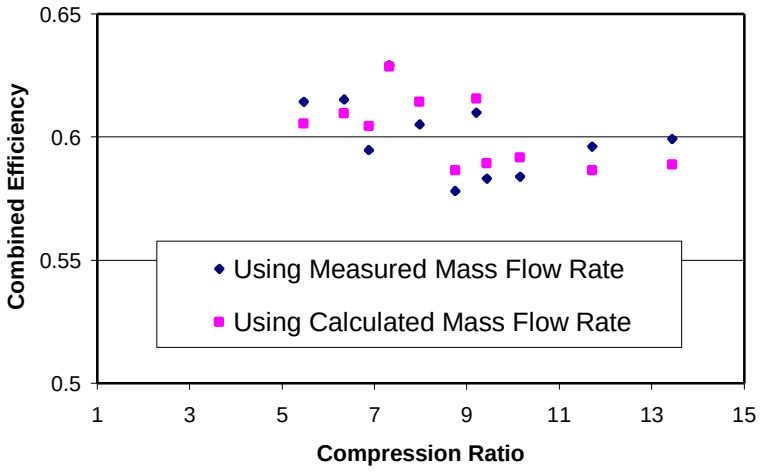

Figure 5-1a: Estimated combined efficiency versus compression ratio for data set A4

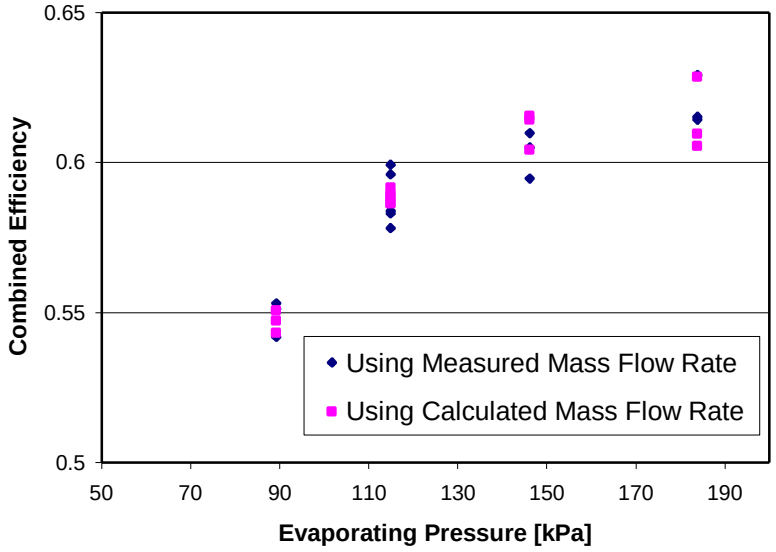

Figure 5-1b: Estimated combined efficiency versus evaporating pressure for data set A4

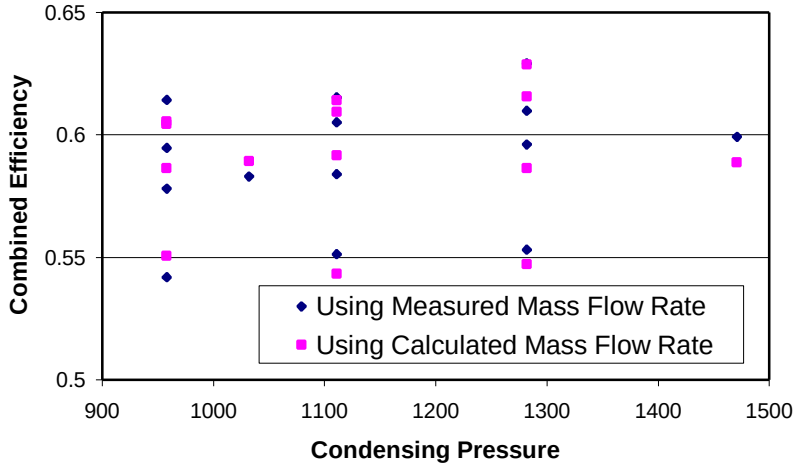

Figure 5-1c: Estimated combined efficiency versus condensing pressure for data set A4

The constant percentage pressure drop model (equation 4-11) was used for the "calculated" mass flow rates for the series of plots in figure 5-1. The figures show that for both the measured mass flow rate and the calculated mass flow rate, the combined efficiency exhibits a strong dependence on evaporating pressure. Because the combined efficiency depends on the evaporating pressure, it will also depend on the compression

ratio; however, the data scatters significantly more when plotted against compression ratio. There seems to be no dependency on the condensing pressure. These trends in the combined efficiency are consistent for all sets of testing data although the efficiency had more scatter for some data sets than for others (even when plotted against evaporating pressure).

The estimated combined efficiency has also been calculated assuming a percentage suction pressure drop as a function of mass flow rate in the mass flow rate model. The numbers do not differ significantly from those obtained with the constant percenntage pressure drop mass flow rate model (equation 4-11). The two models that are being discussed in the next section have also been applied to the case where the percentage suction pressure drop as a function of mass flow rate had been used (equation 4-15). The relative errors obtained are not significantly different from the constant pressure drop mass flow rate model for all sets of calorimeter data. The average relative errors obtained with the two different pressure drop models differ by less than 1% for all data sets. Therefore only the constant percentage suction pressure drop case is presented in the following sections.

Figure 5-1b shows that the ‘measured’ combined efficiency seems to scatter less when the calculated mass flow rate is used to calculate the specific work rather than the measured mass flow rate. The calculated mass flow rate tends to smooth out experimental uncertainty and therefore might be more suitable for use than the measured data. This smoothing trend was observed for most sets of testing data; however, the results depend very much on the quality of the measured mass flow rate data and the resulting mass flow rate curve fit.

The only data set for which the power models fit significantly better when using the measured mass flow rate than when using the calculated mass flow rate is data set B2. This data set has previously been suspected to contain questionable data points because the 'measured' volumetric efficiency plot shows significant scatter and even the ARI curve fit produces errors as large as 15% average relative error for mass flow rate as seen in appendix B. For all other sets of data, using the calculated mass flow rate to fit the power model leads to smaller average errors than using the measured mass flow rate (or the errors are only insignificantly larger). Figure 5-2 shows the 'measured' volumetric efficiency as well as the constant percentage pressure drop model for data set B2

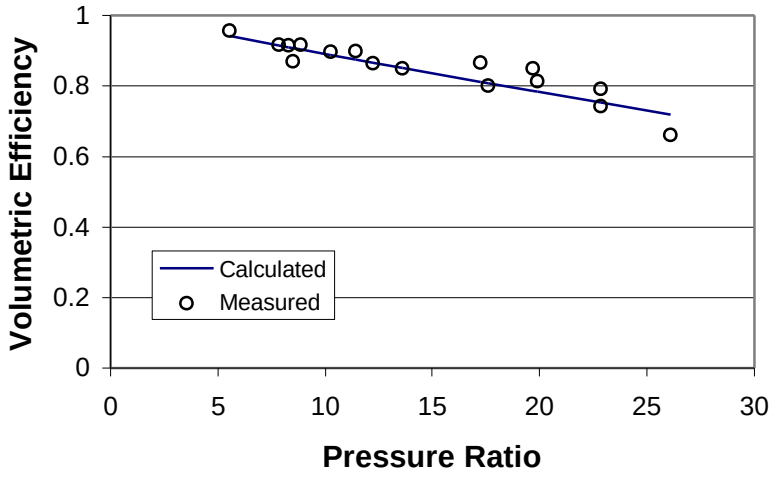

Figure 5-2: 'Measured' and calculated volumetric efficiency for data set B2

In some cases, the average relative error is smaller when using the calculated mass flow rate but the relative errors for some data points are larger. This is the case if there are more than just one or two bad data points in the mass flow rate and these points dominate the curve fit. This way, the errors for good data points become larger. In this case it does not make sense to use the calculated mass flow rate instead of the measured mass flow rate to fit the power model.

In conclusion, the calculated mass flow rate (rather than the measured mass flow rate) should be used to fit the power model because it has the potential to smooth out one or two suspect data points. If there are too many suspect data points, the curve fit cannot make physical sense and the data should not be used.

5.2 Models

Several equations have been examined to identify a relationship between the combined efficiency and evaporating pressure that best represents the experimental data. The goal was to find an equation that fits the data with a minimum of curve fit parameters.

One can conclude from the plots of the combined efficiency that perfectly fits the measured data (figure 5-1b) that the relationship between efficiency and evaporator pressure looks like an exponential. Equation 5-2 shows one relationship that has been investigated:

$$h_{comb} = d + e \cdot \exp\left(f \cdot p_{evap}\right) \qquad (5\text{-}2)$$

with d, e, and f - curve fit parameters

There are 3 parameters in this equation that have to be determined with a non-linear least squares curve fit. Another relationship that results in a curve of similar shape is an inverse proportional equation as shown in equation 5-3.

$$h_{comb} = a + \frac{b}{p_{evap}} \qquad (5\text{-}3)$$

with a and b - curve fit coefficients

This equation has only 2 curve fit parameters and the model is mathematically much easier to solve than equation (5-2) since it is linear with respect to the parameter. Least squares curve fits were performed using both equations for all sets of testing data to determine which model fits the experimental data better.

The exponential relationship (5-2) fits the experimental data slightly better for all data sets; however, the difference is not significant. The average relative errors in mass flow rate are approximately 2 to 3% lower for the exponential model than for the inverse proportional model. Average relative errors in input power are below 3% or less for all but two data sets. Those two data sets are set C1 and C2. The average relative errors in mass flow rate were already larger than for most data sets (3.7% and 3.1% respectively). The ARI curve fit for power also has relatively large errors for these specific data sets as seen in appendix B.

Figure 5-3 shows the power map obtained with the inverse proportional relationship using the combined efficiency (equation 5-3) for data set A4. The figure also shows the experimental data points. The map has been extrapolated beyond the range of operating conditions that were represented in the experimental data.

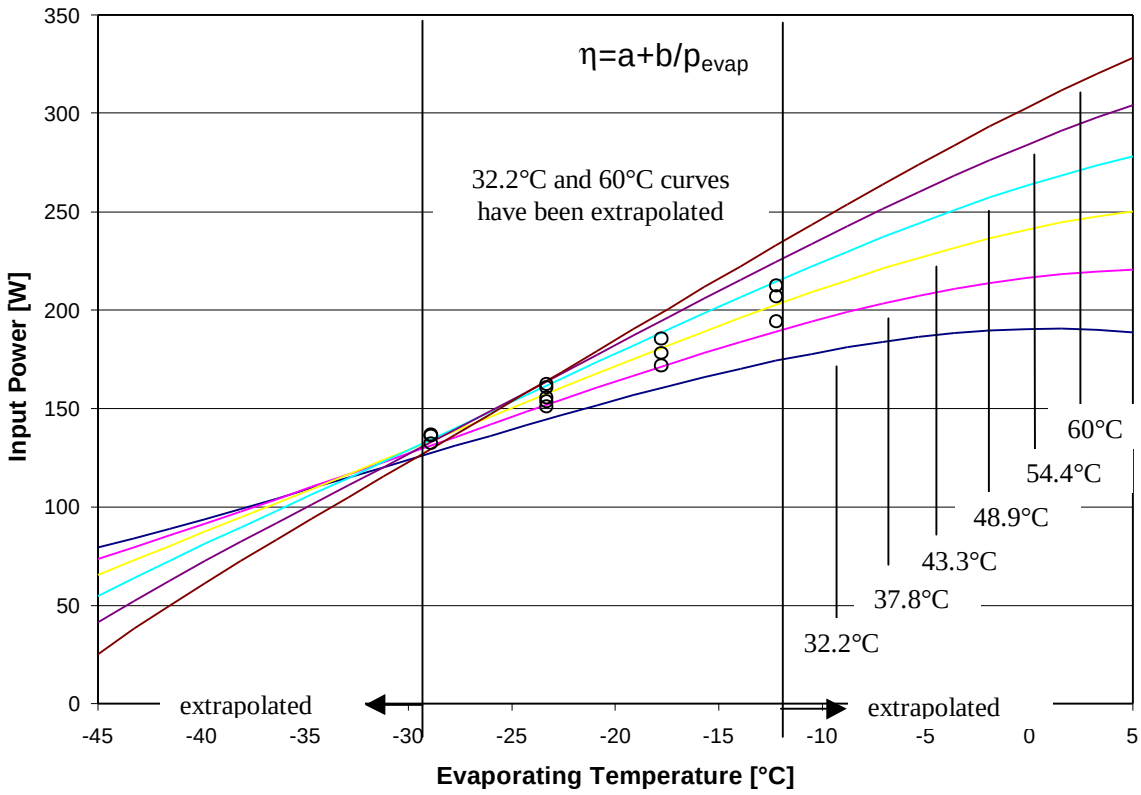

Figure 5-3: Extrapolated power map using the inverse proportional relationship for the combined efficiency for data set A4

The following table shows the errors in power for the model shown in figure 5-3.

T [°C]	T_{cond} [°C]	Mean Weighted Error	Relative Error
-12.2	37.8	-3.0%	-2.6%
-17.8	37.8	-0.2%	-0.2%
-23.3	37.8	0.4%	0.5%
-28.9	37.8	-0.6%	-0.8%
-23.3	40.6	0.8%	0.9%
-12.2	43.3	-2.4%	-1.9%
-17.8	43.3	1.6%	1.5%
-23.3	43.3	1.3%	1.4%
-28.9	43.3	-1.7%	-2.1%
-12.2	48.9	1.4%	1.1%
-17.8	48.9	1.9%	1.7%
-23.3	48.9	0.4%	0.4%
-28.9	48.9	-1.1%	-1.4%
-23.3	54.4	0.8%	0.9%
	averages	1.5%	1.4%

Table 5-1: Errors for the inverse proportional power model for data set A4

The power per unit mass flow rate (specific work) has been plotted against the evaporation temperature in figure 5-4 to get an idea whether the model makes physical sense in the range of operating temperatures where experimental data were provided and beyond.

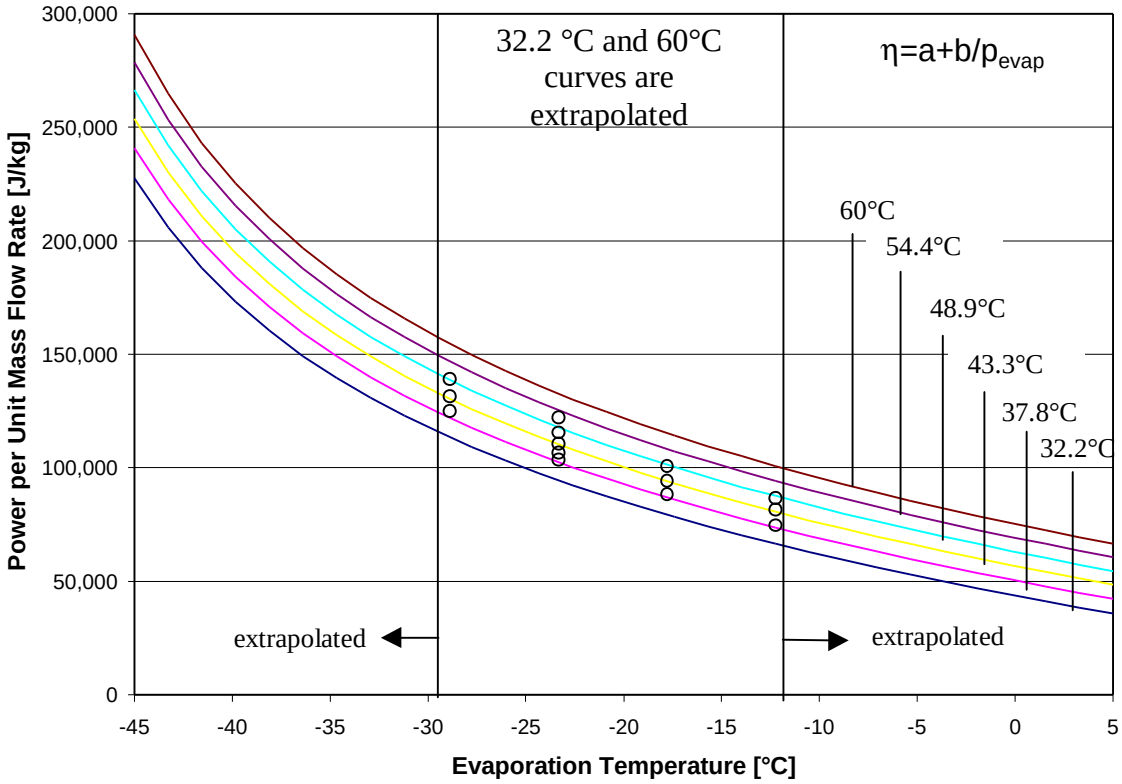

Figure 5-4: Extrapolated power per unit mass flow rate map using the inverse proportional relationship for the combined efficiency for data set A4

Figure 5-5 shows the power map that was obtained when the exponential relationship for the combined efficiency was used to fit the model parameters to data set A4.

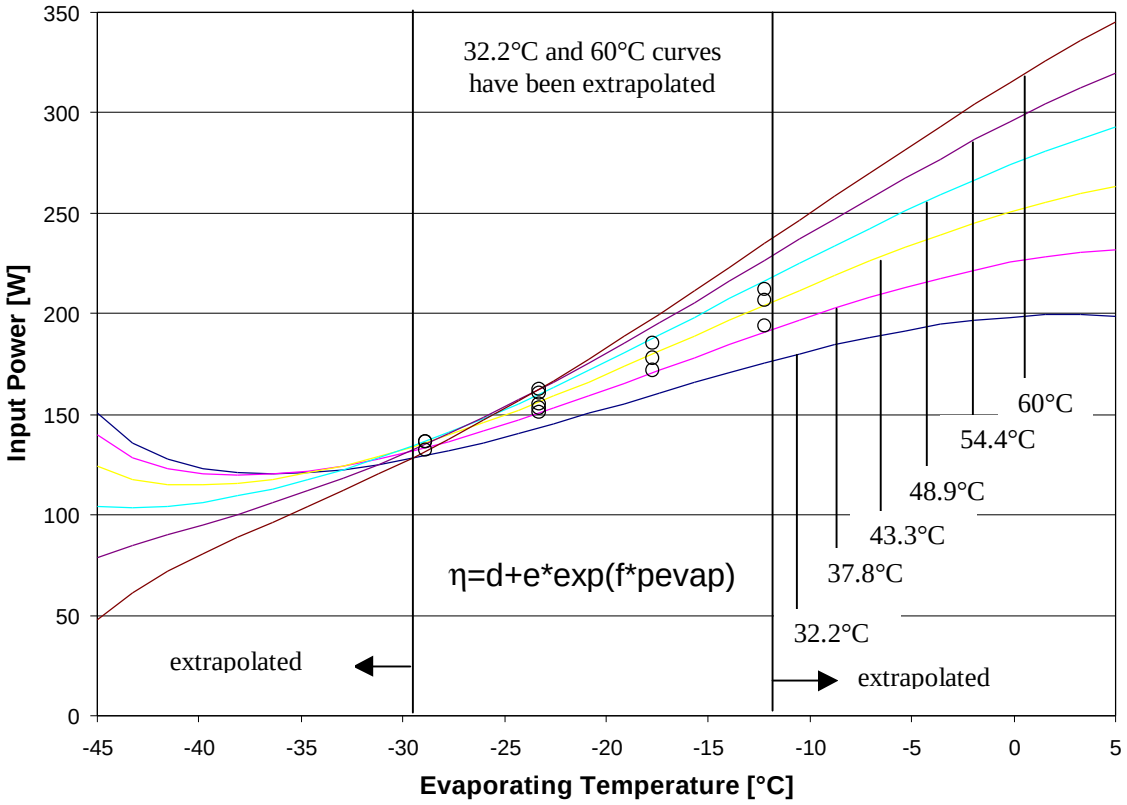

Figure 5-5: Extrapolated power map using the exponential relationship for the combined efficiency for data set A4

The shape of the curves is quite different for the exponential model at low evaporating temperatures. This model seems to fit the data a little bit better for the lowest evaporating temperature that was measured. The relative errors for the three data points at –28.9°C evaporating temperature are 0.8%, -0.6% and 0.1 % respectively for the exponential model as compared to –0.8%, -2.1% and –1.4% for the inverse proportional model. However, the extrapolated power values at low evaporator temperatures appear to be incorrect. The trend that the extrapolated power starts to increase again with decreasing evaporating temperature was found only for 4 out of the 21 data sets. Table 5-2 contains the errors between measured and calculated power for the exponential model for data set A4.

Tevap [°C]	Tcond [°C]	Mean Weighted Error	Relative Error
-12.2	37.8	-2.0%	-1.7%
-17.8	37.8	-0.8%	-0.8%
-23.3	37.8	-0.5%	-0.5%
-28.9	37.8	0.6%	0.8%
-23.3	40.6	-0.1%	-0.1%
-12.2	43.3	-1.4%	-1.1%
-17.8	43.3	0.9%	0.8%
-23.3	43.3	0.4%	0.4%
-28.9	43.3	-0.5%	-0.6%
-12.2	48.9	2.5%	2.0%
-17.8	48.9	1.2%	1.1%
-23.3	48.9	-0.5%	-0.5%
-28.9	48.9	0.1%	0.1%
-23.3	54.4	-0.1%	-0.1%
	averages	1.1%	0.9%

Table 5-2: Errors for the exponential power model for data set A4

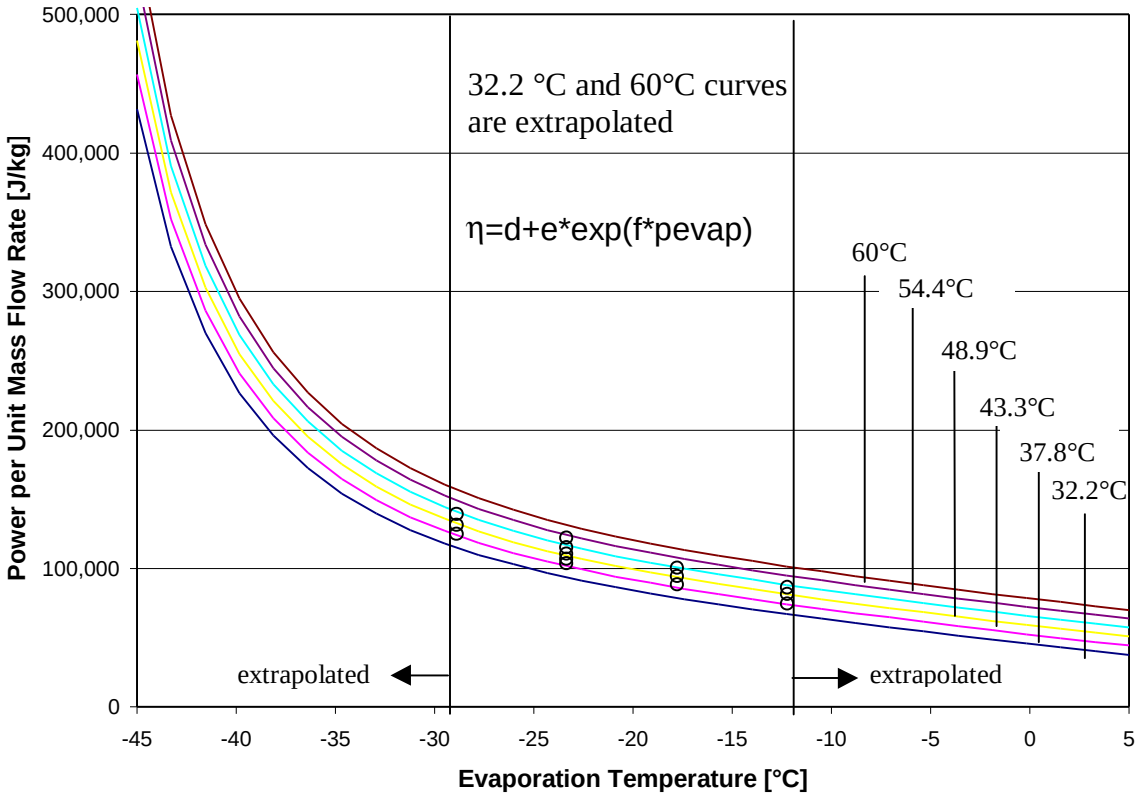

Figure 5-6: Extrapolated power per unit mass flow rate map using the exponential model for the combined efficiency (data set A4)

Figure 5-6 shows the power per unit mass flow rate plotted against the evaporating temperature for the exponential model.

Because the absolute power extrapolated to low evaporation temperature is higher for the exponential model than for the inverse proportional model, the power per unit mass flow rate calculated with the exponential model is much higher than that calculated with the inverse proportional model. Both models explain the experimental data well. Plots of power maps for all 21 sets of calorimeter data are attached in appendix D.

5.3 Conclusion

Two models have been found that explain the compressor power data well. Average relative errors are below 3% for most data sets, and even below 1.5% for about half of the data sets. Both represent the input power to a compressor as the power necessary for a polytropic process including a combined efficiency to account for motor and other inefficiencies. One model uses an exponential and the other an inverse proportional relationship between the combined efficiency and the evaporating pressure. The exponential model contains 3 curve fit coefficients, the inverse proportional one only 2.

Data at higher or lower evaporation and condensing temperatures would be needed to determine which model extrapolates better. See chapter 6 for more on the extrapolation capabilities of the different models.

Chapter 6

Model Performance

6.1 Extrapolation Capabilities

In the previous chapters the parameters of the different models have been fitted using all data points available for the particular data set. However, there are only two parameters in the mass flow rate model and two or three in the power model depending on which expression for the combined efficiency is chosen. This means that, in theory, two or three measurements of mass flow rate and power would be sufficient to fit the parameters.

This section deals with the question how many measured data points are needed to generate accurate compressor maps. If only a few data points are used to fit the model parameters, the measured values at other operating conditions can be used to assess the ability of the model to interpolate and extrapolate.

In this analysis, the constant percentage pressure drop model (equations 3-8 and 4-11) has been used for the mass flow rate while the exponential (equations 5-1 and 5-2) and the inverse proportional model (equations 5-1 and 5-3) have been examined for the power model to determine which model extrapolates better.

This analysis has been performed on two data sets from two different manufacturers. Neither of the two data sets has previously been suspected to contain incorrect data points.

6.1.1 Extrapolation to Lower Condensing Temperatures

The five operating conditions of data set A4 that have the highest condensing temperatures have been used to determine the model parameters of the mass flow rate model and both power models. With only 5 measured data points being used, the errors between measured and calculated values are even smaller than when all 14 data points are used in the fit. The model parameters determined by non-linear regression have then been used to calculate the mass flow rate and power for the 9 other measured operating conditions. Table 6-1 shows the relative errors for all data points.

	Operating Conditions		Relative Errors		
	Condensing Temperature [°C]	Evaporating Temperature [°C]	Mass Flow Rate	Power (inverse proportional)	Power (exponential)
Used for model parameter fitting	48.9	-23.3	-0.9%	0.0%	-0.4%
	48.9	-28.9	0.7%	-0.7%	0.0%
	54.4	-23.3	-0.5%	0.8%	0.4%
	48.9	-12.2	-0.3%	-0.5%	0.0%
	48.9	-17.8	1.1%	0.5%	0.1%
	Average:		**0.7%**	**0.6%**	**0.3%**
Not used for model parameter fitting	37.8	-23.3	1.5%	-0.7%	-1.1%
	37.8	-28.9	2.4%	-1.1%	-0.4%
	40.6	-23.3	1.3%	-0.1%	-0.5%
	43.3	-23.3	1.8%	0.5%	0.1%
	43.3	-28.9	-0.3%	-2.0%	-1.2%
	37.8	-12.2	-2.1%	-4.4%	-4.0%
	37.8	-17.8	1.3%	-1.7%	-2.2%
	43.3	-12.2	-1.4%	-3.7%	-3.2%
	43.3	-17.8	1.4%	0.0%	-0.4%
	Average:		**1.6%**	**2.2%**	**2.0%**

Table 6-1: Relative errors for extrapolation to lower condensing temperatures (data set A4)

The highest relative error encountered is 4.4% of power for the inverse proportional model for a data point with a very low condensing temperature. The relative errors obtained with the inverse proportional and the exponential model are very similar. Figures 6-1 through 6-3 show compressor maps for mass flow rate and for both power models. The figures show the points that have been used to fit the model parameters as circles and the points that have been used to test the extrapolation capabilities of the models as triangles. The lines show the model that has been calculated using those model parameters for condensing temperatures that were represented in the experimental data.

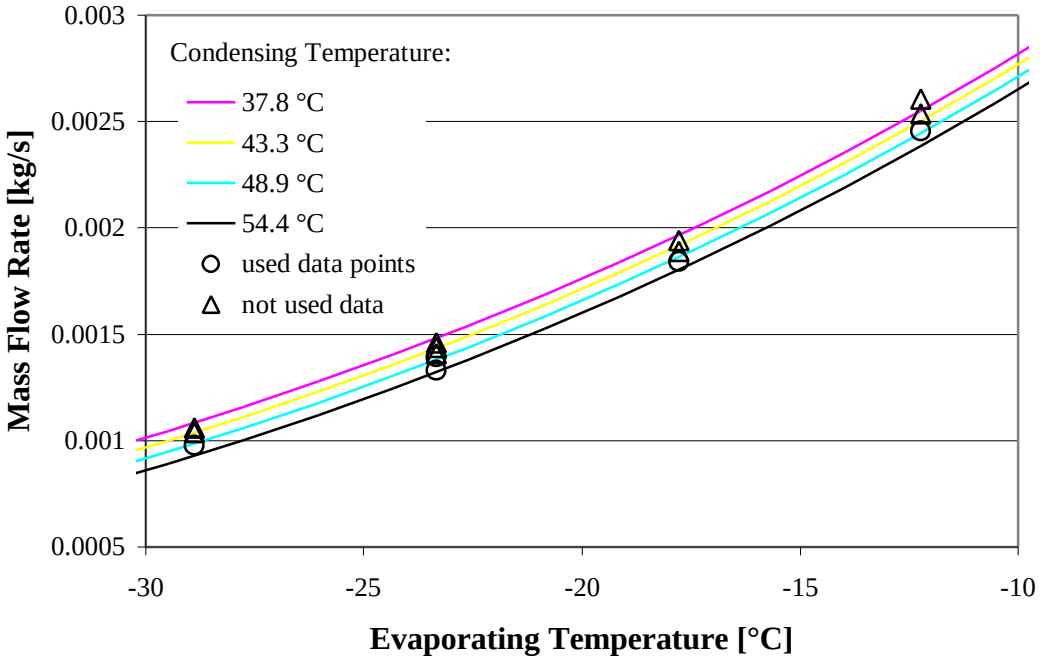

Figure 6-1: Mass flow rate map extrapolating to lower condensing temperatures (data set A4)

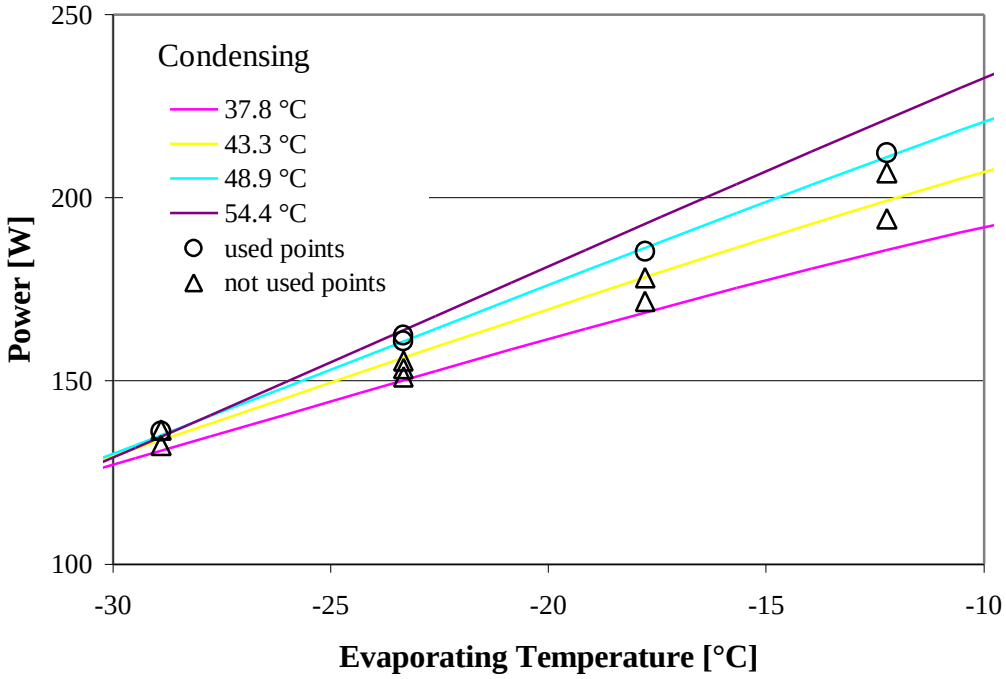

Figure 6-2: Power map extrapolating to lower condensing temperatures (data set A4) using the inverse proportional model

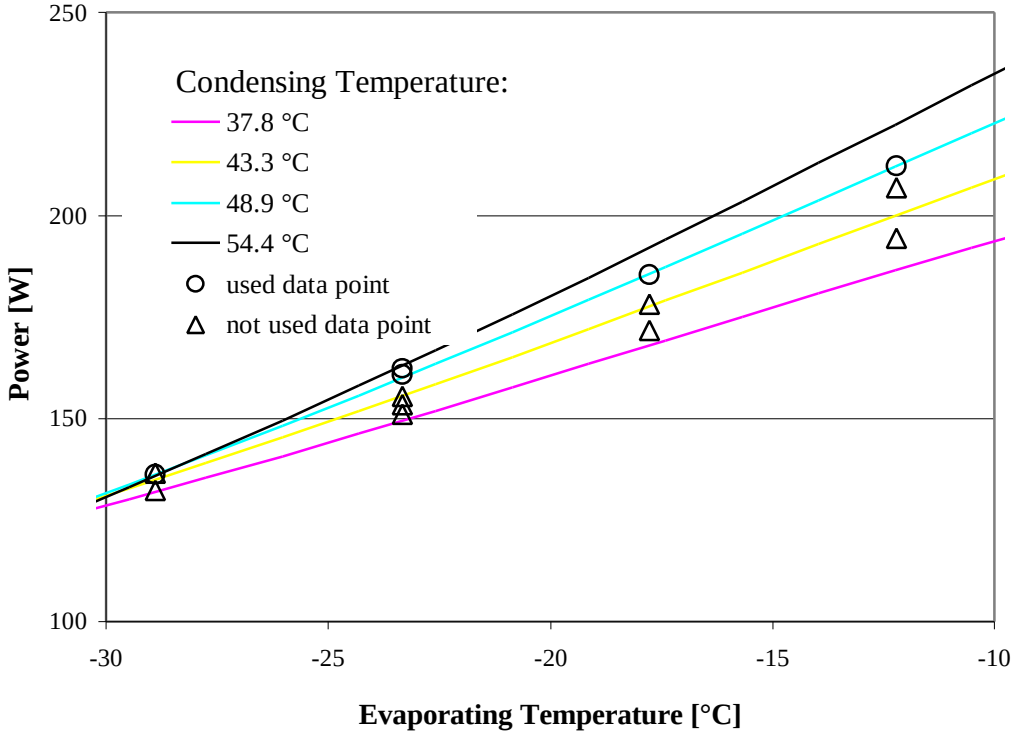

Figure 6-3: Power map extrapolating to lower condensing temperatures (data set A4) using the exponential model

Errors are consistently higher for high evaporating temperatures than for low evaporating temperatures but all errors are below 5%. Extrapolating to condensing temperatures as much as 11.1°C lower than the lowest measured data point leads to very reasonable results.

A similar analysis was conducted using data set B9a. Model parameters were estimated using 4 data points at high condensing. The remaining 5 data points were used to evaluate the model extrapolation capabilities. Table 6-2 shows the relative errors for this data set.

	Operating Conditions		Relative Errors		
	Condensing Temperature [°C]	Evaporating Temperature [°C]	Mass Flow Rate	Power (inverse proportional)	Power (exponential)
Used for model parameter fitting	54.4	-17.8	0.5%	0.0%	0.0%
	54.4	-28.9	-0.6%	-0.5%	-0.5%
	48.9	-17.8	-0.4%	0.0%	0.0%
	48.9	-28.9	0.5%	0.5%	0.5%
	Average:		**0.5%**	**0.4%**	**0.4%**
Not used for model parameter fitting	43.3	-17.8	0.5%	-1.0%	-1.0%
	54.4	-23.3	-2.4%	-2.0%	-1.8%
	48.9	-23.3	-2.1%	-0.9%	-0.7%
	43.3	-23.3	-1.5%	-1.0%	-0.7%
	43.3	-28.9	2.0%	2.9%	2.9%
	Average:		**1.8%**	**1.7%**	**1.7%**

Table 6-2: Relative errors for extrapolation to lower condensing temperatures (data set B9a)

The highest relative error for this data set is 2.9% for power for one of the low condensing temperature points. The map has been extrapolated to a condensing temperature 5.6°C lower than the lowest measured data point.

6.1.2 Extrapolation to Lower Evaporating Temperatures

The 6 data points with the highest evaporating temperature have been chosen to determine the model parameters of the mass flow rate and the power model. Table 6-3 shows the relative errors for data set A4 obtained for the points that have been used to determine the model parameters as well as for those points that have not been used.

	Operating Conditions		Relative Errors		
	Condensing Temperature [°C]	Evaporating Temperature [°C]	Mass Flow Rate	Power (inverse proportional)	Power (exponential)
Used for model parameter fitting	37.8	-12.2	-0.3%	-1.1%	-1.1%
	37.8	-17.8	1.8%	-0.4%	-0.4%
	43.3	-12.2	-0.5%	-0.9%	-0.9%
	43.3	-17.8	0.8%	0.5%	0.5%
	48.9	-12.2	-0.3%	1.6%	1.6%
	48.9	-17.8	-0.8%	-0.1%	-0.1%
	Average:		**0.9%**	**0.9%**	**0.9%**
Not used for model parameter fitting	37.8	-23.3	0.1%	-2.4%	-0.5%
	37.8	-28.9	-1.9%	-7.5%	0.4%
	40.6	-23.3	-0.8%	-2.4%	-0.5%
	43.3	-23.3	-1.1%	-2.6%	-0.6%
	43.3	-28.9	-6.5%	-10.2%	-2.6%
	48.9	-23.3	-5.4%	-4.7%	-2.8%
	48.9	-28.9	-8.2%	-11.4%	-3.9%
	54.4	-23.3	-7.1%	-5.9%	-4.0%
	Average:		**4.9%**	**6.8%**	**2.4%**

Table 6-3: Relative errors for extrapolation to lower evaporating temperatures (data set A4)

Relative errors are larger than when extrapolating to lower condensing temperatures but they are still around 10% and lower, the highest error being at 11.4% for the inverse proportional power model at one of the data points with the lowest evaporating temperature. The exponential power model seems to extrapolate better than

the inverse proportional model. The average relative error for the data points not used for the parameter fit is 6.8% with the inverse proportional model compared to 2.4% with the exponential model. The map has been extrapolated to evaporating temperatures as much as 10.1°C lower than the lowest measured data point.

Figures 6-4 through 6-6 show the compressor maps for mass flow rate and both power models indicating the points that have been used to fit the model parameters and the ones that have not been used.

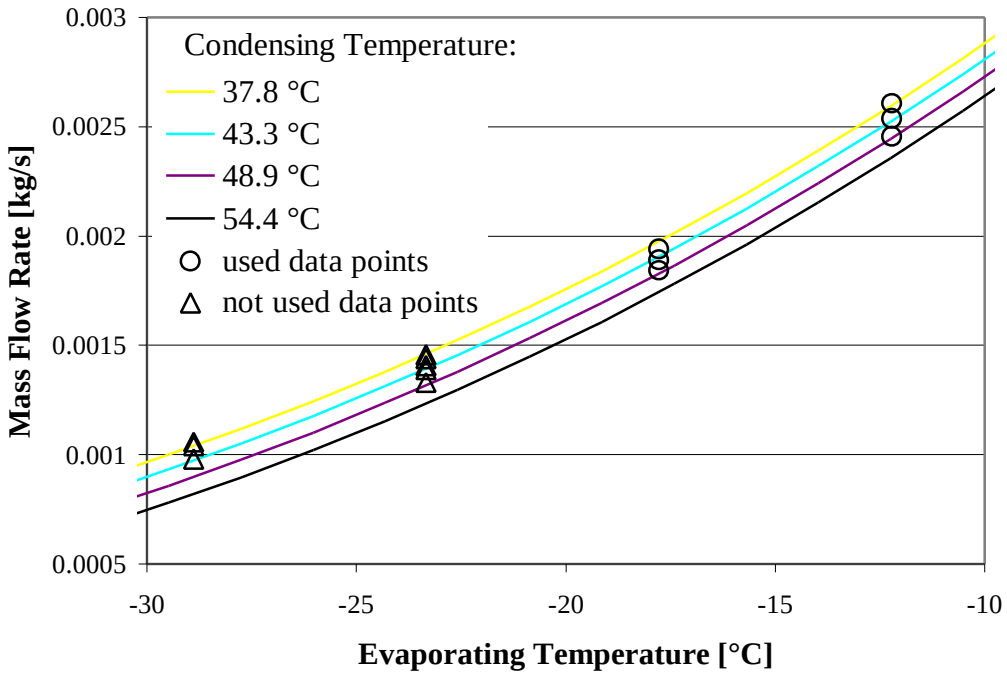

Figure 6-4: Mass flow rate map extrapolating to lower evaporating temperatures (data set A4)

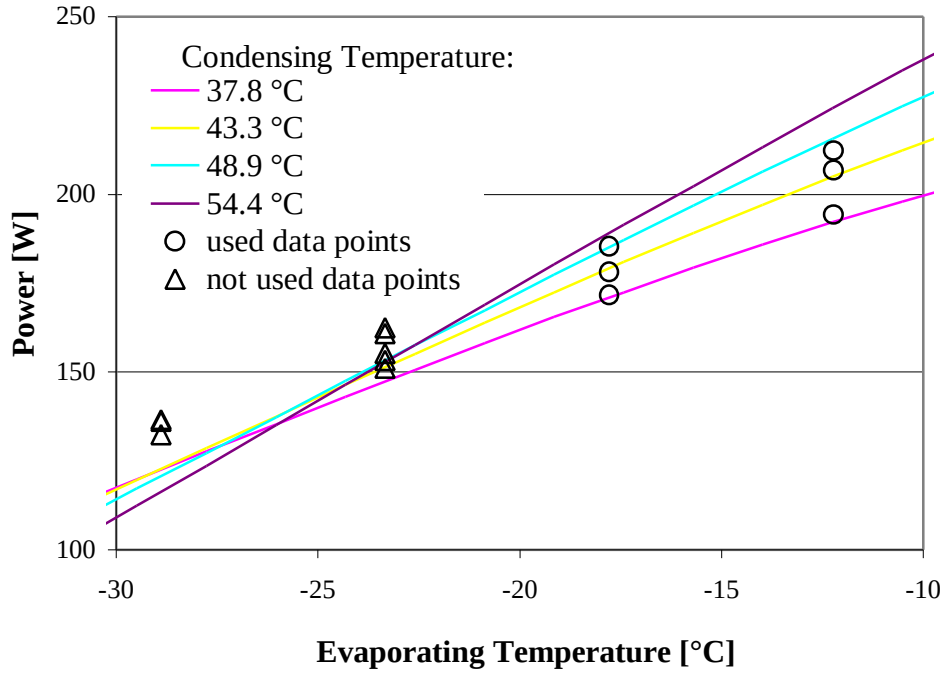

Figure 6-5: Power map extrapolating to lower evaporating temperatures (data set A4) using the inverse proportional model

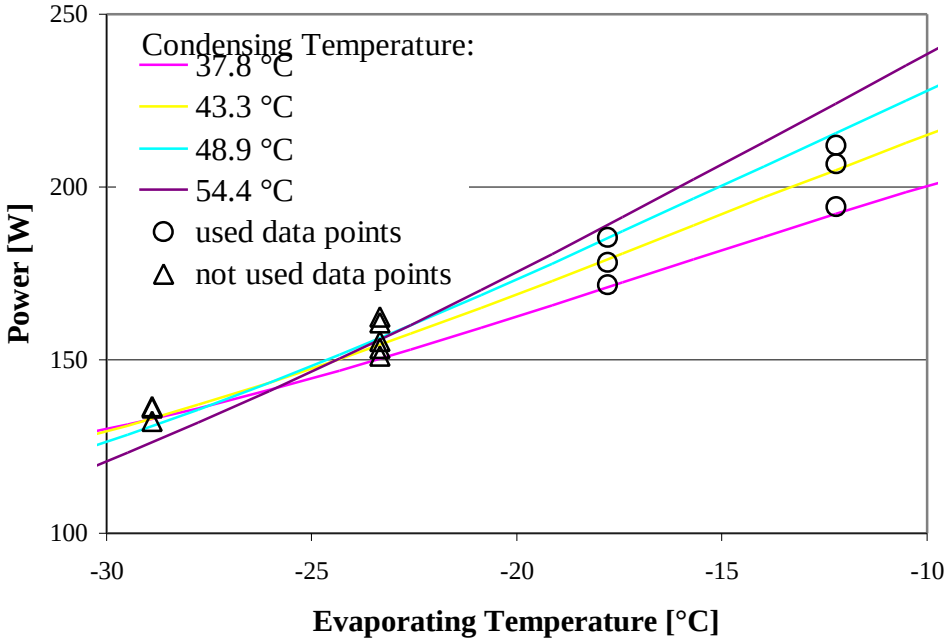

Figure 6-6: Power map extrapolating to lower evaporating temperatures (data set A4) using the exponential model

The maps show that the exponential power model explains the data at low evaporating temperatures significantly better than the inverse proportional model. Table 6-4 shows the relative errors for the corresponding analysis of data set B9a.

	Operating Conditions		Relative Errors		
	Condensing Temperature [°C]	Evaporating Temperature [°C]	Mass Flow Rate	Power (inverse proportional)	Power (exponential)
Used for model parameter fitting	54.4	-17.8	1.3%	0.9%	0.9%
	48.9	-17.8	-0.3%	0.3%	0.3%
	43.3	-17.8	0.1%	-1.2%	-1.2%
	54.4	-23.3	0.0%	0.1%	0.1%
	48.9	-23.3	-0.7%	0.3%	0.3%
	43.3	-23.3	-0.9%	-0.5%	-0.5%
	Average:		**0.7%**	**0.7%**	**0.7%**
Not used for model fitting	54.4	-28.9	4.3%	3.9%	3.2%
	48.9	-28.9	4.0%	3.4%	2.7%
	43.3	-28.9	4.2%	4.7%	4.0%
	Average:		**4.2%**	**4.0%**	**3.3%**

Table 6-4: Relative errors for extrapolation to lower evaporating temperatures (data set B9a)

Again, relative errors are larger than for extrapolating to lower condensing temperatures and the exponential power model fits better than the inverse proportional power model. The highest relative error that occurs is 4.7% for the inverse proportional power model. The map has been extrapolated to evaporating temperatures as much as 5.6°C lower than the lowest measured data point.

6.1.3 Extrapolation to Higher Evaporating and Higher Condensing Temperatures

In this section, 4 data points with low evaporating and low condensing temperature have been chosen to fit the model parameters. The following table (6-5) shows the relative errors obtained for these 4 data points as well as for the 10 other data points of data set A4.

	Operating Conditions		Relative Errors		
	Condensing Temperature [°C]	Evaporating Temperature [°C]	Mass Flow Rate	Power (inverse proportional)	Power (exponential)
Used for model parameter fitting	37.8	-23.3	-0.1%	-0.4%	-0.4%
	37.8	-28.9	1.3%	0.2%	0.2%
	40.6	-23.3	-0.2%	0.4%	0.4%
	43.3	-28.9	-0.8%	-0.2%	-0.2%
	Average:		**0.8%**	**0.3%**	**0.3%**
Not used for model parameter fitting	37.8	-12.2	-4.5%	-5.1%	-2.8%
	37.8	-17.8	-0.9%	-2.1%	-1.2%
	43.3	-12.2	-3.6%	-4.4%	-2.0%
	43.3	-17.8	-0.5%	-0.2%	0.7%
	48.9	-12.2	-2.3%	-1.0%	1.4%
	43.3	-23.3	0.5%	1.1%	1.1%
	48.9	-17.8	-0.4%	0.5%	1.5%
	48.9	-23.3	-1.7%	0.9%	0.9%
	48.9	-28.9	0.9%	1.7%	1.7%
	54.4	-23.3	-0.8%	2.2%	2.2%
	Average:		**2.1%**	**2.5%**	**1.7%**

Table 6-5: Relative errors for extrapolation to higher condensing and higher evaporating temperatures (data set A4)

Figure 6-7 through 6-9 show the corresponding maps for mass flow rate and both power models.

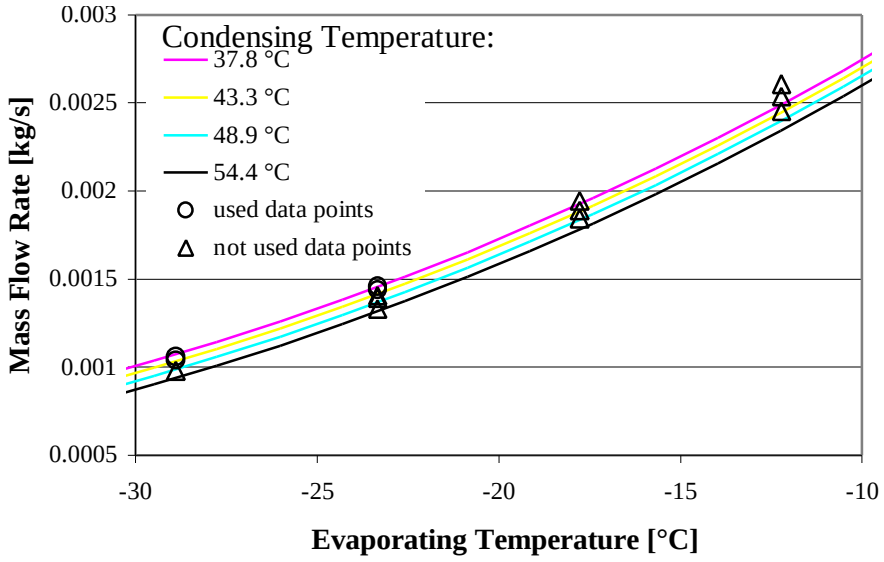

Figure 6-7: Mass flow rate map extrapolating to higher condensing and higher evaporating temperatures (data set A4)

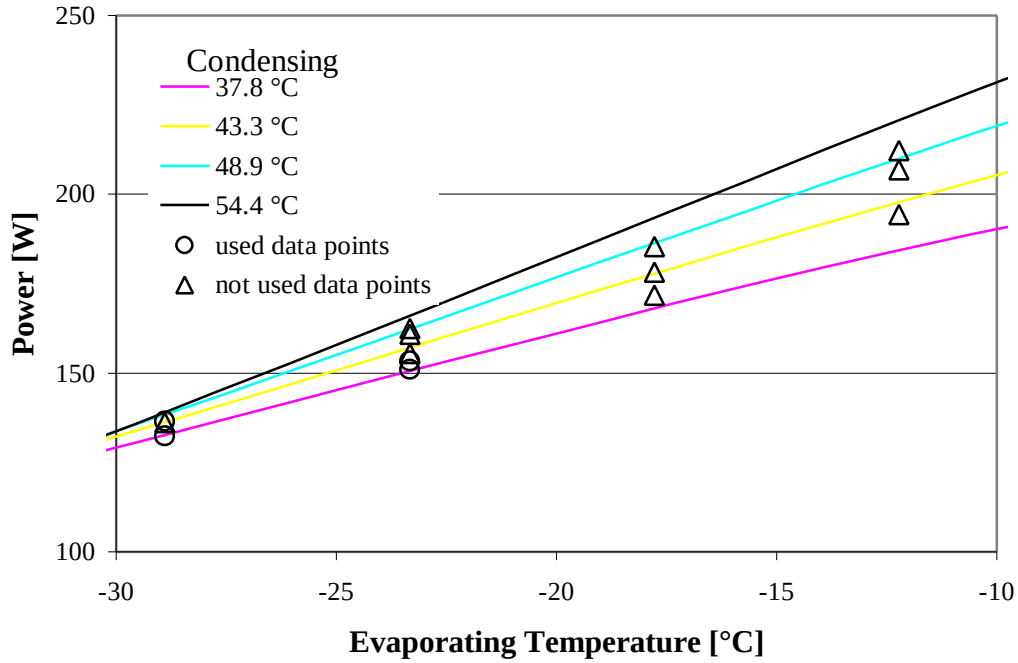

Figure 6-8: Power map extrapolating to higher condensing and higher evaporating temperatures (data set A4) using the inverse proportional model

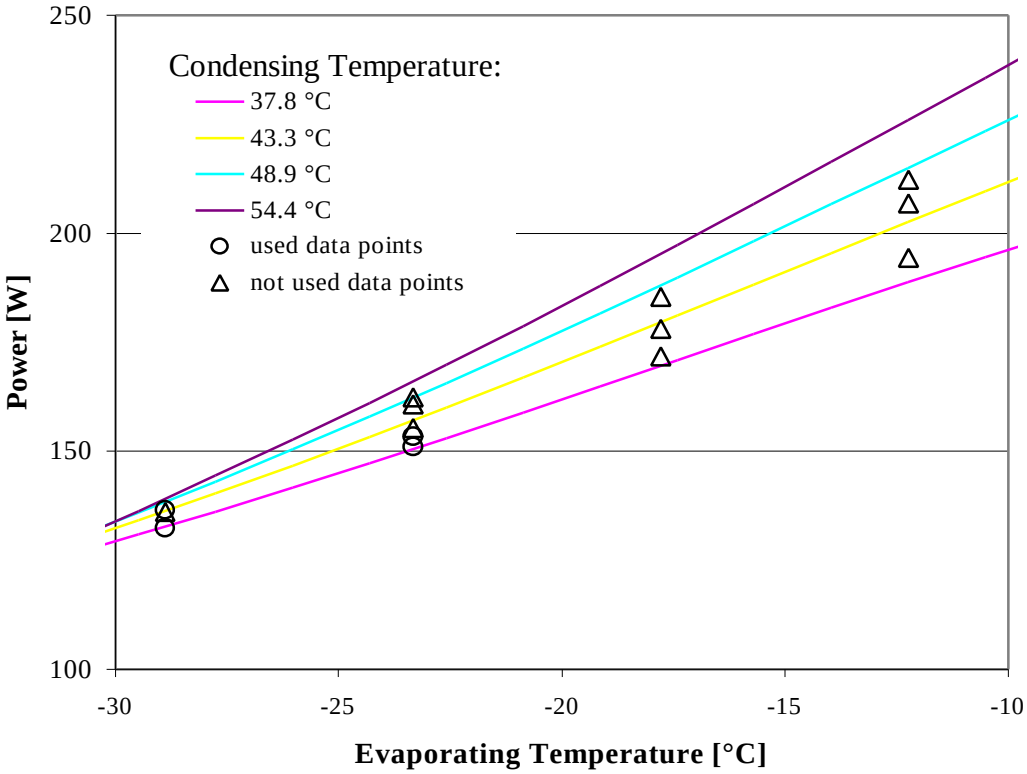

Figure 6-9: Power map extrapolating to higher condensing and higher evaporating temperatures (data set A4) using the exponential model

Errors for the extrapolated points are again smaller for the exponential power model than for the inverse proportional model. The highest relative error is 5.1% for a point extrapolated with the inverse proportional power model. The maps have been extrapolated to condensing and evaporating temperatures 11.1°C higher than the highest measured data points. Figure 6-7 shows that predictions become less accurate the further one extrapolates.

The following table shows the errors for the same analysis for data set B9a. For this data set the inverse proportional and the exponential power model show no significant differences. All relative errors are within 5%.

	Operating Conditions		Relative Errors		
	Condensing Temperature [°C]	Evaporating Temperature [°C]	Mass Flow Rate	Power (inverse proportional)	Power (exponential)
Used for model parameter fitting	48.9	-23.3	-1.3%	-0.4%	-0.4%
	43.3	-23.3	0.2%	0.4%	0.4%
	48.9	-28.9	-1.0%	-2.3%	-2.3%
	43.3	-28.9	2.8%	2.3%	2.3%
	Average:		**1.6%**	**1.6%**	**1.6%**
Not used for model parameter fitting	54.4	-17.8	1.9%	2.0%	1.6%
	48.9	-17.8	1.9%	2.7%	2.2%
	43.3	-17.8	3.5%	2.1%	1.7%
	54.4	-23.3	-2.8%	-2.5%	-2.5%
	54.4	-28.9	-3.9%	-4.9%	-5.0%
	Average:		**2.9%**	**3.0%**	**2.9%**

Table 6-6: Relative errors for extrapolation to higher condensing and higher evaporating temperatures (data set B9a)

6.1.4 Interpolation

The four most extreme data points, i.e. the points with the highest and lowest condensing and evaporating temperatures, have been chosen to verify how well the

models interpolate. These four points were used to determine the model parameters. Table 6-7 shows the relative errors obtained for all data points of data set A4. All relative errors are within 3%. There is no significant difference between the exponential and the inverse proportional power model with an average relative error of the interpolated points of 1.9% for the inverse proportional model and 1.4% for the exponential model.

	Operating Conditions		Relative Errors		
	Condensing Temperature [°C]	Evaporating Temperature [°C]	Mass Flow Rate	Power (inverse proportional)	Power (exponential)
Used for model parameter fitting	37.8	-12.2	-0.6%	-2.1%	-2.0%
	54.4	-23.3	-1.4%	3.0%	2.2%
	48.9	-12.2	0.7%	2.0%	2.1%
	37.8	-28.9	2.1%	0.7%	1.3%
	Average:		**1.4%**	**2.1%**	**1.9%**
Not used for model parameter fitting	37.8	-23.3	2.1%	1.5%	0.7%
	48.9	-28.9	-0.9%	1.1%	1.7%
	48.9	-17.8	1.6%	2.9%	2.1%
	40.6	-23.3	1.7%	2.1%	1.3%
	43.3	-23.3	2.0%	2.6%	1.9%
	43.3	-28.9	-1.1%	-0.2%	0.4%
	48.9	-23.3	-1.1%	2.1%	1.4%
	37.8	-17.8	2.4%	0.5%	-0.2%
	43.3	-12.2	-0.2%	-1.3%	-1.2%
	43.3	-17.8	2.2%	2.4%	1.6%
	Average:		**1.7%**	**1.9%**	**1.4%**

Table 6-7: Relative errors for interpolation between most extreme data points (data set A4)

Figure 6-10 through 6-12 show the corresponding mass flow rate and power maps.

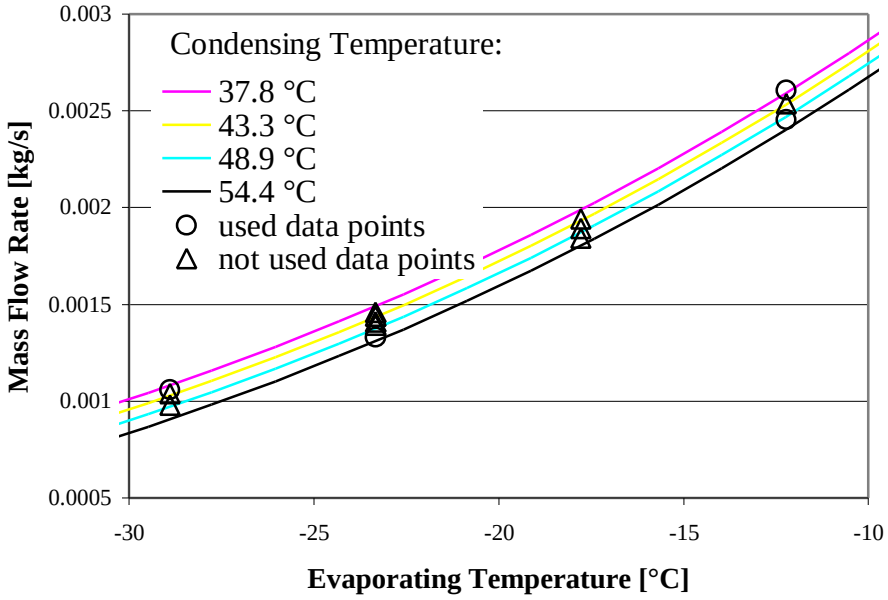

Figure 6-10: Mass flow rate map interpolating between the most extreme measured points (data set A4)

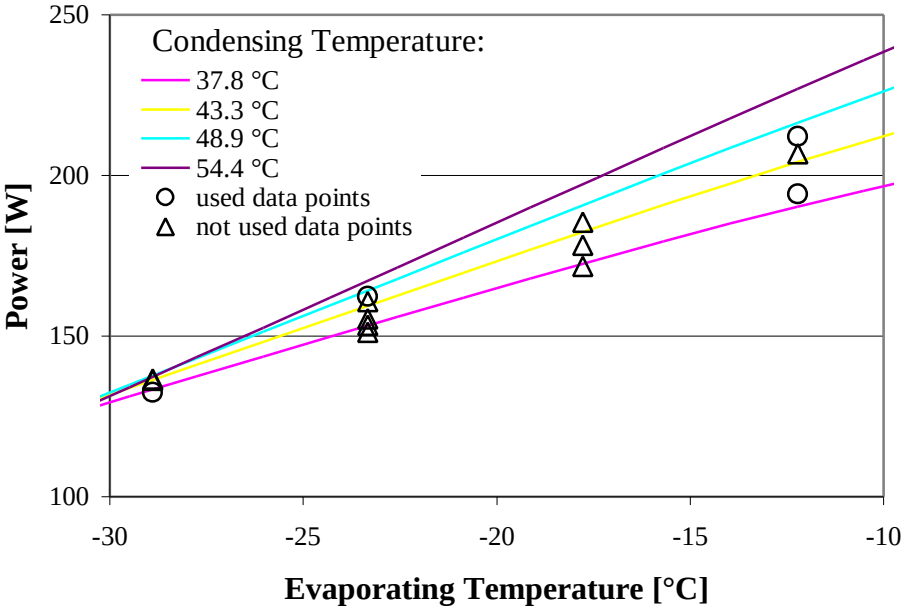

Figure 6-11: Power map interpolating between the most extreme measured points for the inverse proportional model (data set A4)

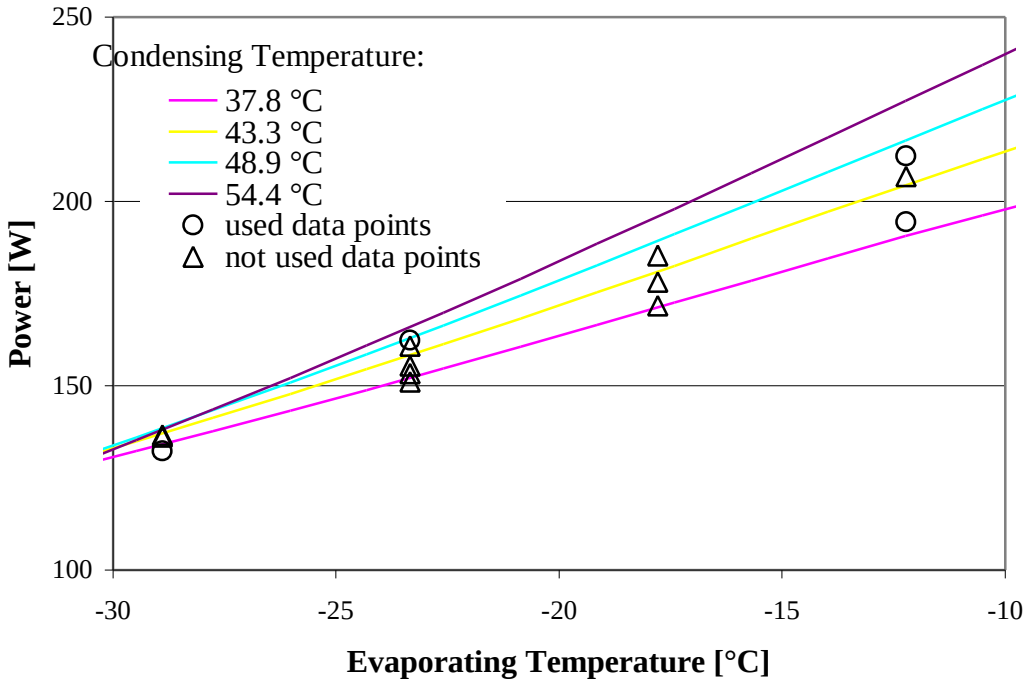

Figure 6-12: Power map interpolating between the most extreme measured points for the exponential model (data set A4)

Table 6-8 shows the errors obtained with this interpolation analysis for data set B9a.

	Operating Conditions		Relative Errors		
	Condensing Temperature [°C]	Evaporating Temperature [°C]	Mass Flow Rate	Power (inverse proportional)	Power (exponential)
Used for model parameter fitting	54.4	-17.8	-0.2%	0.5%	0.5%
	43.3	-17.8	-0.2%	-0.5%	-0.5%
	54.4	-28.9	-1.1%	-2.1%	-2.1%
	43.3	-28.9	2.2%	2.0%	2.0%
	Average:		**1.3%**	**1.5%**	**1.5%**
Not used for model parameter fitting	48.9	-23.3	-2.7%	-1.3%	-1.2%
	43.3	-23.3	-2.2%	-1.4%	-1.2%
	54.4	-23.3	-3.0%	-2.4%	-2.2%
	48.9	-28.9	-0.1%	-1.2%	-1.1%
	48.9	-17.8	-1.1%	0.5%	0.5%
	Average:		**2.1%**	**1.5%**	**1.4%**

Table 6-8: Relative errors for interpolation between most extreme data points (data set B9a)

The relative errors for data set B9a are all below 3%. There is no significant difference between the exponential and the inverse proportional power model. The average relative errors of the interpolated data points are 1.4% and 1.5% respectively.

6.1.5 Calculating the Model Parameters From Two Data Points

The mass flow rate model contains only two unknown parameters that can be calculated directly when two measurements of mass flow rate are taken. The two data points with the lowest evaporating temperatures were used for this analysis. A least squares curve fit is not necessary in this case, the model parameters can be solved for directly. The remaining 12 points for data set A4 were then used to see how well the model extrapolates from those two data points.

Table 6-9 shows the relative errors in mass flow rate for data set A4. The relative errors for the two points that have been used for the fitting procedure have to be equal to zero. The highest relative error for an extrapolated point is 11.2%, which is higher than for most other cases seen in the previous sections; however, it is still surprisingly small considering that this is the worst case that can occur with two measured data points at very similar operating conditions. The following figure (6-13) shows the mass flow rate map obtained with only two measured data points.

	Operating Conditions		Relative Error
	Condensing Temperature [°C]	Evaporating Temperature [°C]	Mass Flow Rate
Used for model fitting	37.8	-28.9	0.0%
	43.3	-28.9	0.0%
	Average:		**0.0%**
Not used for model parameter fitting	40.6	-23.3	-3.4%
	37.8	-23.3	-4.1%
	37.8	-12.2	-11.2%
	37.8	-17.8	-6.6%
	43.3	-12.2	-9.7%
	43.3	-17.8	-5.2%
	48.9	-12.2	-7.5%
	43.3	-23.3	-2.0%
	48.9	-17.8	-3.9%
	48.9	-23.3	-2.4%
	48.9	-28.9	4.1%
	54.4	-23.3	0.4%
	Average		**5.9%**

Table 6-9: Relative errors for extrapolation from two low evaporating temperature data points (data set A4)

The following figure (6-13) shows the mass flow rate map obtained with only two measured data points.

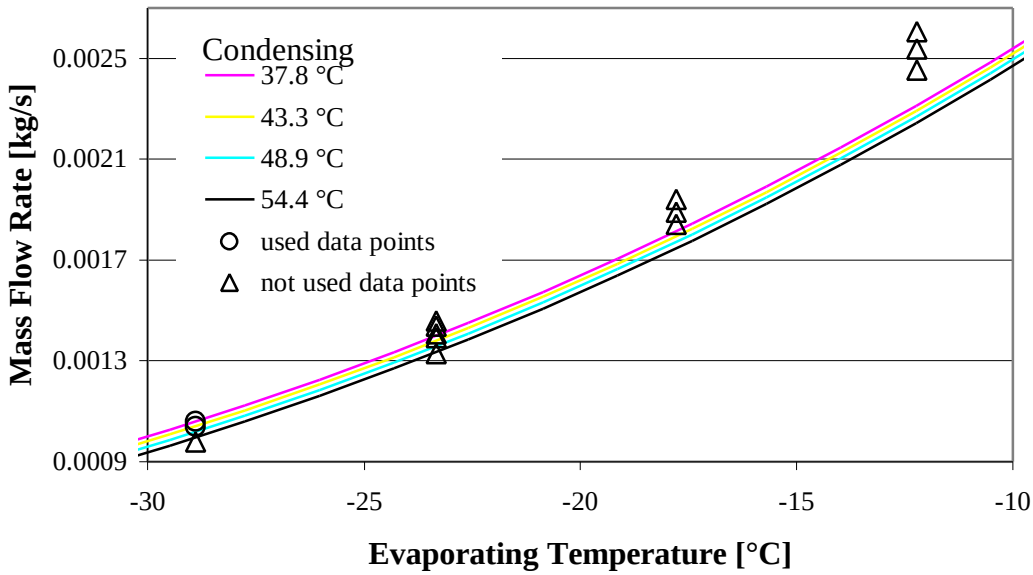

Figure 6-13: Mass flow rate map generated with two measured data points (data set A4)

The map shows that predictions are getting worse the further away the data point is from the measured data. The model is underpredicting almost all of the data points.

6.1.6 Conclusion

The proposed models have been shown to extrapolate reliably 10°C beyond the measured data. The relative errors between the measured data and the model are below 5% for almost every data point for the constant percentage pressure drop model (mass flow rate) and the exponential combined efficiency model (power). Relative errors for the inverse proportional model for power can be as large as 11%.

Extrapolation seems to be more reliable if measurements at at least 2 different condensing and 2 different evaporating temperatures are used to fit the model parameters. To minimize the need to extrapolate, it appears helpful to choose data points at evaporating and condensing temperatures that are very different from each other.

Using only two data points to fit the model parameters leads to relatively big errors in extrapolation. Therefore it seems reasonable to take at least four measurements at operating temperatures very different from each other. To verify the model, it would be useful to measure one more data point in between the four measured points.

6.2 Effect of Ambient Temperature

Standard calorimeter tests are performed at an ambient temperature of 32.2°C (90°F); however, in a real refrigerator the compressor may operate at ambient conditions below 32.2°C (90°F). There are two effects that influence the performance of a

compressor at different ambient temperatures. Generally, the refrigerant is superheated to the ambient temperature. Therefore, the suction temperature of the compressor changes with ambient temperature. A higher suction temperature means that the specific volume at the inlet of the compressor is larger and therefore the mass flow rate of refrigerant that can be pumped and also the power should be smaller. The ambient temperature also affects the amount of heat transfer from the shell to the surroundings.

6.2.1 Experimental Data

There is very little data available in the literature that includes calorimeter tests at different ambient temperatures. Haider, et al. (1997) report calorimeter tests at three different ambient temperatures (43.3°C, 32.2°C and 15.6°C). This data set is going to be called D1 as a compressor of a different manufacturer than the standard test data used in this research was tested. Table 6-10 shows their data points at all operating conditions that were measured at different ambient temperatures as well as the difference in mass flow rate and power in percent between the two ambient temperatures all other conditions being the same. The data at 15.6°C ambient temperature was taken at different condensing temperatures and is therefore not included in table 6-10.

T_{evap} °C	T_{cond} °C	Power at 32.2°C W	Power at 43.3°C W	**Change in Power**	Mass Flow Rate at 32.2°C kg/s	Mass Flow Rate at 43.3°C kg/s	**Change in Mass Flow Rate**
-28.9	54.4	118.3	116.6	**-1.5%**	0.001148	0.001091	**-8.3%**
-28.9	48.9	115.8	114.3	**-1.3%**	0.001184	0.001144	**-6.5%**
-23.3	54.4	135.9	134.5	**-1.0%**	0.001511	0.00149	**-4.4%**
-23.3	48.9	132.4	130.4	**-1.5%**	0.001586	0.001502	**-8.6%**

Table 6-10: Compressor performance measurements at different ambient temperatures (data set D1)

The data reported by Haider et al. indicate that both the mass flow rate and the input power decrease with increasing ambient temperature (the mass flow rate is decreasing faster than the power).

The data reported for compressor model B3 also included measurements at 43.3°C ambient temperature. There are 6 data points that were measured at both 32.2°C and 43.3°C ambient temperature. These data and the changes in power and mass flow rate in percent are shown in table 6-11.

T_{cond} °C	T_{evap} °C	Power at 32.2°C W	Power at 43.3°C W	**Change in Power**	Mass Flow Rate at 32.2°C kg/s	Mass Flow Rate at 43.3°C kg/s	**Change in Mass Flow Rate**
54.4	-23.3	199	208	**+4.5%**	0.001753	0.001738	**-0.9%**
37.8	-20.6	199	197.2	**-0.9%**	0.002213	0.002161	**-2.4%**
48.9	-15.0	245	242.8	**-0.9%**	0.002727	0.002594	**-5.1%**
60.0	-26.1	184	189.6	**+3.0%**	0.001401	0.001446	**+3.2**
37.8	-40.0	114	114.8	**+0.7%**	0.000755	0.000759	**+0.5%**
43.3	-40.0	114	117.2	**+2.8%**	0.000718	0.000724	**+0.9%**

Table 6-11: Compressor performance measurements at different ambient temperatures (compressor model B3)

As seen in table 6-11, power and mass flow rate both increase and decrease with increasing ambient temperature depending on the operating conditions. There is not a physical explanation for this behavior.

6.2.2 Comparison of Predictions and Experiments

The mass flow rate and power model developed in chapters 4 and 5 accounts for a change in ambient temperature only by changing the suction temperature to the compressor which is assumed to be equal to the ambient temperature. Figure 6-14 shows how the mass flow rate and power changes with the ambient temperature for constant

condensing and evaporating conditions (43.3°C and –23.3°C respectively) for data set B3.

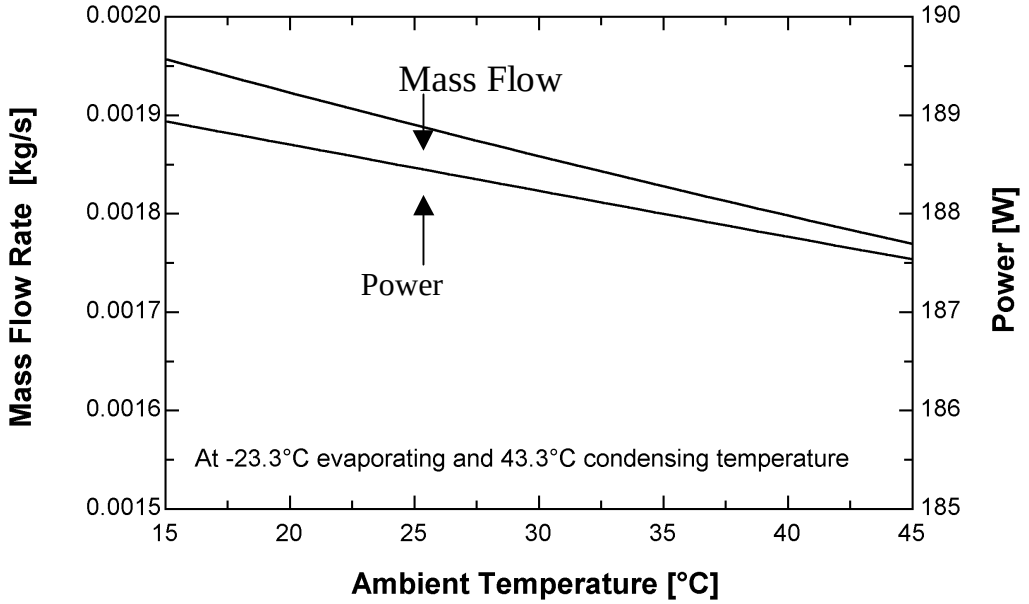

Figure 6-14: Changes in mass flow rate and power with ambient temperature for the new model (data set B3)

Both the mass flow rate and the power decrease with increasing ambient temperature. The effect is stronger for mass flow rate than for power. The mass flow rate changes 10.1% over the range of ambient temperatures (15°C - 45°C). The power changes only 0.7% over the same range. Both equations (for mass flow rate and for power) contain the specific volume at the suction side of the compressor. To calculate the power however, the changed mass flow rate is used and the effects of mass flow rate and specific volume tend to almost cancel.

The experimental data reported by Haider et al. (1997) have been used to test how well the model predicts calorimeter data taken at different ambient temperatures. Measurements at 9 different operating conditions and an ambient temperature of 32.2°C were available to fit the 5 model parameters, C, Δp, d, e, f. These parameters were then

used to determine the mass flow rate and power for the other measured data points at different ambient temperatures. For comparison, the mass flow rate and power were also calculated for these points ignoring the changed suction conditions. Table 6-12 shows all the data points and the relative errors between measure and calculated mass flow rate and power.

Ambient Tempera-ture [°C]	T_{cond} [°C]	T_{evap} [°C]	Mass Flow Rate			Power		
			meas. [kg/s]	calc. [kg/s]	Relative Error	meas. [kg/s]	calc. [kg/s]	Relative Error
32.2	54.4	-28.9	0.001148	0.001138	-0.9%	118.3	118.2	-0.1%
	48.9	-28.9	0.001184	0.001184	0.0%	115.8	116.2	0.3%
	43.3	-28.9	0.001225	0.001225	0.0%	113.6	113.2	-0.4%
	54.4	-23.3	0.001511	0.001528	1.1%	135.9	136.6	0.5%
	48.9	-23.3	0.001586	0.001575	-0.7%	132.4	132.3	-0.1%
	43.3	-23.3	0.00162	0.001617	-0.2%	127.7	127.1	-0.5%
	54.4	-17.8	0.00197	0.001994	1.2%	154.4	155.6	0.8%
	48.9	-17.8	0.002039	0.002041	0.1%	148.9	148.9	0.0%
	43.3	-17.8	0.002113	0.002084	-1.4%	142.6	141.2	-1.0%
43.3°C	54.4	-28.9	0.001091	0.001097	0.5%	116.6	117.9	1.1%
	48.9	-28.9	0.001144	0.001141	-0.3%	114.3	115.9	1.4%
	54.4	-23.3	0.00149	0.001473	-1.1%	134.5	136.2	1.3%
	48.9	-23.3	0.001502	0.001518	1.1%	130.4	132	1.2%
15.6°C	26.7	-28.9	0.001376	0.001408	2.3%	106.9	98.71	-7.7%
	23.9	-28.9	0.001436	0.001424	-0.8%	104.6	95.46	-8.7%
	26.7	-23.3	0.001846	0.001825	-1.1%	117.3	106.0	-9.6%
	23.9	-23.3	0.001885	0.001841	-2.3%	115.1	101.7	-11.6%
Data below uses 32.2°C (90°F) as suction temperature instead of ambient temperature								
43.3°C	54.4	-28.9	0.001091	0.001138	4.3%	116.6	118.2	1.4%
	48.9	-28.9	0.001144	0.001184	3.5%	114.3	116.2	1.7%
	54.4	-23.3	0.00149	0.001528	2.6%	134.5	136.6	1.6%
	48.9	-23.3	0.001502	0.001575	4.9%	130.4	132.3	1.5%
15.6°C	26.7	-28.9	0.001376	0.00133	-3.3%	106.9	98.44	-7.9%
	23.9	-28.9	0.001436	0.001345	-6.3%	104.6	95.21	-9.0%
	26.7	-23.3	0.001846	0.001724	-6.6%	117.3	105.8	-9.8%
	23.9	-23.3	0.001885	0.001739	-7.7%	115.1	101.5	-11.8%

Table 6-12: Predicting at different ambient temperatures (measured data from Haider et al. (1997), compressor D1

The model predicts both mass flow rate and power at 43.3°C very well. Relative errors are below 1.5% for all data points. At an ambient temperature of 15.5°C, the relative errors for mass flow rate are below 2.5% but the relative error in power is as high as 11.6%. When using the model without using the ambient temperature as suction temperature (i.e. using a suction temperature of 32.2°C for all data points) the predictions of power are very similar to those obtained when using the correct ambient temperature; however, predictions of mass flow rate differ with relative errors as high as 7.8%.

The measurements taken at an ambient temperature of 15.6°C were conducted using much lower condensing temperatures than the measurements at both 32.2°C and 43.3°C ambient temperature. As seen in the previous section on extrapolation, extrapolation becomes less and less reliable the further one moves away from the conditions that the model parameters were fitted at. The values at 15.6°C ambient temperature are extrapolated to condensing temperatures as low as 19.4°C lower than the lowest condensing temperature that was used to fit the model parameters. This is almost twice as far as extrapolations in the previous section were performed. The predictions calculated using 32.2°C as the suction temperature for all data points show that the large errors in power predictions at 15.6°C ambient temperature are mostly due to errors in extrapolation in condensing temperature. The effect of ambient temperature appears to be much smaller and is confounded with the extrapolation effects.

Another comparison of the percentage change of mass flow rate and power for different operating conditions including different ambient temperatures has been made. This percentage has been calculated for experimental data provided by Clark Bullard

(1998). In this experiment the performance of a compressor inside a refrigerator has been measured at different ambient temperatures. These percentages have been compared to the change in mass flow rate and power that the model predicts for the same operating and ambient conditions as in the experiment. Only the percentages between the different operating conditions can be compared because calorimeter measurements were not available for the compressor used in these tests. A different compressor model has been used for the calculations. The following table (6-13) shows this comparison in terms of percent variation from the first data point.

T_{amb} [°C]	T_{cond} [°C]	T_{evap} [°C]	Mass Flow Rate [%]		Power [%]	
			meas	calc	meas	calc
32.8	27.1	-31.6	-	-	-	-
16	35.9	-27.3	-33.6%	-30.6%	-33.4%	-44.9%
24.3	45.3	-23.5	-16.1%	-12.4%	-17.8%	-19.9%
38.5	49.4	-23.2	-6.0%	-2.8%	+2.0%	+3.5%

Table 6-13: Percentage change in mass flow rate and power for different operating conditions. Eperimental data supplied by Clark Bullard (1998), calculated data using data set B3.

The operating conditions are different for each data point. The model predicts changes in mass flow rate in the correct direction and in the same order of magnitude than the experimental data.

6.2.3 Conclusion

The influence of the ambient temperature on power and mass flow rate has been found to be fairly small. The model captures the effect reasonably well through changes in the suction temperature. It seems more important to perform the calorimeter test at

condensing and evaporating conditions close to those that the compressor will be operating at than at the correct ambient temperature. Predictions with the model become less and less reliable the more the operating conditions differ from the test conditions at which the parameters were fitted.

Chapter 7

Heat Transfer and Discharge Temperature

As mentioned in chapter 3, the heat transfer from the shell of refrigerator compressors can be very significant, therefore, the refrigerant discharge temperature at the outlet of the shell may be substantially lower than the temperature at the outlet of the cylinder. Knowing the discharge temperature at the outlet of the shell is useful for determining the overall heat transfer from the compressor and necessary for systems-level modeling.

Popovic and Shapiro (1995) use a heat transfer loss coefficient to correlate the overall compressor efficiency. The heat transfer loss coefficient is defined as the heat loss from the compressor shell divided by the heat loss from the motor, the heat loss from the motor being defined as the difference between the measured electrical power input and the polytropic work (equation 3-11) and the mass flow rate. The compressors investigated by Popovic and Shapiro (1995) are larger than those investigated here (3 tons refrigeration capacity) and the heat transfer loss coefficients are in the order of 0.2. The corresponding heat transfer loss coefficients for the refrigerator/freezer compressors investigated in this research are much larger (1-2.5). Popovic and Shapiro (1995) use a linear curve fit of the overall compressor effiency versus the heat transfer loss coefficient to model the electrical power input.

For the data sets collected during the course of this research for which the discharge temperatures were available, the heat transfer loss coefficient (as described

above) was calculated and plotted against the overall compressor efficiency defined as the enthalpy change across the compressor divided by the electrical power input. Figure 7-1 shows these plots for a few of the data sets. Note that values of negative compressor efficiency indicate that the enthalpy of the refrigerant leaving the compressor is lower than the enthalpy entering the compressor. Such a situation arises when the heat loss from the compressor shell is large.

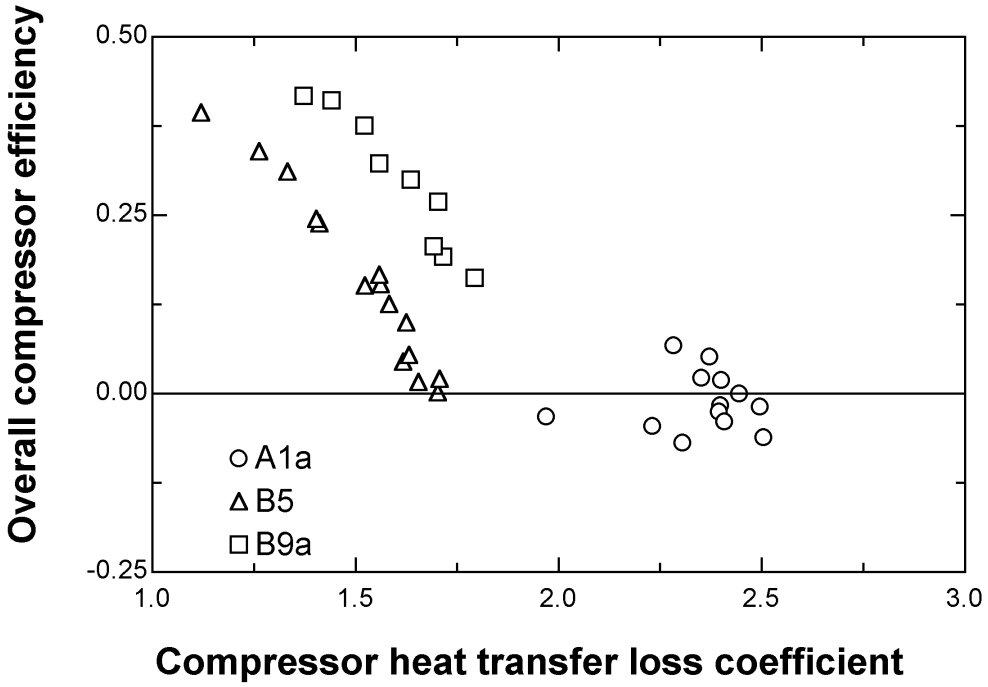

Figure 7-1:Overall compressor efficiency versus compressor heat transfer loss coefficient for several data sets.

The overall compressor efficiencies obtained are much lower than the values that Popovic and Shapiro obtained from their data indicating that there is considerably more heat transfer over the shell of small compressors than over the shell of large compressors. Nevertheless, except for one data set there is a trend in the data that could be correlated with a linear relation.

Figure 7-2 shows the heat loss from the compressor shell divided by the compression ratio for several data sets. The heat loss from the compressor shell can be calculated if the discharge temperature is known. The discharge temperature appears to be linearly correlated with compression ratio. An equation of the form

$$\frac{Power - \dot{m}\left(h_{discharge} - h_{suction}\right)}{Power} = a + b \cdot CR \qquad (7\text{-}1)$$

with h - enthalpy

CR - compression ratio

would allow to predict the discharge temperature of the refrigerant. This relation is useful for modeling an entire refrigeration cycle.

Two parameters (a and b) have to be determined from measured data of discharge temperature, mass flow rate and power. The discharge temperature can than be calculated using the calculated mass flow rate and power. This correlation adds two parameters to the model but allows calculation of the discharge temperature for different operating conditions.

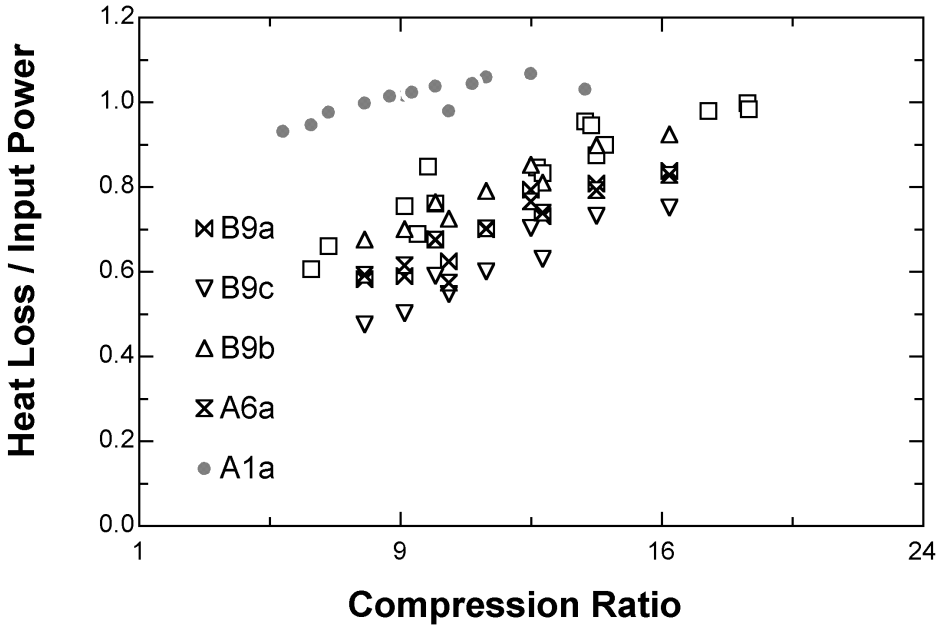

Figure 7-2: Heat loss over power input versus compression ratio for several data sets

The ratio between heat loss from the shell and power input ranges from around 0.5 to 1.1. The above considerations have been evaluated only for small refrigerator/freezer compressors with capacities in the range of approximately 50-350 W (0.02-0.09 tons, 1 ton=12,000 Btu/hr). Heat loss ratios in this range are likely not to be valid for larger compressors such as those used in the study by Popovic and Shapiro (1995). The validity of equation 7-1 for larger compressor needs to be established with additional data.

Chapter 8

Conclusions and Recommendations

8.1 Conclusions

Calorimeter testing data for compressors used in domestic refrigerators have been collected. 21 data sets from 3 manufacturers containing 9 to 16 data points of mass flow rate or capacity and power at different operating conditions were used in this research. Most of the data were taken at an ambient, compressor suction and liquid line temperature of 32.2°C (90°F). A total of 276 data points at these conditions has been used. The data were plotted in form of compressor maps against evaporating temperature to identify any suspect data points. Plotting the power per unit mass flow rate against evaporating temperature helped to identify these suspect points. One manufacturer also supplied data at 43.3°C (110°F) ambient temperature. One data set at different ambient temperatures was measured by Clark Bullard (1998), another data set was found in the literature [Haider et al. (1997)].

A semi-empirical model has been developed to represent the performance of reciprocating refrigeration compressors. The model can be used to generate compressor maps from four or more measurements of refrigerant mass flow rate and electrical power input.

The current method of representing compressor performance data (ARI standard 540-91) has been investigated as well as several variations of the semi-empirical model proposed in this research.

8.1.1 Advantages and Disadvantages of the Different Models

ARI Method

The current ARI procedure, presented in ARI Standard 540-91, was used to generate compressor maps for all experimental data. The procedure for fitting the parameters is very simple because the model is linear with respect to all curve fit parameters and linear regression can be applied.

The current method to present compressor performance has been found to be unreliable for extrapolation and interpolation. To fit the 10 parameters in the polynomials that describe the mass flow rate and input power as a function of evaporating and condensing temperature, at least 10 measurements of both mass flow rate and power have to be taken. The more measurements are taken the more reliable extrapolation and interpolation gets.

Whether or not the curve fit make physical sense can be checked by plotting the power per unit mass flow rate. Most ARI curve fits for the experimental data were questionable for extrapolated low evaporating temperatures and extrapolated condensing temperatures. The ARI curve fit for one data set that contained only 10 data points perfectly represents the measured data but interpolation and extrapolation are very inaccurate.

The semi-empirical model that has been developed, is based on the assumption of a polytropic compression process. The compression process in the cylinder itself is assumed to be adiabatic; therefore, the isentropic exponent k for the given refrigerant can be used instead of the unknown polytropic exponent n.

Recommended Mass Flow Rate Model

The mass flow rate can be represented by equation (4-1).

$$\dot{m} = \left[1 + C - C\left(\frac{p_{discharge}}{p_{suction}} \right)^{\frac{1}{n}} \right] \cdot \frac{V \cdot RPM}{v_{suction}} \tag{4-1}$$

The displacement volume, V, and the motor speed, RPM, for the particular compressor model are required inputs. The discharge pressure is assumed to be equal to the condensing pressure. Small increases in discharge pressure due to pressure drops across the valves have little effect on power or mass flow rate. The specific volume at the suction side of the compressor can be calculated using the ideal gas law. The suction pressures in refrigerator/freezer compressors are low enough so that the ideal gas assumption is accurate. The suction temperature is assumed to be equal to the ambient temperature which is 32.2°C (90°F) for standard testing. A suction pressure drop is assumed so that the suction pressure is lower than the evaporating pressure. The suction pressure drop can be represented by one of the following equations:

$$\Delta p_{suction} = p_{evap} - p_{suction} \tag{4-10}$$

$$p_{suction} = p_{evap}\left(1 - \Delta p_{suction}\right) \tag{4-11}$$

$$\Delta p_{suction} = \frac{k \cdot \dot{m}^{2}}{p_{evap}} \tag{4-14}$$

It was found that a percentage pressure drop (equation (4-11)) represents the data better than a constant pressure drop (equation (4-10)). Although the pressure drop, physically, is a function of the mass flow rate through the suction line and muffler, it has

been found that using equation (4-14) rather than (4-11) does not benefit the model enough to justify the mathematically much more complicated model.

Equations (4-11) and (4-14) together are the recommended model for mass flow rate. It should be noted that the model parameters C and Δp do not necessarily represent the actual clearance volume and the suction pressure drop respectively. Rather, they should be called the *effective* clearance volume and pressure drop because all physical phenomena that are not accounted for by the assumed form of the model are being lumped together in these two parameters. The values that best fit the experimental data are larger than physically reasonable. Values for C range from 1.5% to 5% and for the pressure drop from 0 to 21% in the 21 sets of refrigeration compressor data investigated.

The average relative errors in mass flow rate are below 3% for all sets of experimental data except a few data sets that contain suspect data points. Most relative errors are below 5% with a few data points having relative errors up to 7 or 8%.

Recommended Power Model

The polytropic work divided by a 'combined' efficiency has been used to represent the electrical input power. The combined efficiency takes motor inefficiencies as well as all other inefficiencies such as frictional effects into account. Equation (5-1) shows the expression that has been used to represent the power input to the compressor.

$$Power \cdot h_{comb} = \dot{m} \cdot \frac{n}{n-1} \cdot p_{suction} \cdot v_{suction} \left[\left(\frac{p_{discharge}}{p_{suction}} \right)^{\frac{n-1}{n}} - 1 \right] \qquad (5\text{-}1)$$

Again, the isentropic exponent k has been used instead of the polytropic exponent; the same suction pressure drop as for the mass flow rate is used. The mass flow rate itself is also needed to determine the power. It has been found that using the calculated mass flow rate rather than the measured value tends to smooth out errors in the mass flow rate measurements and therefore leads to a better curve fit in power.

The combined efficiency in equation (5-1) is not a constant. Several parameters have been investigated to find a parameter to explain the variation of the combined efficiency. It was shown that the data scatter very little when the combined efficiency is plotted against the evaporating pressure. Two relationships between combined efficiency and evaporating pressure have been found to fit the data reasonably well. These relationships are shown in equations (5-2) and (5-3).

$$h_{comb} = d + e \cdot \exp\left(f \cdot p_{evap}\right) \tag{5-2}$$

$$h_{comb} = a + \frac{b}{p_{evap}} \tag{5-3}$$

The exponential model (equation 5-2) contains 3 curve fit parameters (d, e, and f), the inverse proportional model only 2 (a and b). It was found that both models fit the data reasonably well but the exponential model extrapolates better especially to lower evaporating temperatures. The exponential model is preferred if extrapolation is expected although the model is mathematically more complicated than the inverse proportional one.

Average relative errors in power are below 4.5% for all data sets for the exponential model and below 5.2% for the inverse proportional model. There are a small number of data points that have errors are large as 14% for the inverse proportional

model and 10% for the exponential model. Values of the combined efficiency range from 40 to 60% for all sets of testing data.

Interpolation and Extrapolation

It was found that the model interpolates and extrapolates reliably up to 10°C higher or lower evaporating or condensing temperatures. Relative errors in mass flow rate and power are below 5% when using the exponential model for power. When the inverse proportional model is used the relative errors are generally higher; some data points have errors as high as 12%.

Required Number of Tests

To minimize the need to extrapolate, it would be useful to take four measurements at operating conditions very different from one another to fit the 5 model parameters (C, Δp, d, e, and f). A fifth measurement should be taken at an intermediate evaporating and condensing temperature to verify the model.

Effect of Ambient Temperature

A change in ambient temperature is represented in the model by a change in the specific volume of the refrigerant at the suction side of the compressor. Very little experimental data taken at ambient temperatures other than 32.2°C (90°F) are available in the literature. The data available from Haider et al. (1997), Bullard (1998) and manufacturer B were used to compare the results from the model with the experimental

data. The effect of a change in ambient temperature seems to be well represented in the model. It agrees well with the experimental data.

Heat Transfer and Discharge Temperature

It has been found that measured data of the refrigerant discharge temperature at different operating conditions can be used to correlate the heat transfer from the compressor shell divided by the electrical power input to the compression ratio. Two model parameters that have been determined this way can be used to calculate the refrigerant discharge temperature at different operating conditions.

This has been shown for the data sets for which the discharge temperature was available. All of the data was taken at 32.2°C (90°F) ambient temperature. More research is needed at different ambient temperature and using different compressor models and sizes.

8.1.2 Modeling Procedure

A non-linear least squares curve fit has to be carried out to estimate the model parameters using the experimental data. Four or more measurements of mass flow rate and electrical power input have to be taken. First, the two parameters of the mass flow rate model are determined with a least squares curve fit. The values obtained for the pressure drop and the mass flow rate itself are then used for fitting the power model. Another least squares curve fit is performed to estimate the remaining 2 or 3 parameters that describe the combined efficiency.

The computer program 'Engineering Equation Solver' (EES, Klein and Alvarado (1999)) has been used in this research to perform the non-linear least squares curve fits. Copies of the programs for mass flow rate and power are attached in appendix E.

8.1.3 Generality

This study has emphasized on domestic refrigerator compressors. All the experimental data is from compressors with a refrigeration capacity below 1200 Btu/hr. However, the model that has been developed is more general and should also be valid for larger compressors.

In the literature, calorimeter testing data for a large air-conditioning compressor is available [Marriott (1973)]. This compressor has a refrigeration capacity of 18,500 But/hr at standard rating point conditions. There are 12 measured operating conditions. The model parameters were determined using all measured data. The average relative error in mass flow rate is 0.35% with a maximum error of 0.55% and an average relative error in power of 0.92% with a maximum error of 1.7%. The values for C and Δp that best fit the data are 0.0882 and 0.088 respectively. The combined efficiency varies between 49% and 51%.

8.2 Recommendations

In this research, the experimental data that were available was limited. It was only possible to test the extrapolation capabilities of the developed models at evaporating and

condensing temperature 10°C higher and lower than the data points used to fit the model. It would be useful to test the extrapolation capabilities over a wider range.

The model for the electrical power input developed in this research contains purely empirical parameters. It is desirable to develop a more physically-based model that would be more reliable for extrapolating.

A detailed study of larger compressors is necessary to determine whether the proposed model is valid for larger compressors than the models studied in this research.

Rating Point Recommendation

To generate an accurate compressor map, at least four measurements of mass flow rate and power at different condensing and evaporating conditions should be taken. The single rating point conditions currently used for rating compressors are -10°F (-23.3°C) evaporating and 130°F (54.4°C) condensing temperature at an ambient, suction and liquid line temperature of 90°F (32.2°C). This rating point is considerably different than conditions that refrigeration compressor typically operate at in systems today. A condensing temperature of 110°F (43.3°C) would better represent the actual operating conditions in a 90°F (32.2°C) ambient in today's products. The actual ambient temperature that most domestic refrigerator compressors operate at is lower than the standard test conditions of 32.2°C (90°F). But as seen in section 6.2, the influence of the ambient temperature on mass flow rate and power is fairly small and the proposed model seems to represent this change reasonable well.

Recommended Measurements During Testing

To fit the model parameters, measurements at at least four different operating conditions have to be made. It would be useful to take a fifth measurement at an operating condition in between the other four measurements to verify the model. This is at least 6 less than are necessary for the ARI method. While only measurements of electrical power and mass flow rate are necessary at these conditions, it would be useful to also report discharge and shell temperatures. Although these measurements have not been found useful in this investigation, it takes very little effort to report this additional information and it could help to understand the heat transfer off the shell and possibly help to model the combined efficiency or power.

Appendix A: Plots of All Measured Data

This appendix contains plots of the measured data of all 21 data sets. The data are plotted in form of compressor maps as mass flow rate and power versus evaporating temperatures. In addition, the data have been plotted as power per unit mass flow rate versus evaporating temperature.

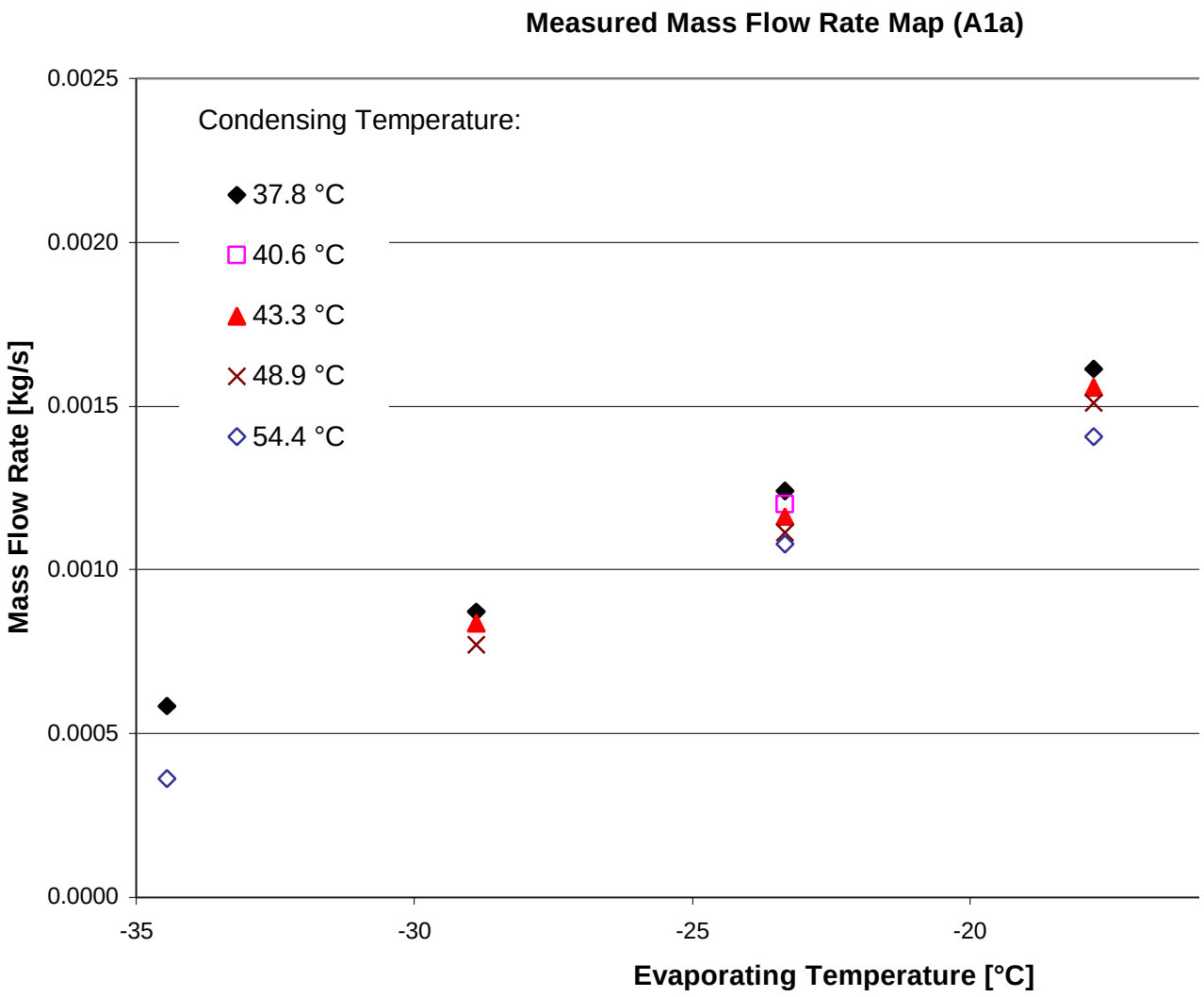
Measured Mass Flow Rate Map (A1a)
Mass Flow Rate [kg/s]
0.0025
0.0020
0.0015
0.0010
0.0005
0.0000
Condensing Temperature:
37.8 °C
40.6 °C
43.3 °C
48.9 °C
54.4 °C
-35
-30
-25
-20
Evaporating Temperature [°C]

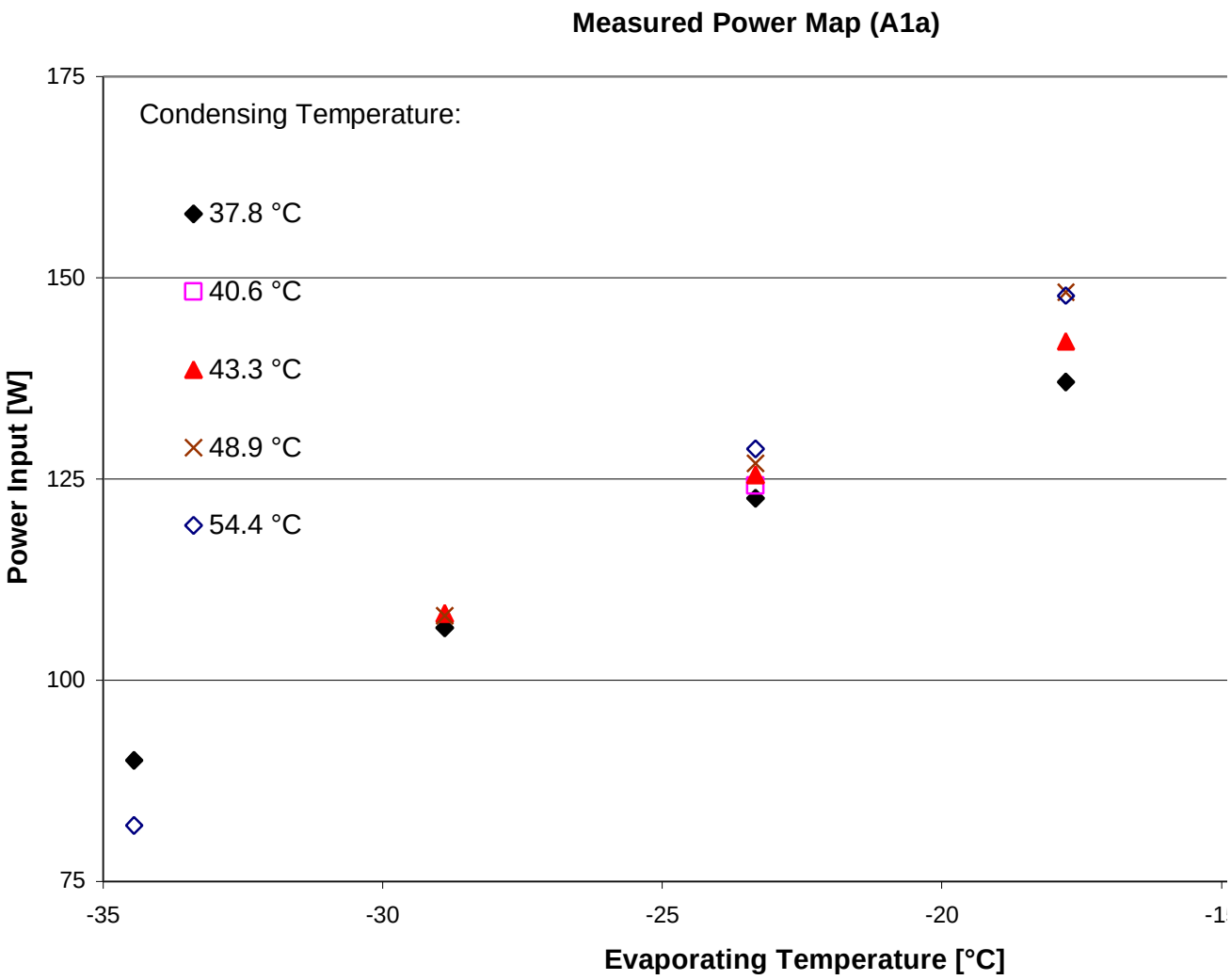
Measured Power Map (A1a)
Condensing Temperature:
37.8 °C
40.6 °C
43.3 °C
48.9 °C
54.4 °C
Power Input [W]
175
150
125
100
75
-35
-30
-25
-20
Evaporating Temperature [°C]

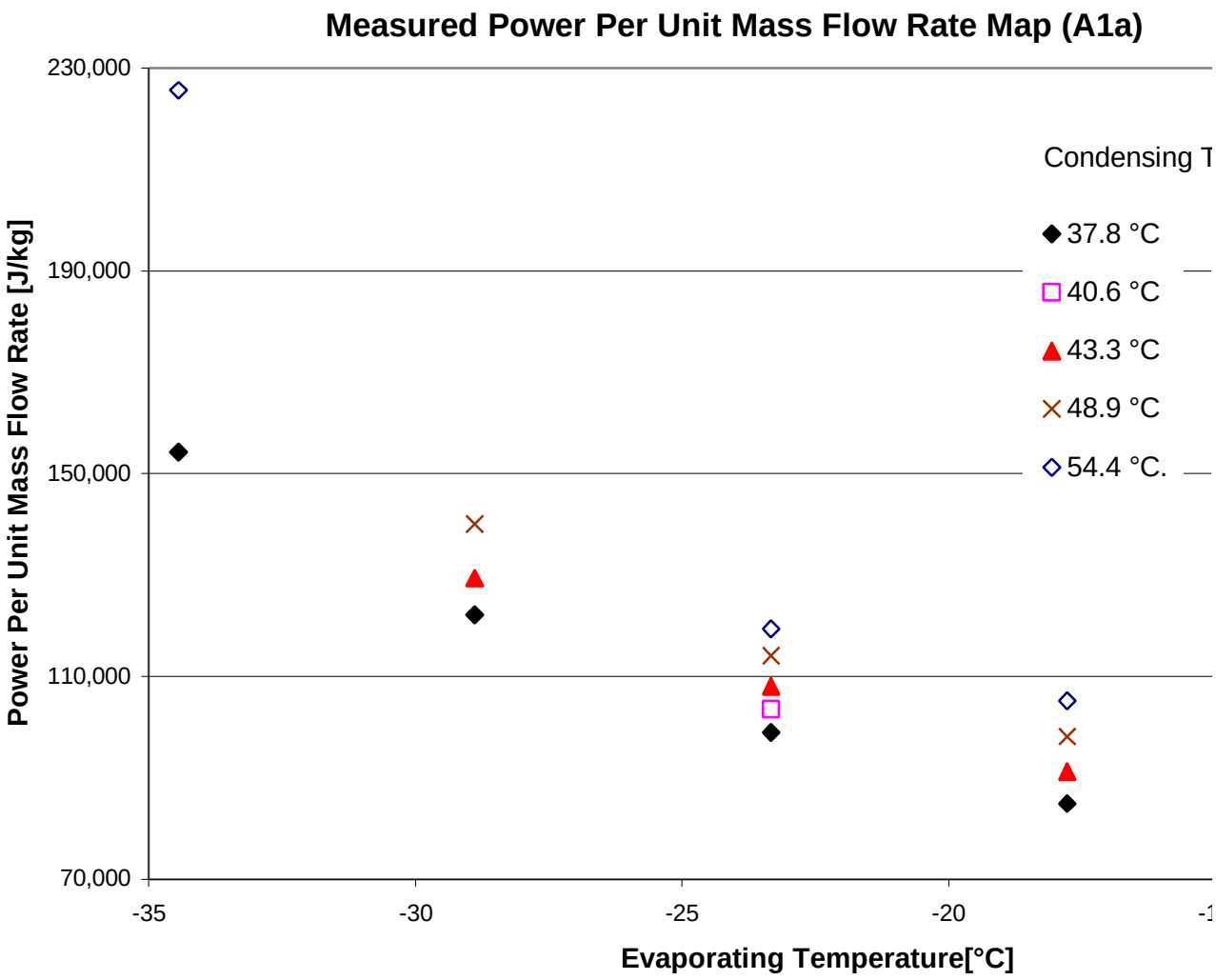
Measured Power Per Unit Mass Flow Rate Map (A1a)
Power Per Unit Mass Flow Rate [J/kg]
230,000
190,000
150,000
110,000
70,000
-35
-30
-25
-20
Evaporating Temperature[°C]
Condensing T
37.8 °C
40.6 °C
43.3 °C
48.9 °C
54.4 °C.

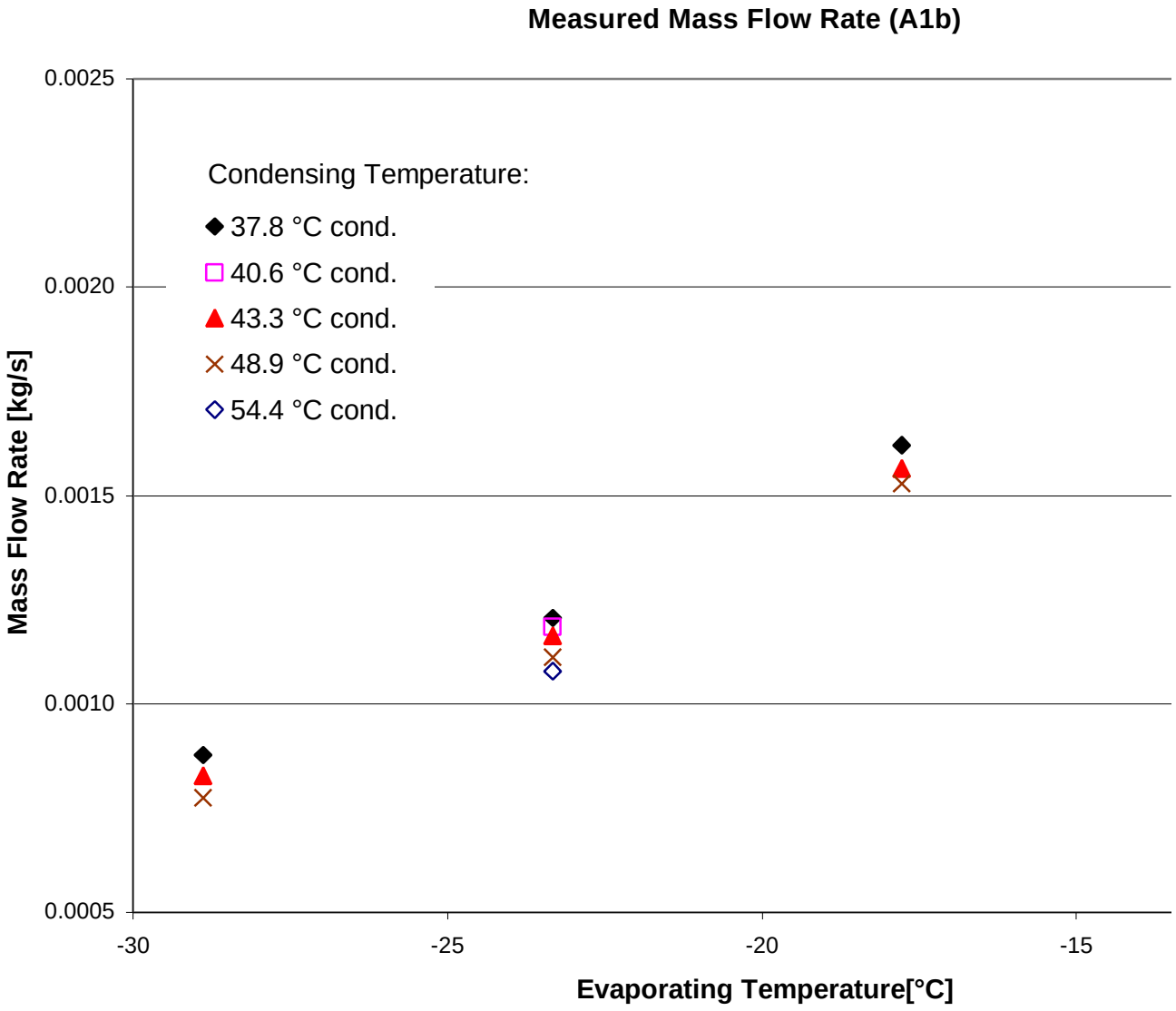
Measured Mass Flow Rate (A1b)
Mass Flow Rate [kg/s]
0.0025
0.0020
0.0015
0.0010
0.0005
Condensing Temperature:
37.8 °C cond.
40.6 °C cond.
43.3 °C cond.
48.9 °C cond.
54.4 °C cond.
-30
-25
-20
-15
Evaporating Temperature[°C]

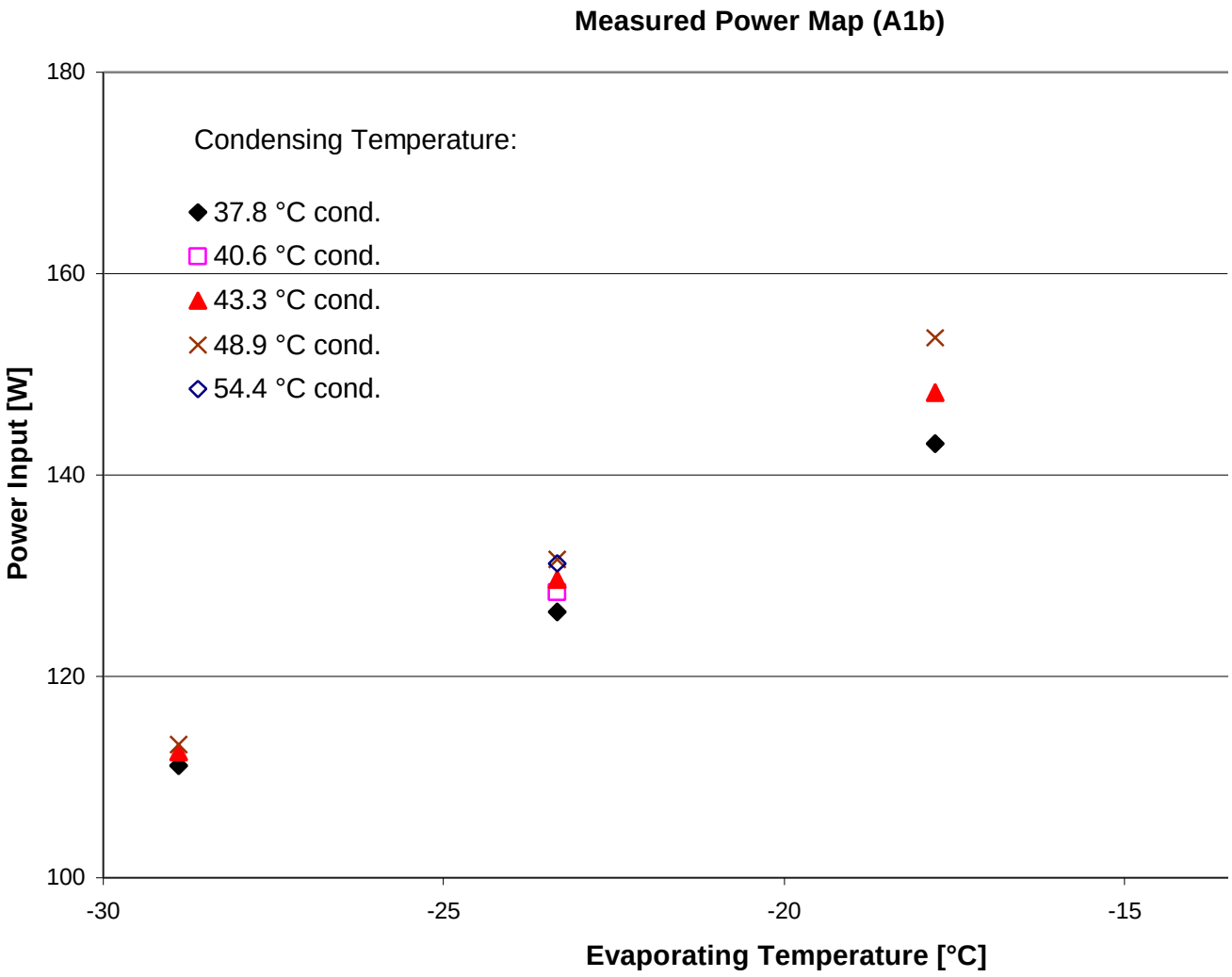
Measured Power Map (A1b)
Condensing Temperature:
37.8 °C cond.
40.6 °C cond.
43.3 °C cond.
48.9 °C cond.
54.4 °C cond.
Power Input [W]
180
160
140
120
100
-30
-25
-20
-15
Evaporating Temperature [°C]

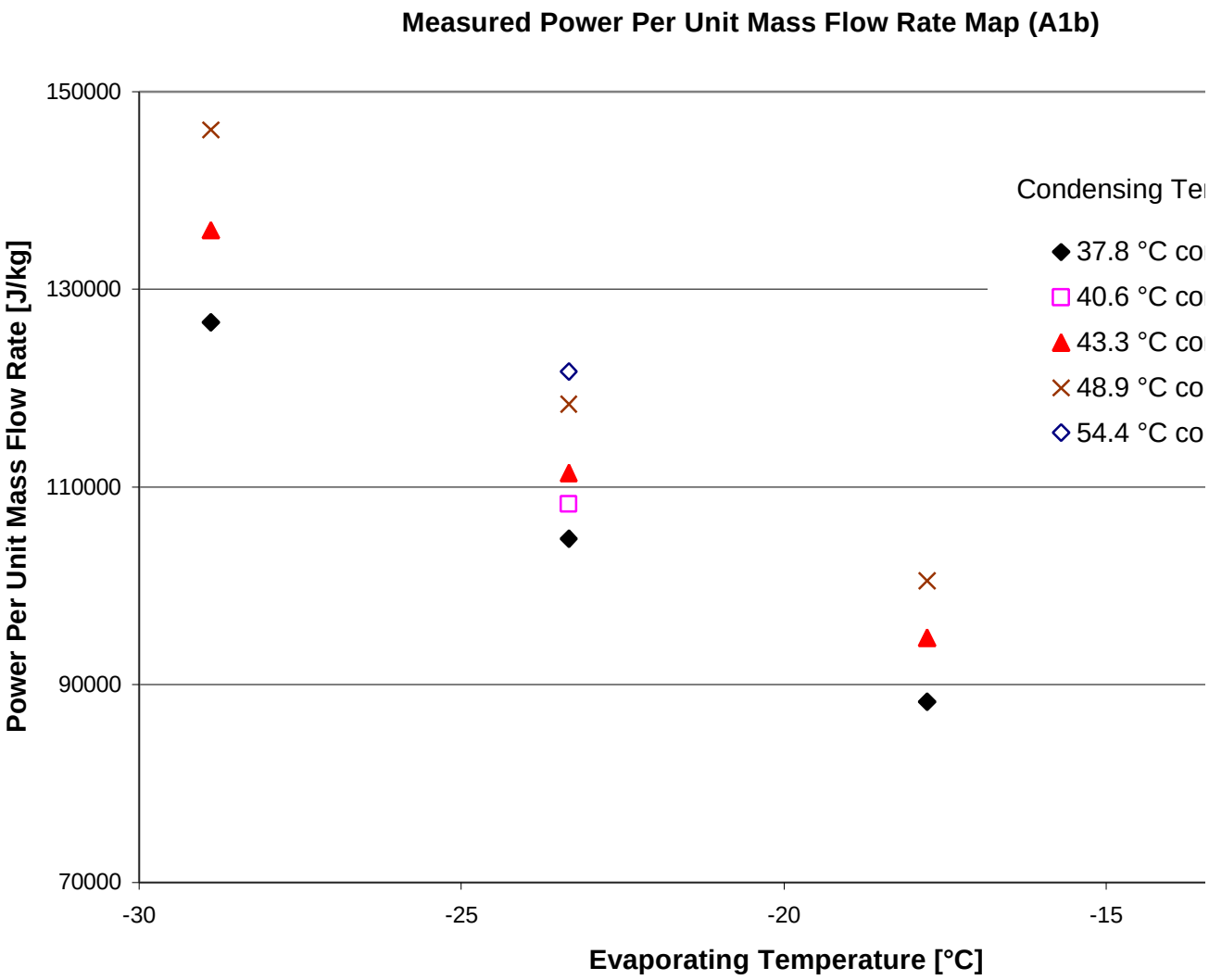
Measured Power Per Unit Mass Flow Rate Map (A1b)
Power Per Unit Mass Flow Rate [J/kg]
150000
130000
110000
90000
70000
-30
-25
-20
-15
Evaporating Temperature [°C]
Condensing Te
37.8 °C co
40.6 °C co
43.3 °C co
48.9 °C co
54.4 °C co

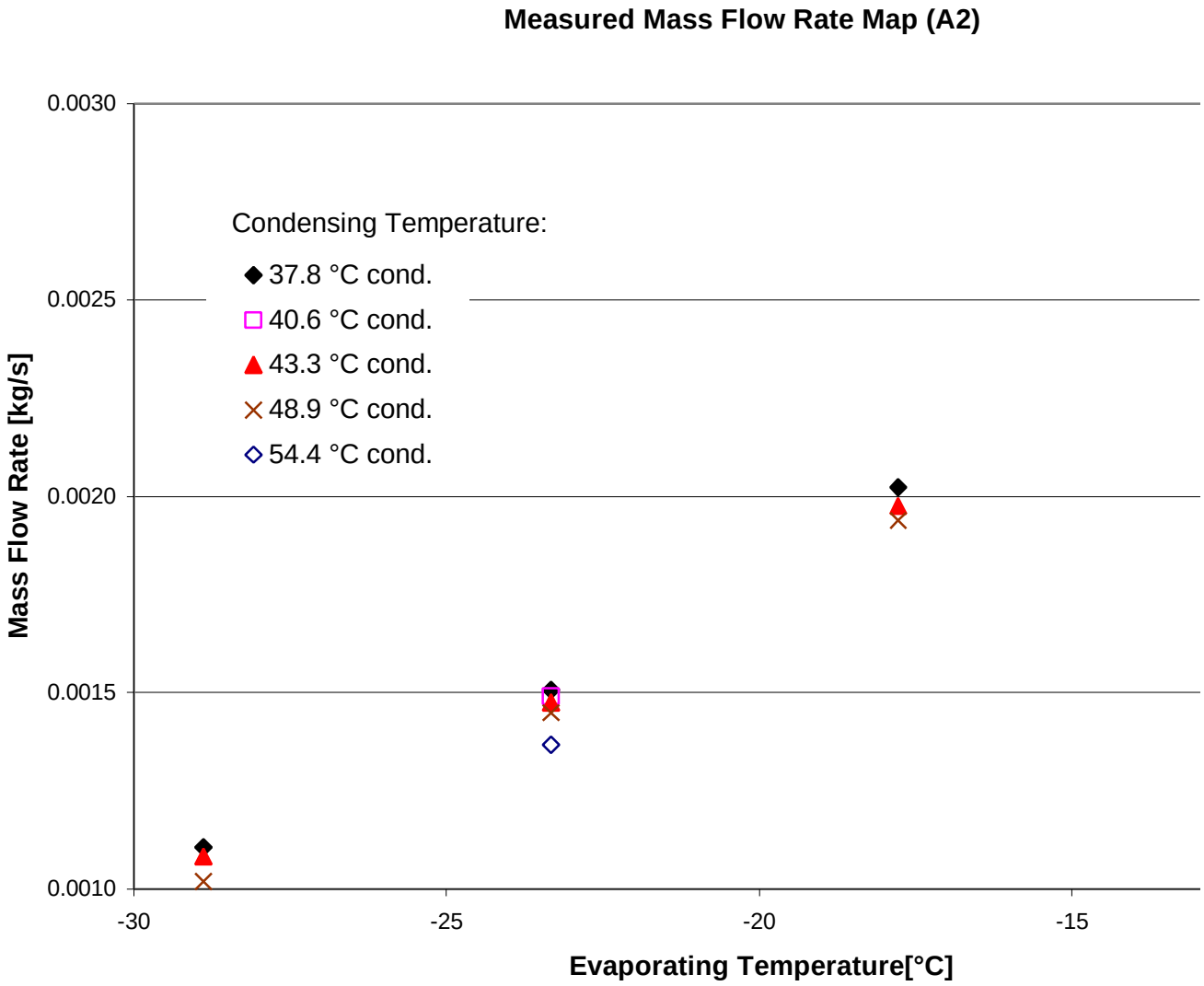
Measured Mass Flow Rate Map (A2)
0.0030
0.0025
0.0020
0.0015
0.0010
Mass Flow Rate [kg/s]
Condensing Temperature:
37.8 °C cond.
40.6 °C cond.
43.3 °C cond.
48.9 °C cond.
54.4 °C cond.
-30
-25
-20
-15
Evaporating Temperature[°C]

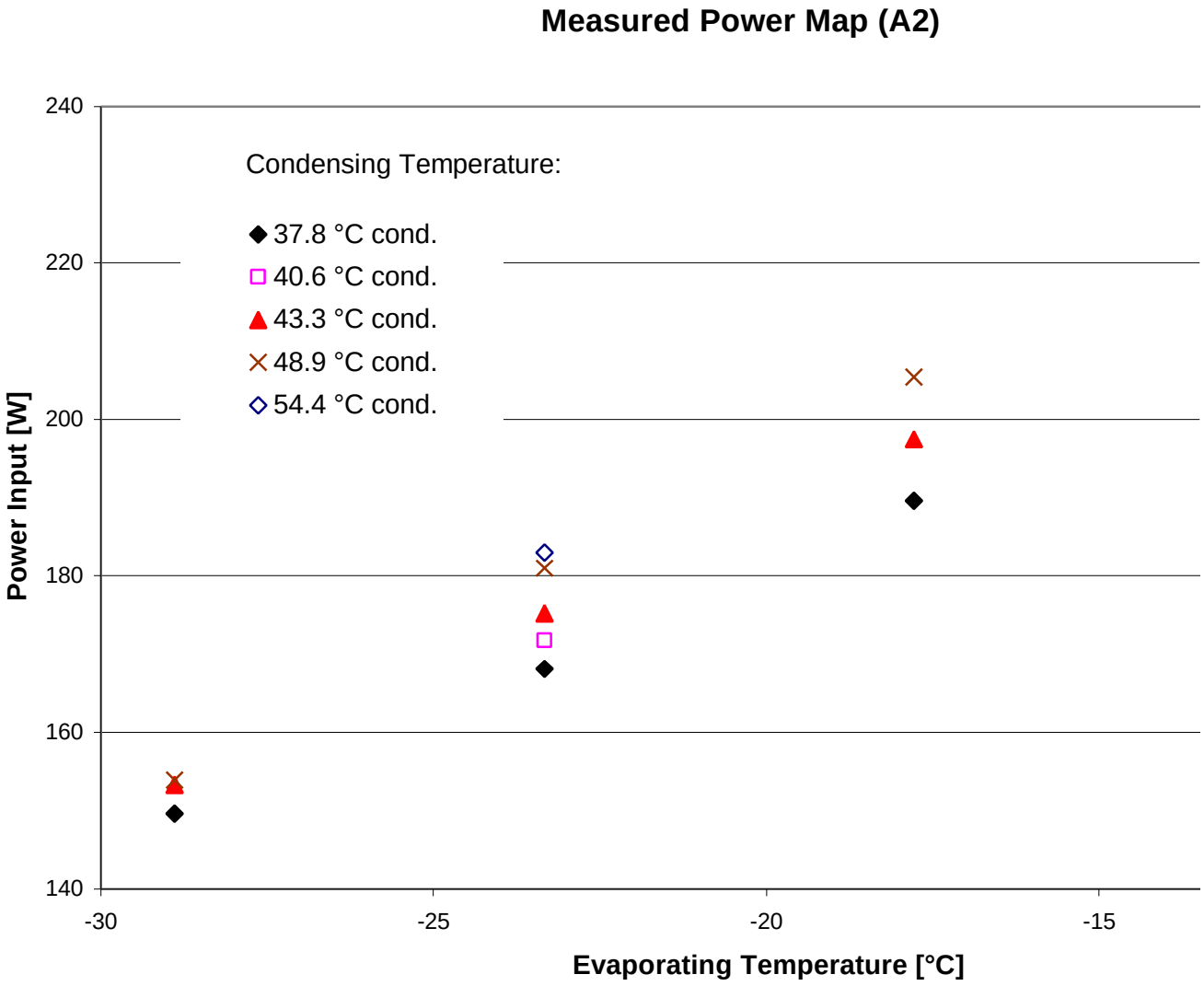
Measured Power Map (A2)
Condensing Temperature:
37.8 °C cond.
40.6 °C cond.
43.3 °C cond.
48.9 °C cond.
54.4 °C cond.
Power Input [W]
240
220
200
180
160
140
-30
-25
-20
-15
Evaporating Temperature [°C]

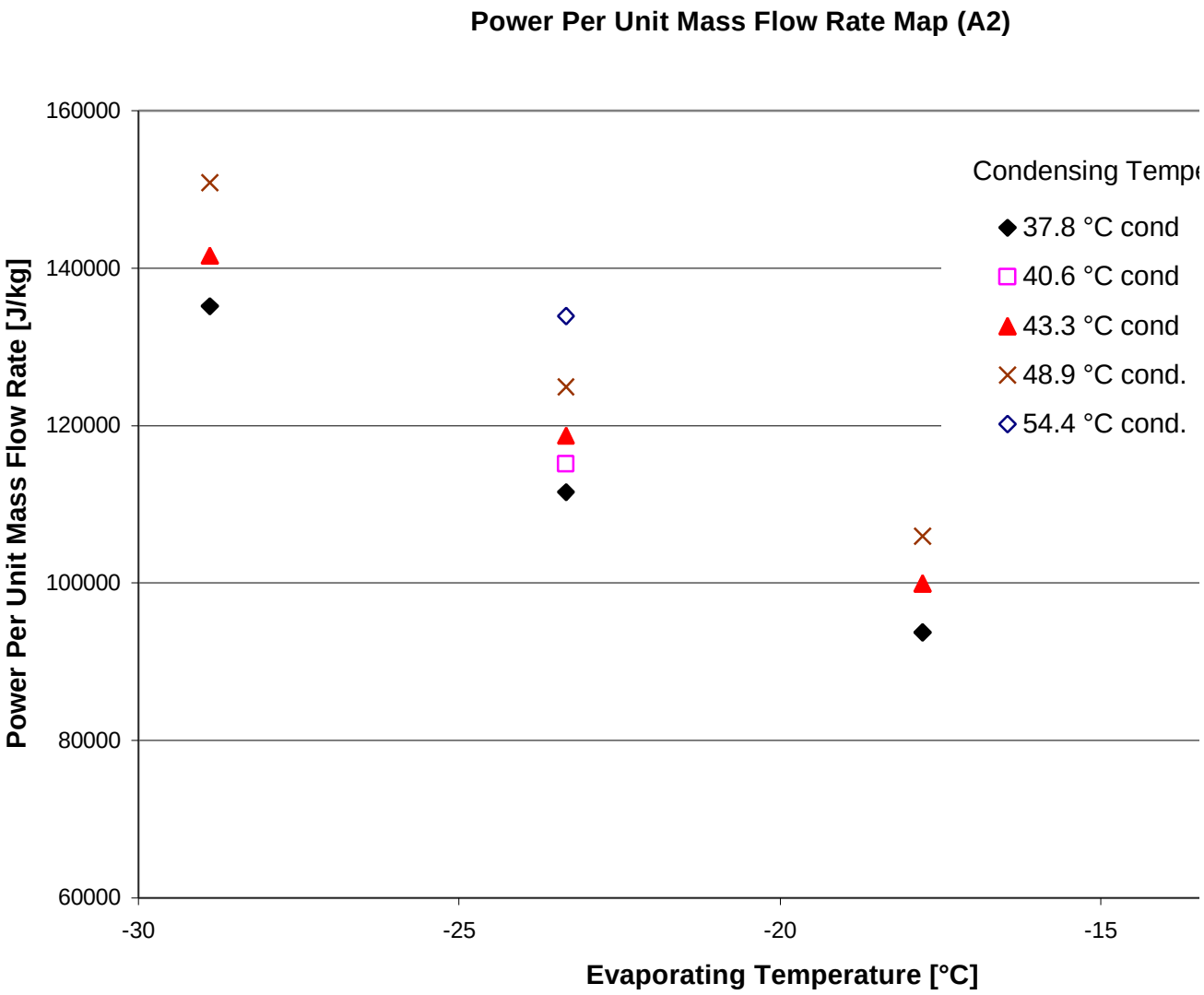
Power Per Unit Mass Flow Rate Map (A2)
Power Per Unit Mass Flow Rate [J/kg]
160000
140000
120000
100000
80000
60000
-30
-25
-20
-15
Evaporating Temperature [°C]
Condensing Tempe
37.8 °C cond
40.6 °C cond
43.3 °C cond
48.9 °C cond.
54.4 °C cond.

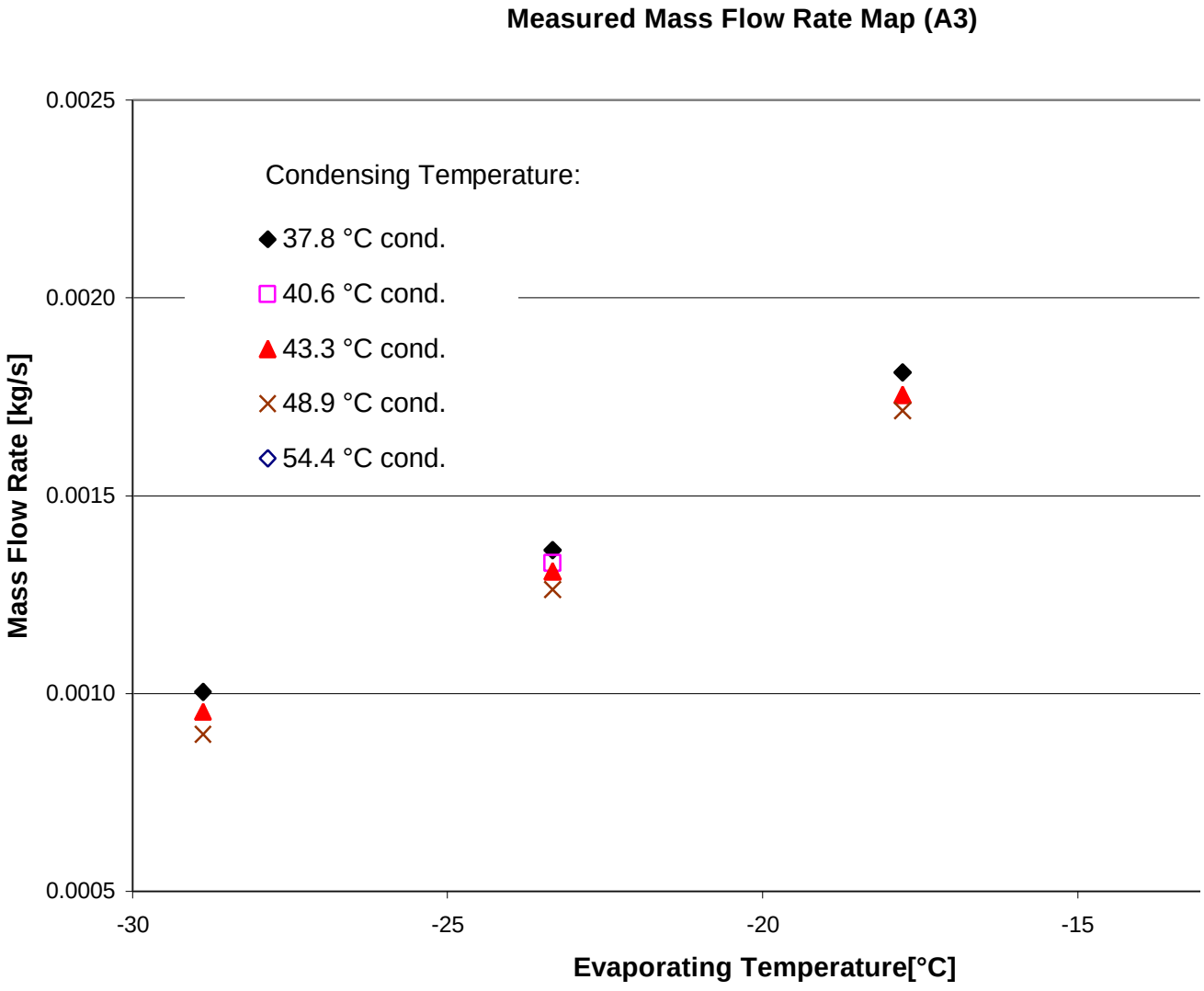
Measured Mass Flow Rate Map (A3)
Mass Flow Rate [kg/s]
0.0025
0.0020
0.0015
0.0010
0.0005
Condensing Temperature:
37.8 °C cond.
40.6 °C cond.
43.3 °C cond.
48.9 °C cond.
54.4 °C cond.
-30
-25
-20
-15
Evaporating Temperature[°C]

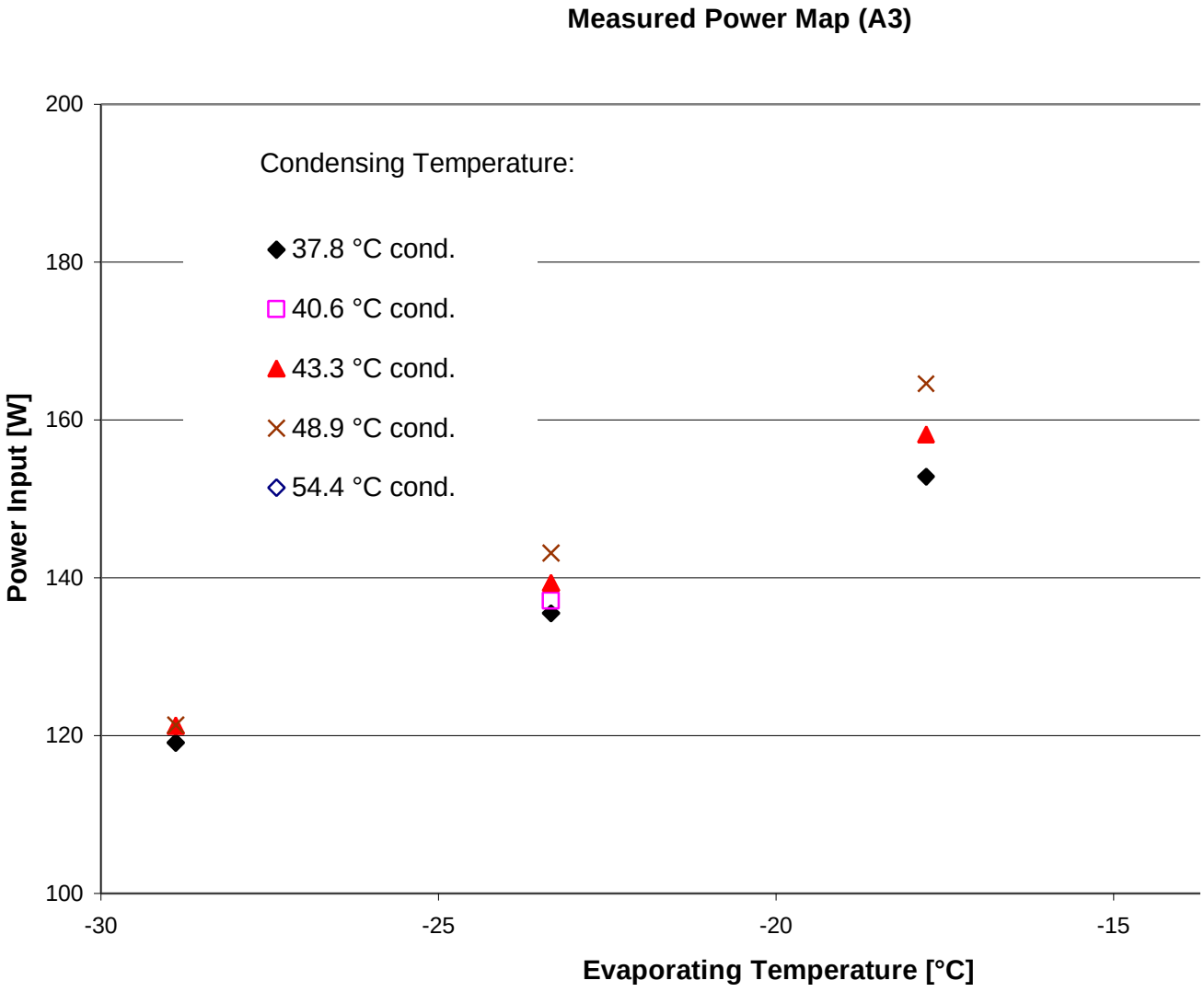
Measured Power Map (A3)
Condensing Temperature:
37.8 °C cond.
40.6 °C cond.
43.3 °C cond.
48.9 °C cond.
54.4 °C cond.
Power Input [W]
200
180
160
140
120
100
-30
-25
-20
-15
Evaporating Temperature [°C]

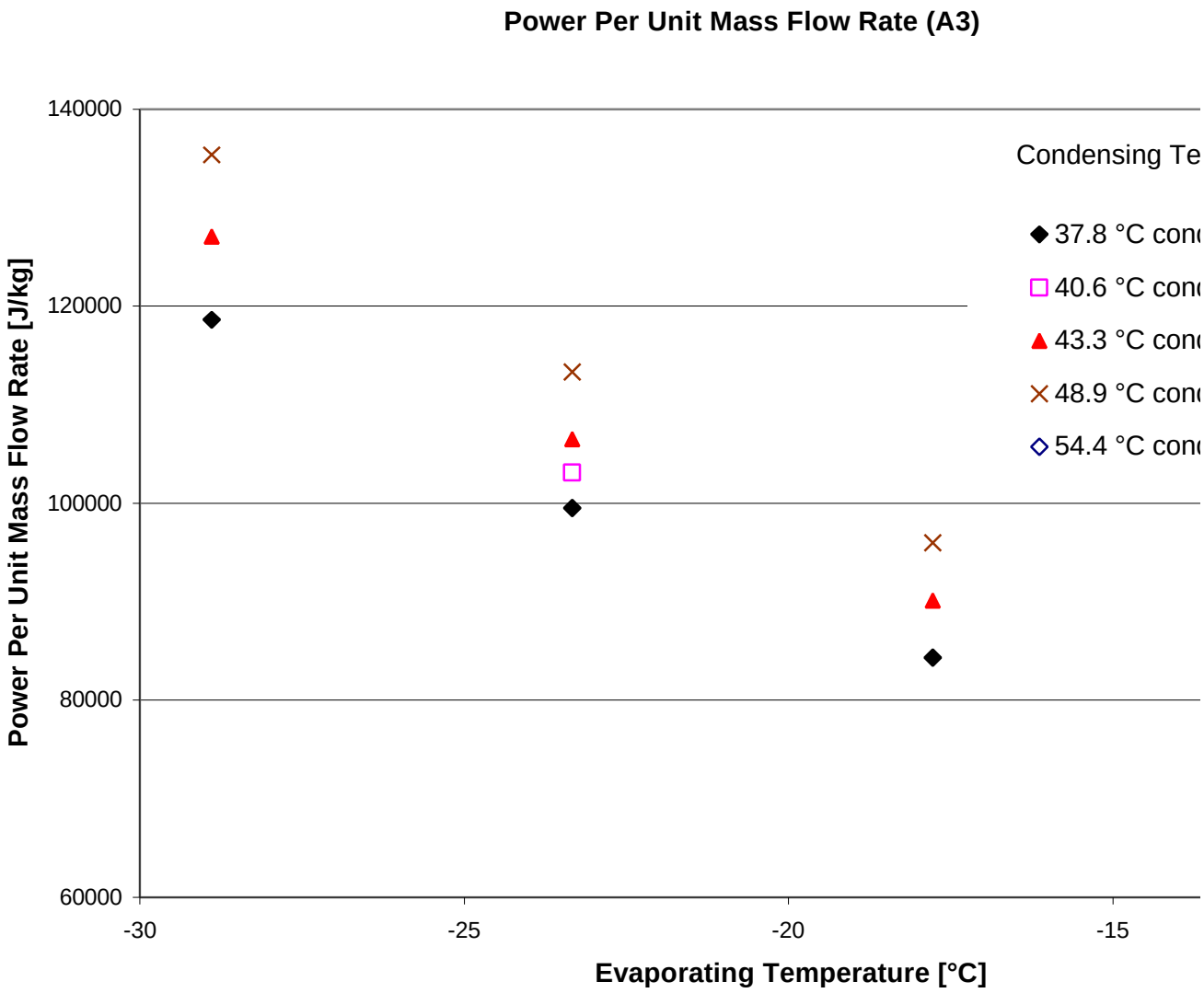
Power Per Unit Mass Flow Rate (A3)
Power Per Unit Mass Flow Rate [J/kg]
140000
120000
100000
80000
60000
-30
-25
-20
-15
Evaporating Temperature [°C]
Condensing Te
37.8 °C cond
40.6 °C cond
43.3 °C cond
48.9 °C cond
54.4 °C cond

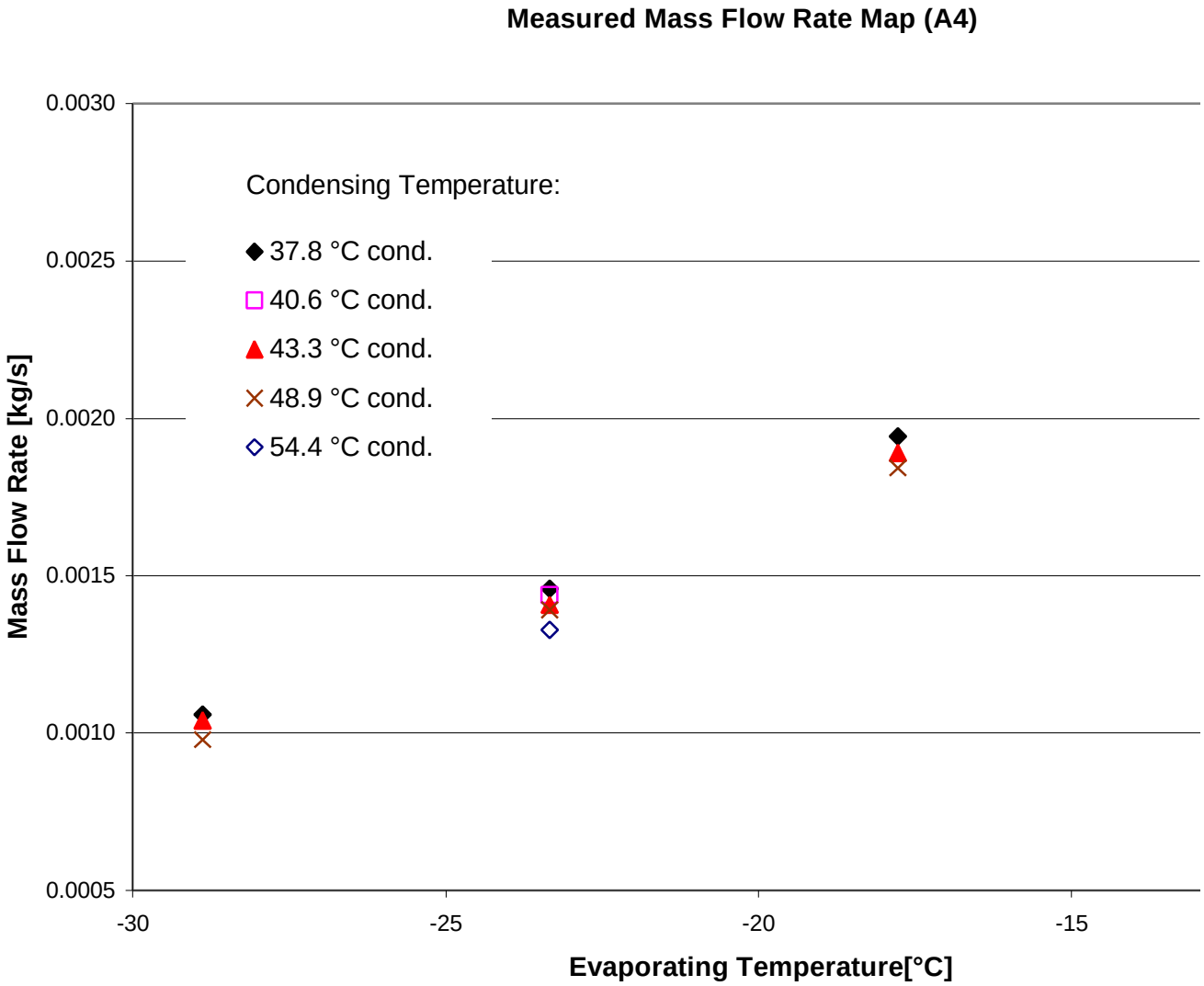
Measured Mass Flow Rate Map (A4)
Mass Flow Rate [kg/s]
0.0030
0.0025
0.0020
0.0015
0.0010
0.0005
Condensing Temperature:
37.8 °C cond.
40.6 °C cond.
43.3 °C cond.
48.9 °C cond.
54.4 °C cond.
-30
-25
-20
-15
Evaporating Temperature[°C]

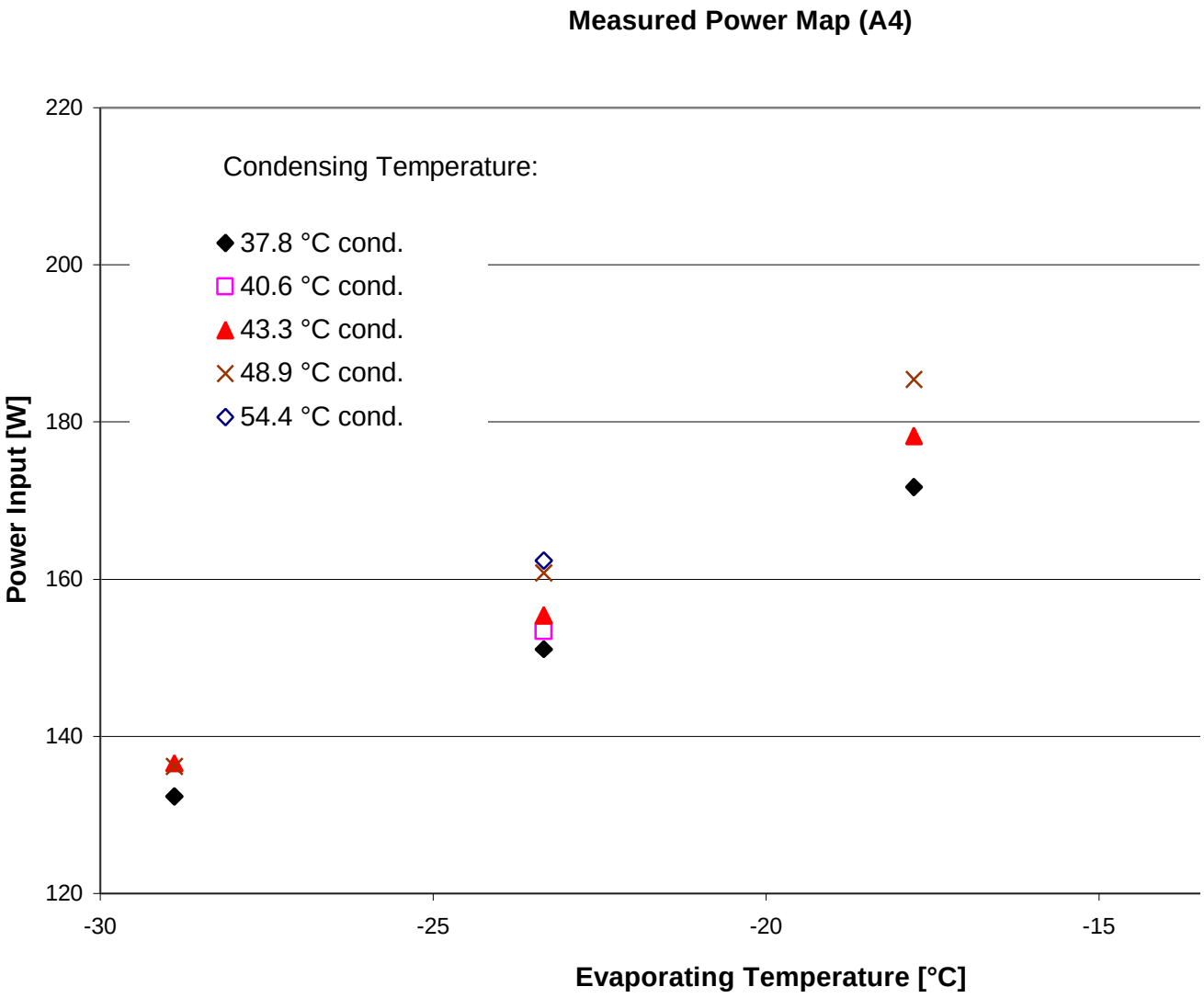
Measured Power Map (A4)
Condensing Temperature:
37.8 °C cond.
40.6 °C cond.
43.3 °C cond.
48.9 °C cond.
54.4 °C cond.
Power Input [W]
220
200
180
160
140
120
-30
-25
-20
-15
Evaporating Temperature [°C]

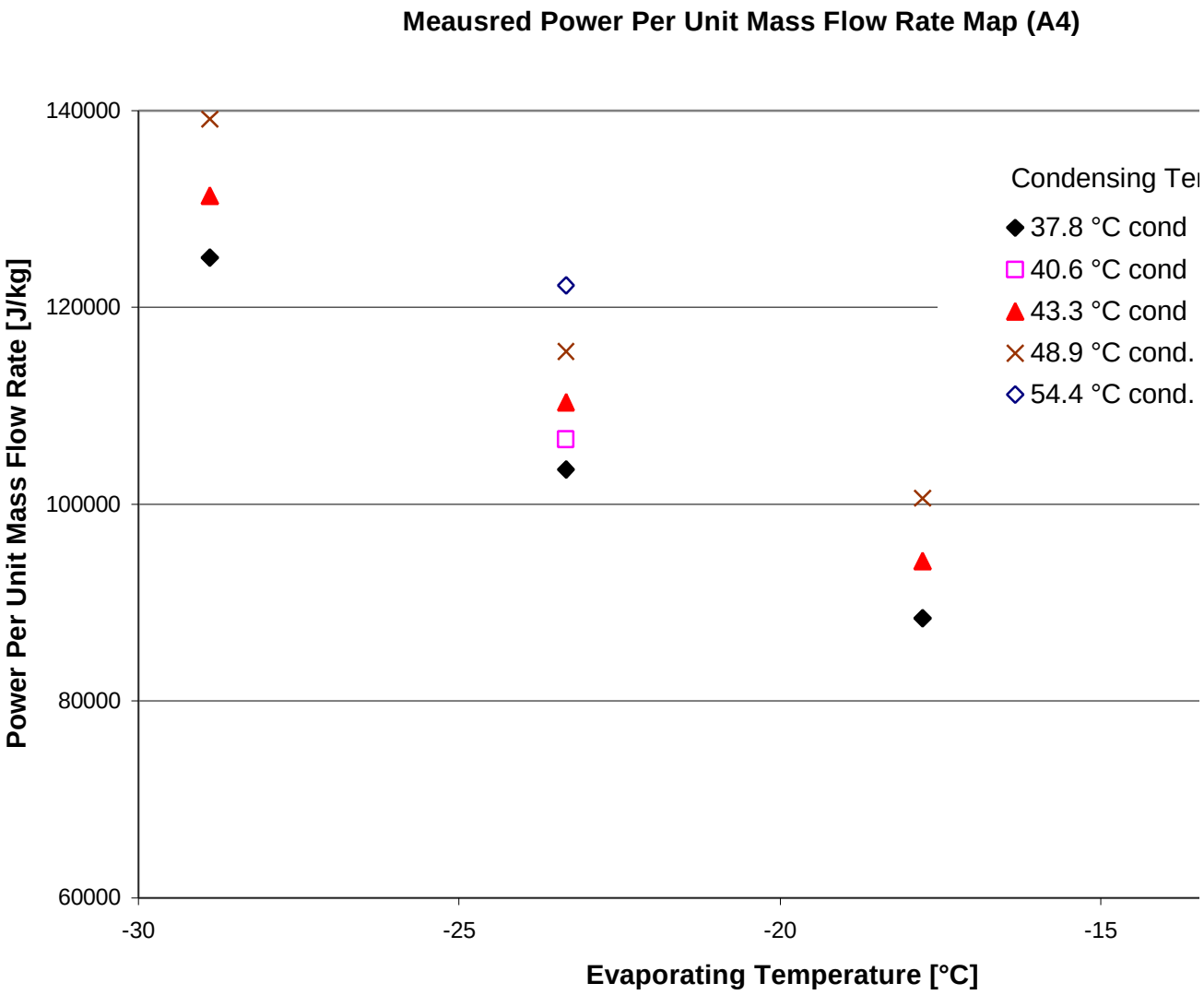
Meausred Power Per Unit Mass Flow Rate Map (A4)
Power Per Unit Mass Flow Rate [J/kg]
140000
120000
100000
80000
60000
-30
-25
-20
-15
Evaporating Temperature [°C]
Condensing Tei
37.8 °C cond
40.6 °C cond
43.3 °C cond
48.9 °C cond.
54.4 °C cond.

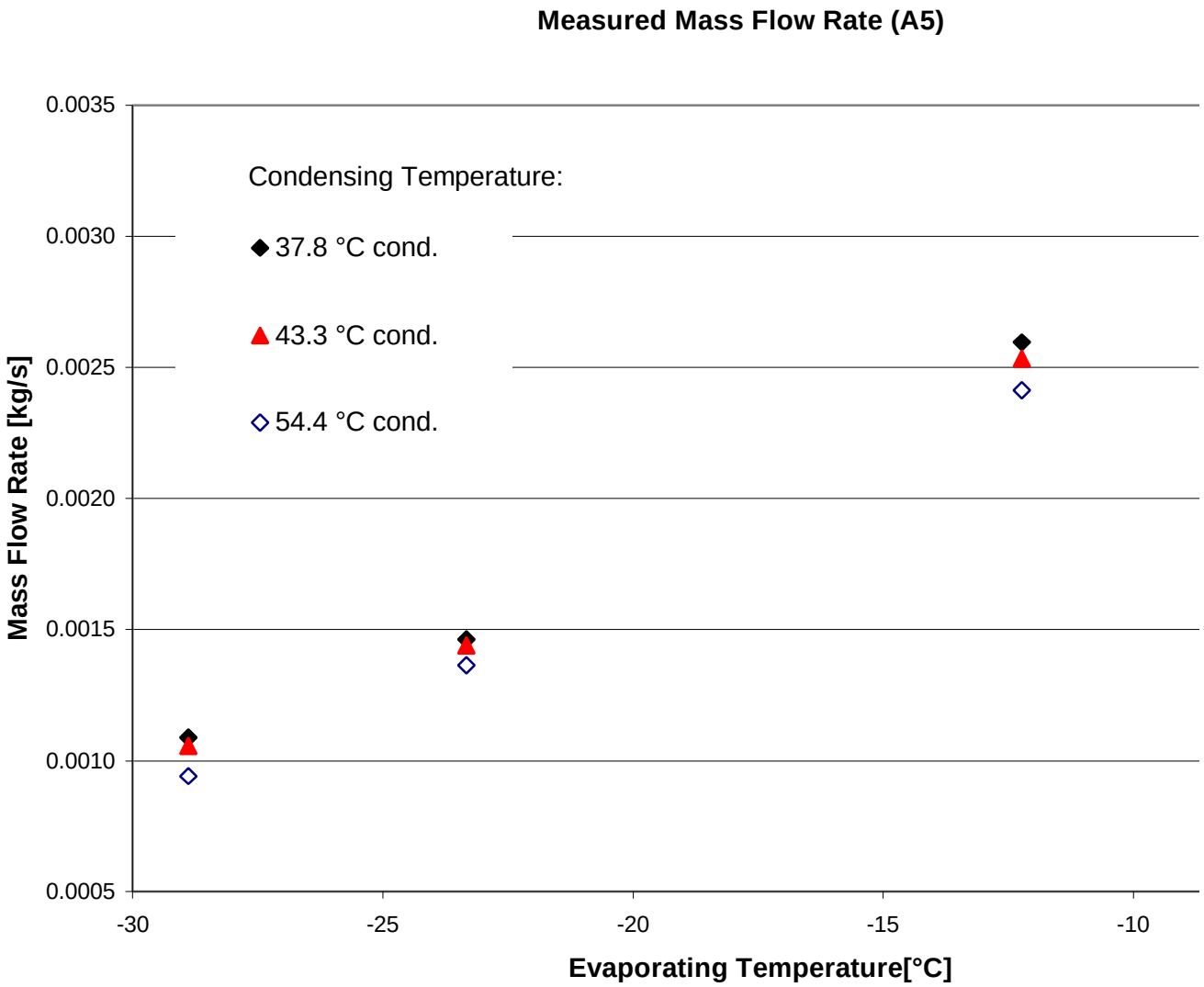
Measured Mass Flow Rate (A5)
Mass Flow Rate [kg/s]
0.0035
0.0030
0.0025
0.0020
0.0015
0.0010
0.0005
Condensing Temperature:
37.8 °C cond.
43.3 °C cond.
54.4 °C cond.
-30
-25
-20
-15
-10
Evaporating Temperature[°C]

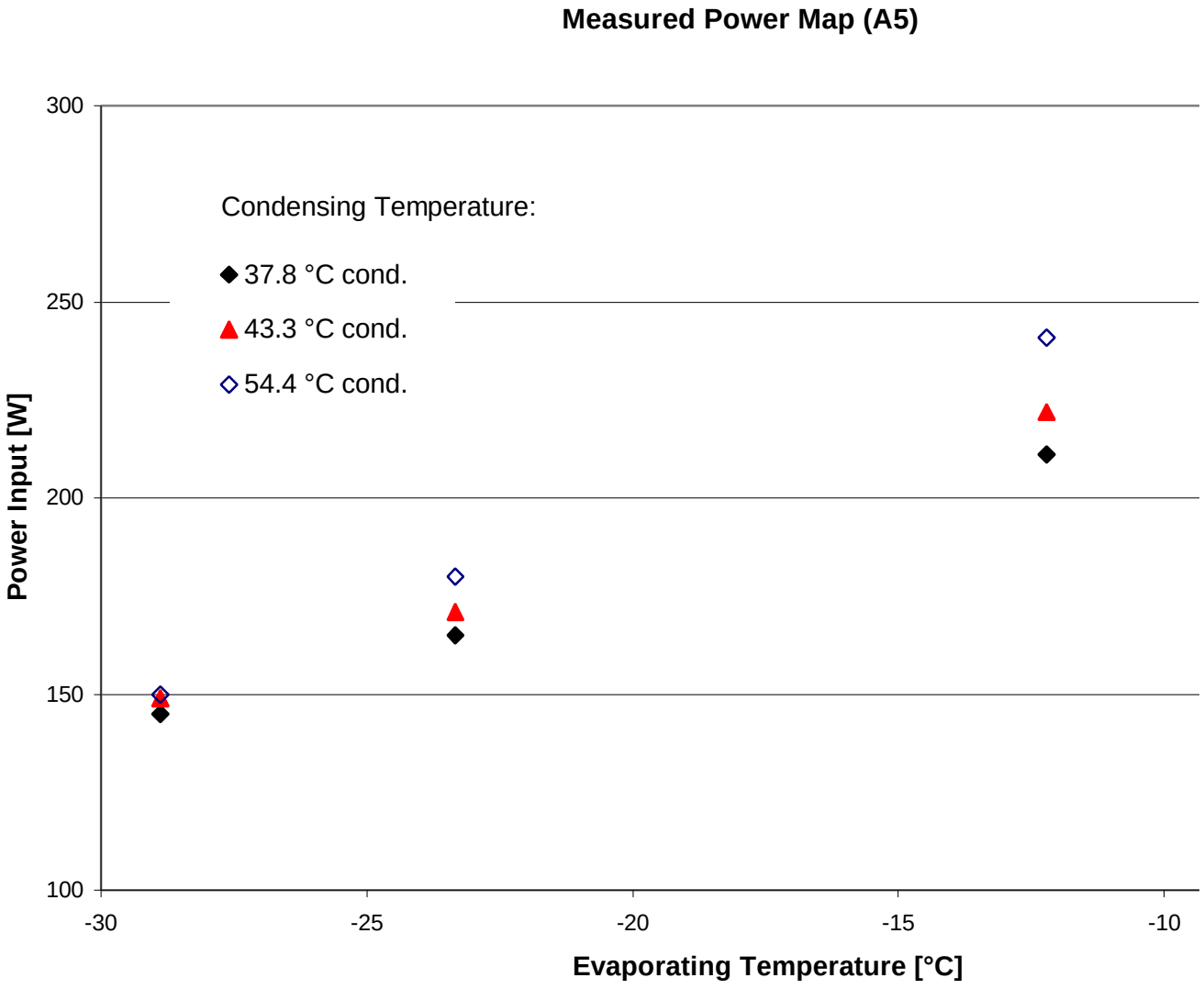
Measured Power Map (A5)
Power Input [W]
300
250
200
150
100
Condensing Temperature:
37.8 °C cond.
43.3 °C cond.
54.4 °C cond.
-30
-25
-20
-15
-10
Evaporating Temperature [°C]

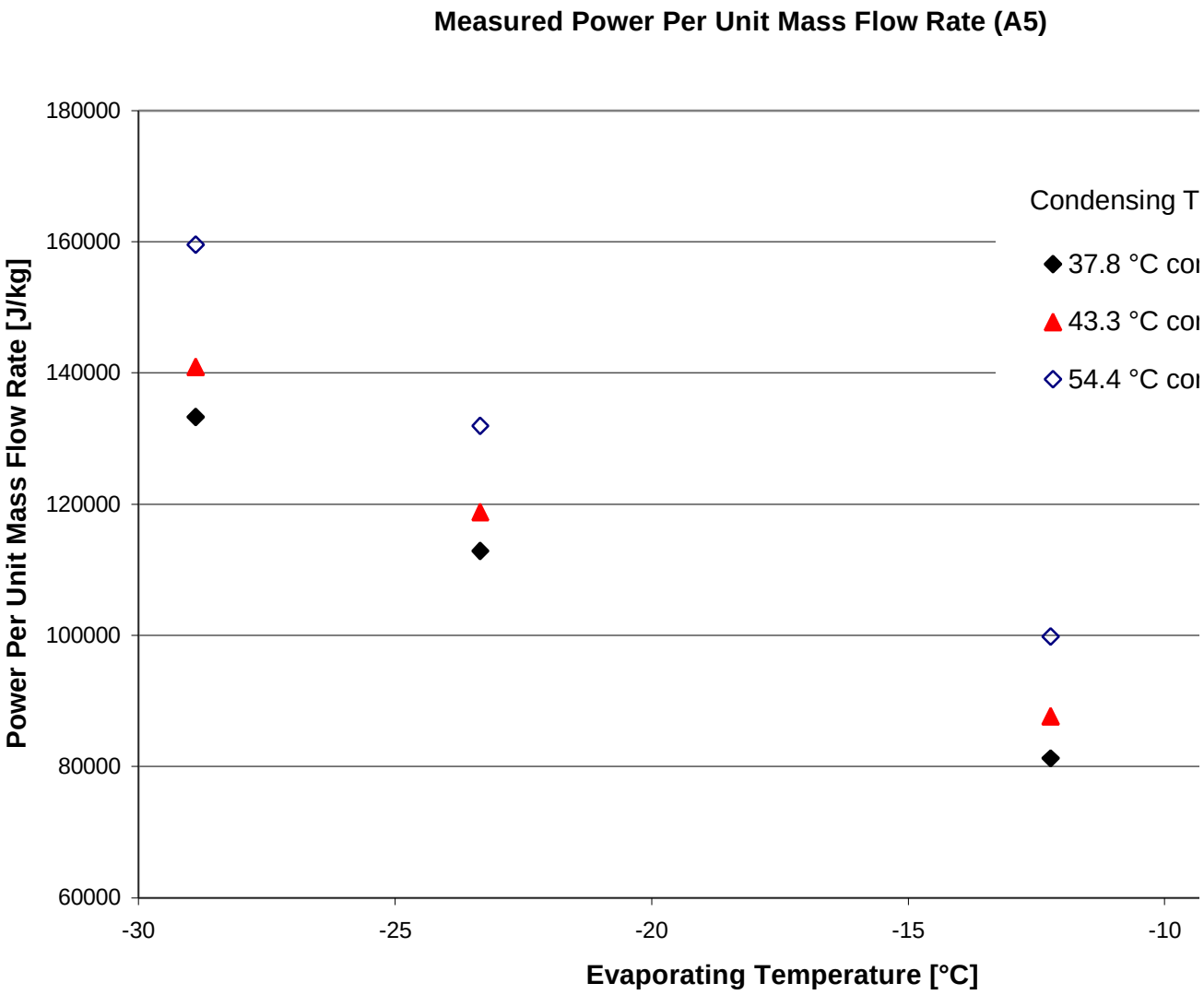
Measured Power Per Unit Mass Flow Rate (A5)
Power Per Unit Mass Flow Rate [J/kg]
180000
160000
140000
120000
100000
80000
60000
-30
-25
-20
-15
-10
Evaporating Temperature [°C]
Condensing T
37.8 °C co
43.3 °C co
54.4 °C co

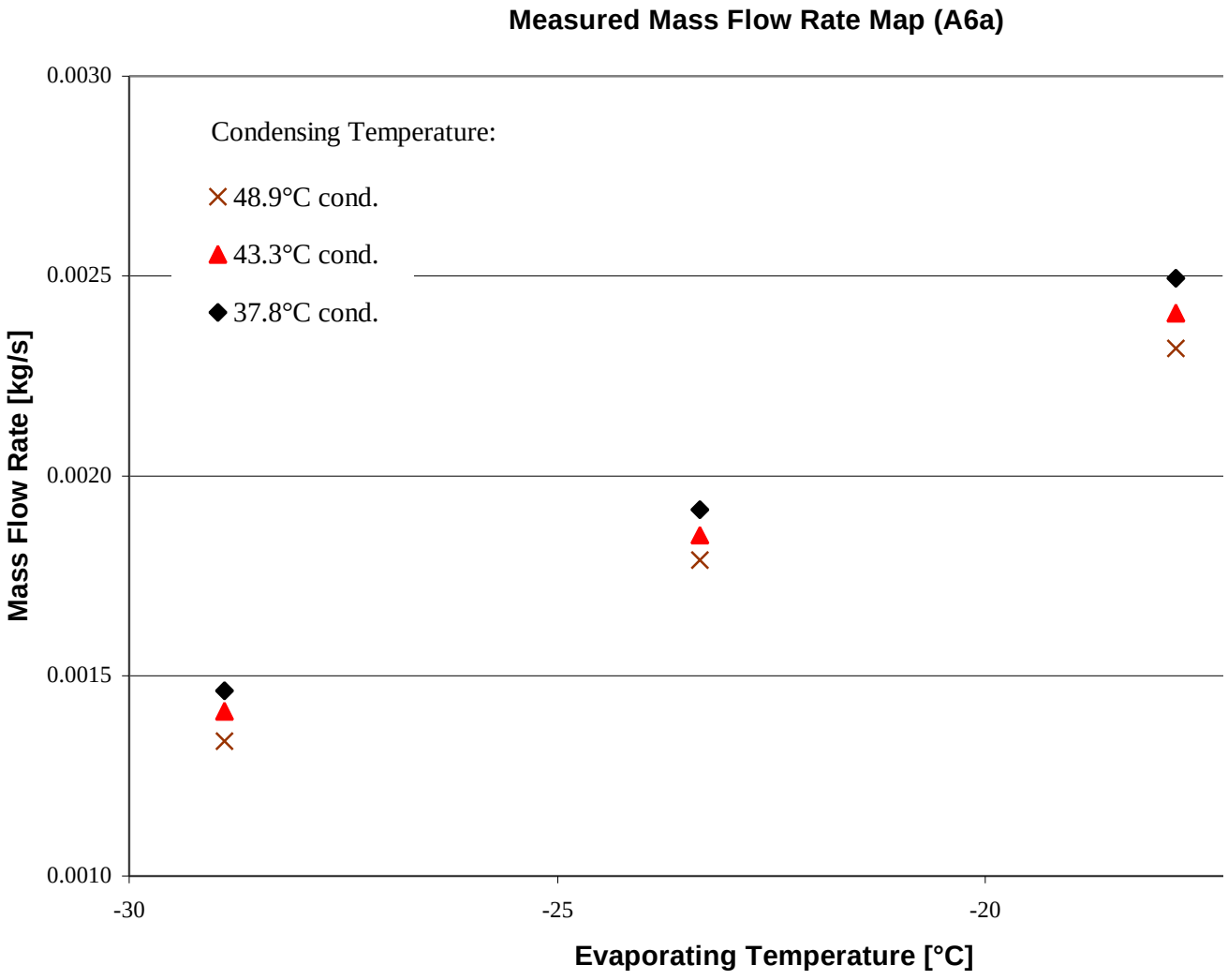
Measured Mass Flow Rate Map (A6a)
Mass Flow Rate [kg/s]
0.0030
0.0025
0.0020
0.0015
0.0010
Condensing Temperature:
48.9°C cond.
43.3°C cond.
37.8°C cond.
-30
-25
-20
Evaporating Temperature [°C]

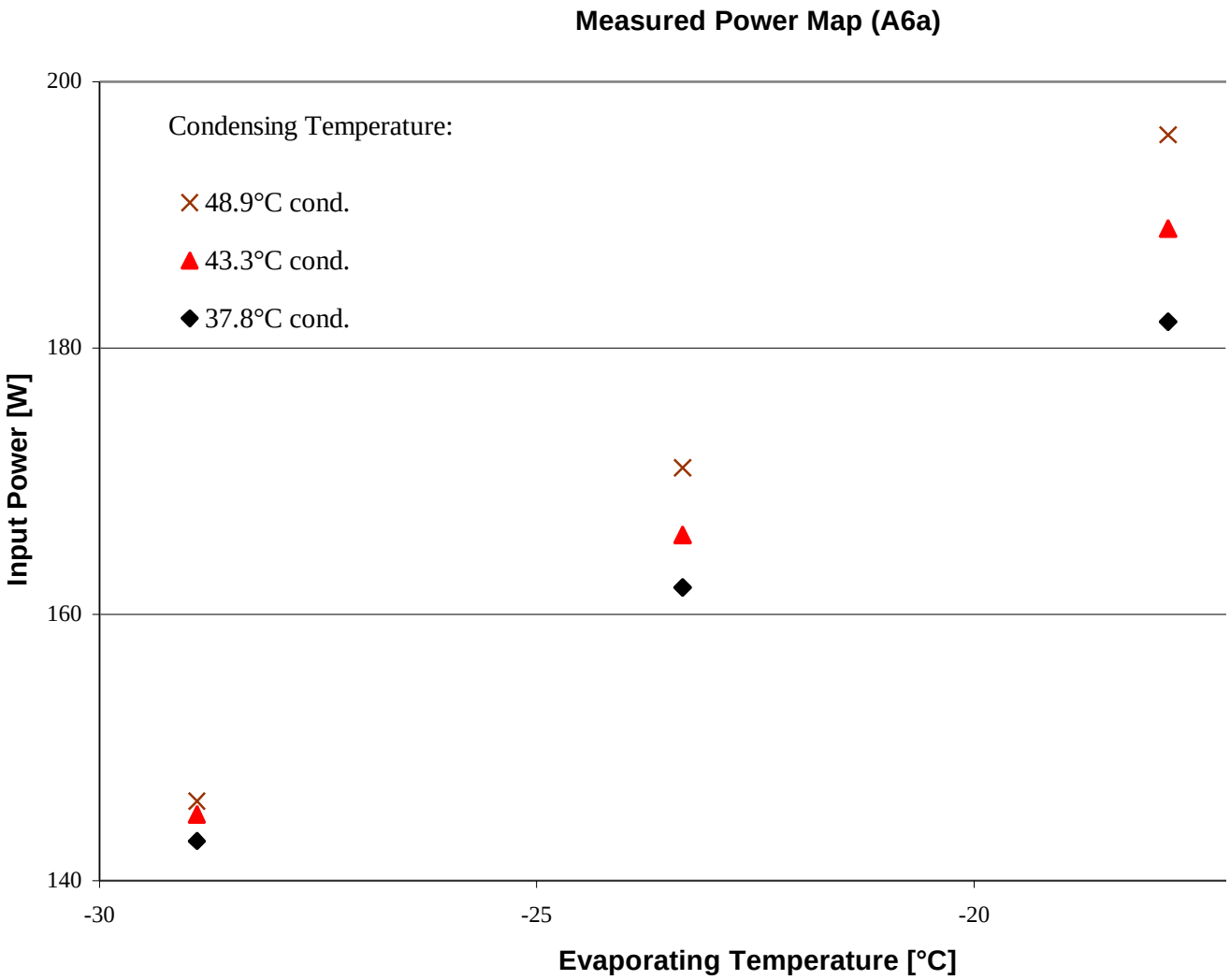
Measured Power Map (A6a)
Condensing Temperature:
48.9°C cond.
43.3°C cond.
37.8°C cond.
Input Power [W]
200
180
160
140
-30
-25
-20
Evaporating Temperature [°C]

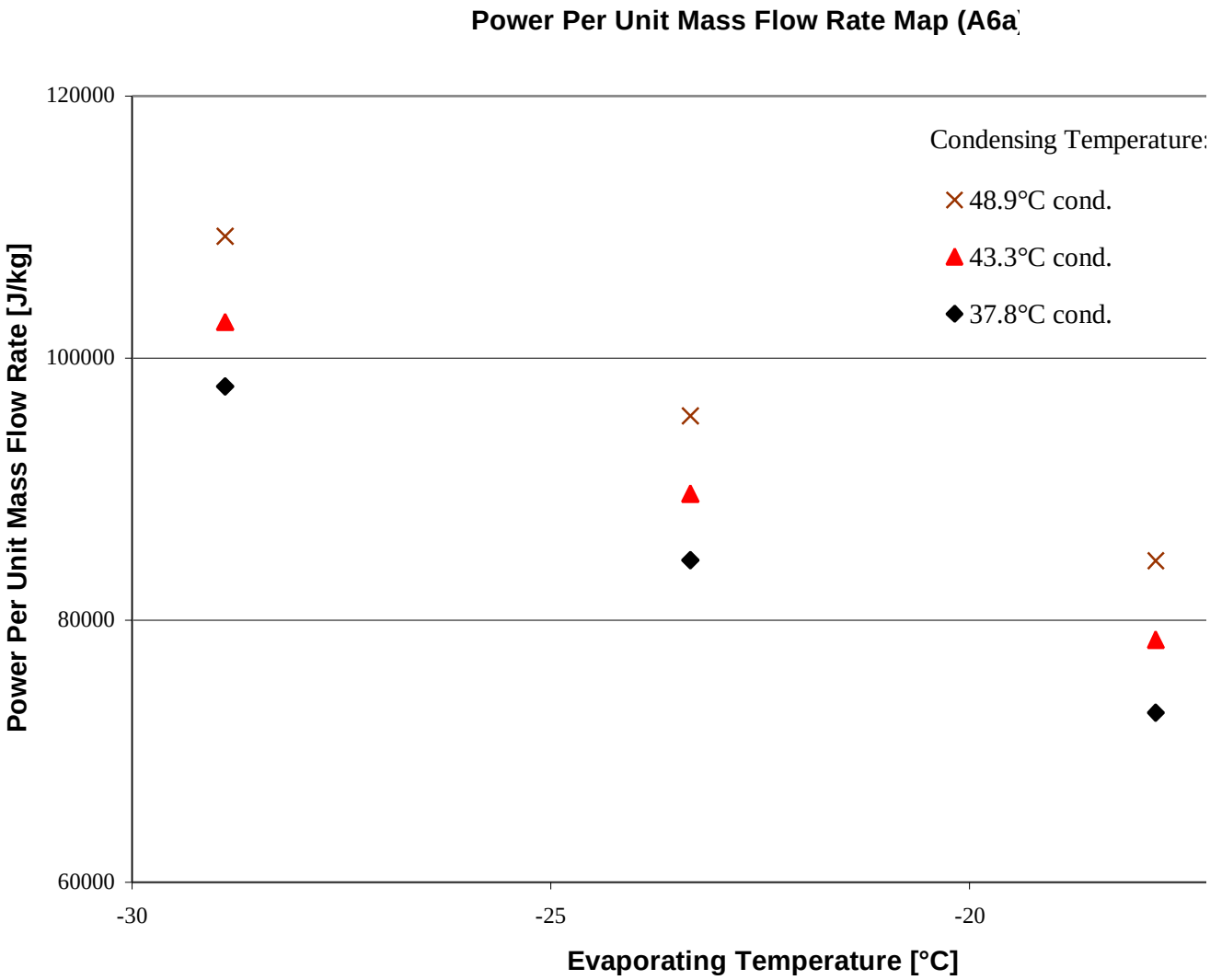
Power Per Unit Mass Flow Rate Map (A6a)
Power Per Unit Mass Flow Rate [J/kg]
120000
100000
80000
60000
-30
-25
-20
Evaporating Temperature [°C]
Condensing Temperature:
48.9°C cond.
43.3°C cond.
37.8°C cond.

Measured Mass Flow Rate Map (A6b)

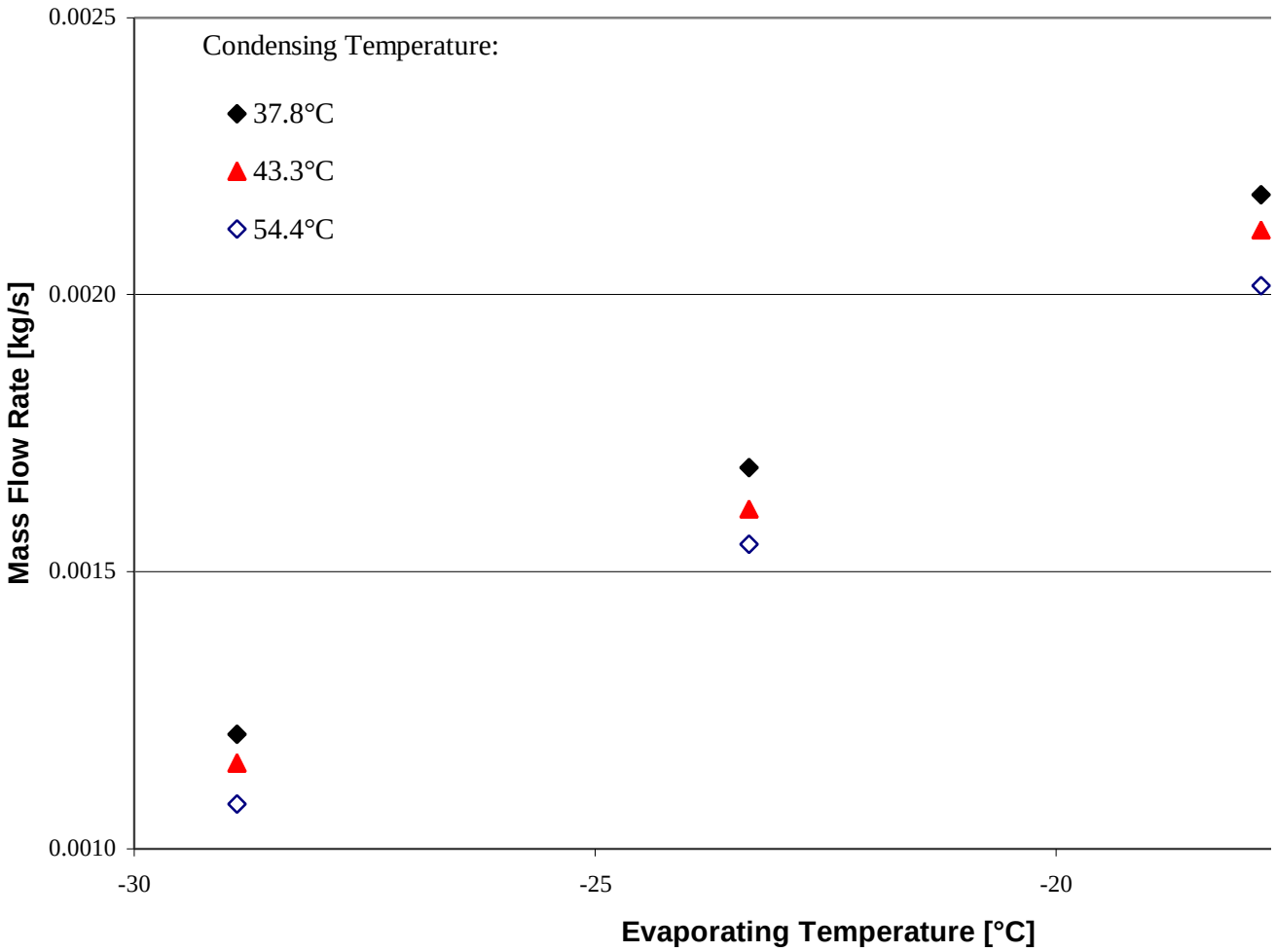

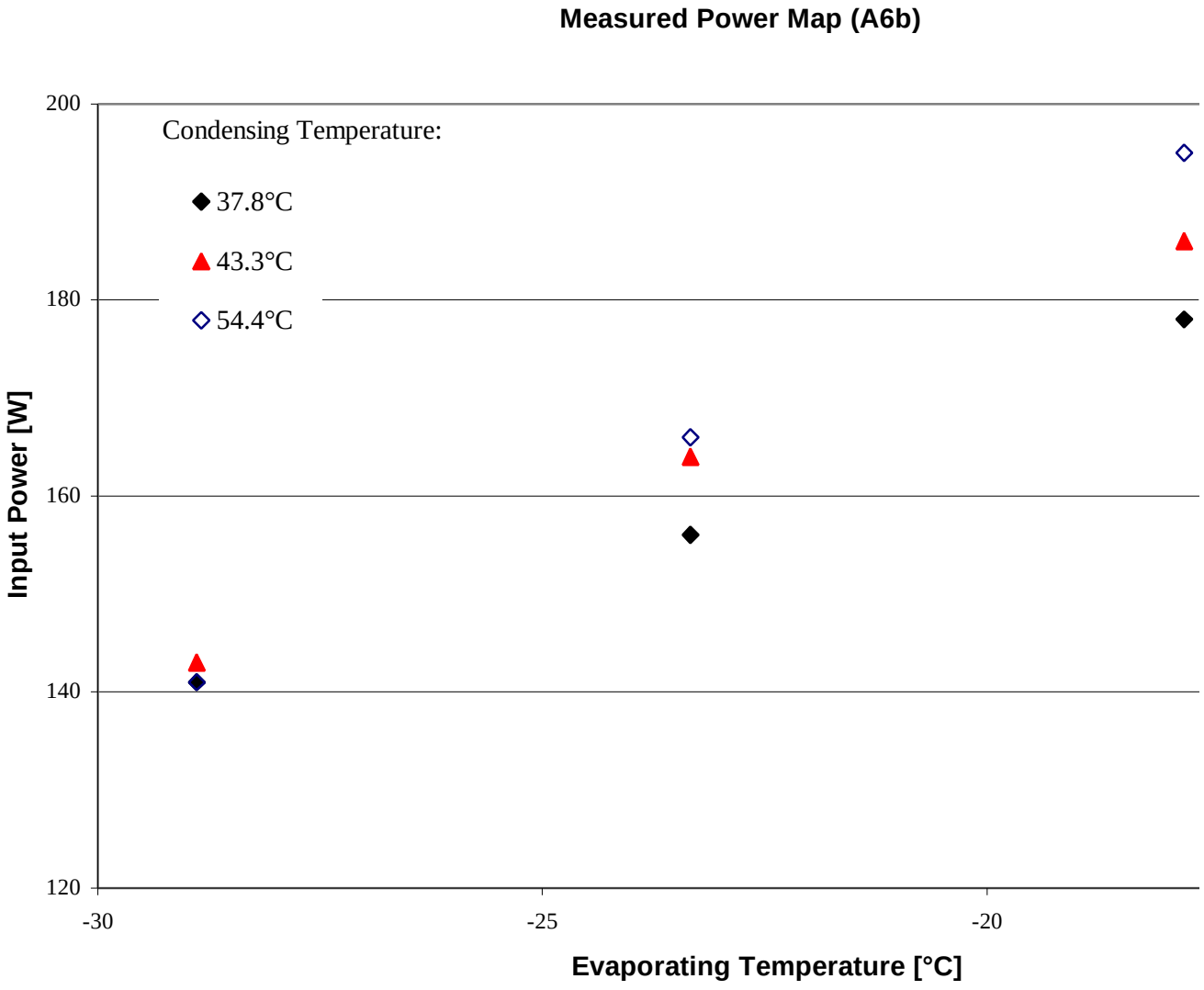
Measured Power Map (A6b)
Condensing Temperature:
37.8°C
43.3°C
54.4°C
Input Power [W]
200
180
160
140
120
-30
-25
-20
Evaporating Temperature [°C]

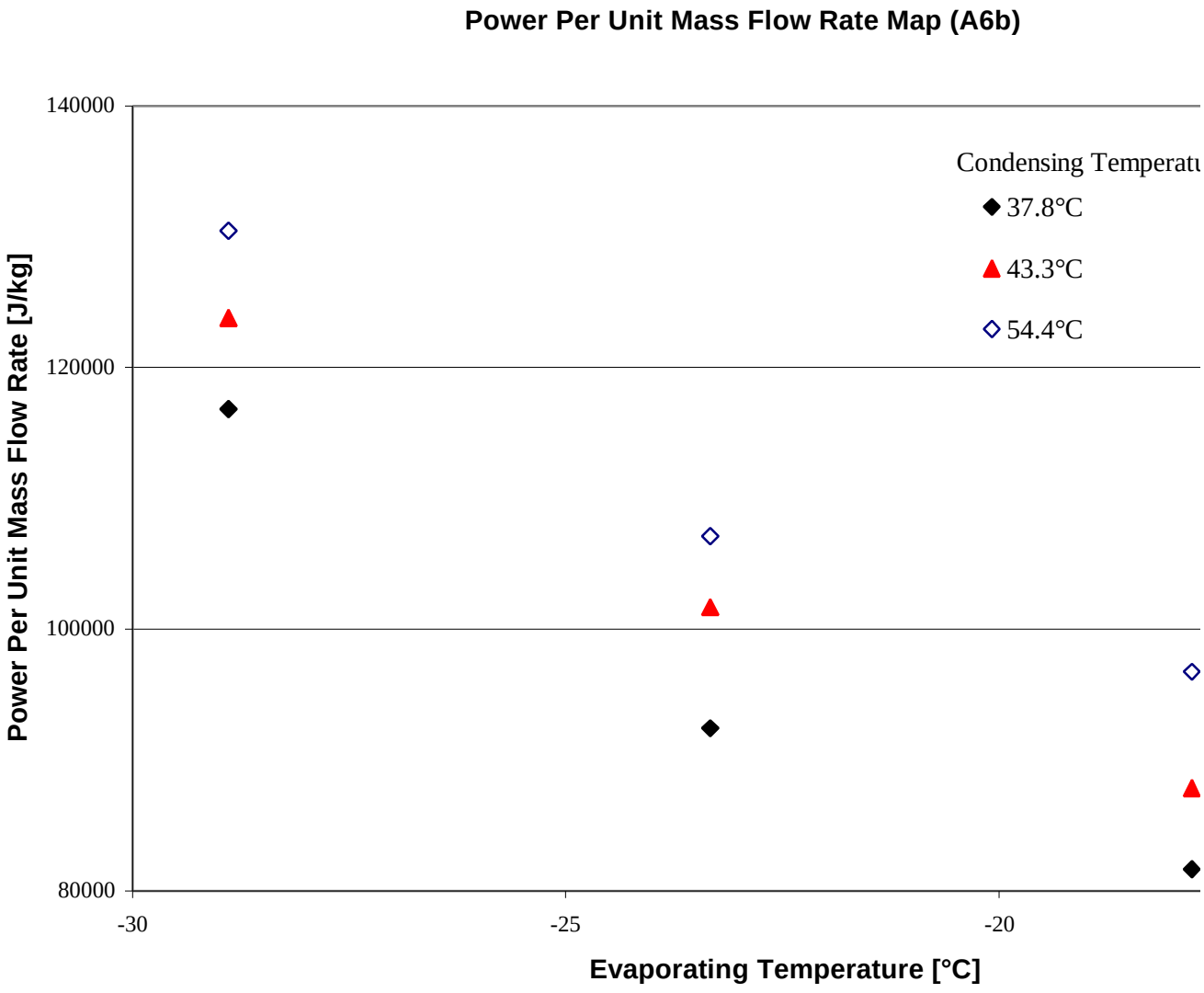
Power Per Unit Mass Flow Rate Map (A6b)
140000
120000
100000
80000
Power Per Unit Mass Flow Rate [J/kg]
-30
-25
-20
Evaporating Temperature [°C]
Condensing Temperatu
37.8°C
43.3°C
54.4°C

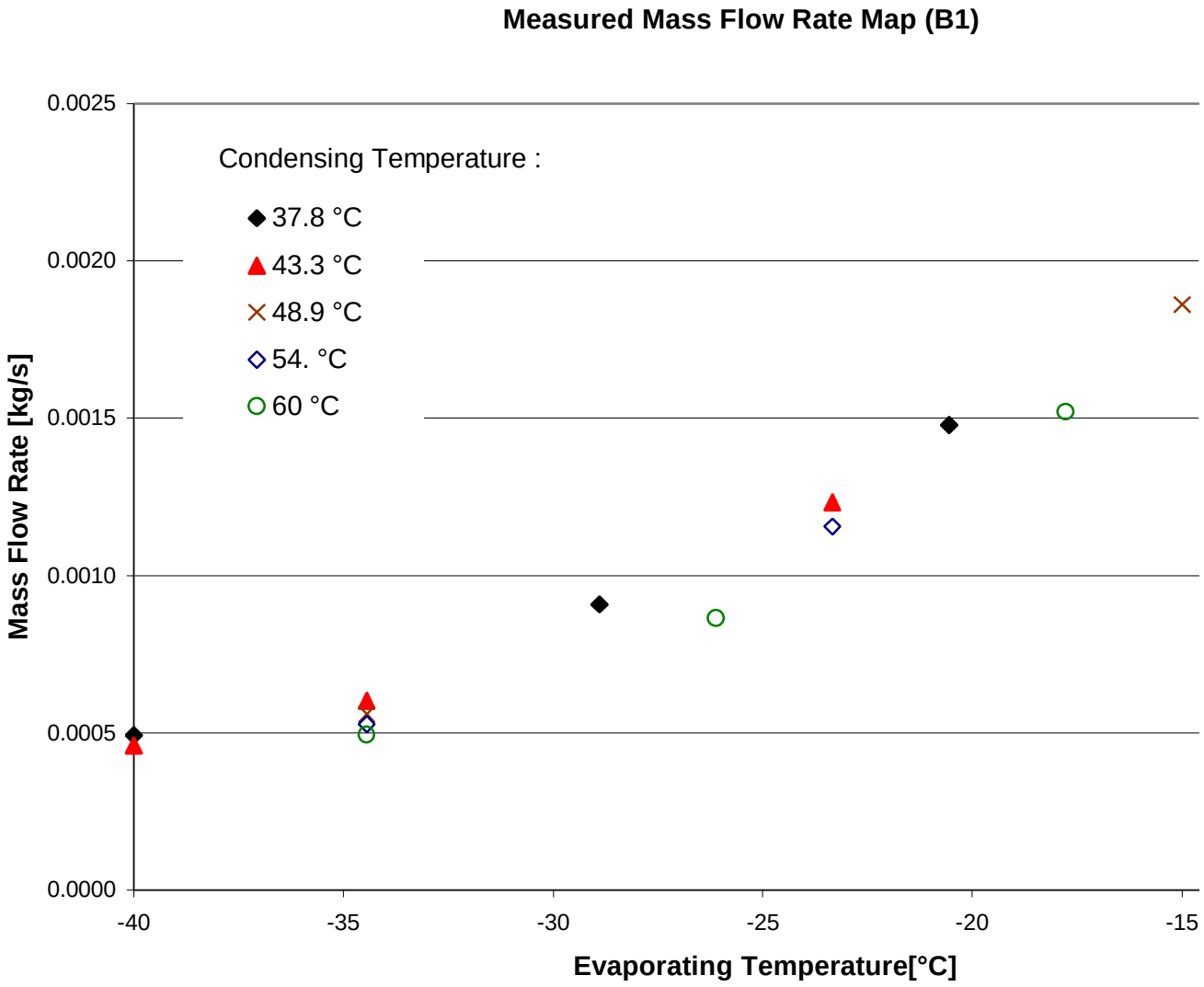
Measured Mass Flow Rate Map (B1)
Mass Flow Rate [kg/s]
0.0025
0.0020
0.0015
0.0010
0.0005
0.0000
Condensing Temperature :
37.8 °C
43.3 °C
48.9 °C
54. °C
60 °C
-40
-35
-30
-25
-20
-15
Evaporating Temperature[°C]

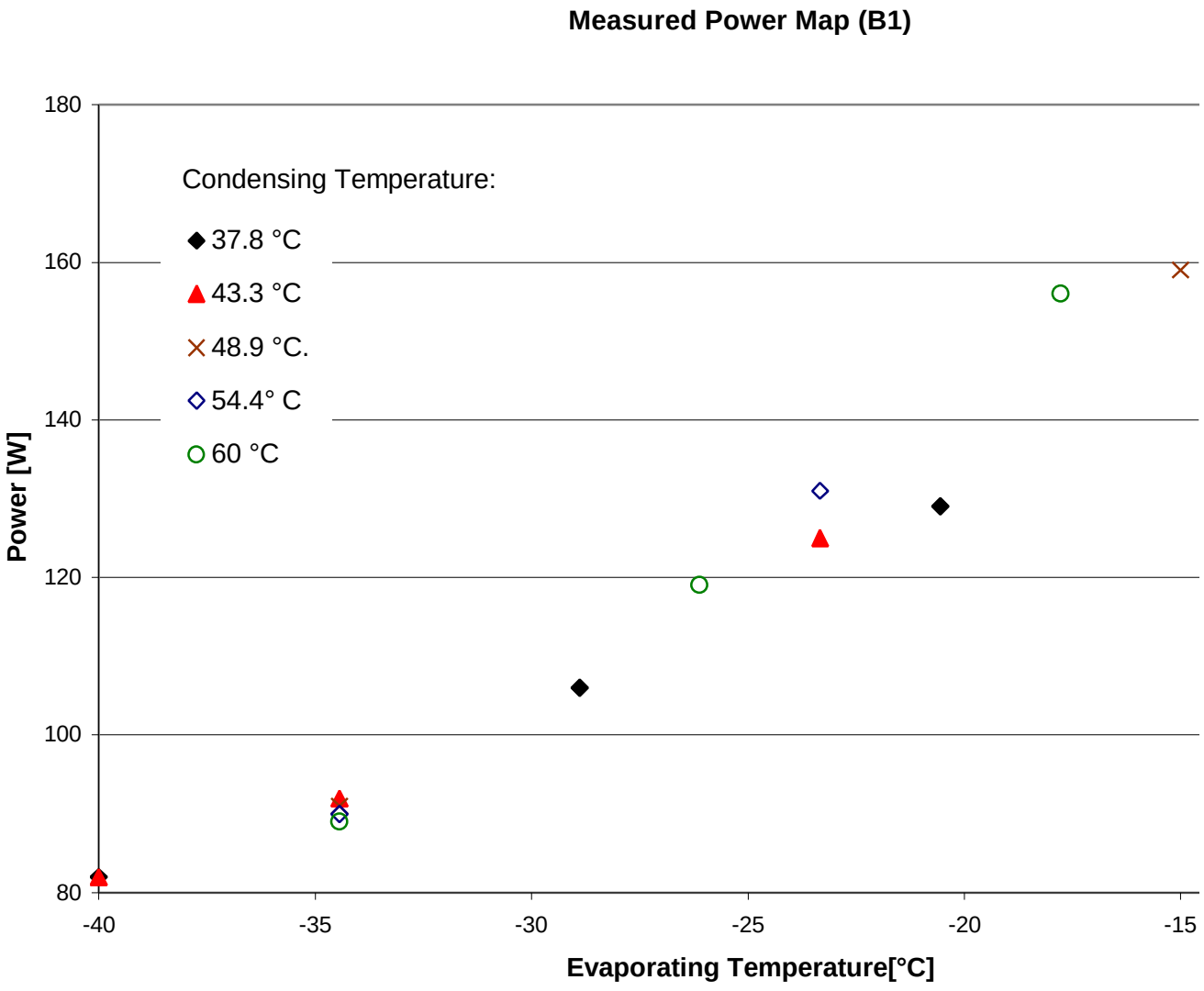
Measured Power Map (B1)
Condensing Temperature:
37.8 °C
43.3 °C
48.9 °C.
54.4° C
60 °C
Power [W]
180
160
140
120
100
80
-40
-35
-30
-25
-20
-15
Evaporating Temperature[°C]

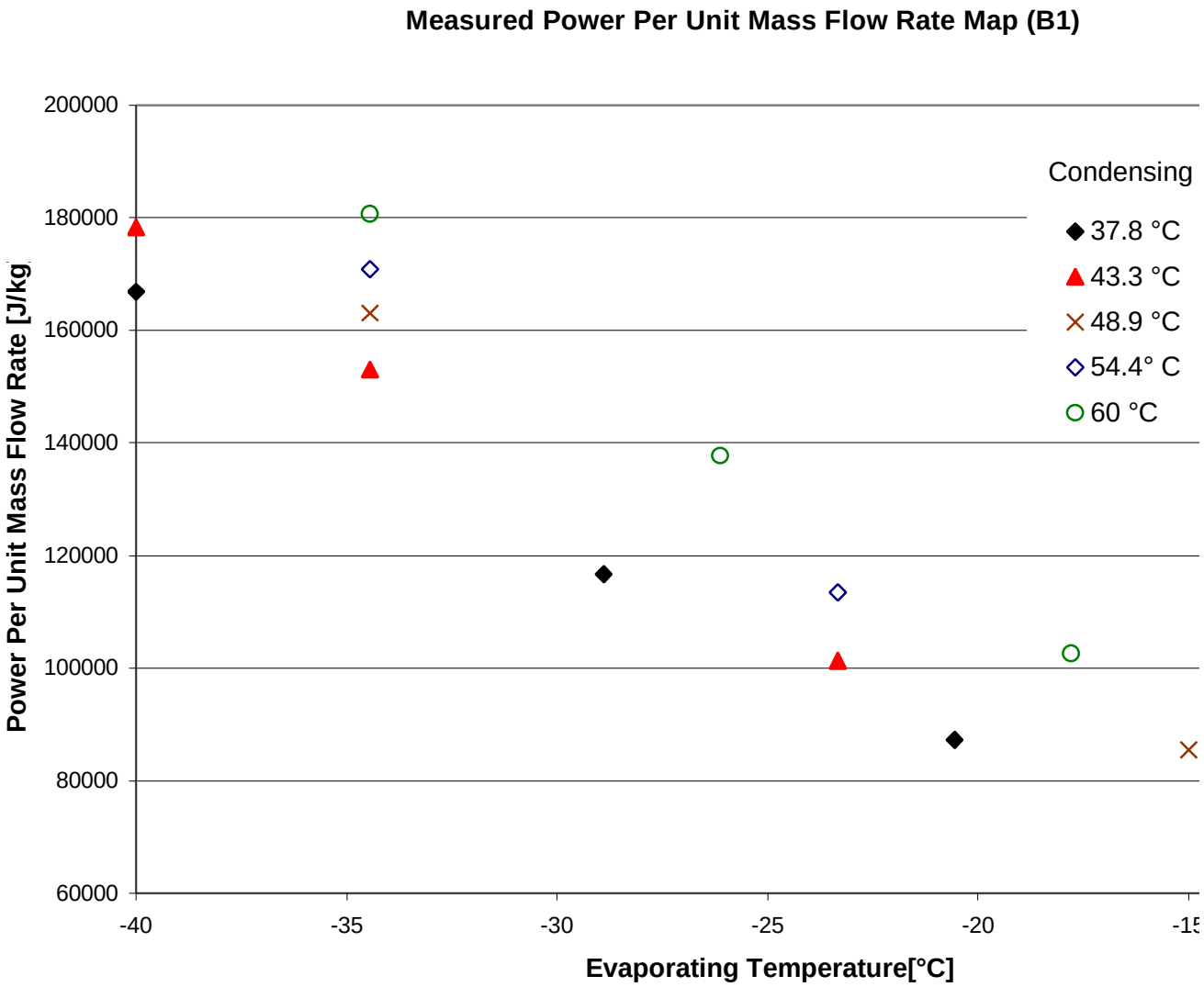
Measured Power Per Unit Mass Flow Rate Map (B1)
Power Per Unit Mass Flow Rate [J/kg]
200000
180000
160000
140000
120000
100000
80000
60000
-40
-35
-30
-25
-20
-15
Evaporating Temperature[°C]
Condensing
37.8 °C
43.3 °C
48.9 °C
54.4° C
60 °C

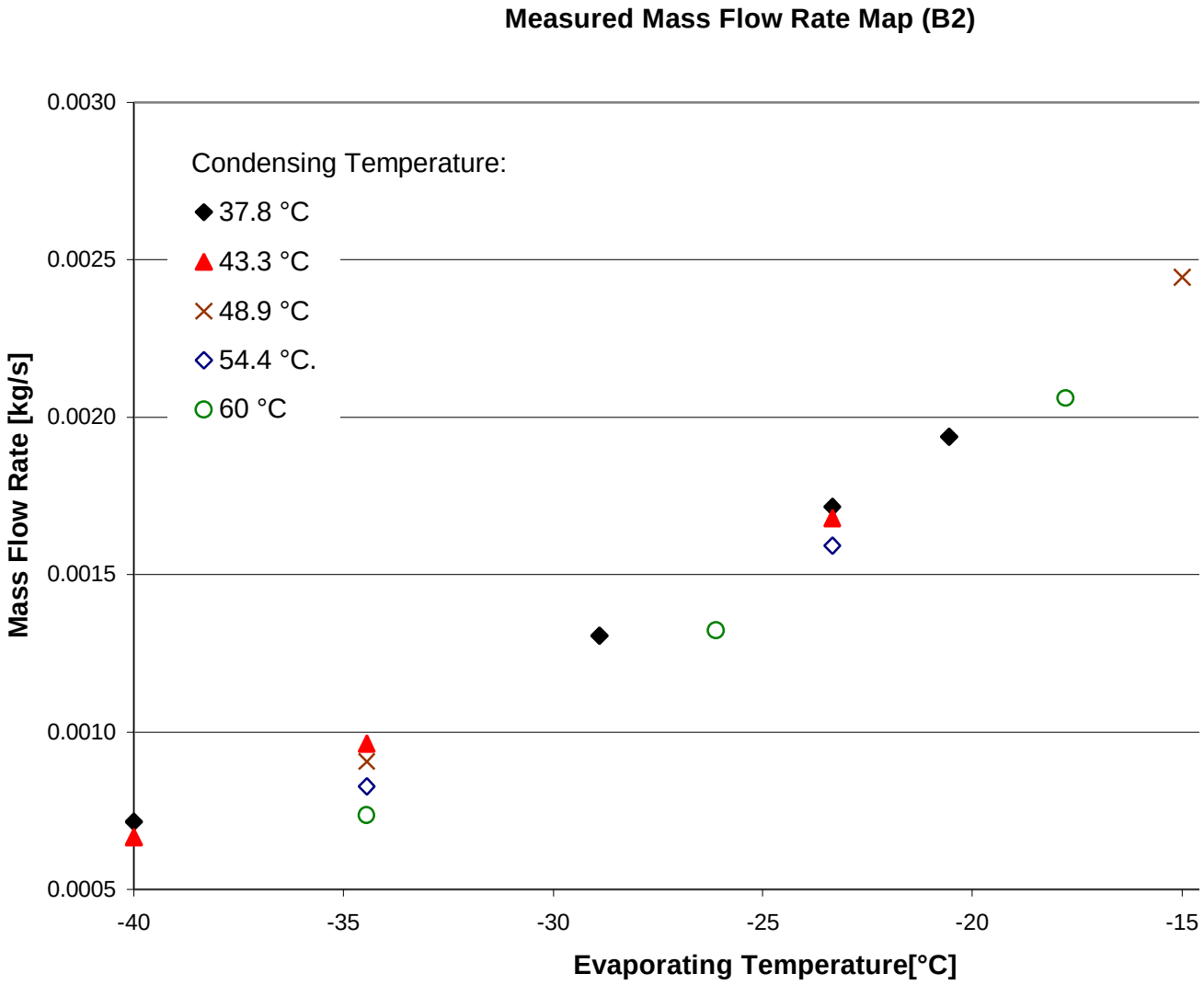
Measured Mass Flow Rate Map (B2)
Mass Flow Rate [kg/s]
0.0030
0.0025
0.0020
0.0015
0.0010
0.0005
Condensing Temperature:
37.8 °C
43.3 °C
48.9 °C
54.4 °C.
60 °C
-40
-35
-30
-25
-20
-15
Evaporating Temperature[°C]

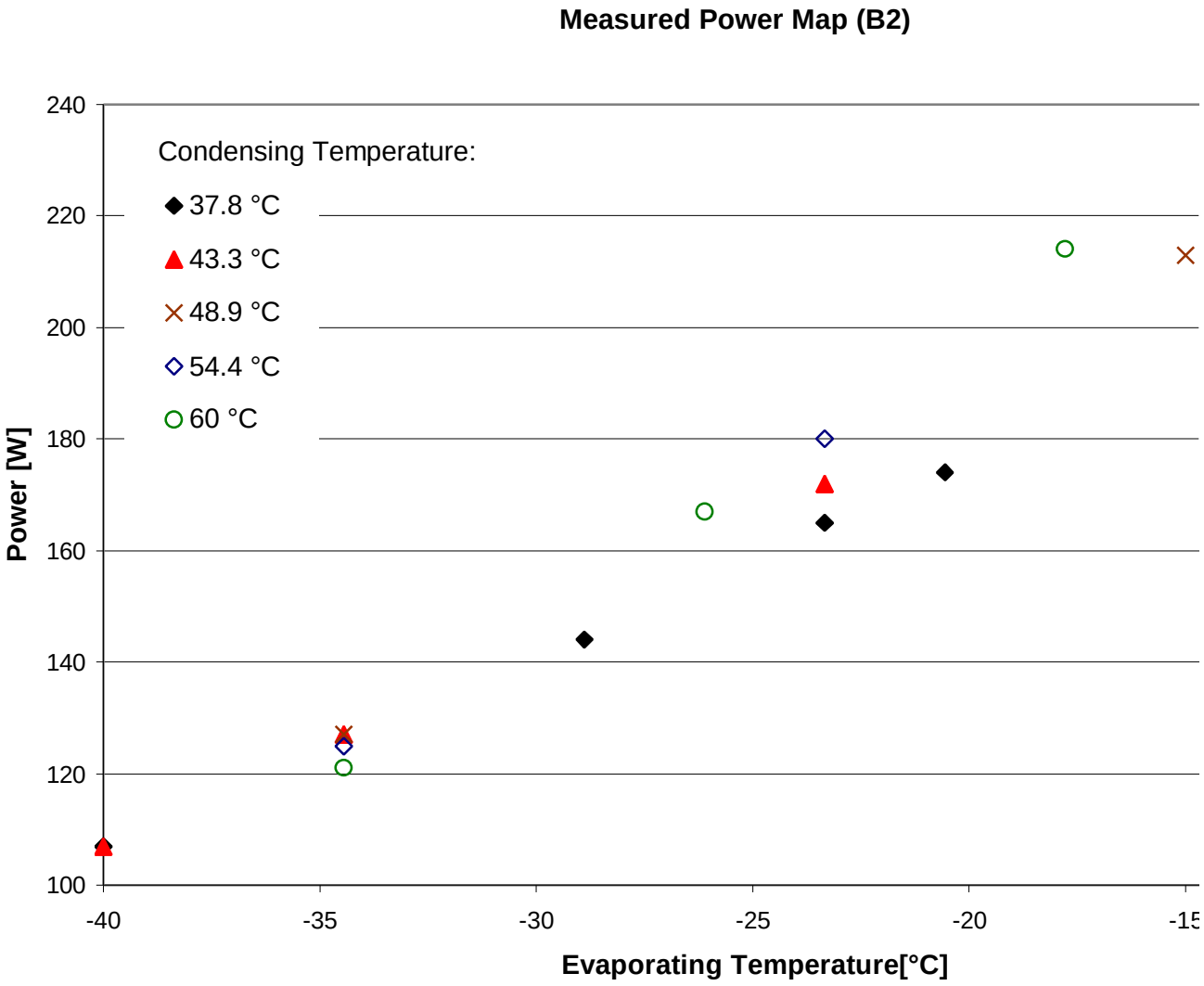
Measured Power Map (B2)
Condensing Temperature:
37.8 °C
43.3 °C
48.9 °C
54.4 °C
60 °C
Power [W]
240
220
200
180
160
140
120
100
-40
-35
-30
-25
-20
-15
Evaporating Temperature[°C]

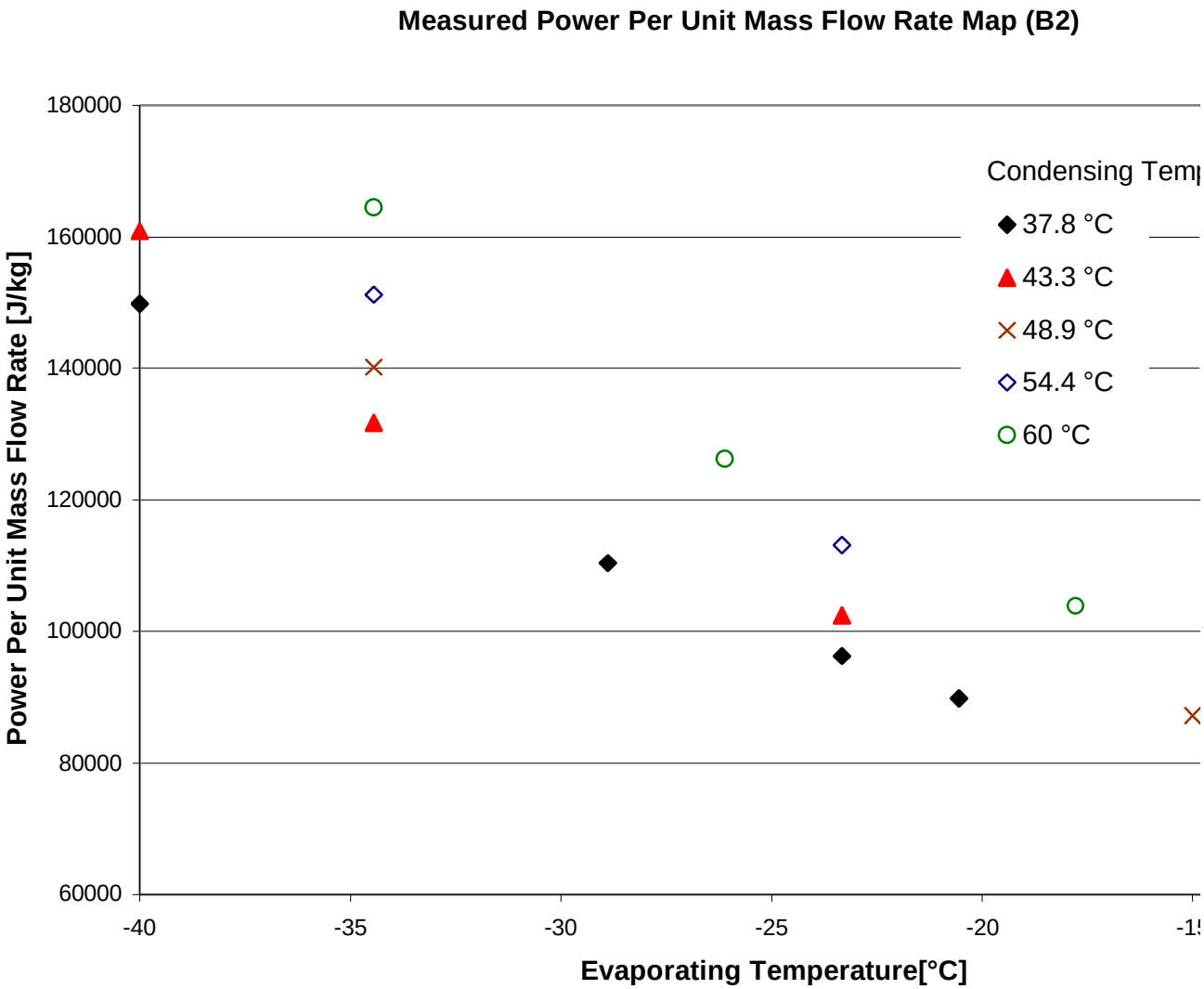
Measured Power Per Unit Mass Flow Rate Map (B2)
Power Per Unit Mass Flow Rate [J/kg]
180000
160000
140000
120000
100000
80000
60000
-40
-35
-30
-25
-20
Evaporating Temperature[°C]
Condensing Temp
37.8 °C
43.3 °C
48.9 °C
54.4 °C
60 °C

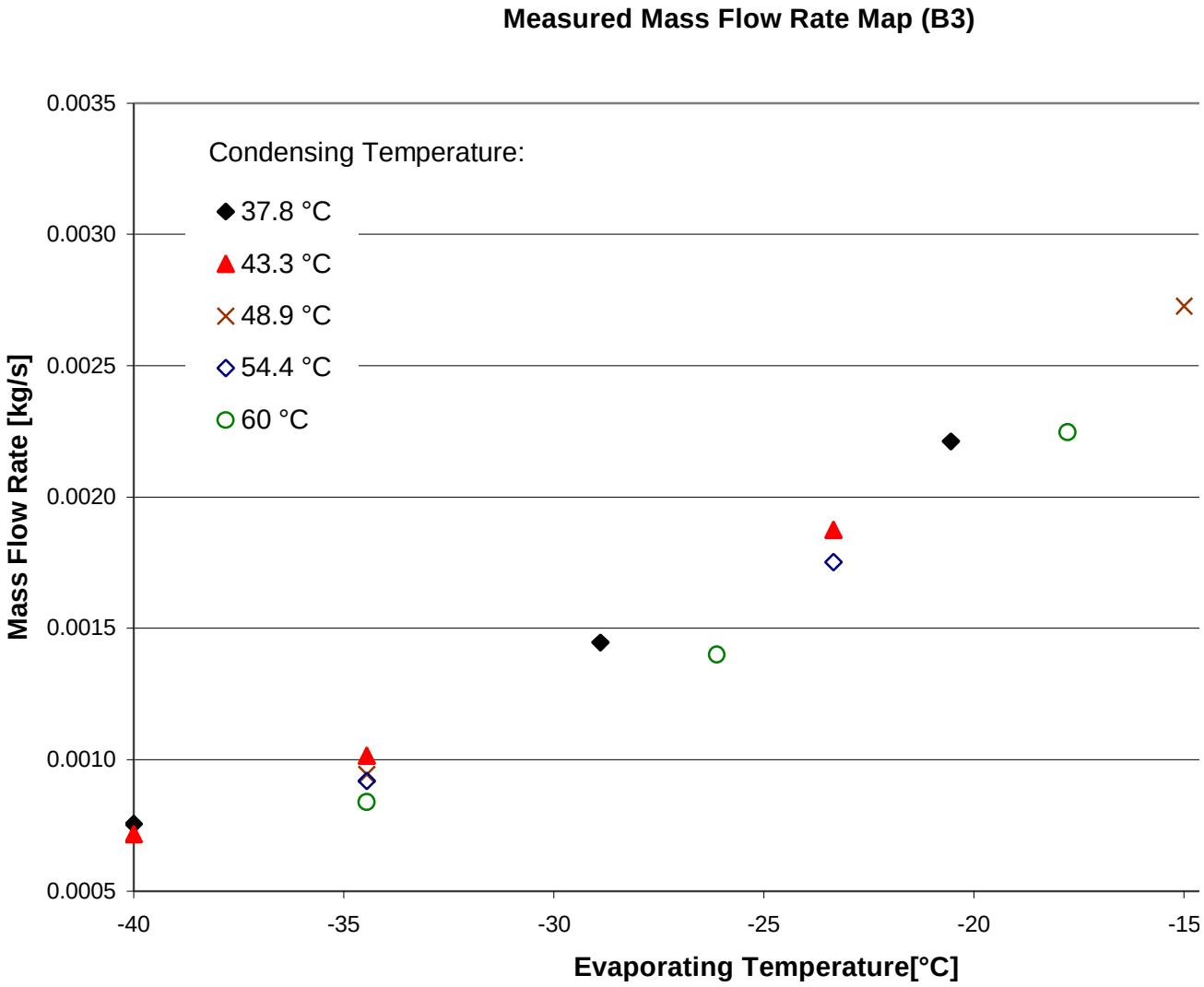
Measured Mass Flow Rate Map (B3)
Condensing Temperature:
37.8 °C
43.3 °C
48.9 °C
54.4 °C
60 °C
Mass Flow Rate [kg/s]
0.0035
0.0030
0.0025
0.0020
0.0015
0.0010
0.0005
-40
-35
-30
-25
-20
-15
Evaporating Temperature[°C]

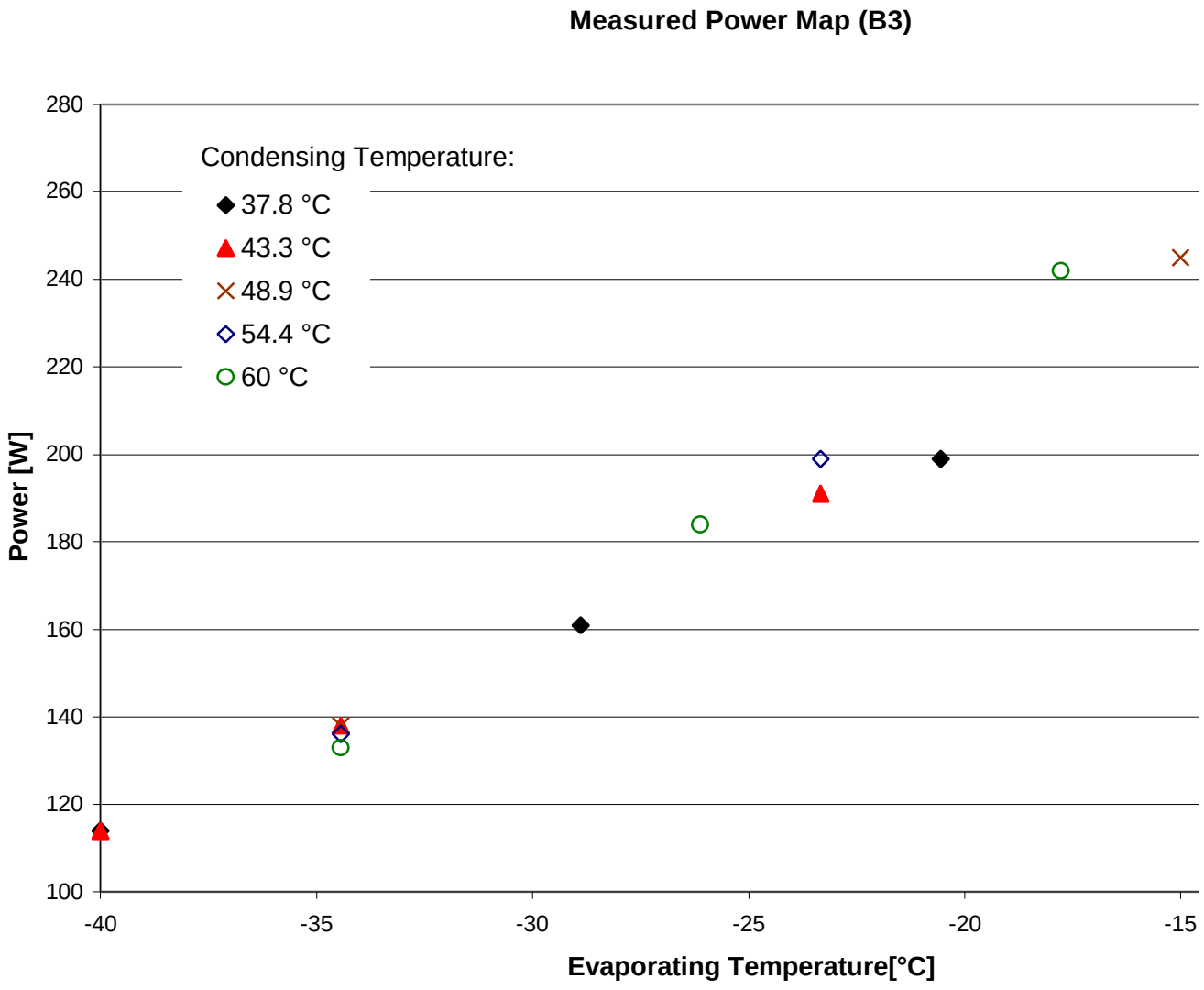
Measured Power Map (B3)
Condensing Temperature:
37.8 °C
43.3 °C
48.9 °C
54.4 °C
60 °C
Power [W]
280
260
240
220
200
180
160
140
120
100
-40
-35
-30
-25
-20
-15
Evaporating Temperature[°C]

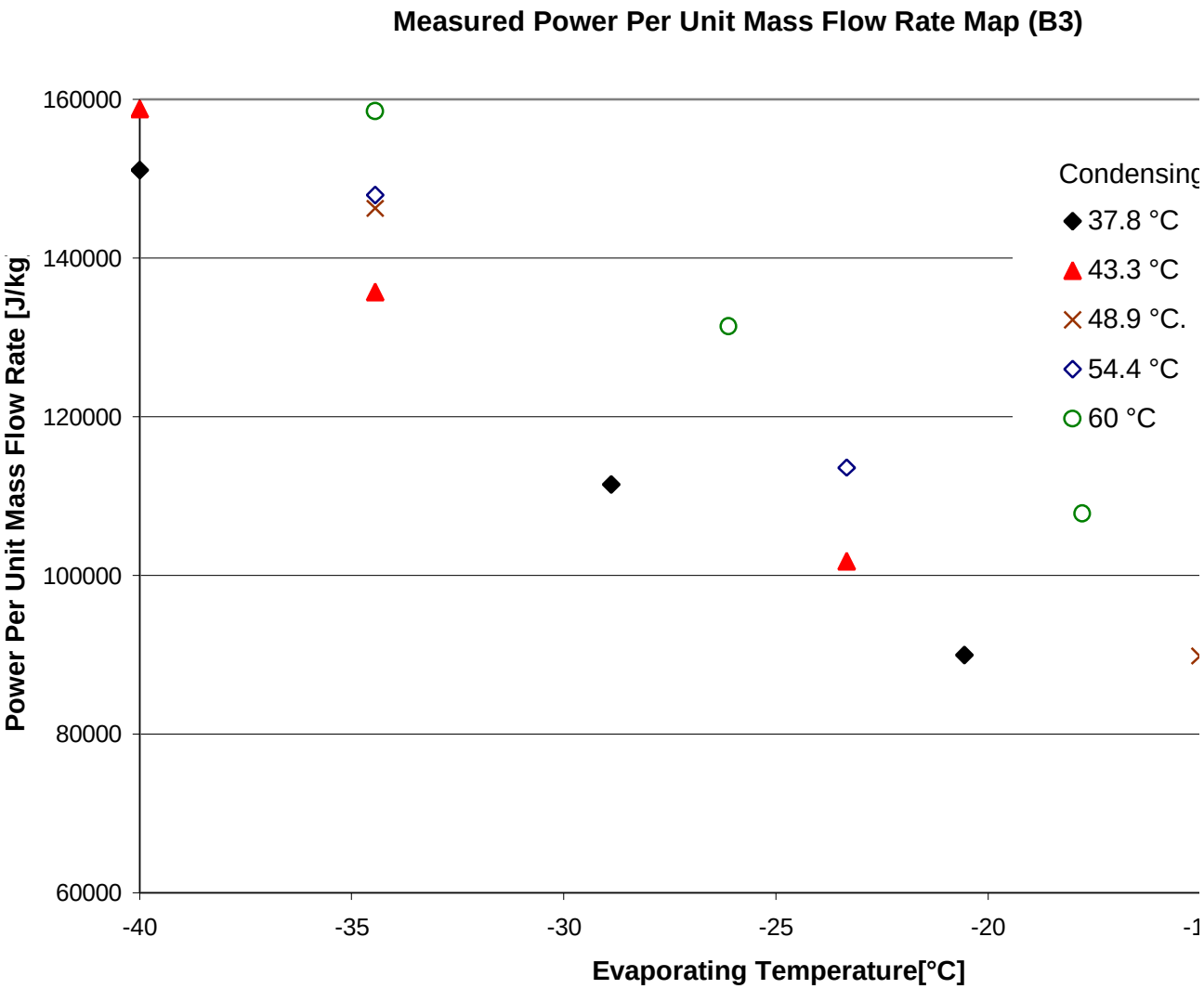
Measured Power Per Unit Mass Flow Rate Map (B3)
Power Per Unit Mass Flow Rate [J/kg
160000
140000
120000
100000
80000
60000
-40
-35
-30
-25
-20
Evaporating Temperature[°C]
Condensing
37.8 °C
43.3 °C
48.9 °C.
54.4 °C
60 °C

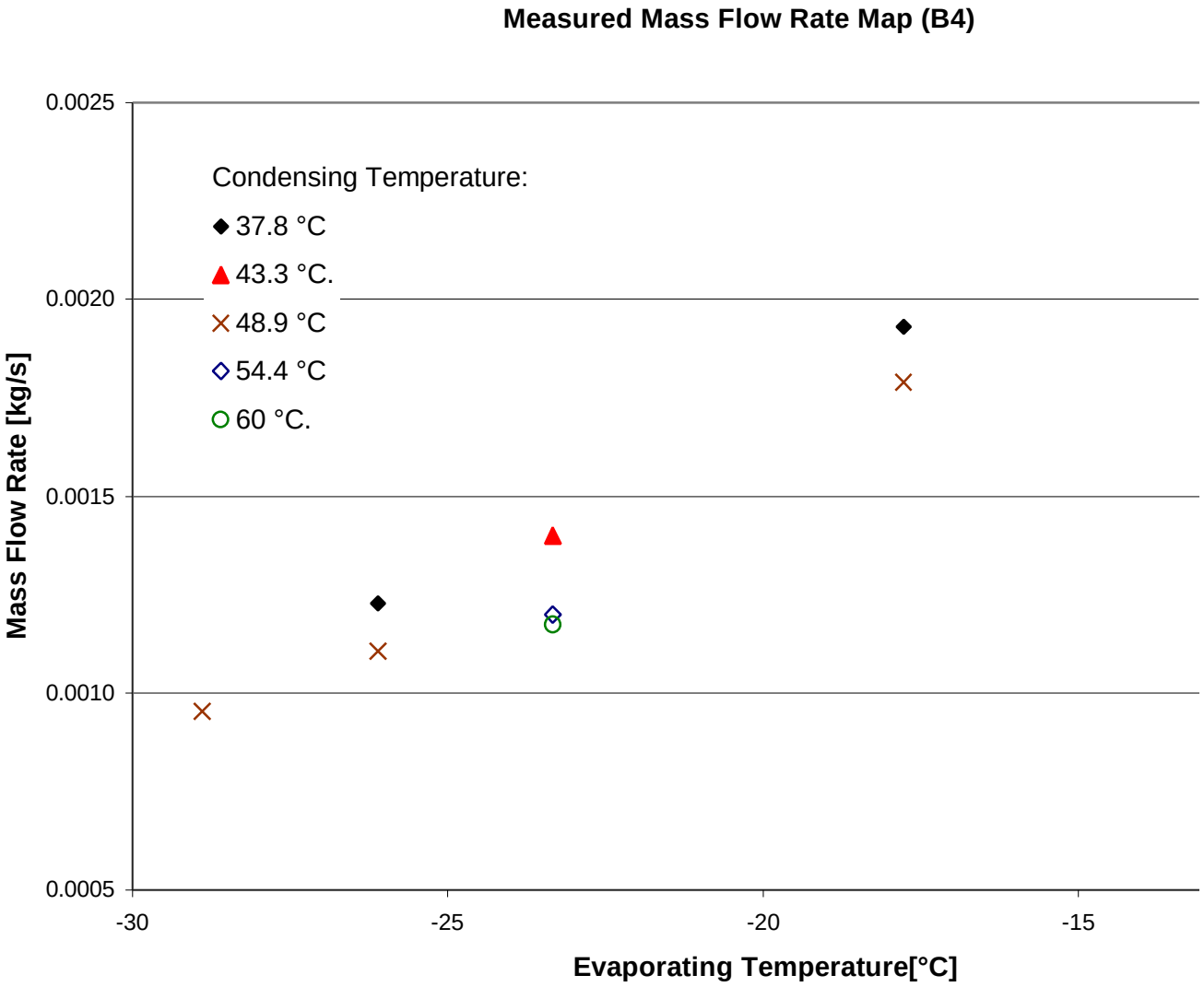
Measured Mass Flow Rate Map (B4)
Mass Flow Rate [kg/s]
0.0025
0.0020
0.0015
0.0010
0.0005
Condensing Temperature:
37.8 °C
43.3 °C.
48.9 °C
54.4 °C
60 °C.
-30
-25
-20
-15
Evaporating Temperature[°C]

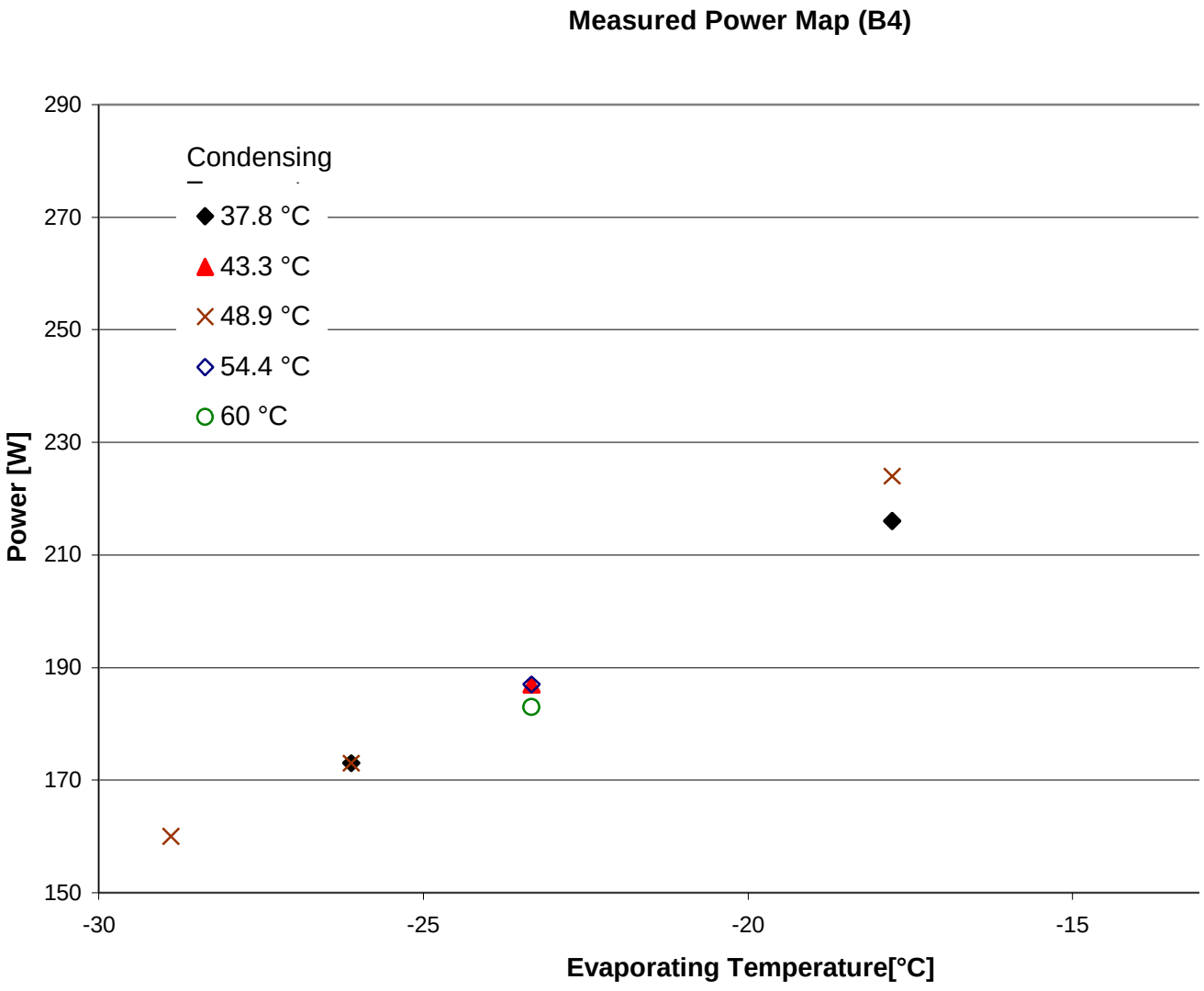
Measured Power Map (B4)
290
270
250
230
210
190
170
150
Power [W]
Condensing
37.8 °C
43.3 °C
48.9 °C
54.4 °C
60 °C
-30
-25
-20
-15
Evaporating Temperature[°C]

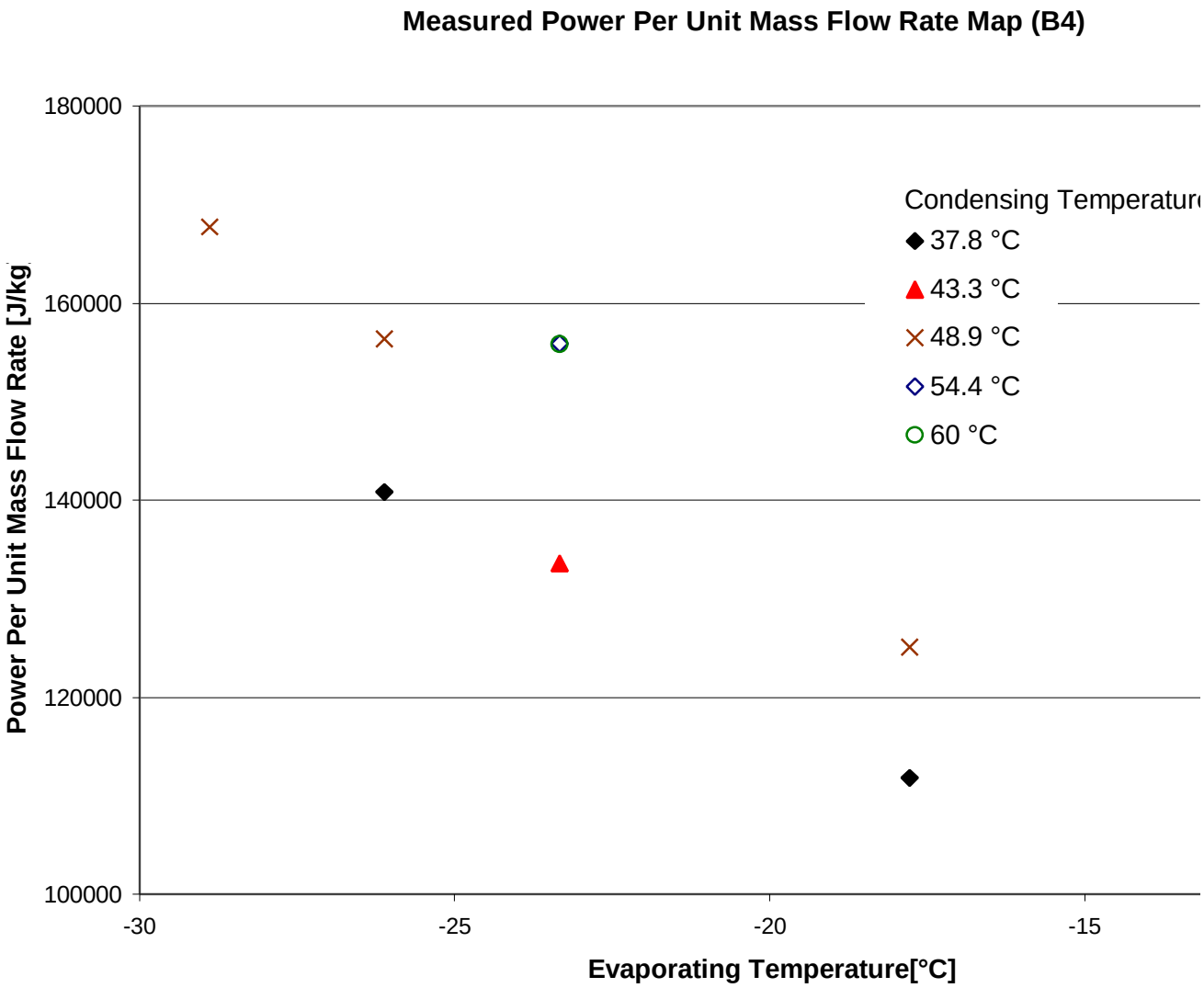
Measured Power Per Unit Mass Flow Rate Map (B4)
Power Per Unit Mass Flow Rate [J/kg]
180000
160000
140000
120000
100000
-30
-25
-20
-15
Evaporating Temperature[°C]
Condensing Temperatur
37.8 °C
43.3 °C
48.9 °C
54.4 °C
60 °C

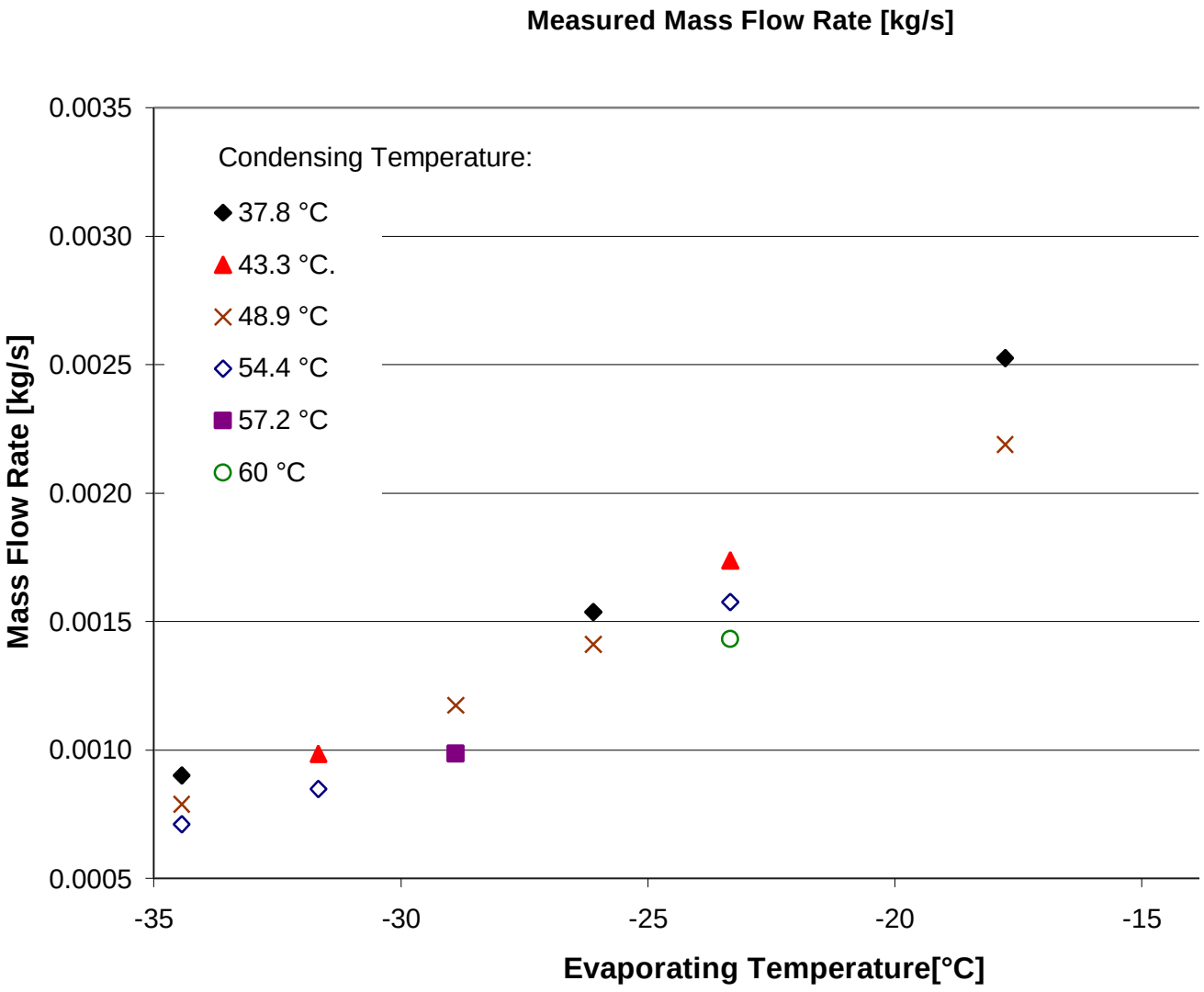
Measured Mass Flow Rate [kg/s]
Condensing Temperature:
37.8 °C
43.3 °C.
48.9 °C
54.4 °C
57.2 °C
60 °C
Mass Flow Rate [kg/s]
0.0035
0.0030
0.0025
0.0020
0.0015
0.0010
0.0005
-35
-30
-25
-20
-15
Evaporating Temperature[°C]

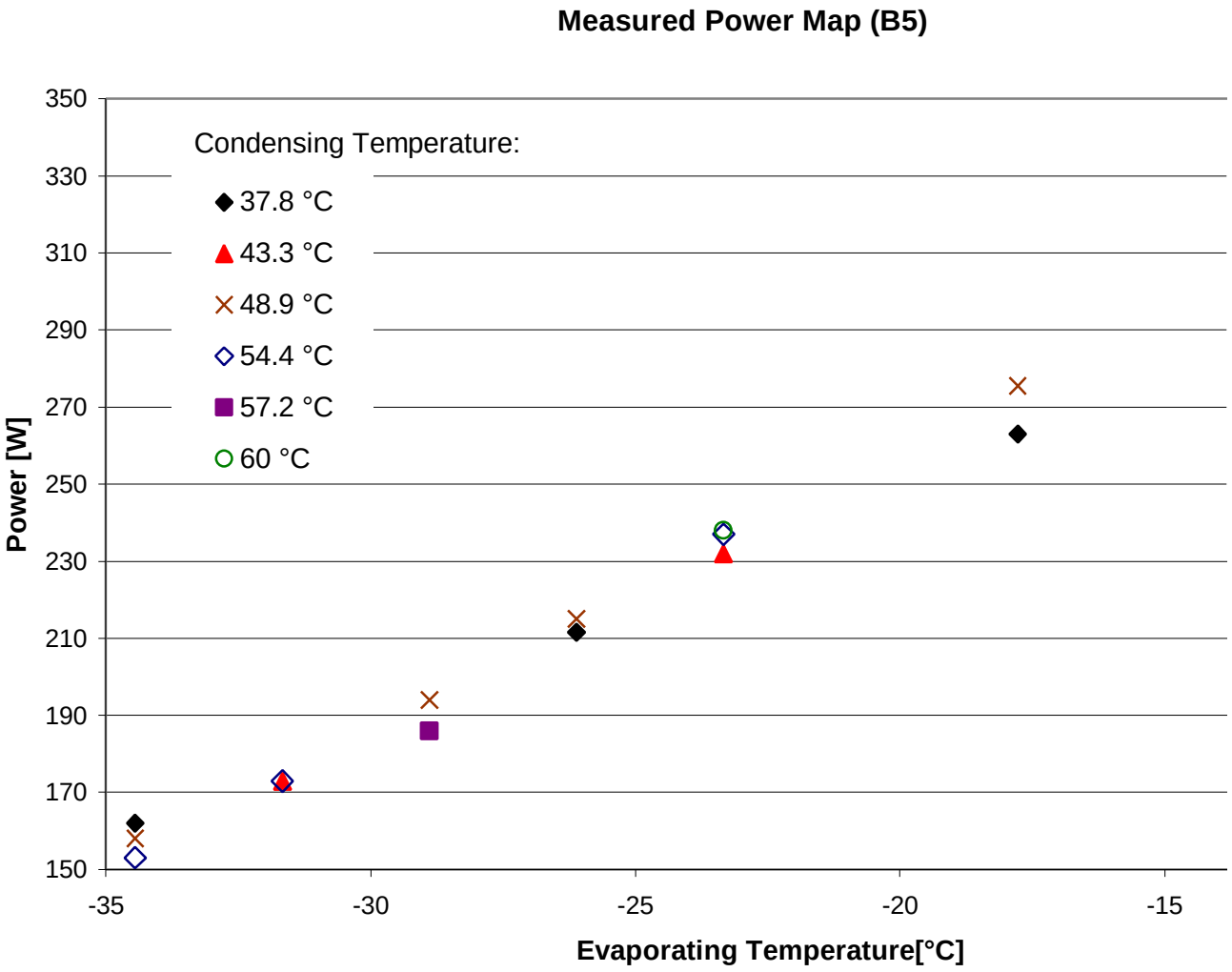
Measured Power Map (B5)
Condensing Temperature:
37.8 °C
43.3 °C
48.9 °C
54.4 °C
57.2 °C
60 °C
Power [W]
350
330
310
290
270
250
230
210
190
170
150
-35
-30
-25
-20
-15
Evaporating Temperature[°C]

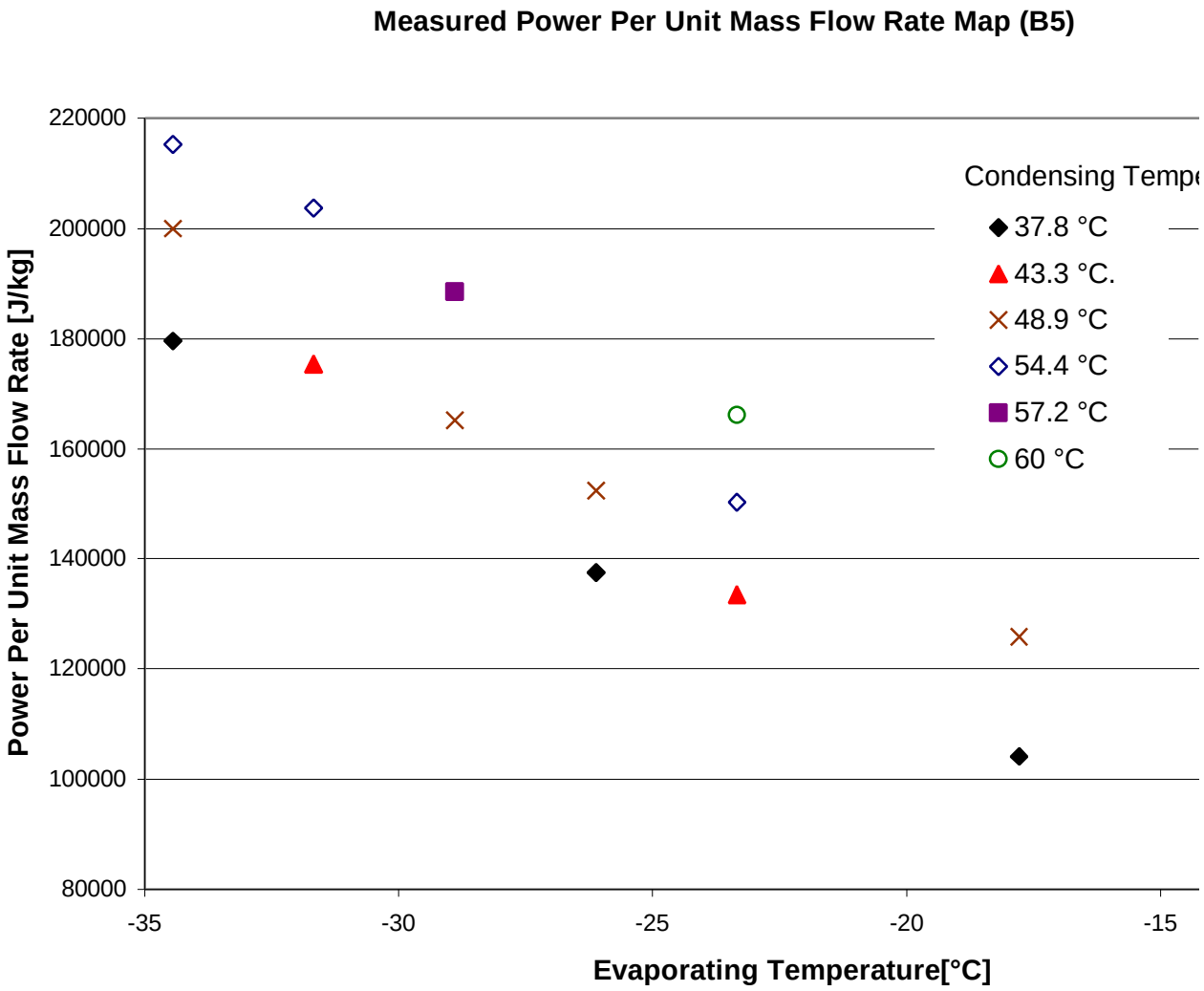
Measured Power Per Unit Mass Flow Rate Map (B5)
Power Per Unit Mass Flow Rate [J/kg]
220000
200000
180000
160000
140000
120000
100000
80000
-35
-30
-25
-20
-15
Evaporating Temperature[°C]
Condensing Tempe
37.8 °C
43.3 °C.
48.9 °C
54.4 °C
57.2 °C
60 °C

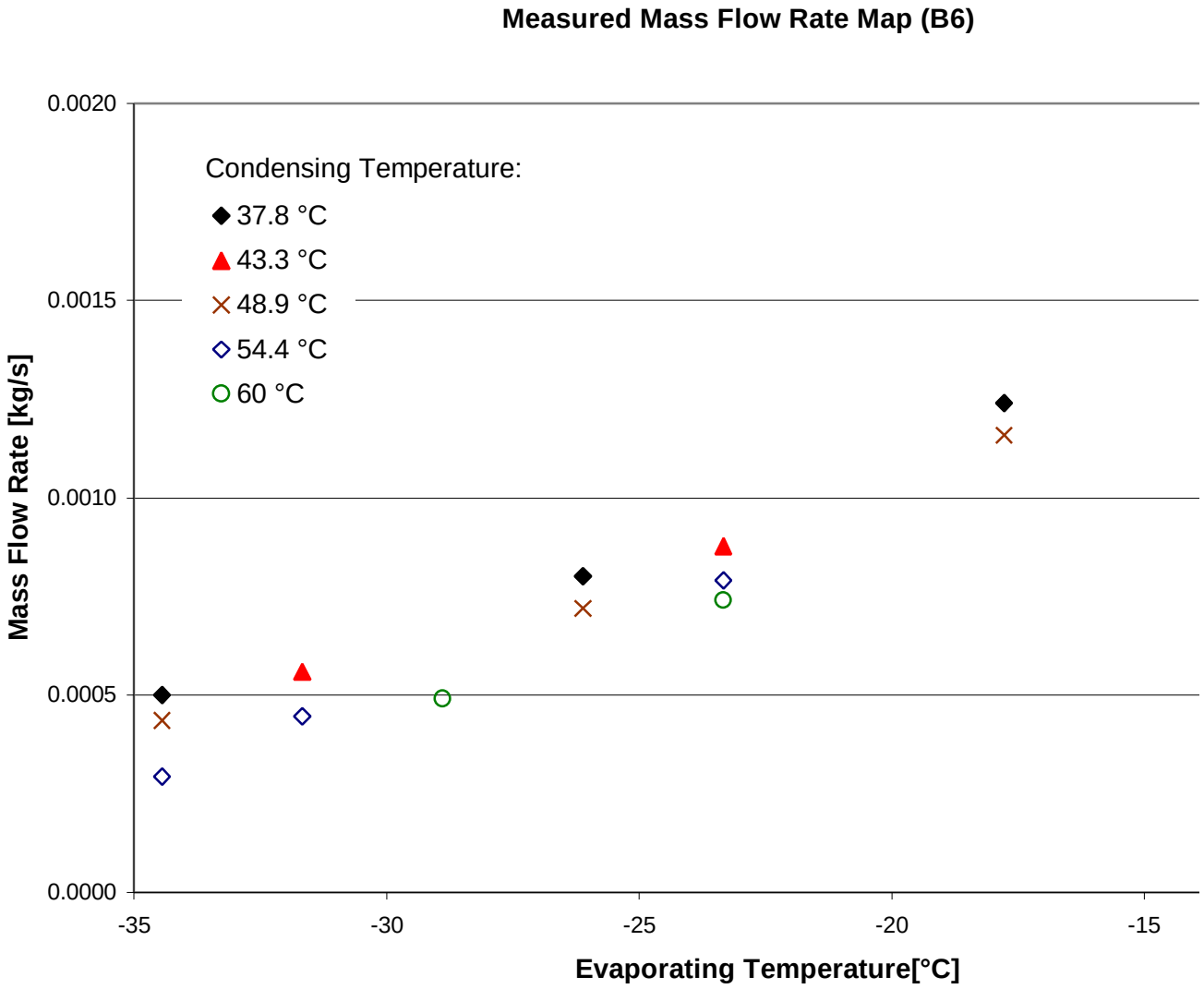
Measured Mass Flow Rate Map (B6)
Mass Flow Rate [kg/s]
0.0020
0.0015
0.0010
0.0005
0.0000
Condensing Temperature:
37.8 °C
43.3 °C
48.9 °C
54.4 °C
60 °C
-35
-30
-25
-20
-15
Evaporating Temperature[°C]

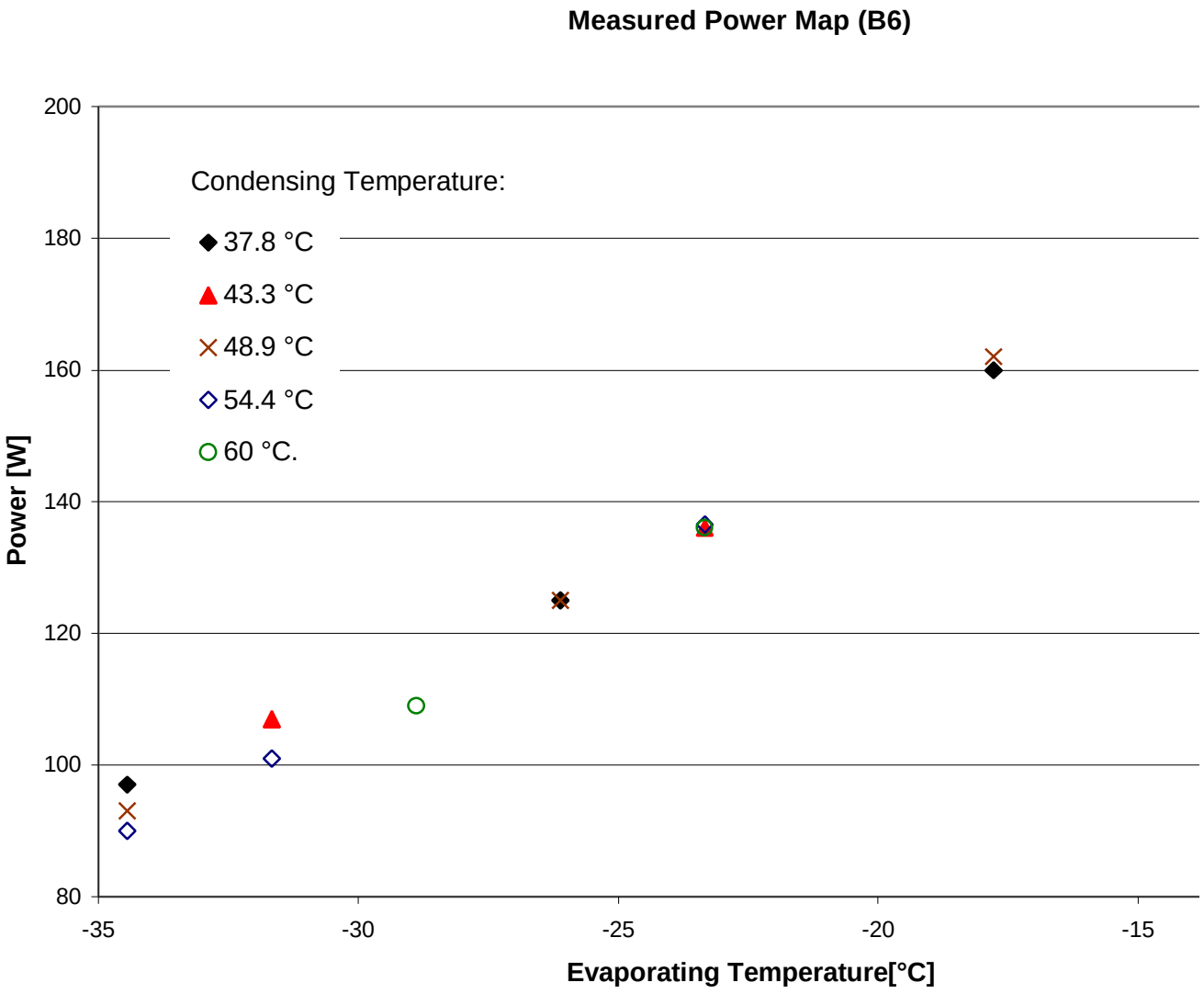
Measured Power Map (B6)
Condensing Temperature:
37.8 °C
43.3 °C
48.9 °C
54.4 °C
60 °C.
Power [W]
200
180
160
140
120
100
80
-35
-30
-25
-20
-15
Evaporating Temperature[°C]

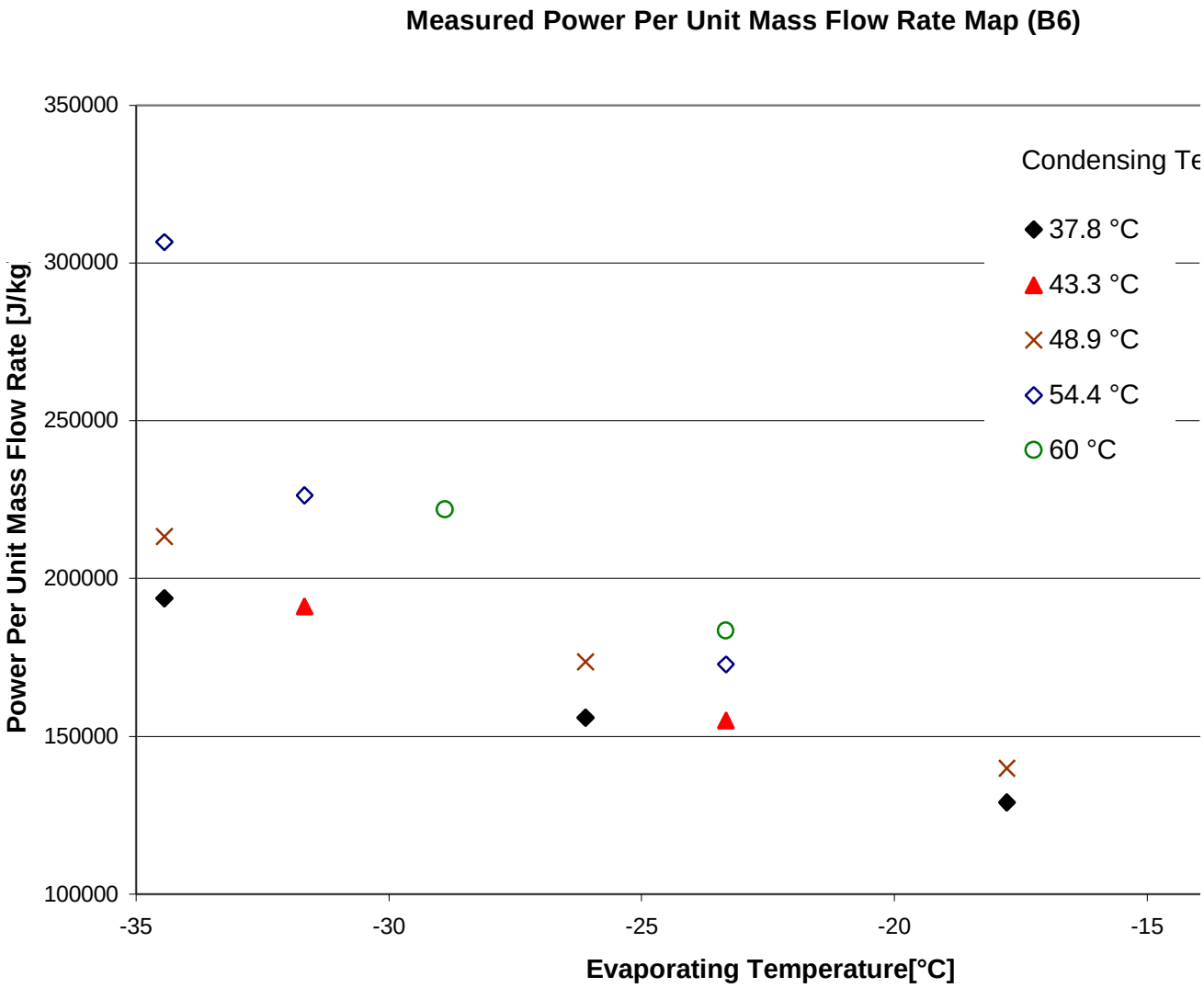
Measured Power Per Unit Mass Flow Rate Map (B6)
Power Per Unit Mass Flow Rate [J/kg]
350000
300000
250000
200000
150000
100000
-35
-30
-25
-20
-15
Evaporating Temperature[°C]
Condensing Te
37.8 °C
43.3 °C
48.9 °C
54.4 °C
60 °C

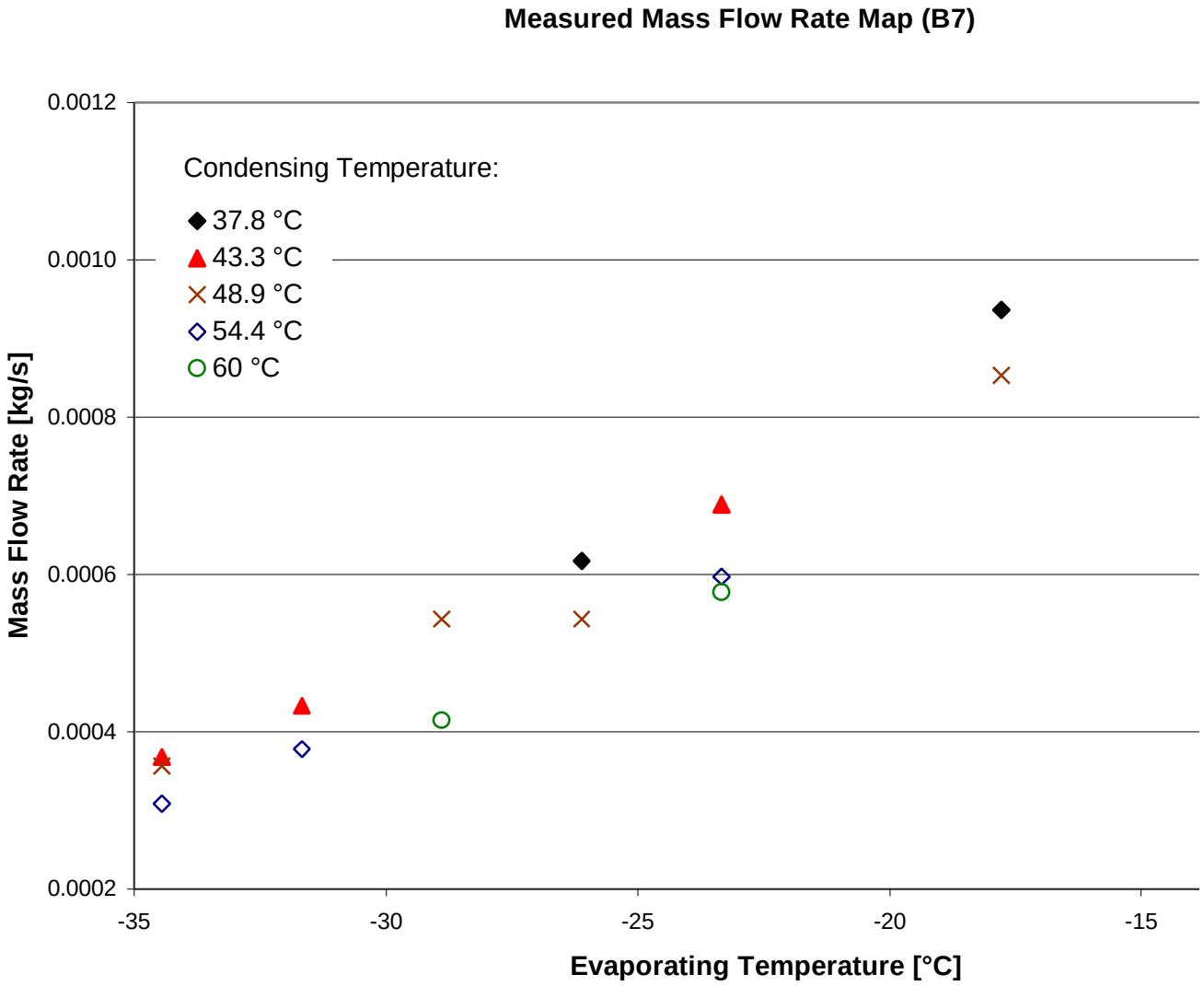
Measured Mass Flow Rate Map (B7)
Mass Flow Rate [kg/s]
0.0012
0.0010
0.0008
0.0006
0.0004
0.0002
Condensing Temperature:
37.8 °C
43.3 °C
48.9 °C
54.4 °C
60 °C
-35
-30
-25
-20
-15
Evaporating Temperature [°C]

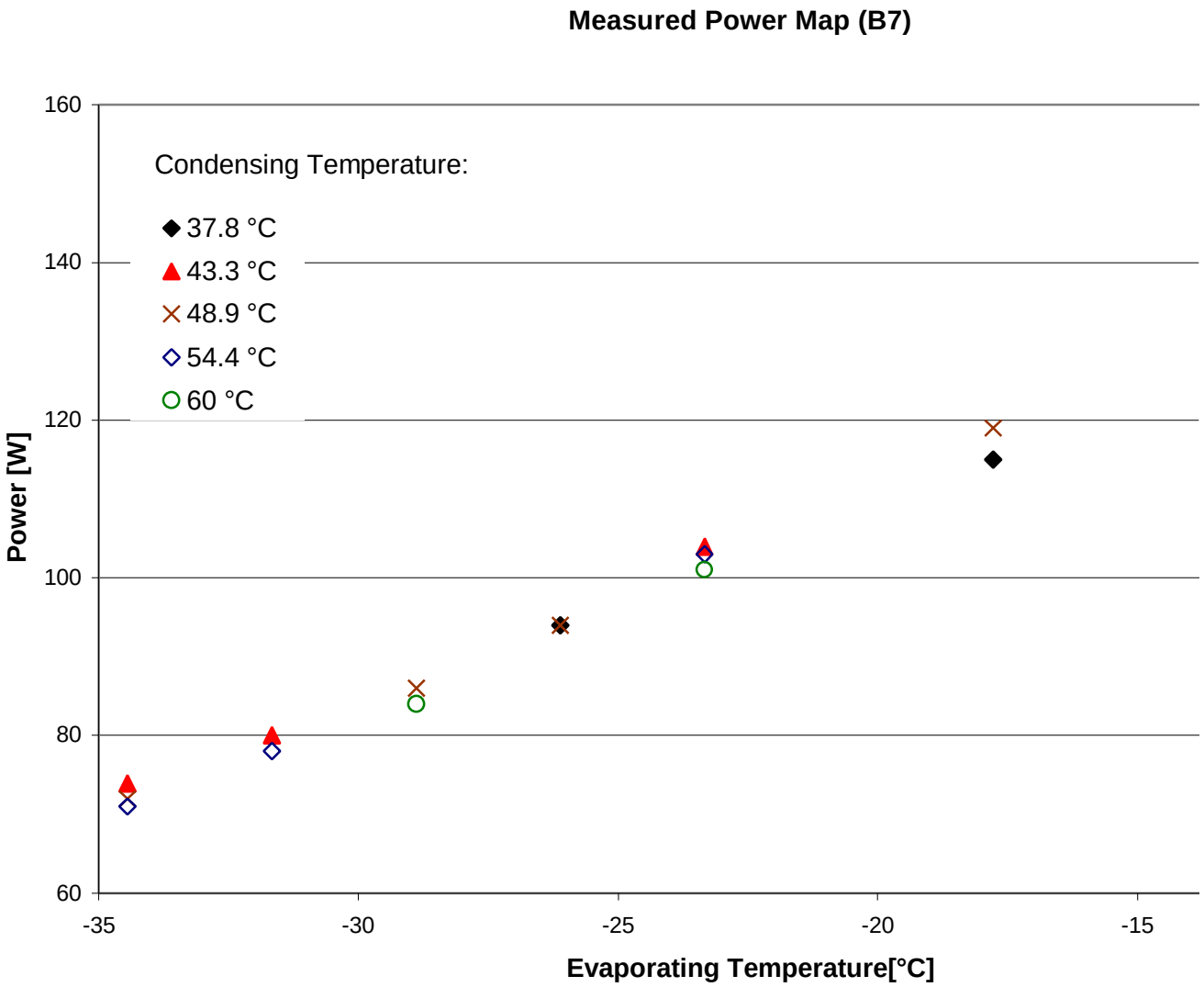
Measured Power Map (B7)
Condensing Temperature:
37.8 °C
43.3 °C
48.9 °C
54.4 °C
60 °C
Power [W]
160
140
120
100
80
60
-35
-30
-25
-20
-15
Evaporating Temperature[°C]

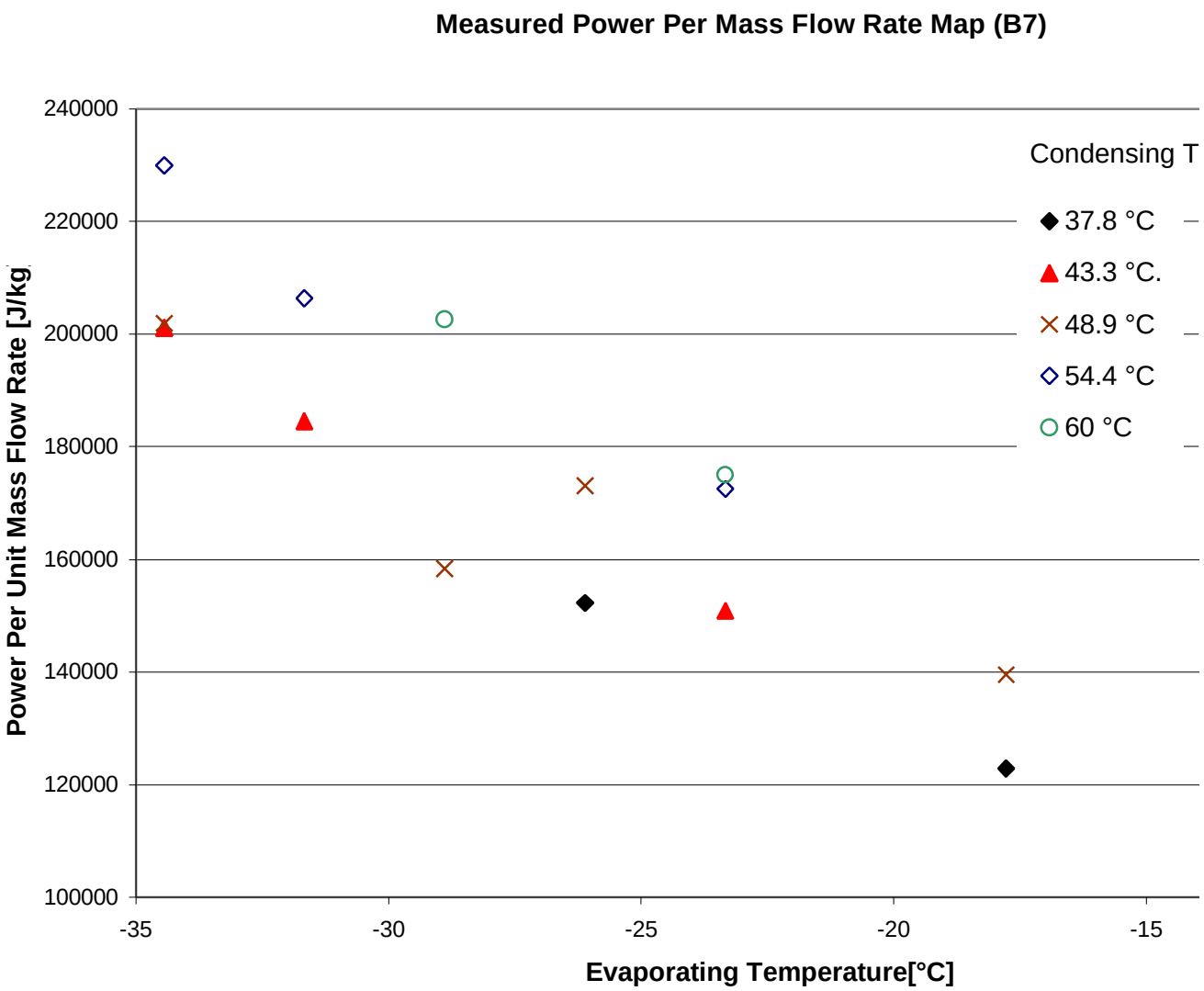
Measured Power Per Mass Flow Rate Map (B7)
Power Per Unit Mass Flow Rate [J/kg]
240000
220000
200000
180000
160000
140000
120000
100000
-35
-30
-25
-20
-15
Evaporating Temperature[°C]
Condensing T
37.8 °C
43.3 °C.
48.9 °C
54.4 °C
60 °C

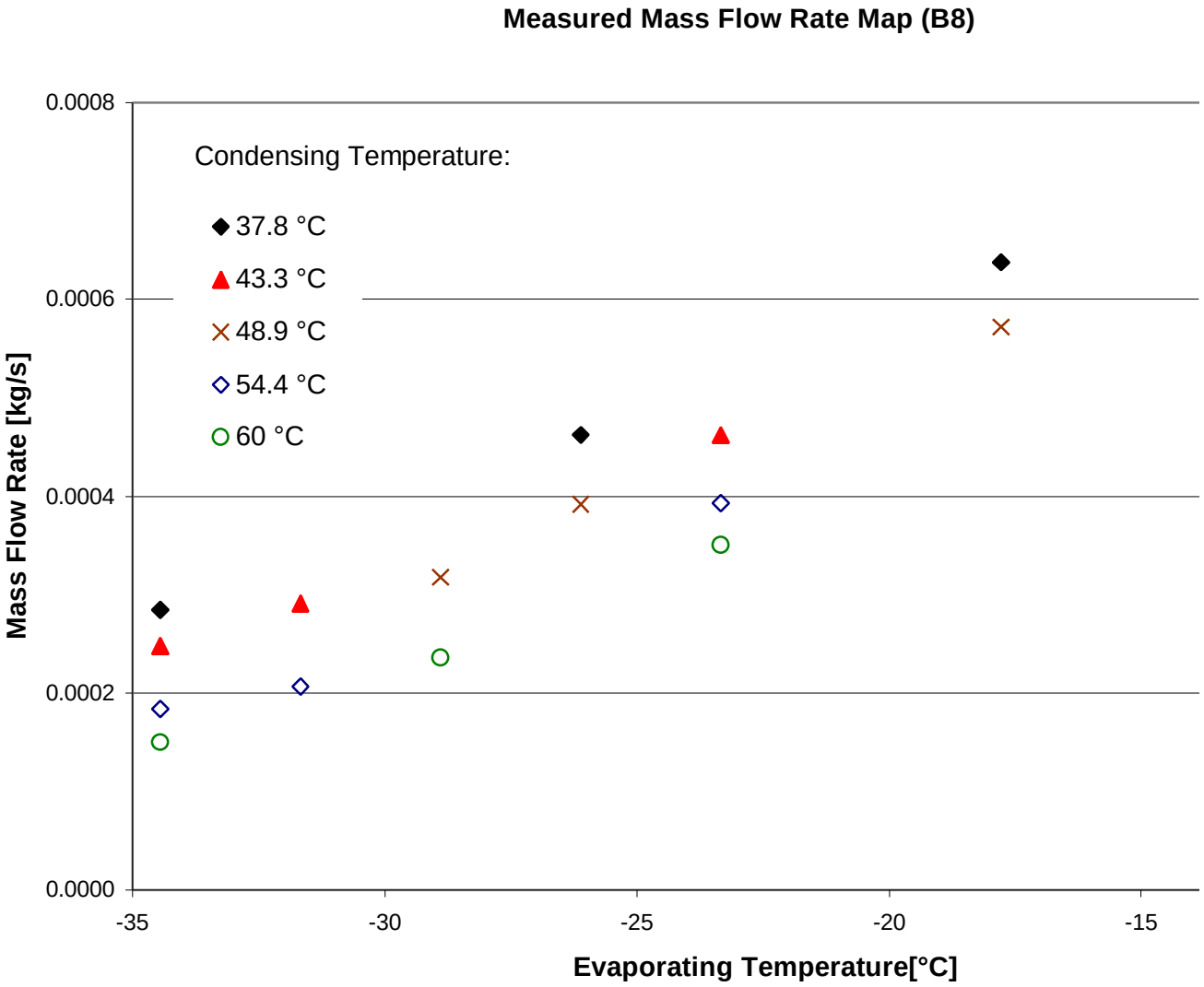
Measured Mass Flow Rate Map (B8)
Condensing Temperature:
37.8 °C
43.3 °C
48.9 °C
54.4 °C
60 °C
Mass Flow Rate [kg/s]
0.0008
0.0006
0.0004
0.0002
0.0000
-35
-30
-25
-20
-15
Evaporating Temperature[°C]

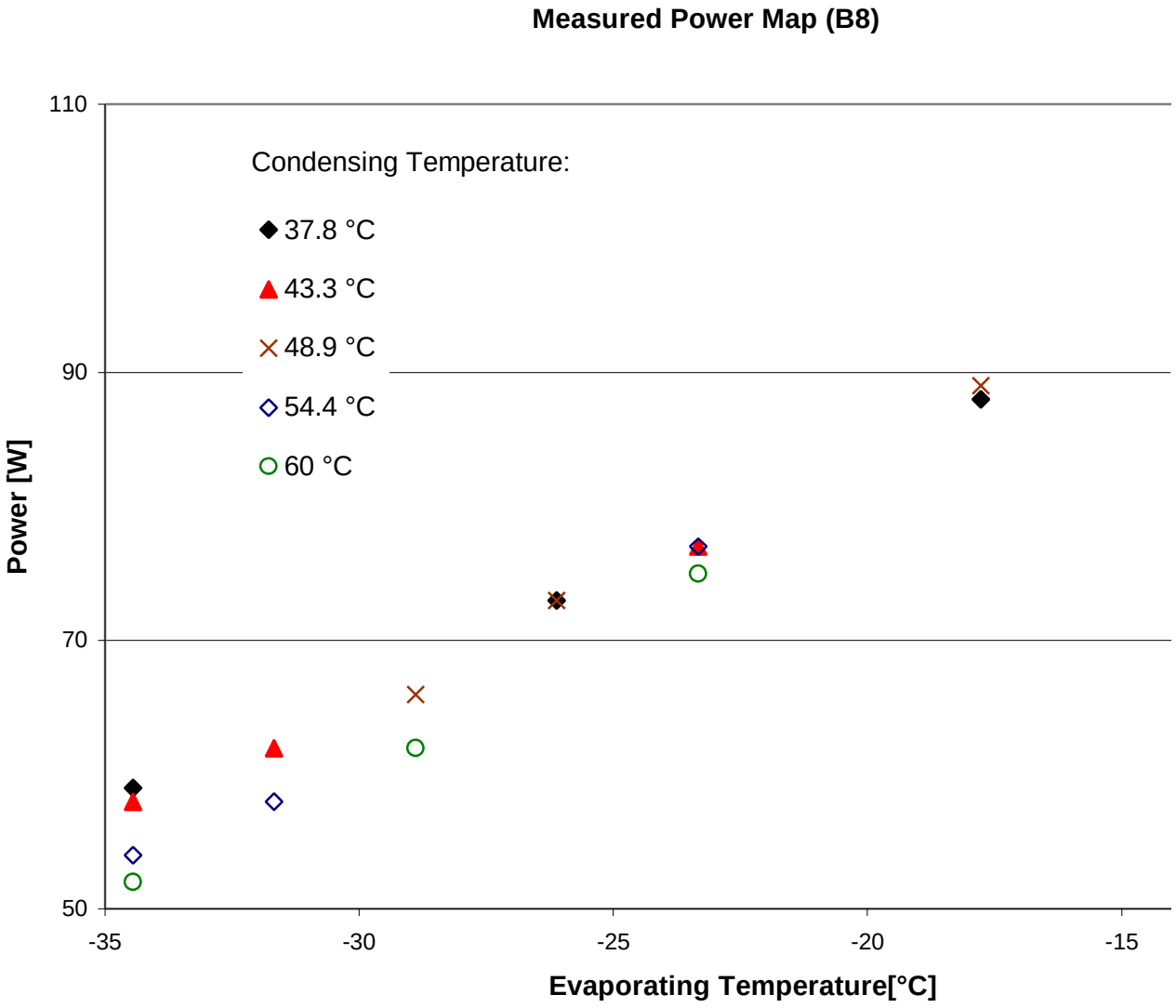
Measured Power Map (B8)
110
90
70
50
Power [W]
Condensing Temperature:
37.8 °C
43.3 °C
48.9 °C
54.4 °C
60 °C
-35
-30
-25
-20
-15
Evaporating Temperature[°C]

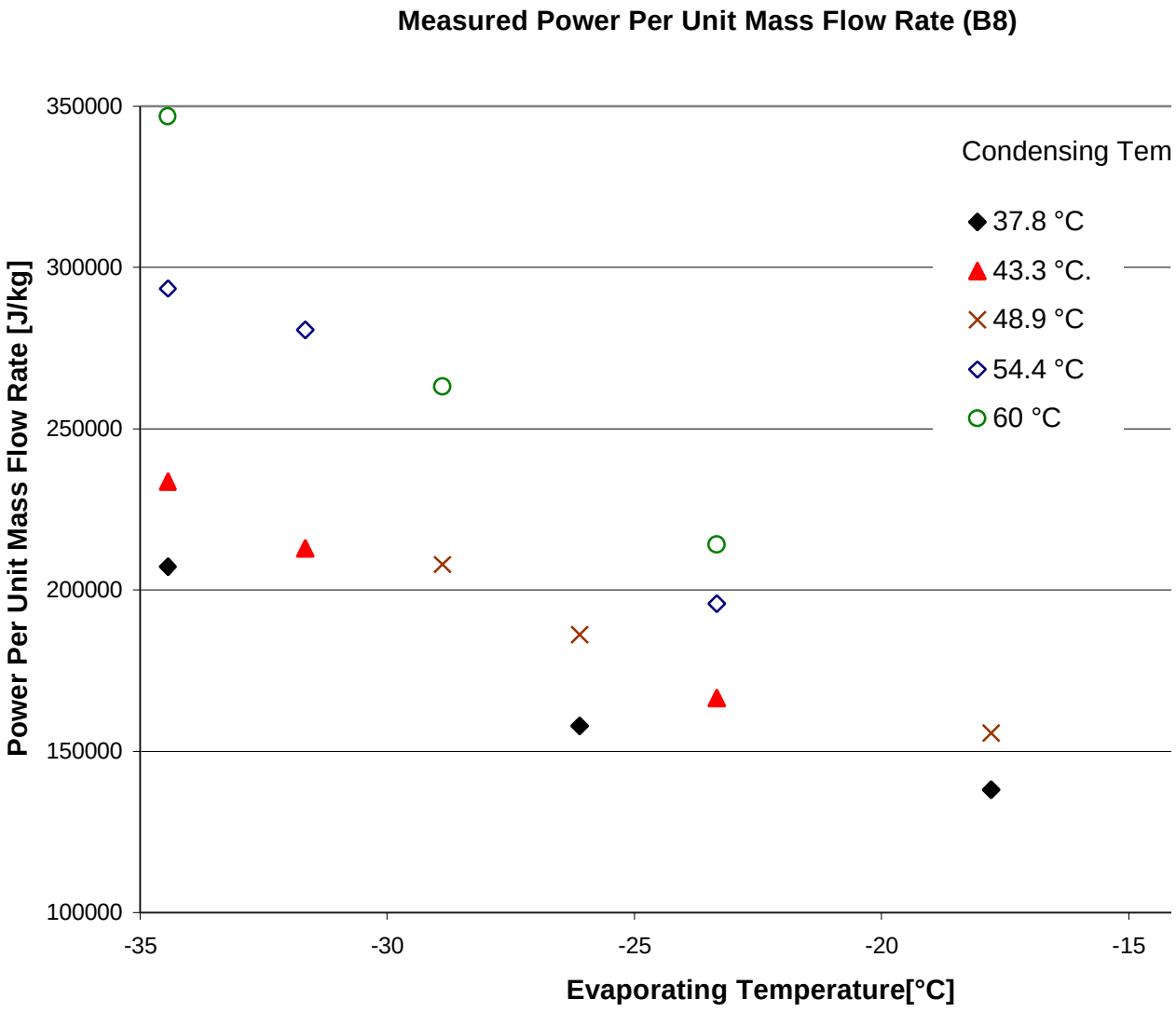
Measured Power Per Unit Mass Flow Rate (B8)
Power Per Unit Mass Flow Rate [J/kg]
350000
300000
250000
200000
150000
100000
-35
-30
-25
-20
-15
Evaporating Temperature[°C]
Condensing Tem
37.8 °C
43.3 °C.
48.9 °C
54.4 °C
60 °C

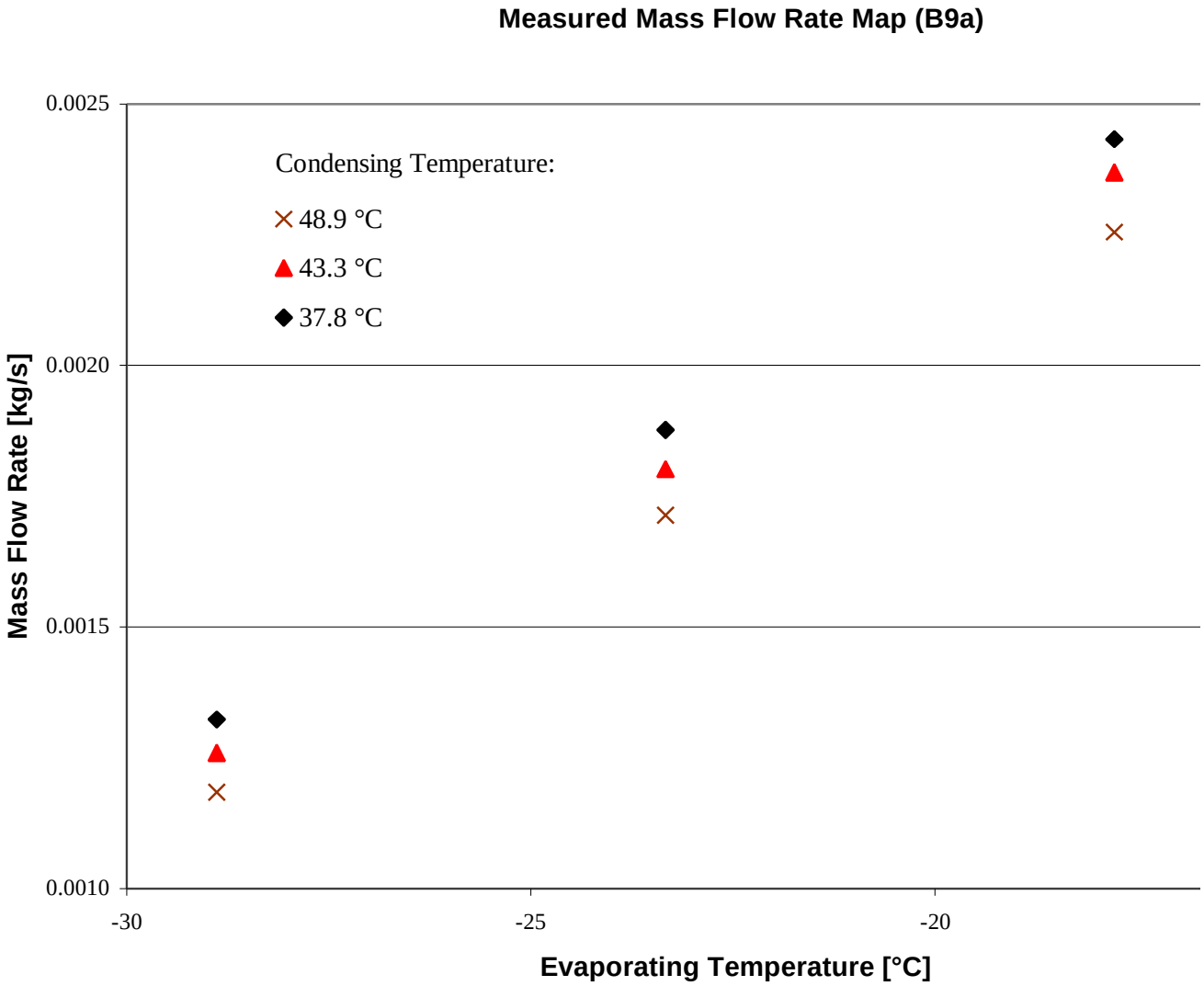
Measured Mass Flow Rate Map (B9a)
Condensing Temperature:
48.9 °C
43.3 °C
37.8 °C
Mass Flow Rate [kg/s]
0.0025
0.0020
0.0015
0.0010
-30
-25
-20
Evaporating Temperature [°C]

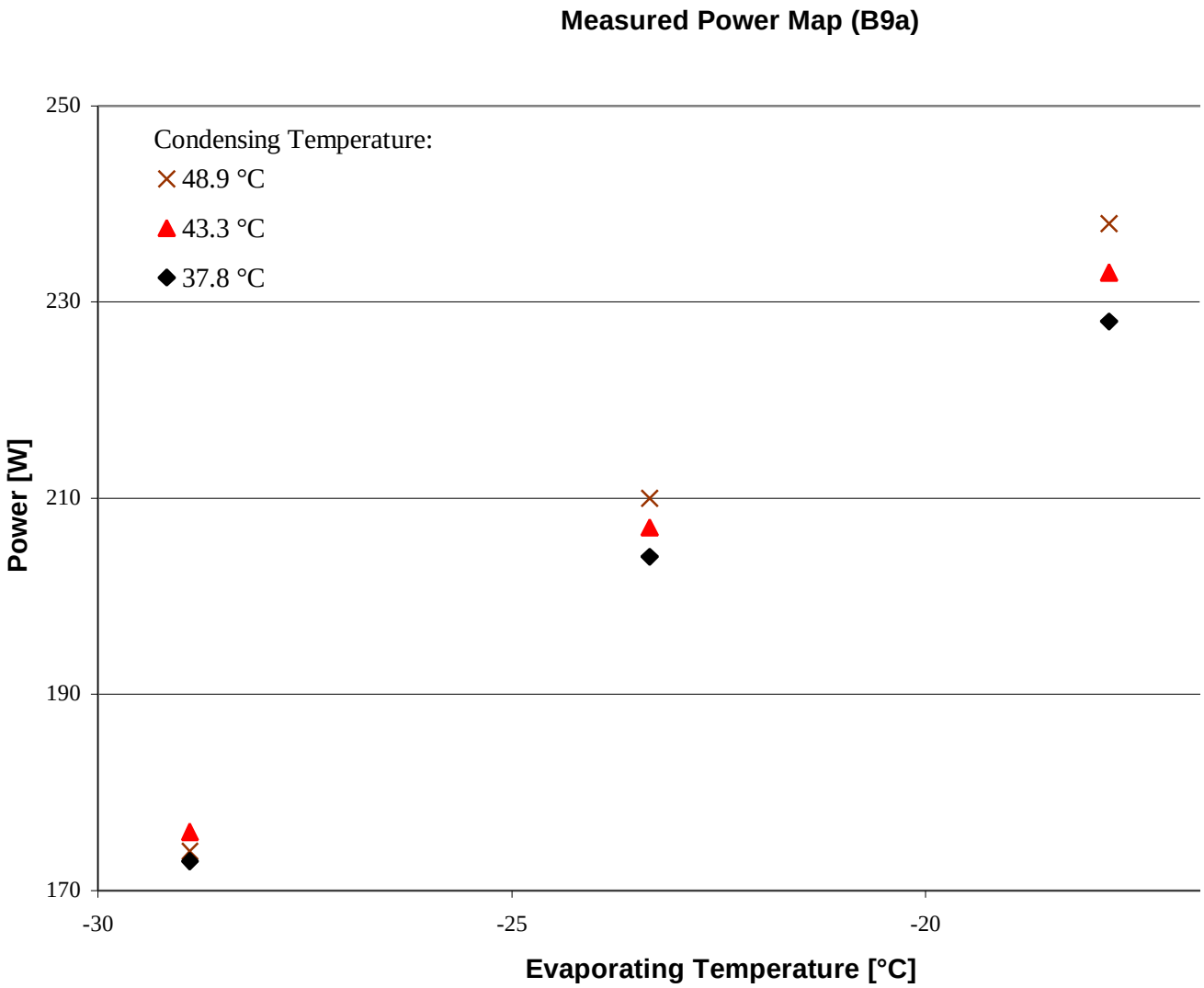
Measured Power Map (B9a)
250
230
210
190
170
Power [W]
Condensing Temperature:
48.9 °C
43.3 °C
37.8 °C
-30
-25
-20
Evaporating Temperature [°C]

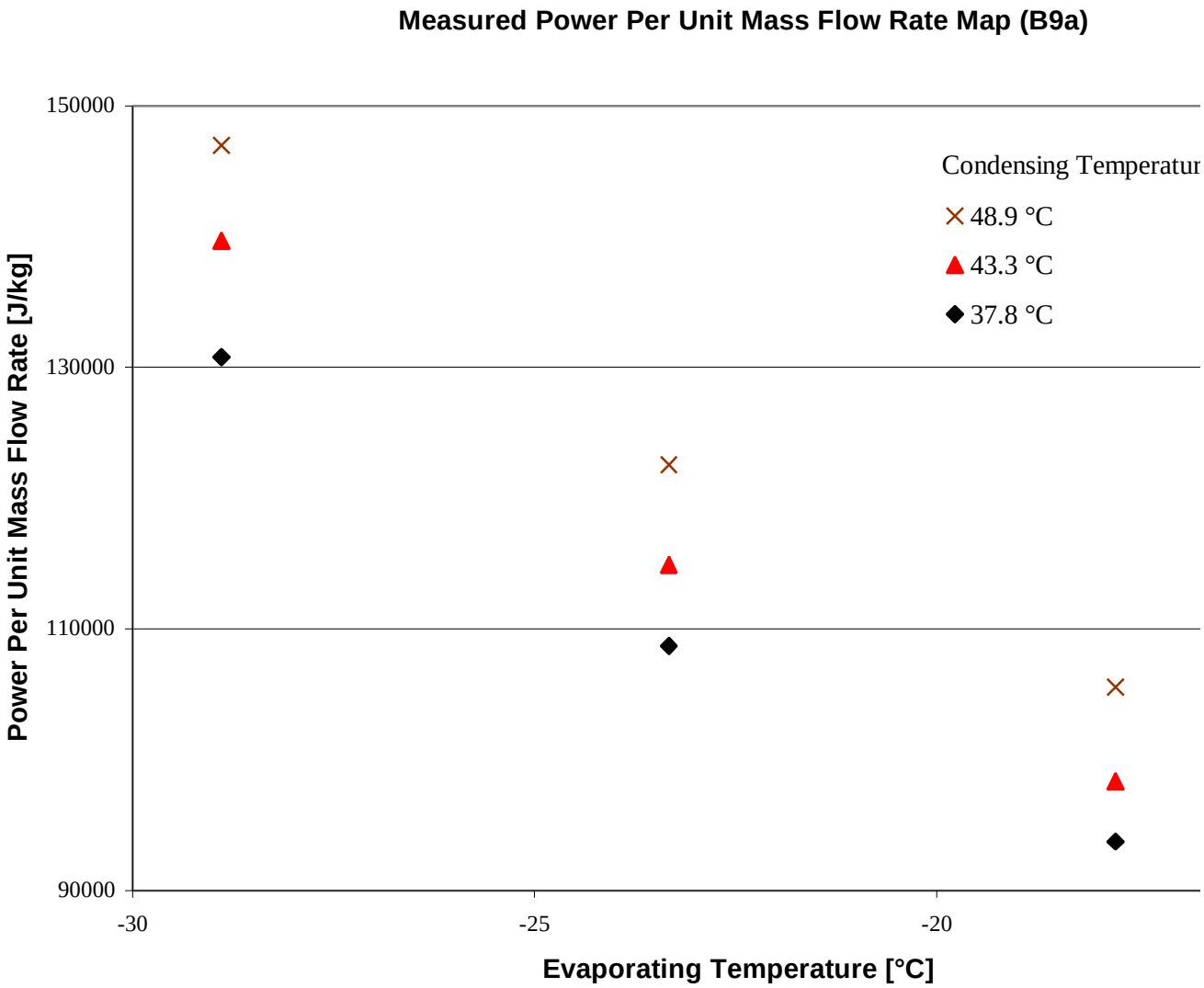
Measured Power Per Unit Mass Flow Rate Map (B9a)
Power Per Unit Mass Flow Rate [J/kg]
150000
130000
110000
90000
-30
-25
-20
Evaporating Temperature [°C]
Condensing Temperatur
48.9 °C
43.3 °C
37.8 °C

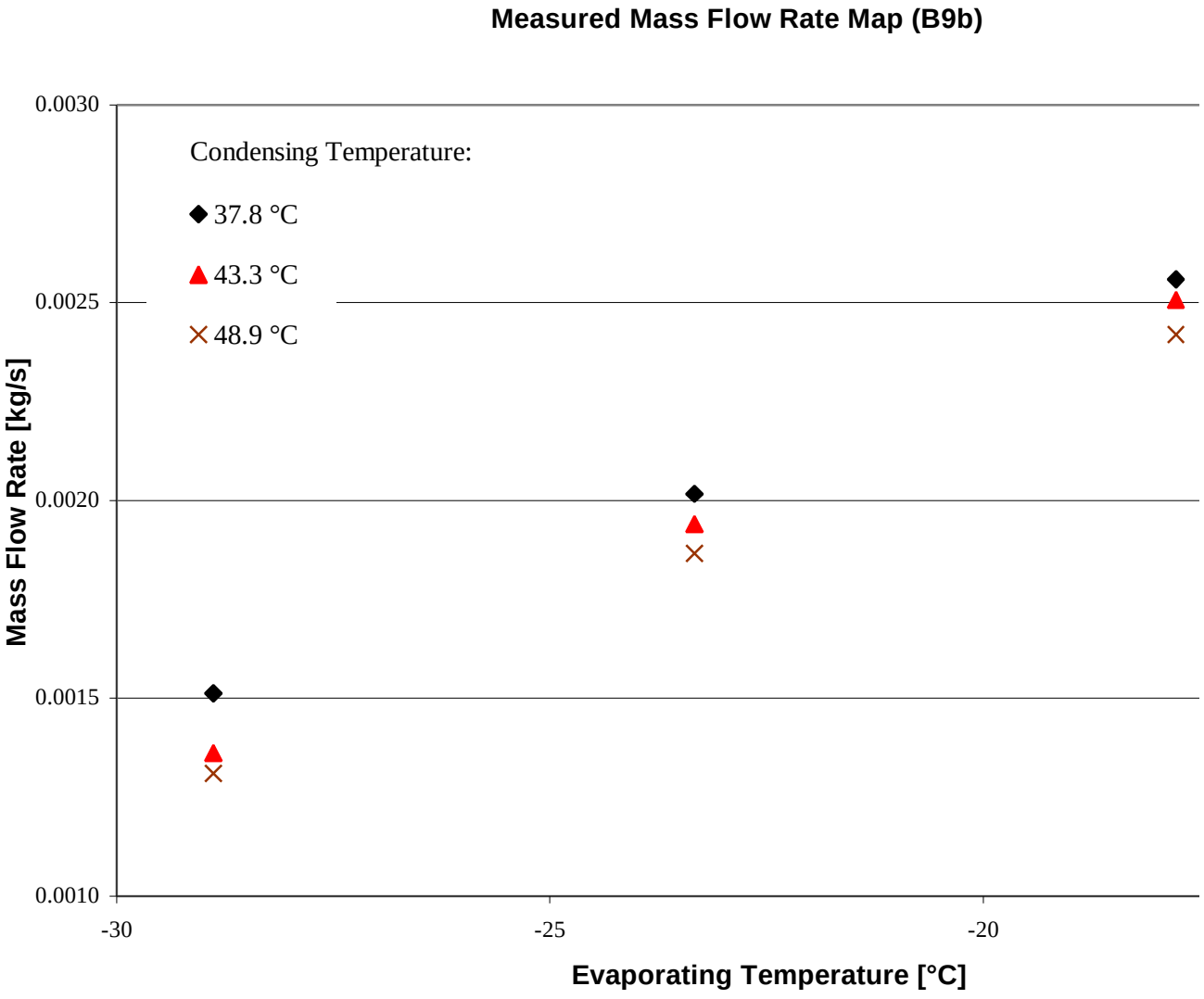
Measured Mass Flow Rate Map (B9b)
Condensing Temperature:
37.8 °C
43.3 °C
48.9 °C
0.0030
0.0025
0.0020
0.0015
0.0010
Mass Flow Rate [kg/s]
-30
-25
-20
Evaporating Temperature [°C]

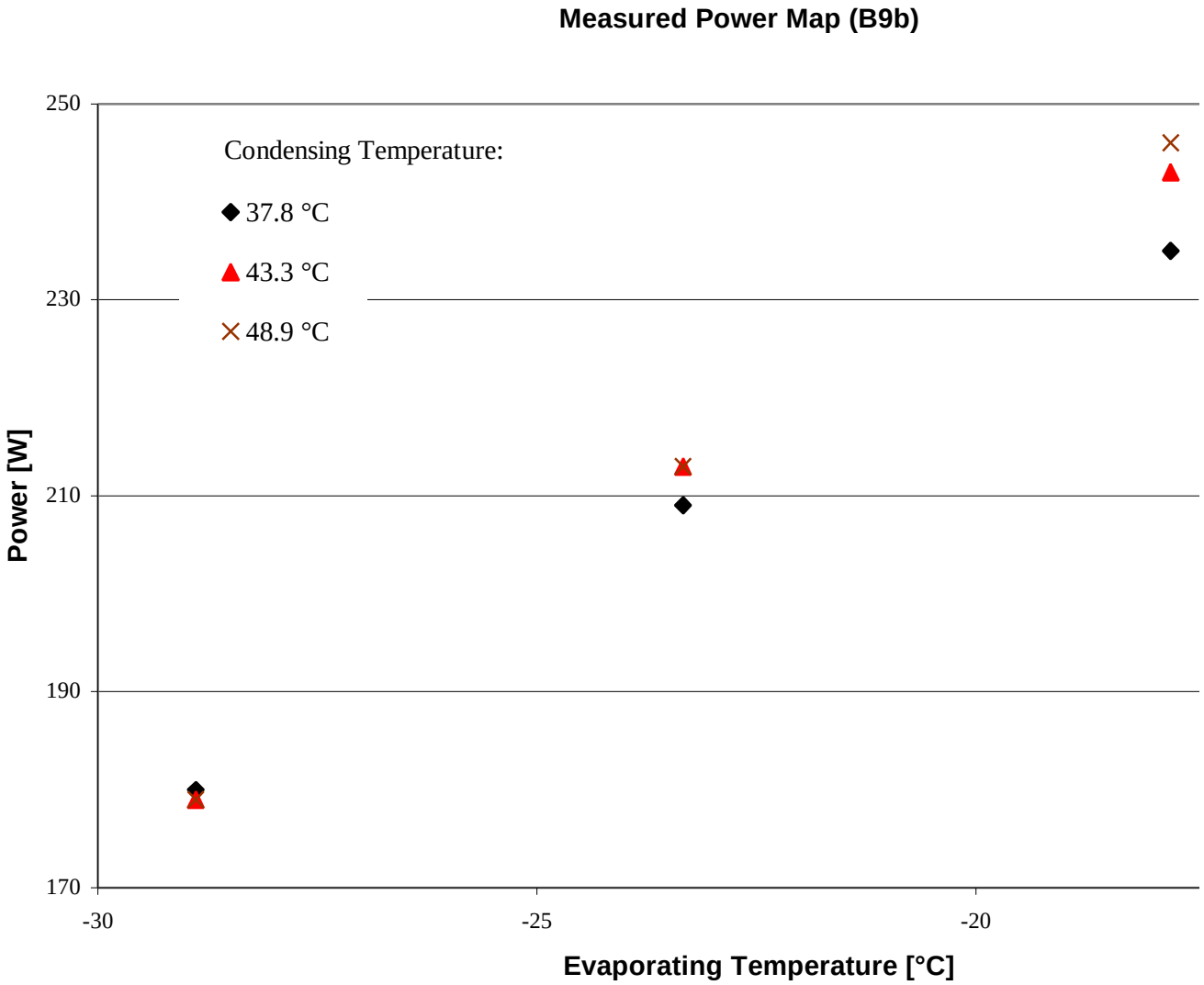
Measured Power Map (B9b)
Condensing Temperature:
37.8 °C
43.3 °C
48.9 °C
Power [W]
250
230
210
190
170
-30
-25
-20
Evaporating Temperature [°C]

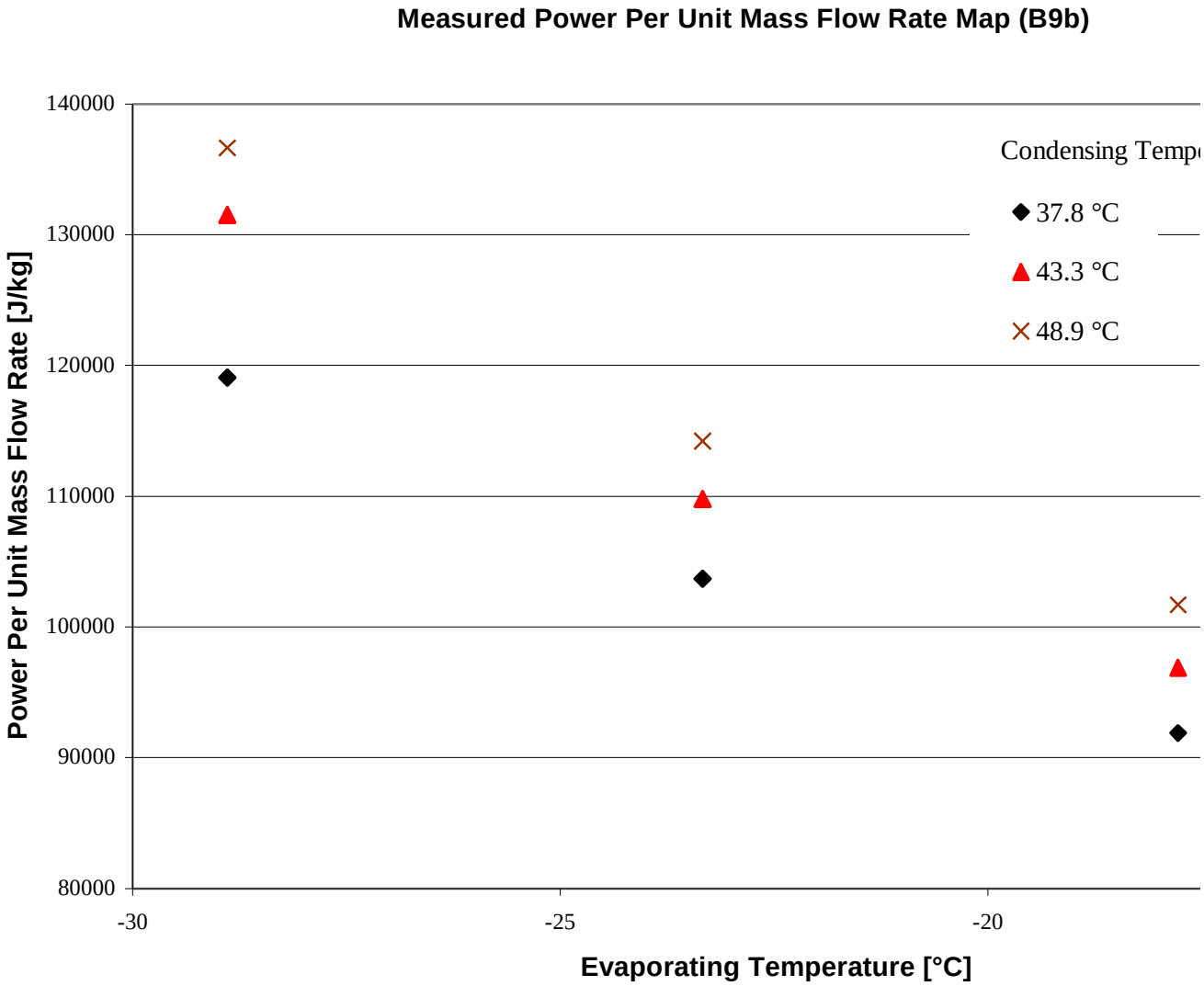
Measured Power Per Unit Mass Flow Rate Map (B9b)
Power Per Unit Mass Flow Rate [J/kg]
140000
130000
120000
110000
100000
90000
80000
-30
-25
-20
Evaporating Temperature [°C]
Condensing Temp
37.8 °C
43.3 °C
48.9 °C

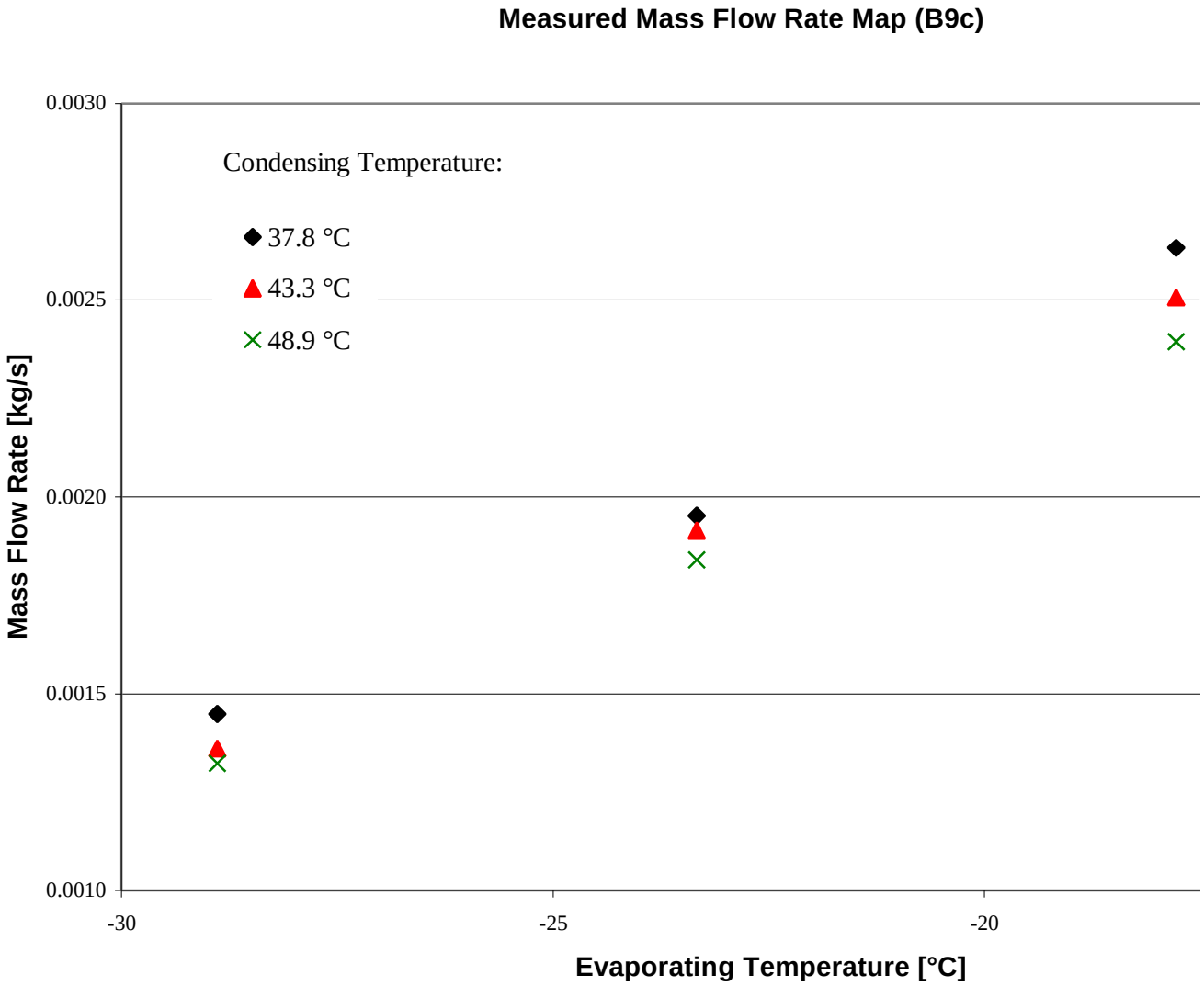
Measured Mass Flow Rate Map (B9c)
Condensing Temperature:
37.8 °C
43.3 °C
48.9 °C
Mass Flow Rate [kg/s]
0.0030
0.0025
0.0020
0.0015
0.0010
-30
-25
-20
Evaporating Temperature [°C]

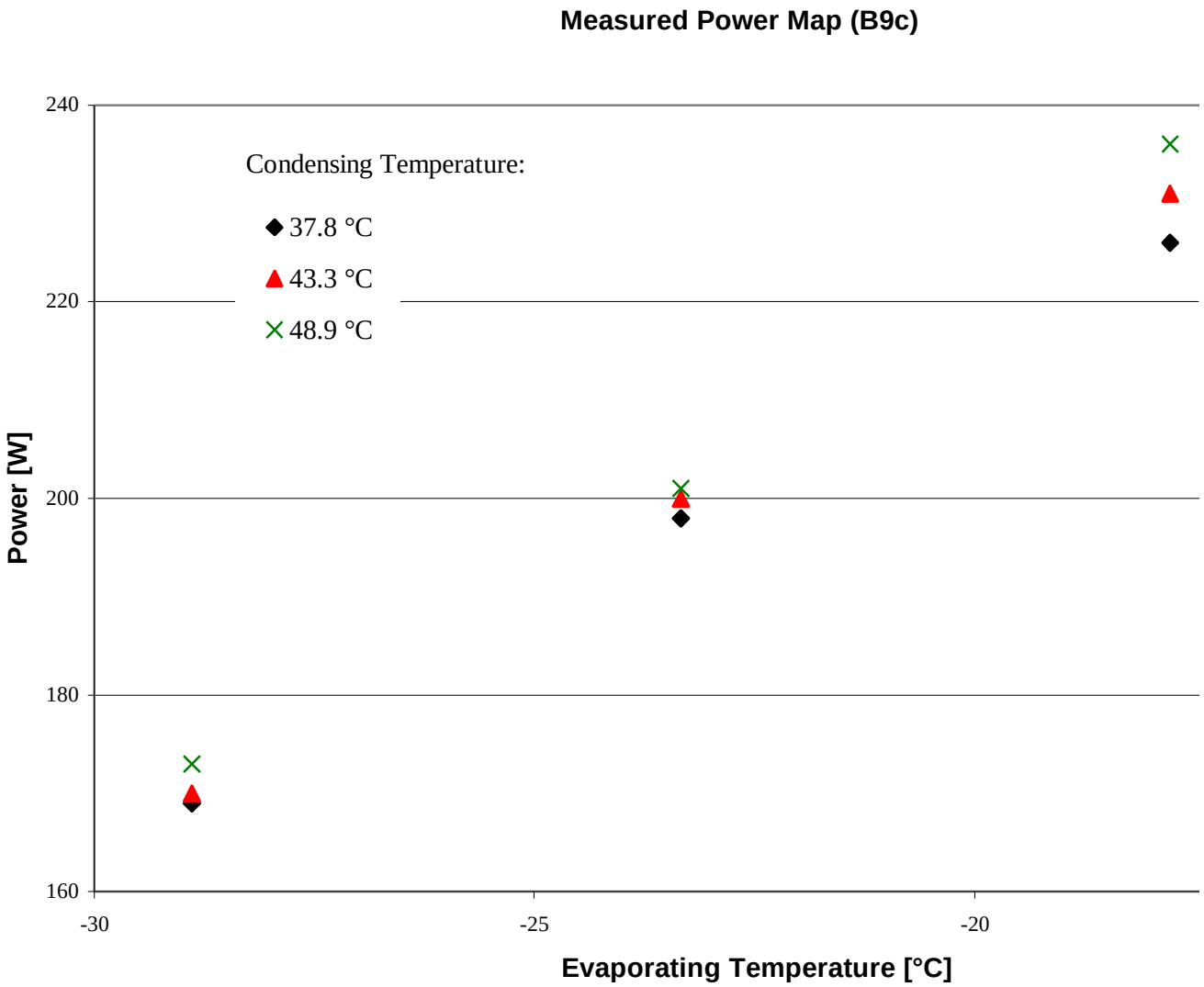
Measured Power Map (B9c)
Condensing Temperature:
37.8 °C
43.3 °C
48.9 °C
Power [W]
240
220
200
180
160
-30
-25
-20
Evaporating Temperature [°C]

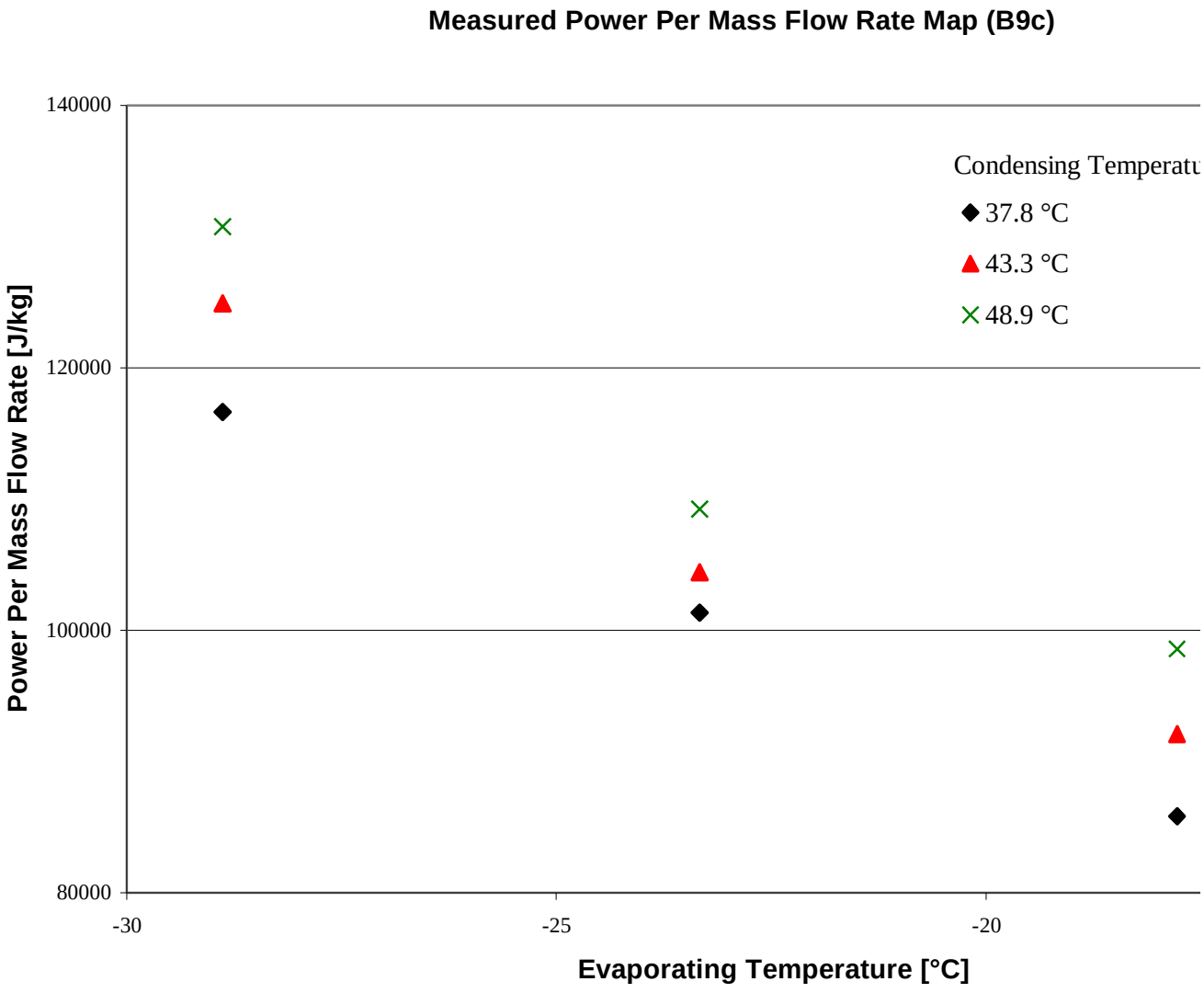
Measured Power Per Mass Flow Rate Map (B9c)
Power Per Mass Flow Rate [J/kg]
140000
120000
100000
80000
-30
-25
-20
Evaporating Temperature [°C]
Condensing Temperatu
37.8 °C
43.3 °C
48.9 °C

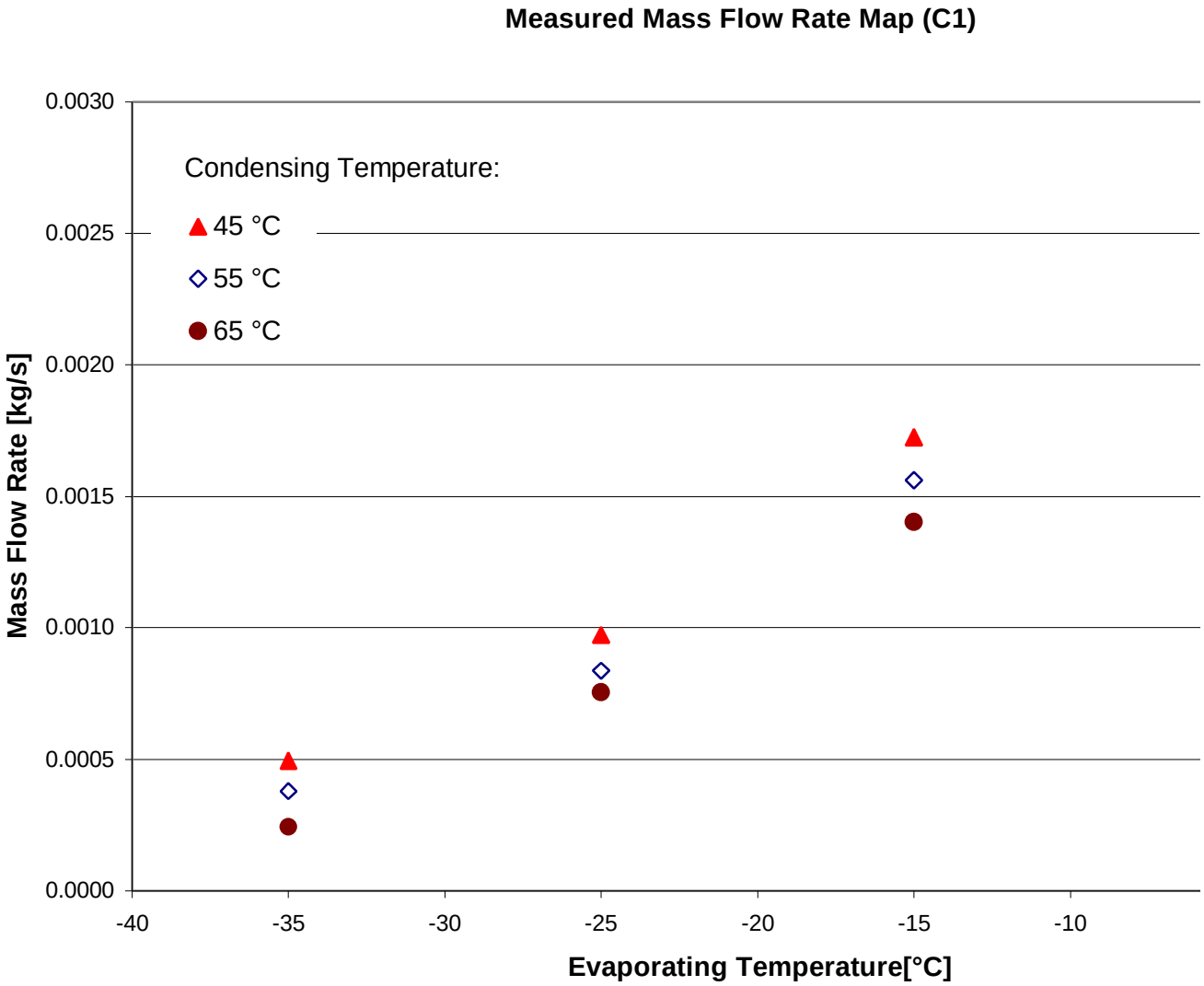
Measured Mass Flow Rate Map (C1)
Condensing Temperature:
45 °C
55 °C
65 °C
Mass Flow Rate [kg/s]
0.0030
0.0025
0.0020
0.0015
0.0010
0.0005
0.0000
-40
-35
-30
-25
-20
-15
-10
Evaporating Temperature[°C]

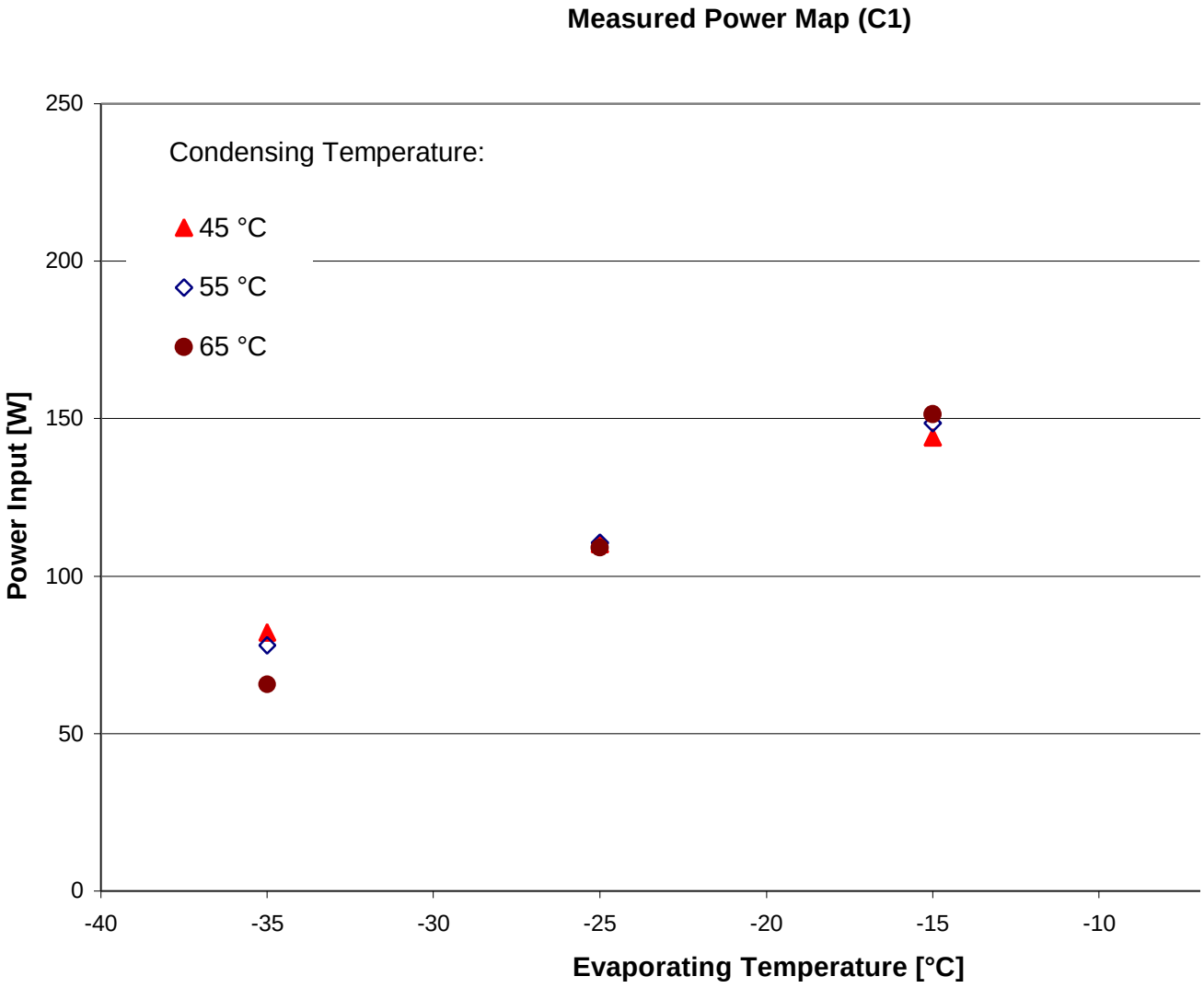
Measured Power Map (C1)
Condensing Temperature:
45 °C
55 °C
65 °C
Power Input [W]
250
200
150
100
50
0
-40
-35
-30
-25
-20
-15
-10
Evaporating Temperature [°C]

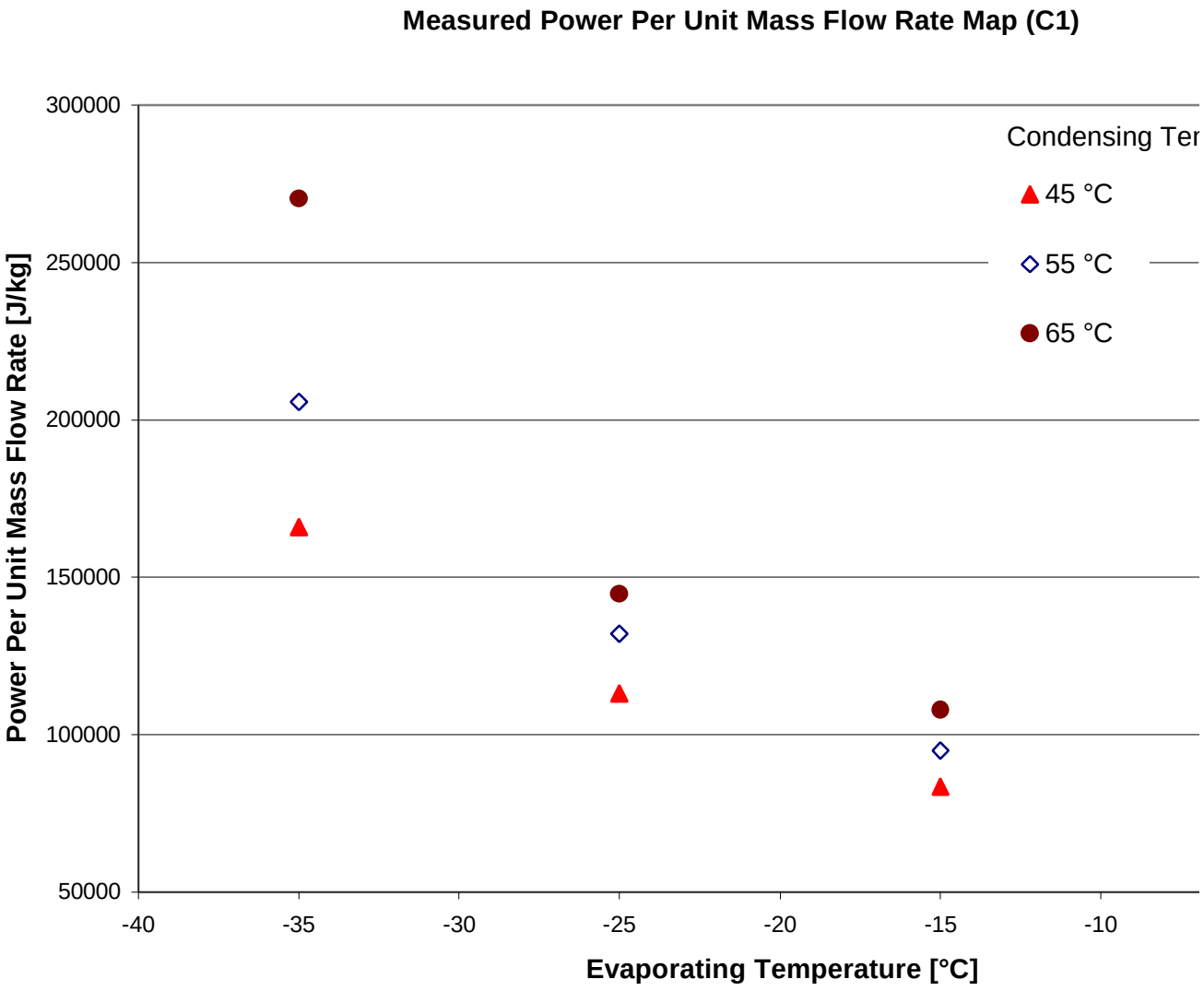
Measured Power Per Unit Mass Flow Rate Map (C1)
Power Per Unit Mass Flow Rate [J/kg]
300000
250000
200000
150000
100000
50000
-40
-35
-30
-25
-20
-15
-10
Evaporating Temperature [°C]
Condensing Ter
45 °C
55 °C
65 °C

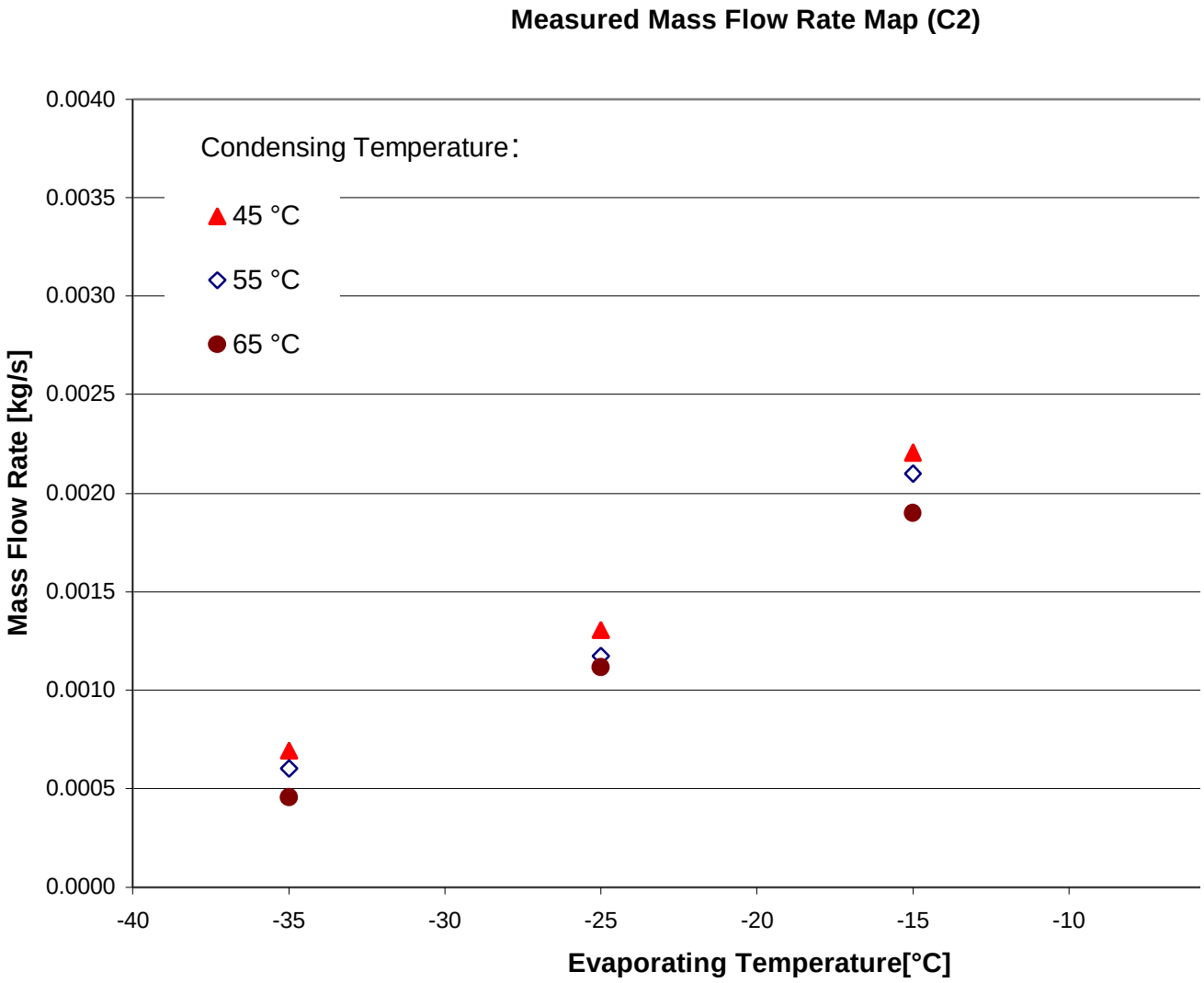
Measured Mass Flow Rate Map (C2)
Mass Flow Rate [kg/s]
0.0040
0.0035
0.0030
0.0025
0.0020
0.0015
0.0010
0.0005
0.0000
Condensing Temperature:
45 °C
55 °C
65 °C
-40
-35
-30
-25
-20
-15
-10
Evaporating Temperature[°C]

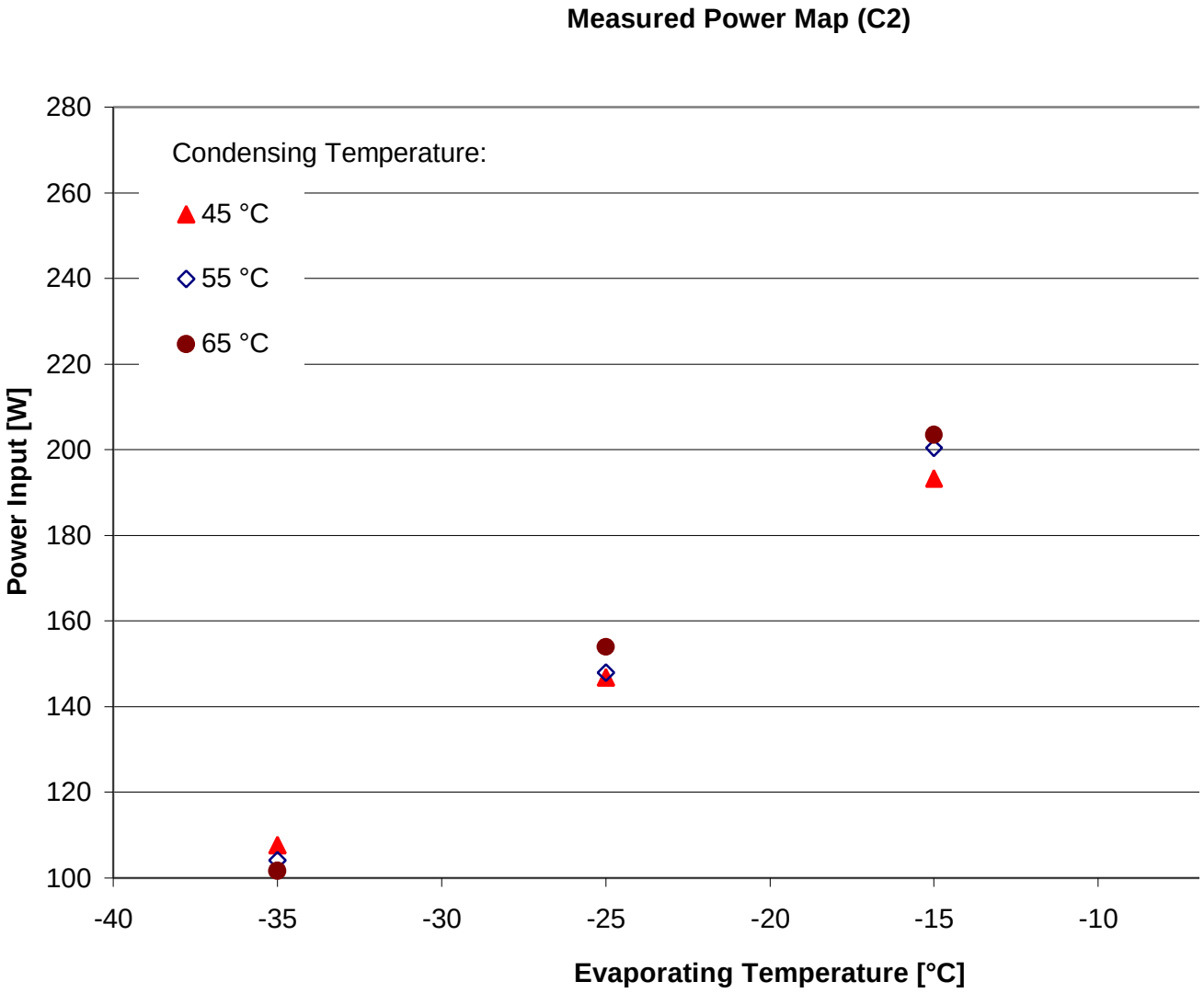
Measured Power Map (C2)
Condensing Temperature:
45 °C
55 °C
65 °C
Power Input [W]
280
260
240
220
200
180
160
140
120
100
-40
-35
-30
-25
-20
-15
-10
Evaporating Temperature [°C]

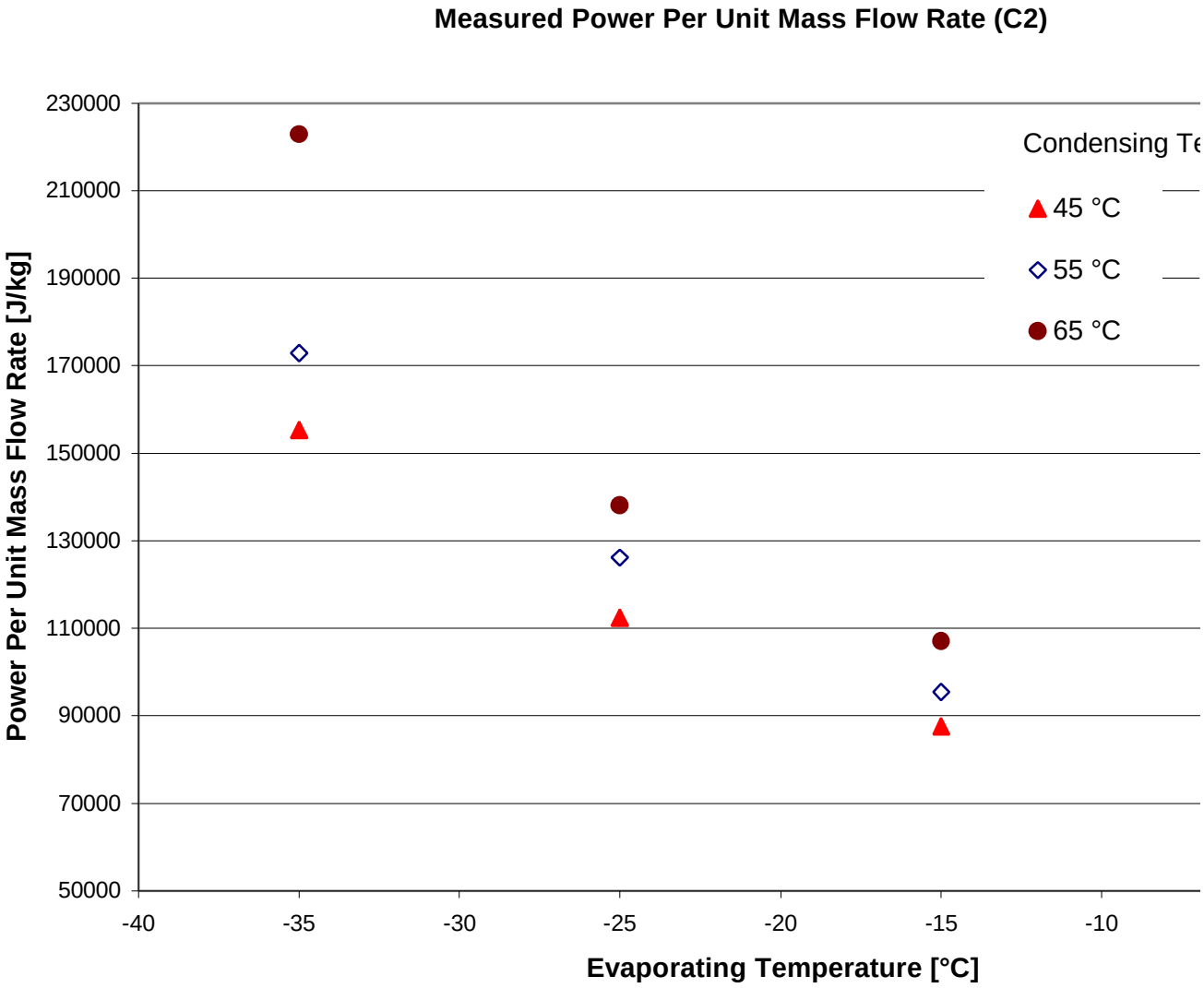
Measured Power Per Unit Mass Flow Rate (C2)
Power Per Unit Mass Flow Rate [J/kg]
230000
210000
190000
170000
150000
130000
110000
90000
70000
50000
-40
-35
-30
-25
-20
-15
-10
Evaporating Temperature [°C]
Condensing Te
45 °C
55 °C
65 °C

Appendix B: ARI Maps

The following plots show compressor maps for all 21 sets of testing data that were generated using the ARI curve fit method. For each data set, there is a mass flow rate, a power and a power per unit mass flow rate plot. The experimental data points that were used to generate these maps are also shown.

ARI Curve Fits (A1a)

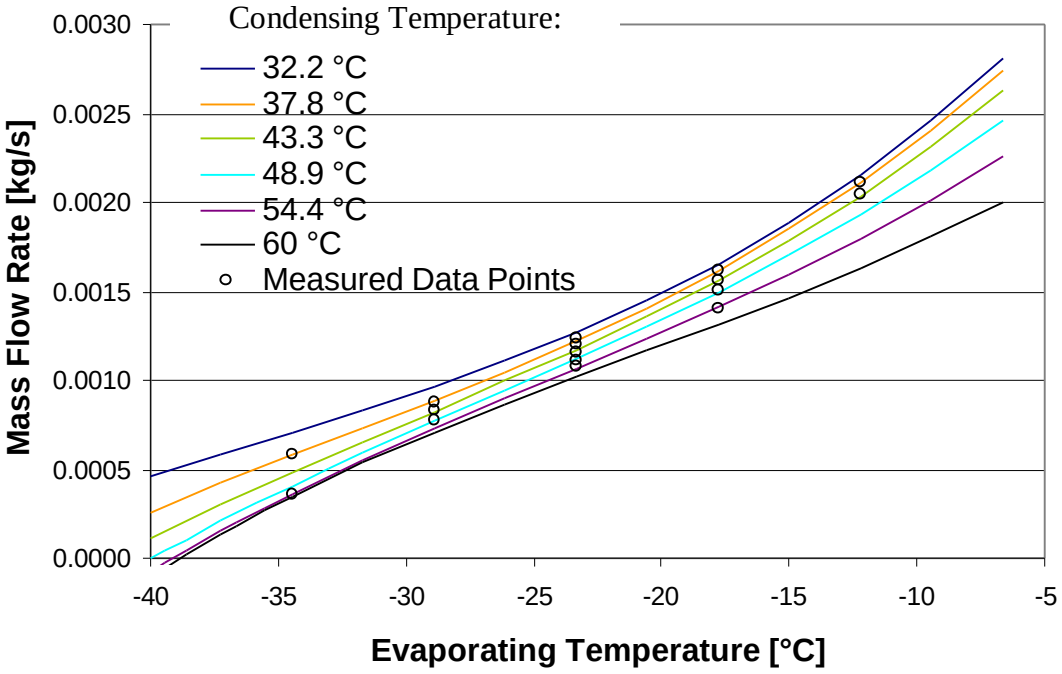

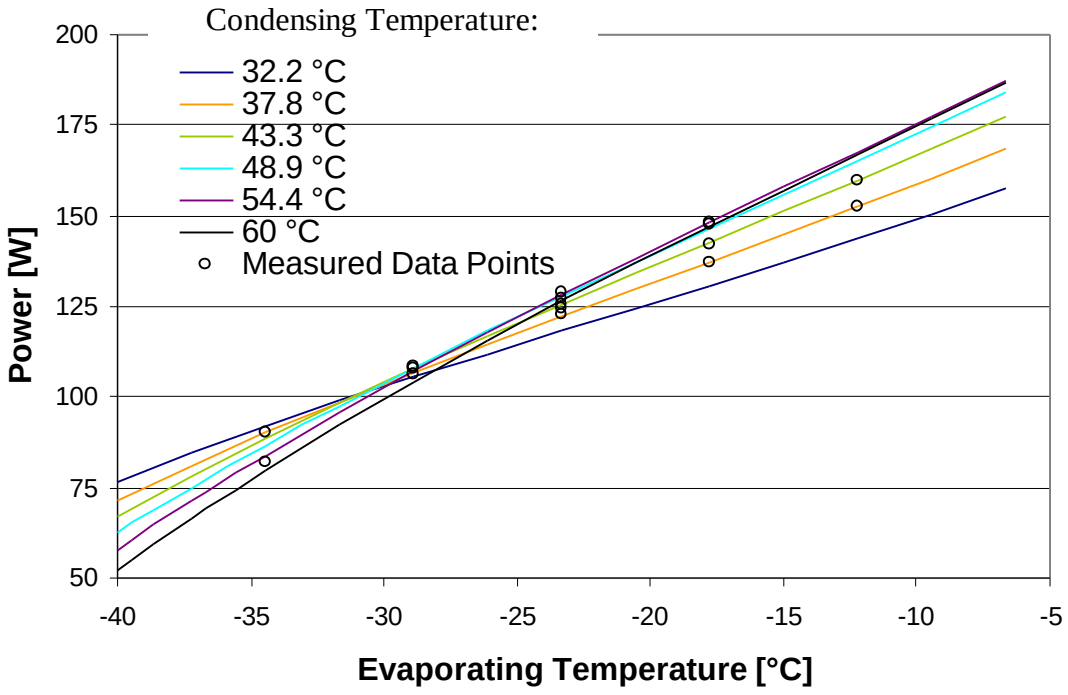

ARI Curve Fit (A1a)

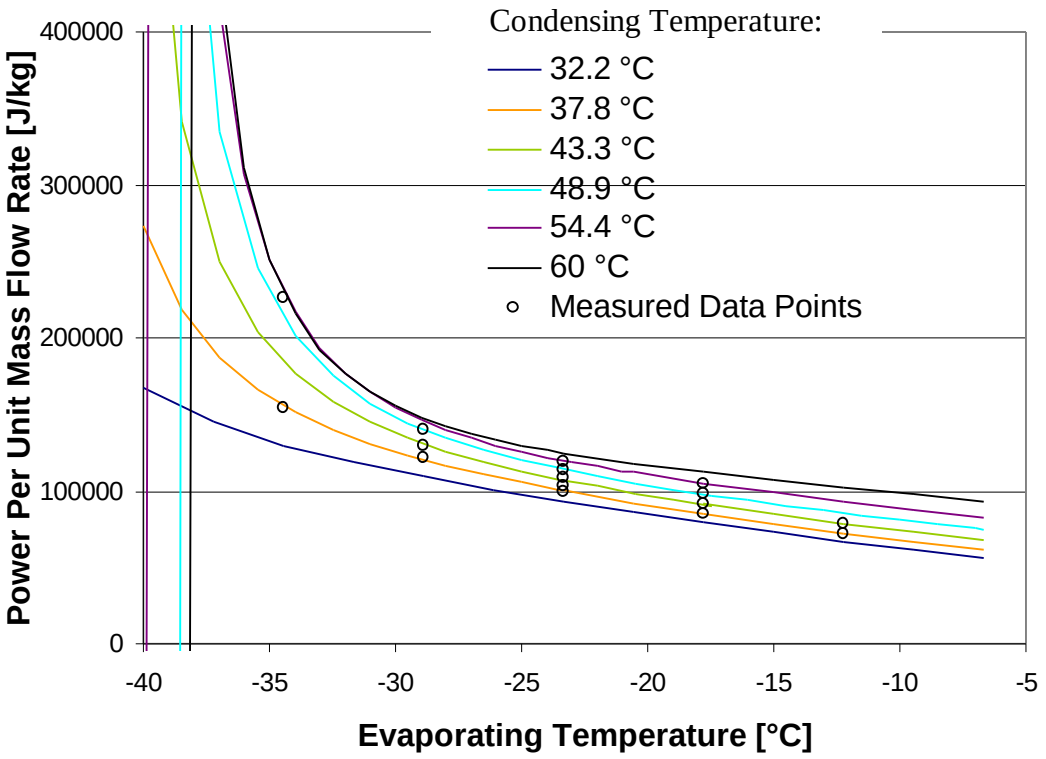

ARI Curve Fit (A1b)

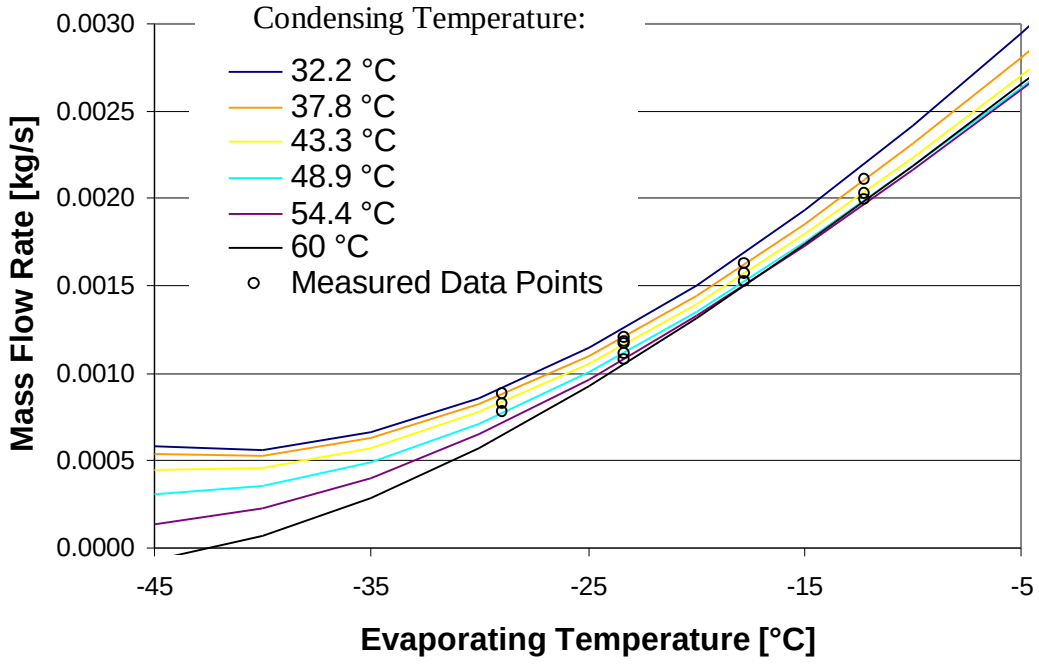

ARI Curve Fits (A1b)

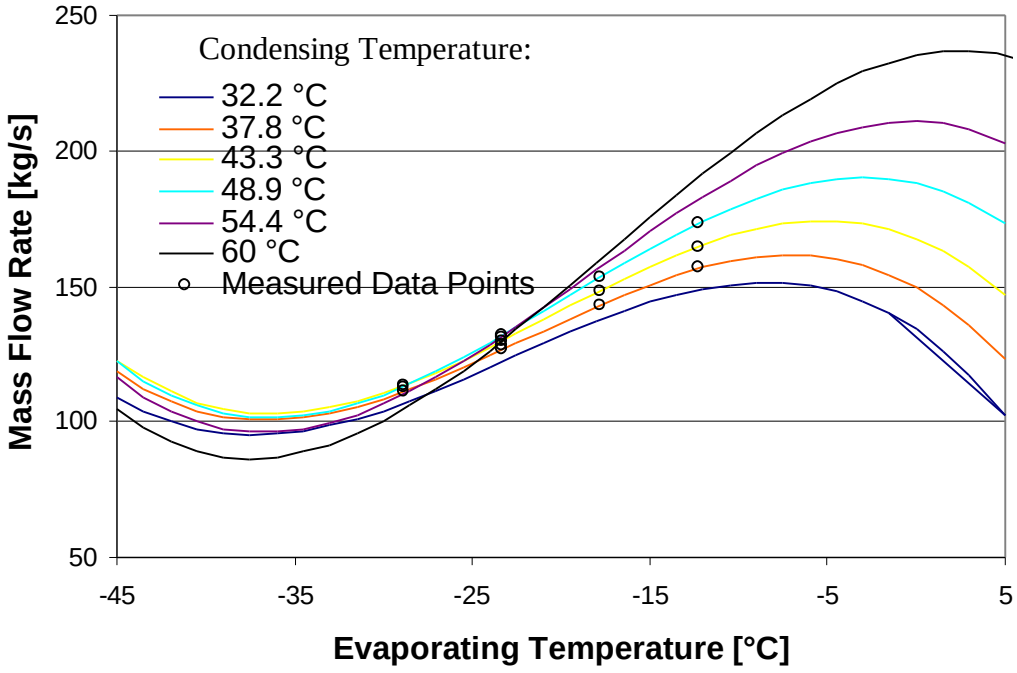

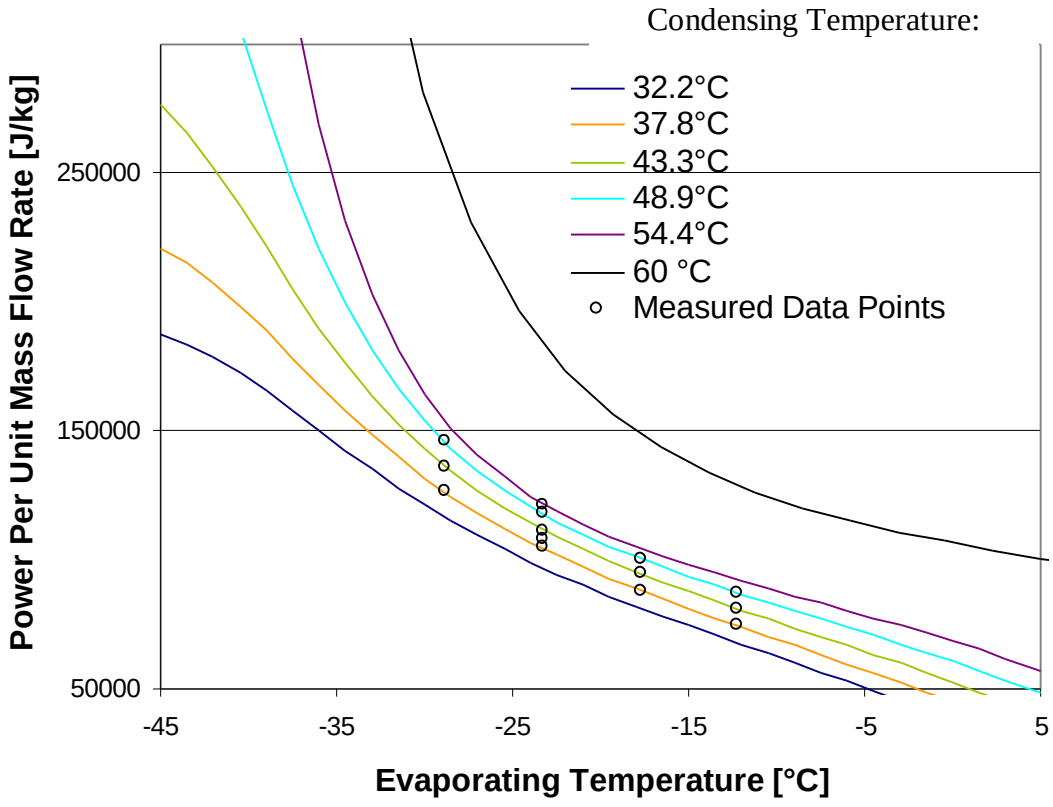

ARI Curve Fits (A2)

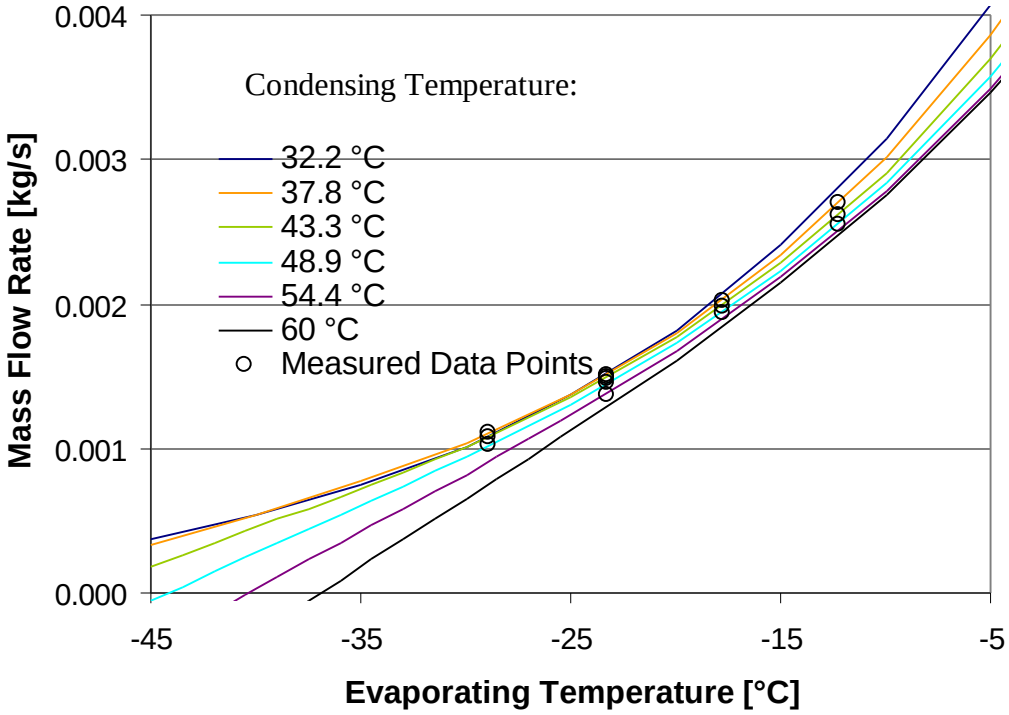

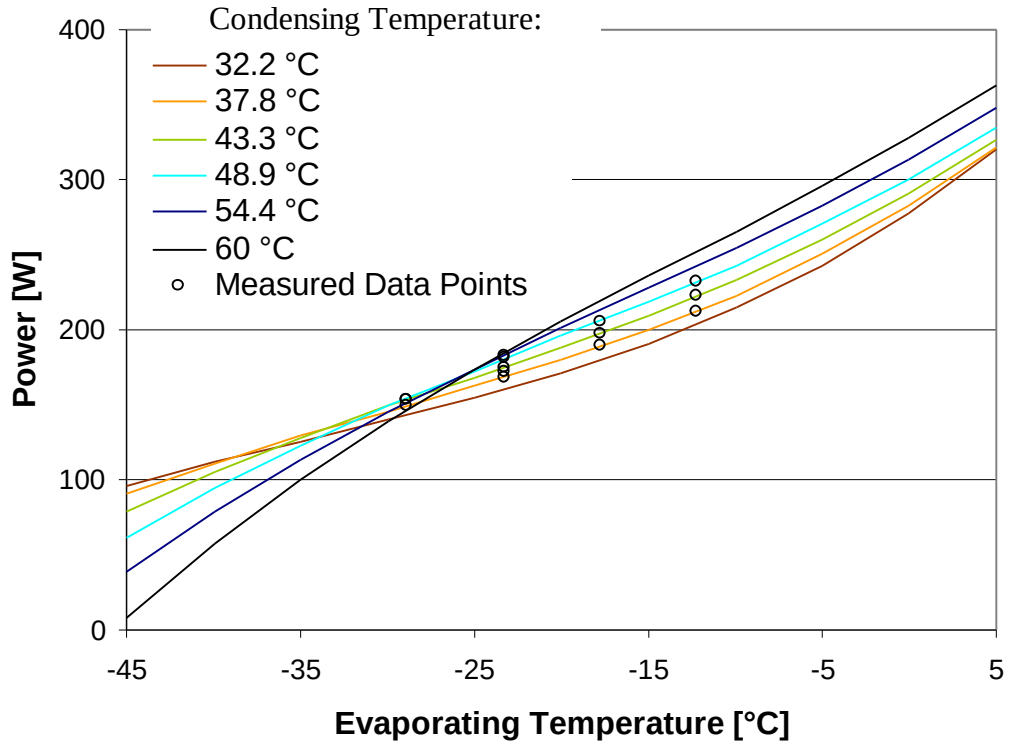

ARI Curve Fit (A2)

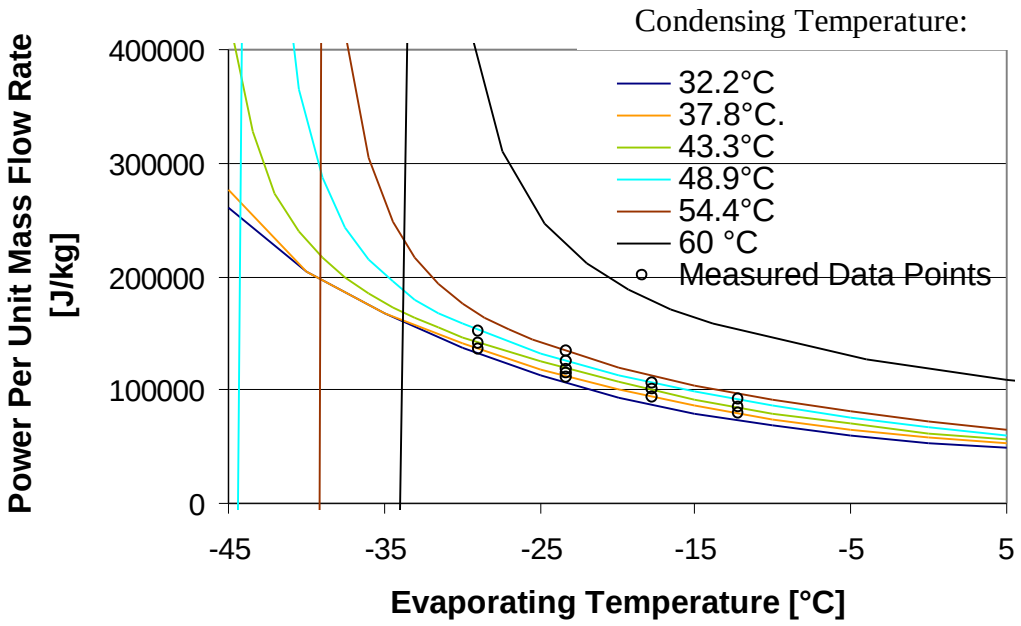

ARI Curve Fit (A3)

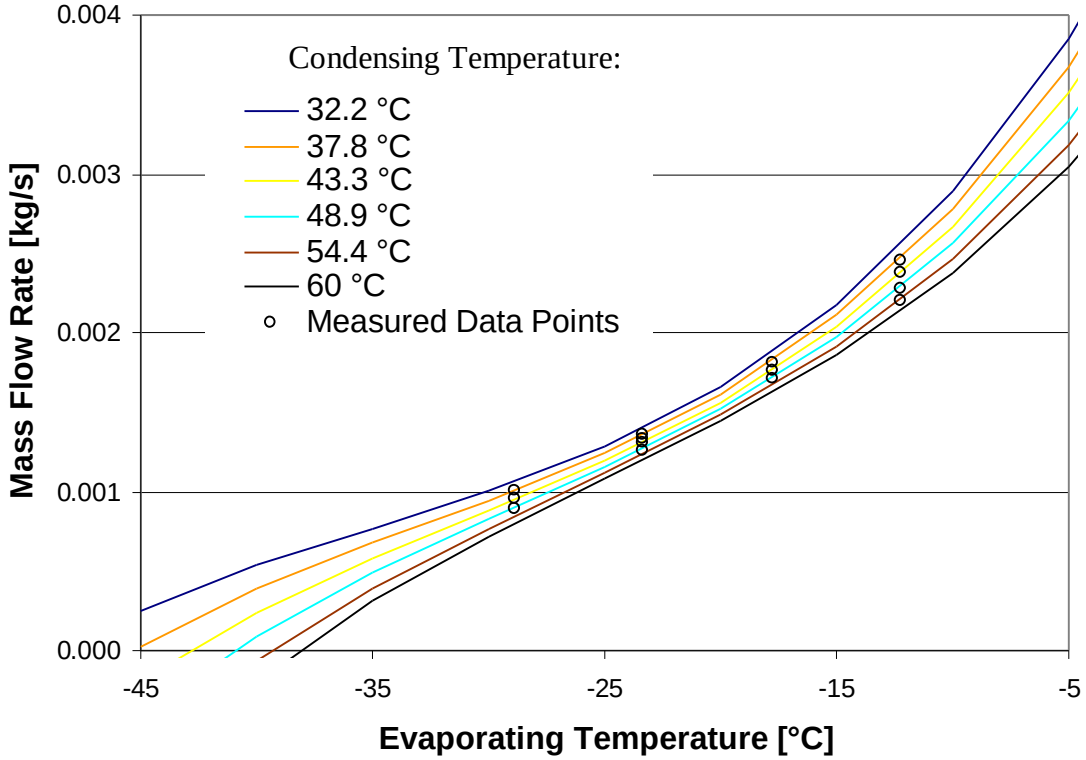

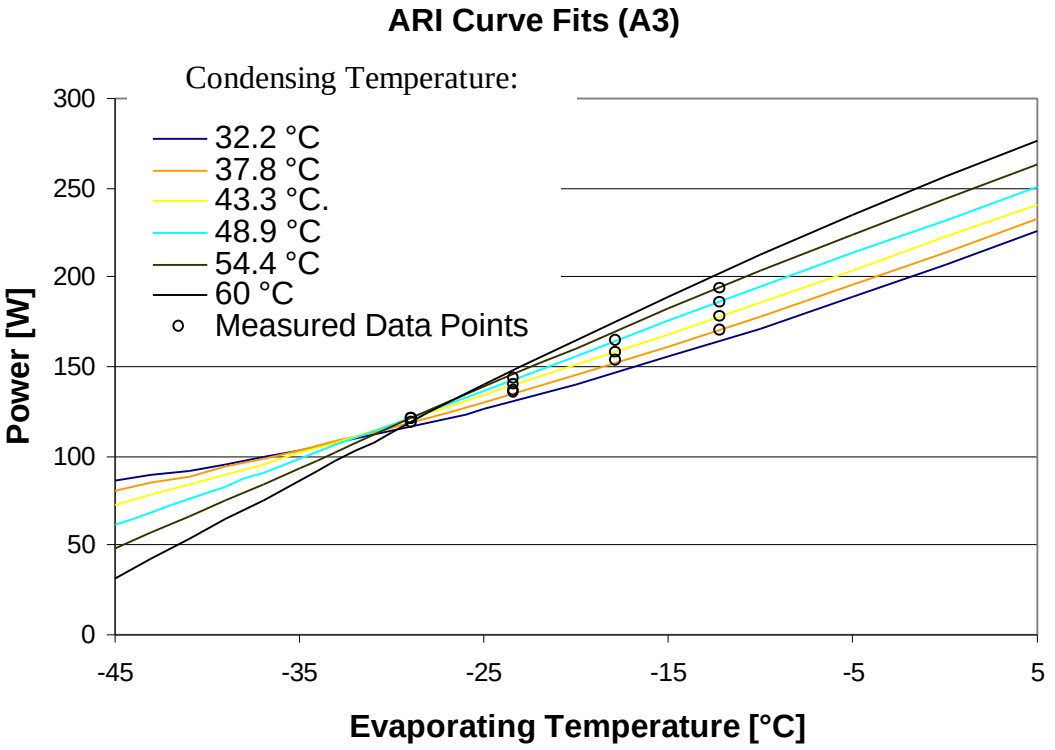
ARI Curve Fits (A3)
Condensing Temperature:
32.2 °C
37.8 °C
43.3 °C.
48.9 °C
54.4 °C
60 °C
Measured Data Points
Power [W]
300
250
200
150
100
50
0
-45
-35
-25
-15
-5
5
Evaporating Temperature [°C]

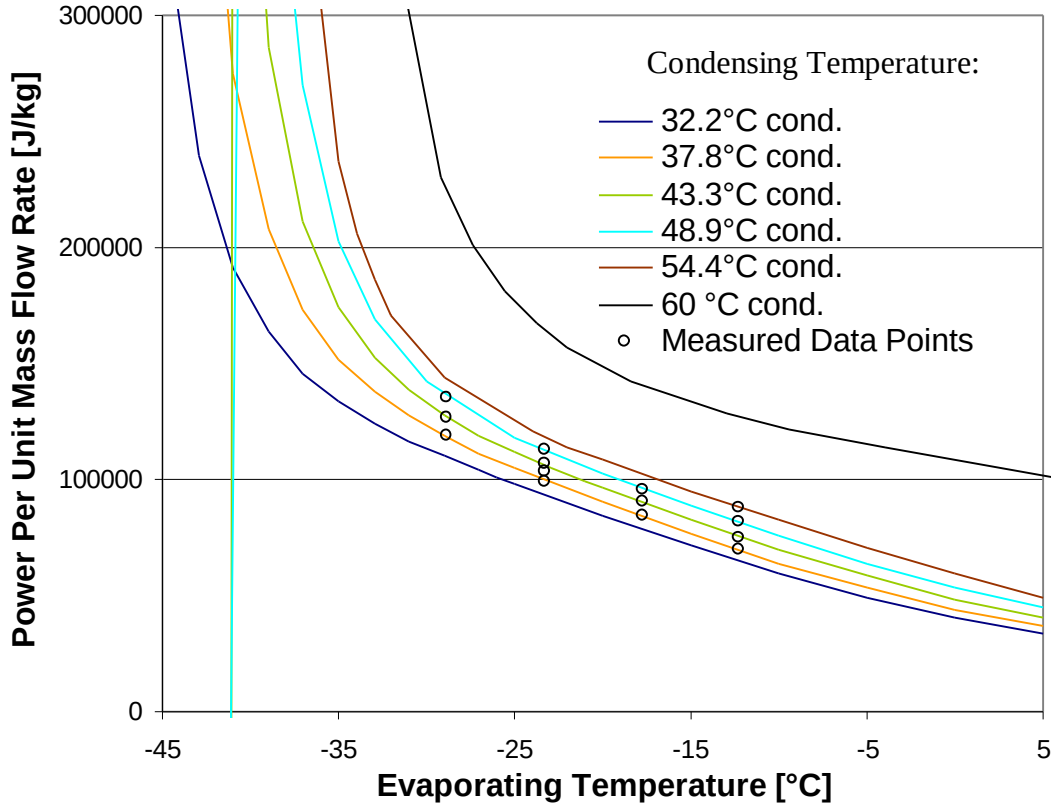
Condensing Temperature:
32.2°C cond.
37.8°C cond.
43.3°C cond.
48.9°C cond.
54.4°C cond.
60 °C cond.
Measured Data Points
Power Per Unit Mass Flow Rate [J/kg]
300000
200000
100000
0
-45
-35
-25
-15
-5
5
Evaporating Temperature [°C]

ARI Curve Fits (A4)

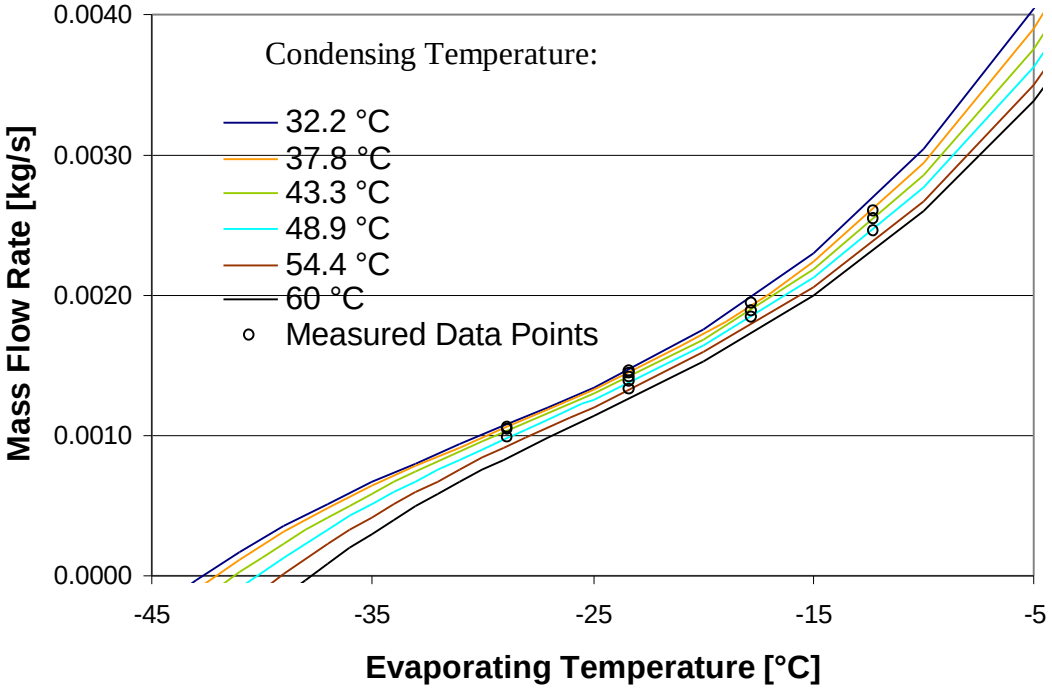

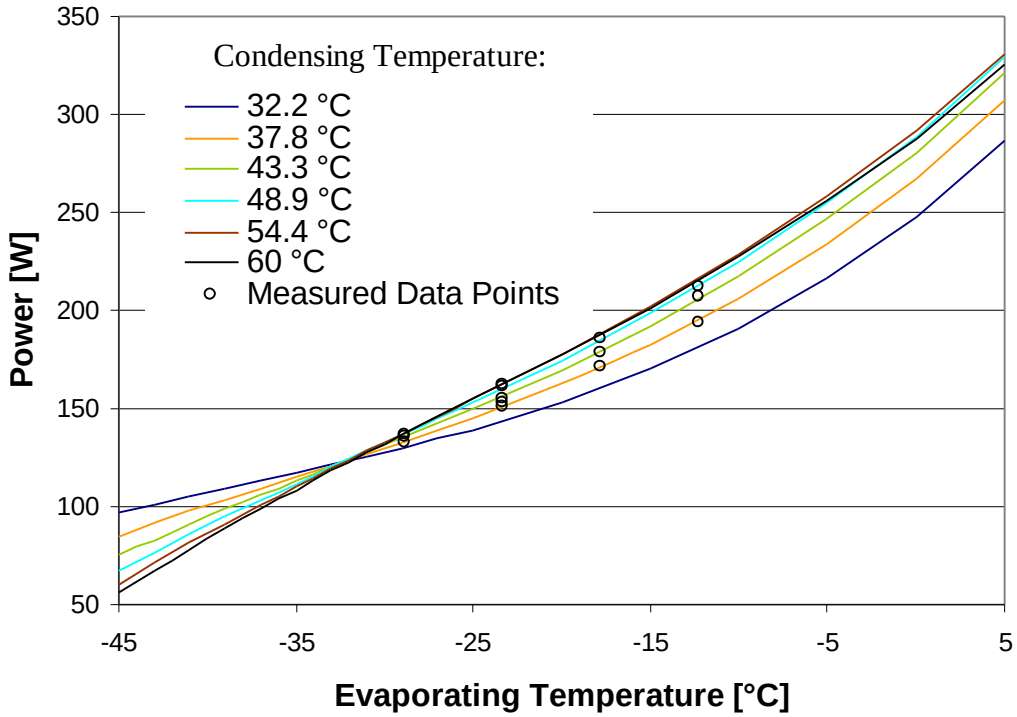

ARI Curve Fit (A4)

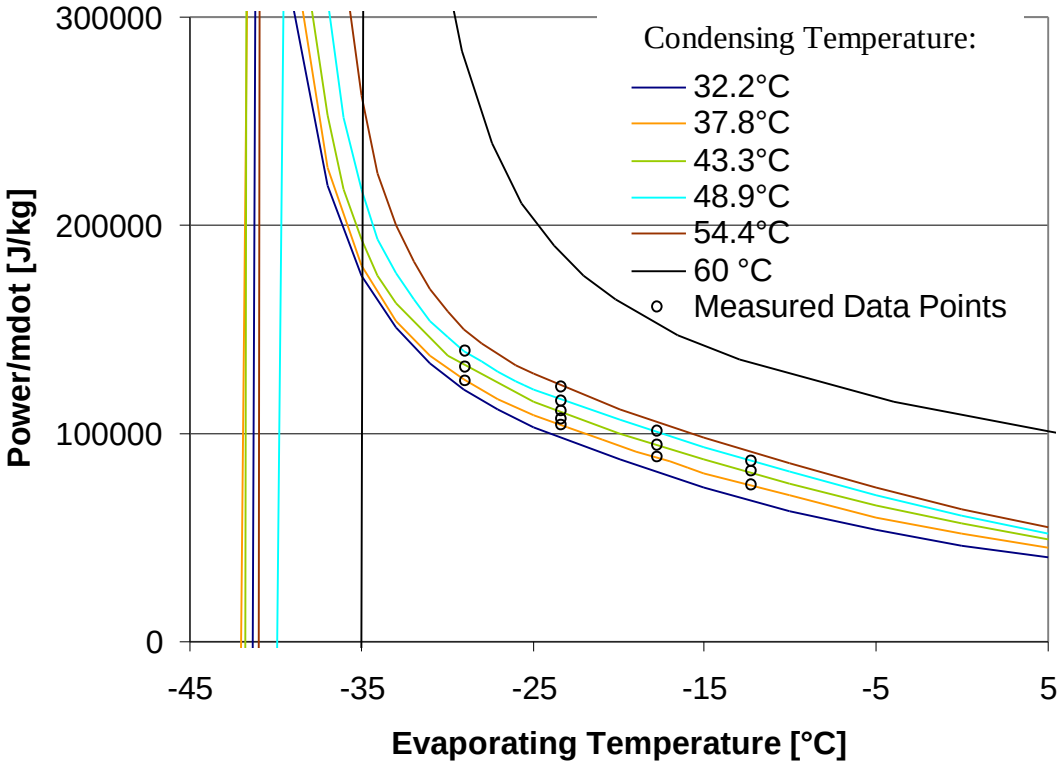

ARI Curve Fit (A5)

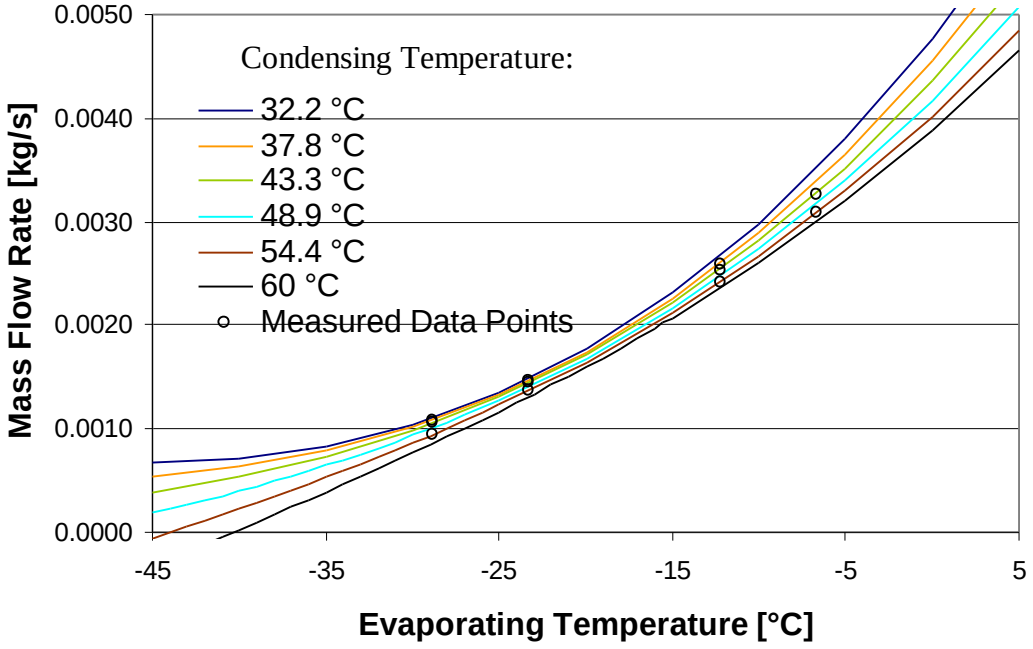

ARI Curve Fits (A5)

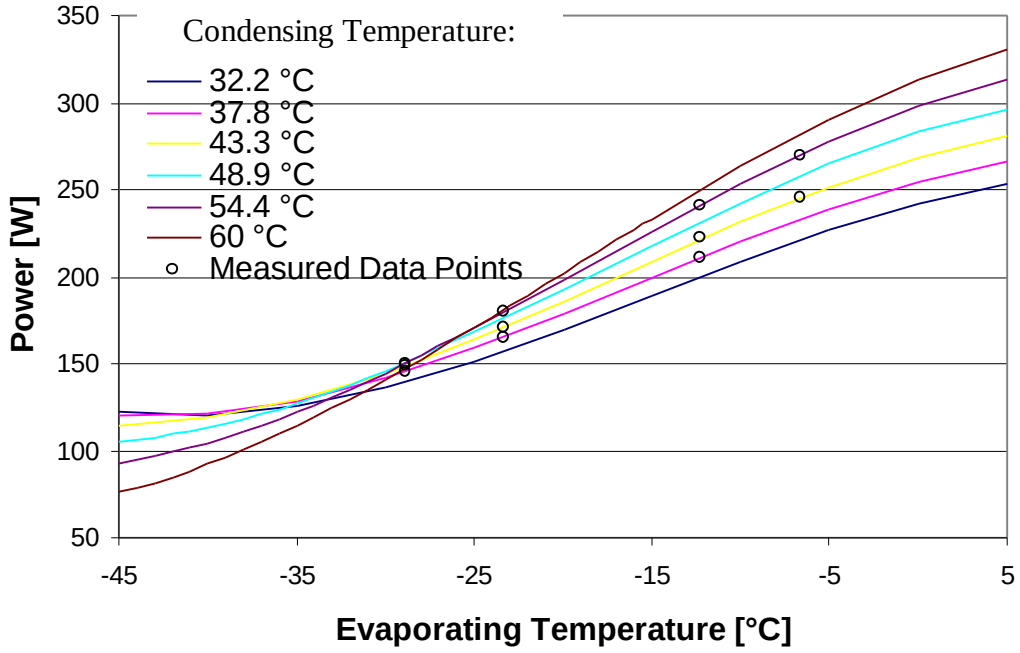

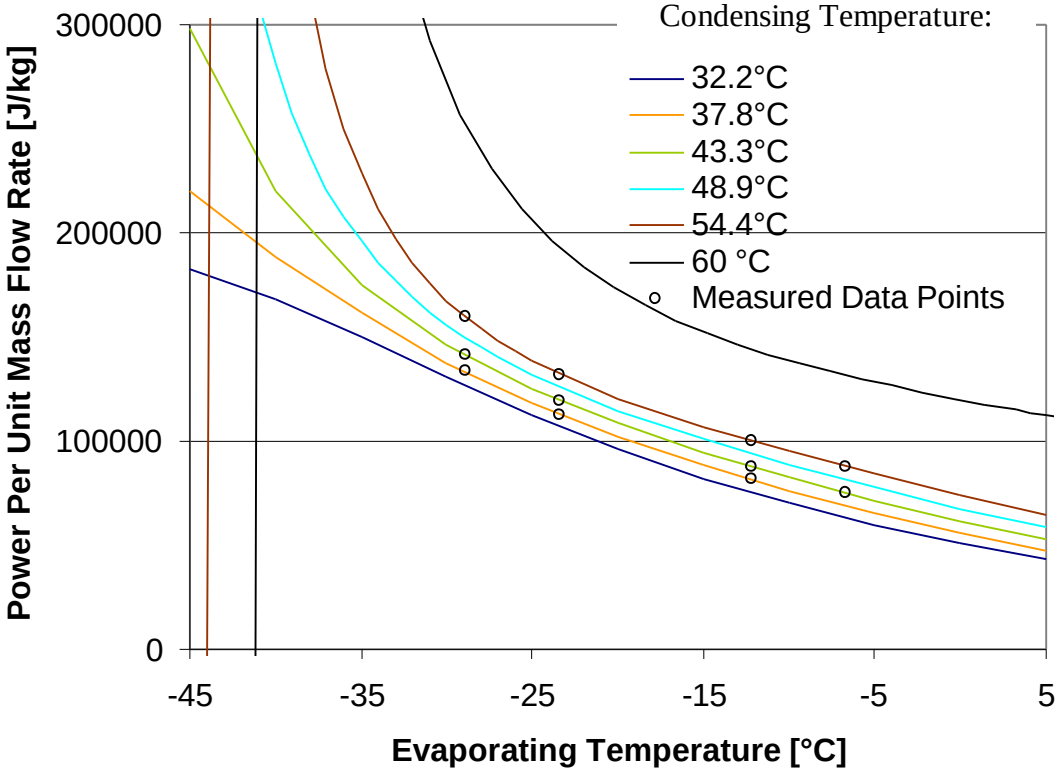

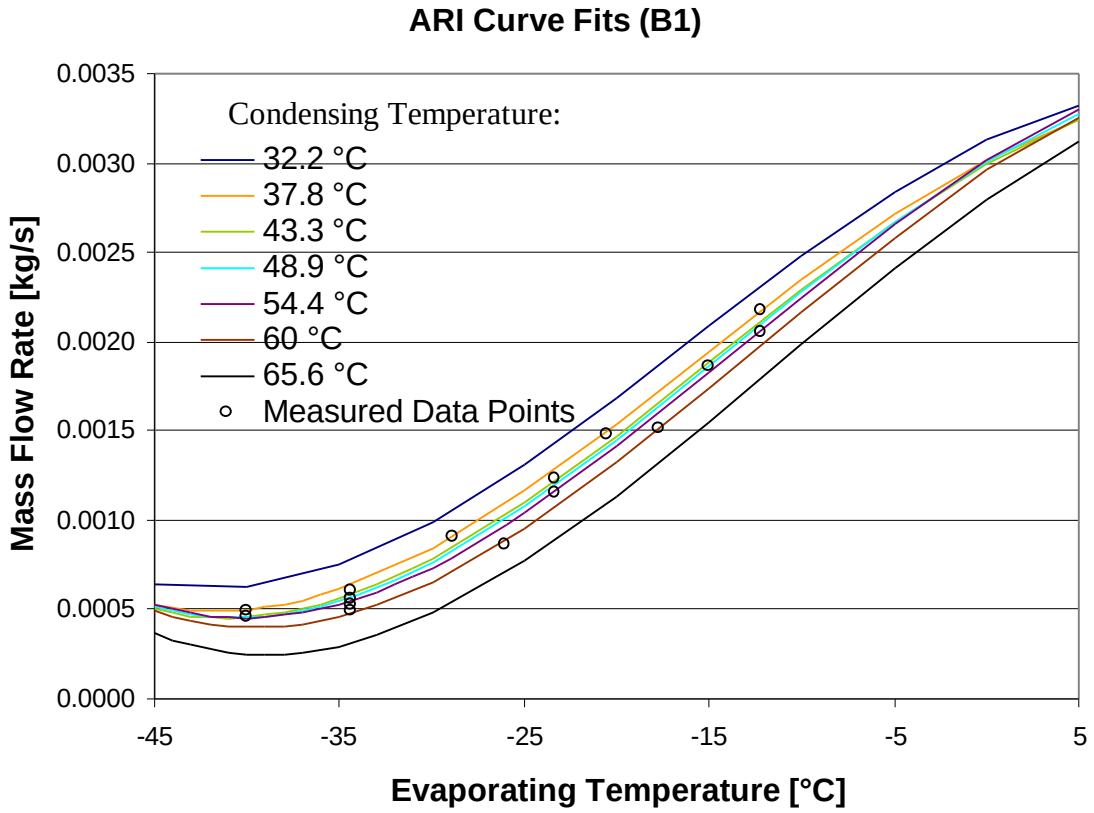
ARI Curve Fits (B1)
Mass Flow Rate [kg/s]
0.0035
0.0030
0.0025
0.0020
0.0015
0.0010
0.0005
0.0000
Condensing Temperature:
32.2 °C
37.8 °C
43.3 °C
48.9 °C
54.4 °C
60 °C
65.6 °C
Measured Data Points
-45
-35
-25
-15
-5
5
Evaporating Temperature [°C]

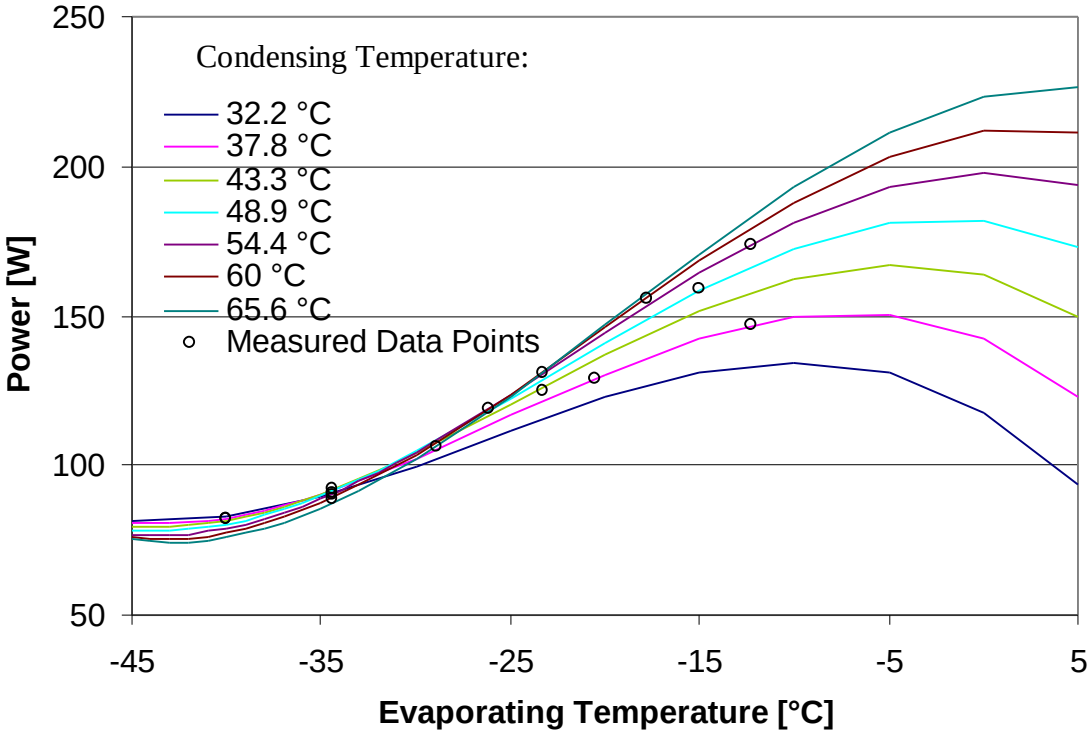
Power [W]
250
200
150
100
50
Condensing Temperature:
32.2 °C
37.8 °C
43.3 °C
48.9 °C
54.4 °C
60 °C
65.6 °C
Measured Data Points
-45
-35
-25
-15
-5
5
Evaporating Temperature [°C]

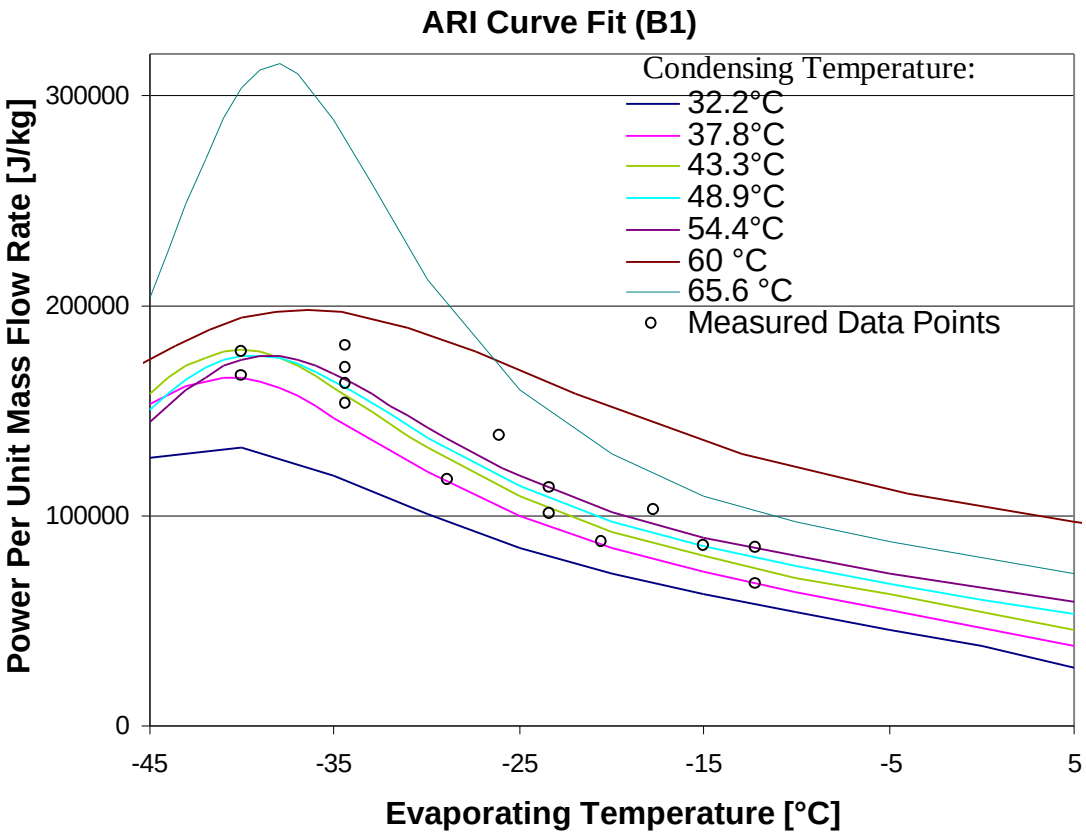
ARI Curve Fit (B1)
Condensing Temperature:
32.2°C
37.8°C
43.3°C
48.9°C
54.4°C
60 °C
65.6 °C
Measured Data Points
Power Per Unit Mass Flow Rate [J/kg]
300000
200000
100000
0
-45
-35
-25
-15
-5
5
Evaporating Temperature [°C]

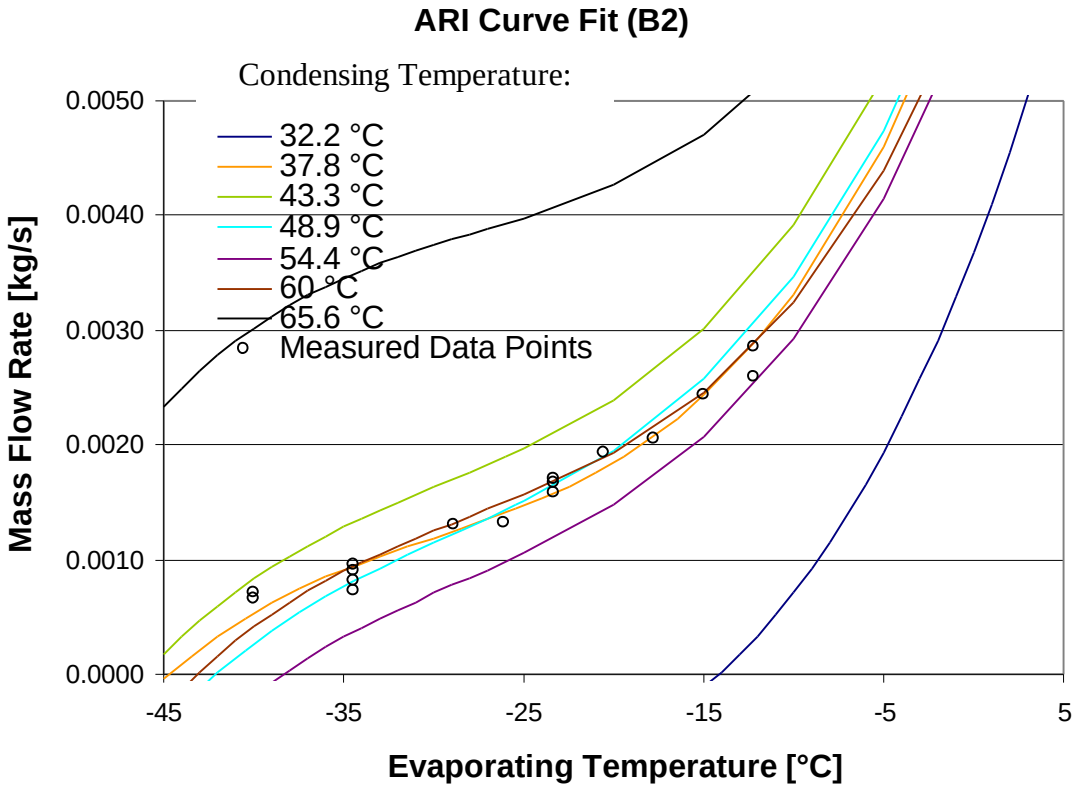
ARI Curve Fit (B2)
Condensing Temperature:
32.2 °C
37.8 °C
43.3 °C
48.9 °C
54.4 °C
60 °C
65.6 °C
Measured Data Points
Mass Flow Rate [kg/s]
0.0050
0.0040
0.0030
0.0020
0.0010
0.0000
-45
-35
-25
-15
-5
5
Evaporating Temperature [°C]

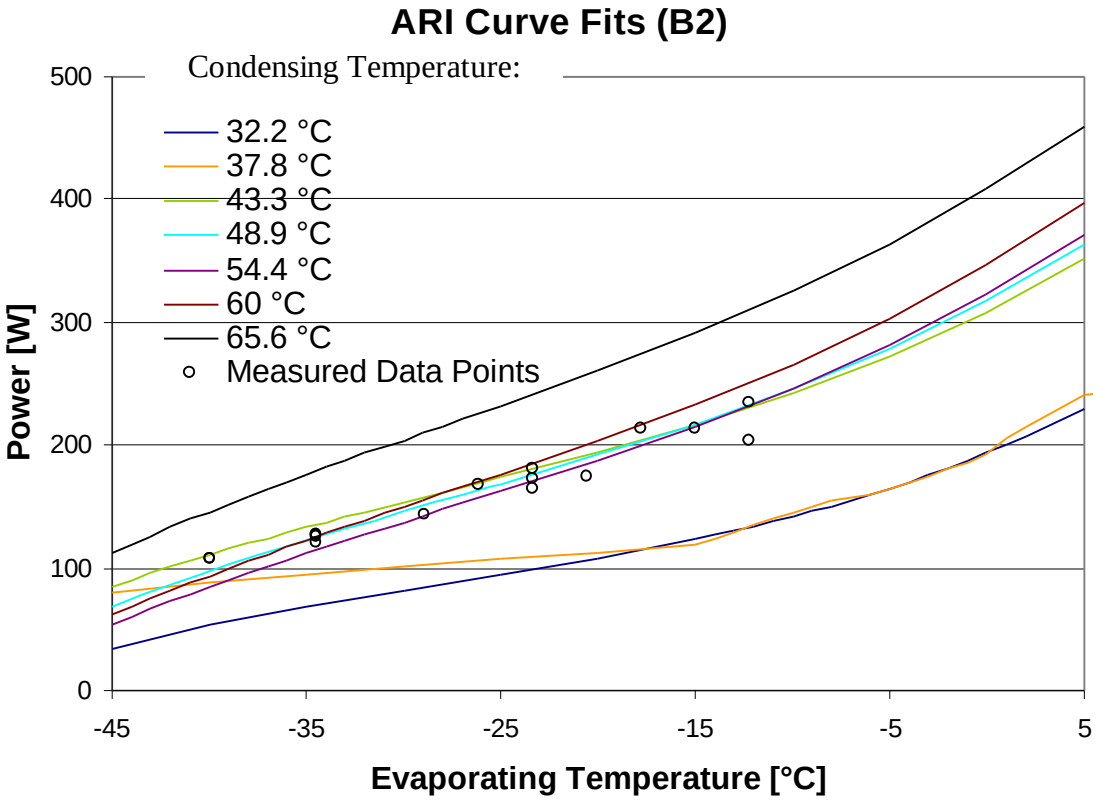
ARI Curve Fits (B2)
Condensing Temperature:
32.2 °C
37.8 °C
43.3 °C
48.9 °C
54.4 °C
60 °C
65.6 °C
Measured Data Points
Power [W]
500
400
300
200
100
0
-45
-35
-25
-15
-5
5
Evaporating Temperature [°C]

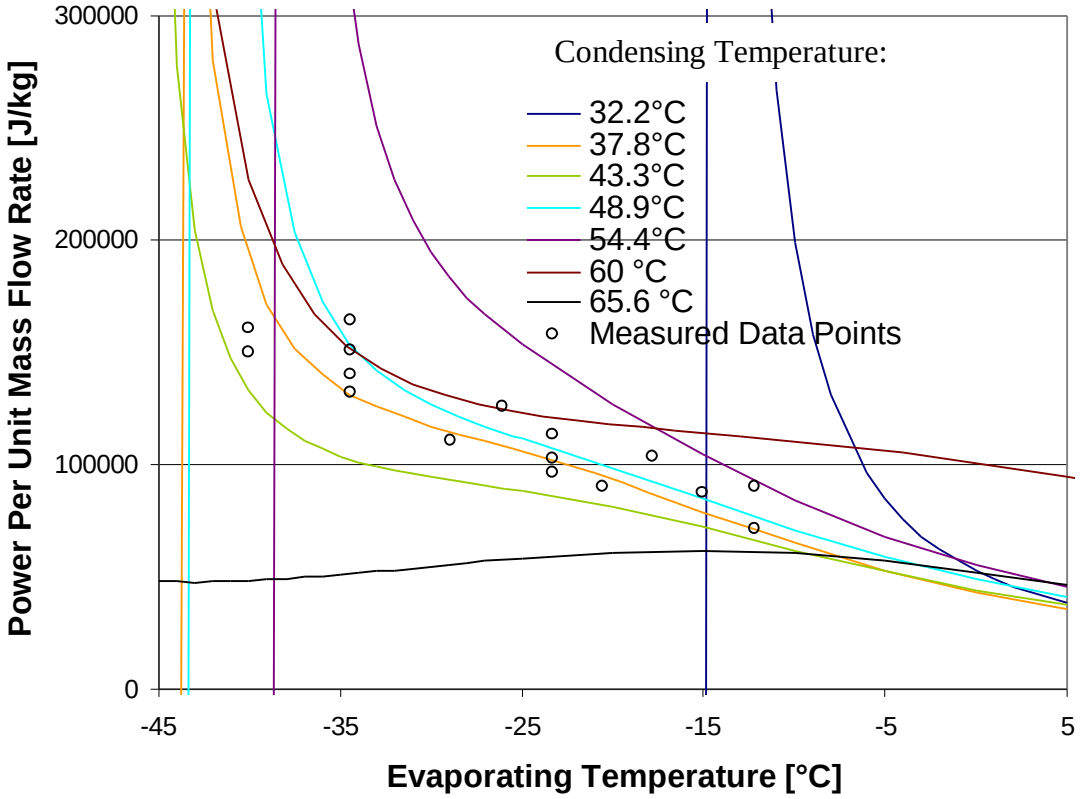
Condensing Temperature:
32.2°C
37.8°C
43.3°C
48.9°C
54.4°C
60 °C
65.6 °C
Measured Data Points
Power Per Unit Mass Flow Rate [J/kg]
300000
200000
100000
0
-45
-35
-25
-15
-5
5
Evaporating Temperature [°C]

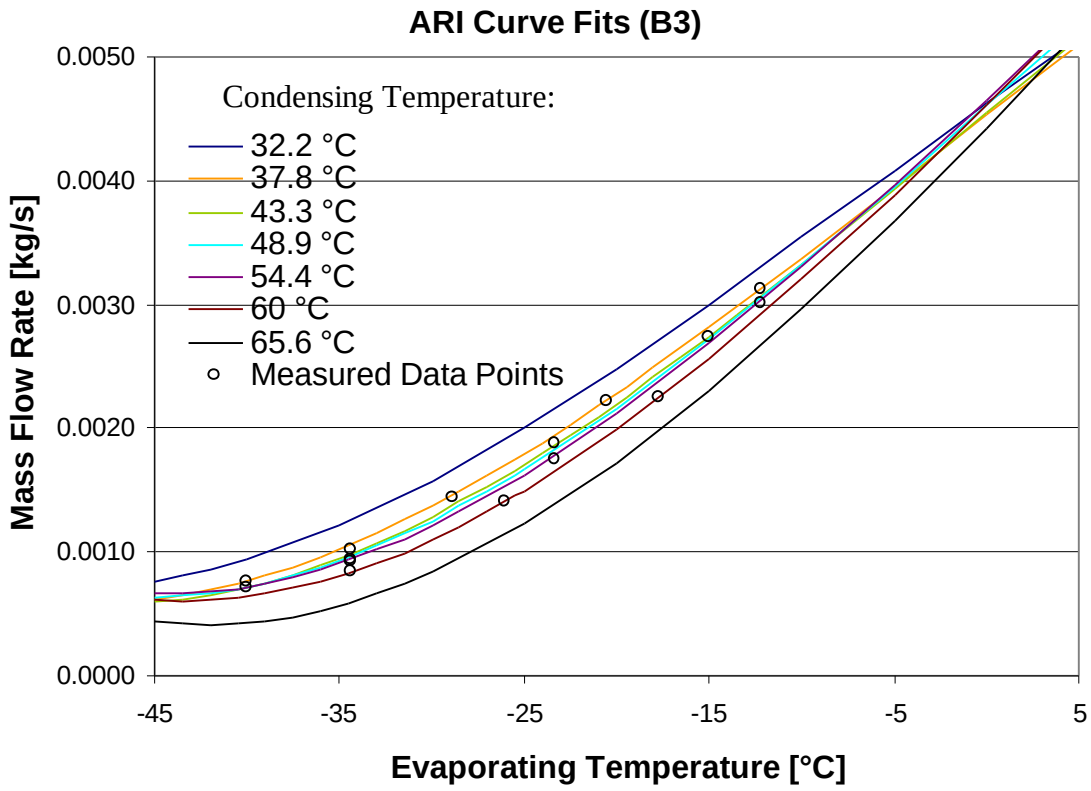
ARI Curve Fits (B3)
Mass Flow Rate [kg/s]
0.0050
0.0040
0.0030
0.0020
0.0010
0.0000
Condensing Temperature:
32.2 °C
37.8 °C
43.3 °C
48.9 °C
54.4 °C
60 °C
65.6 °C
Measured Data Points
-45
-35
-25
-15
-5
5
Evaporating Temperature [°C]

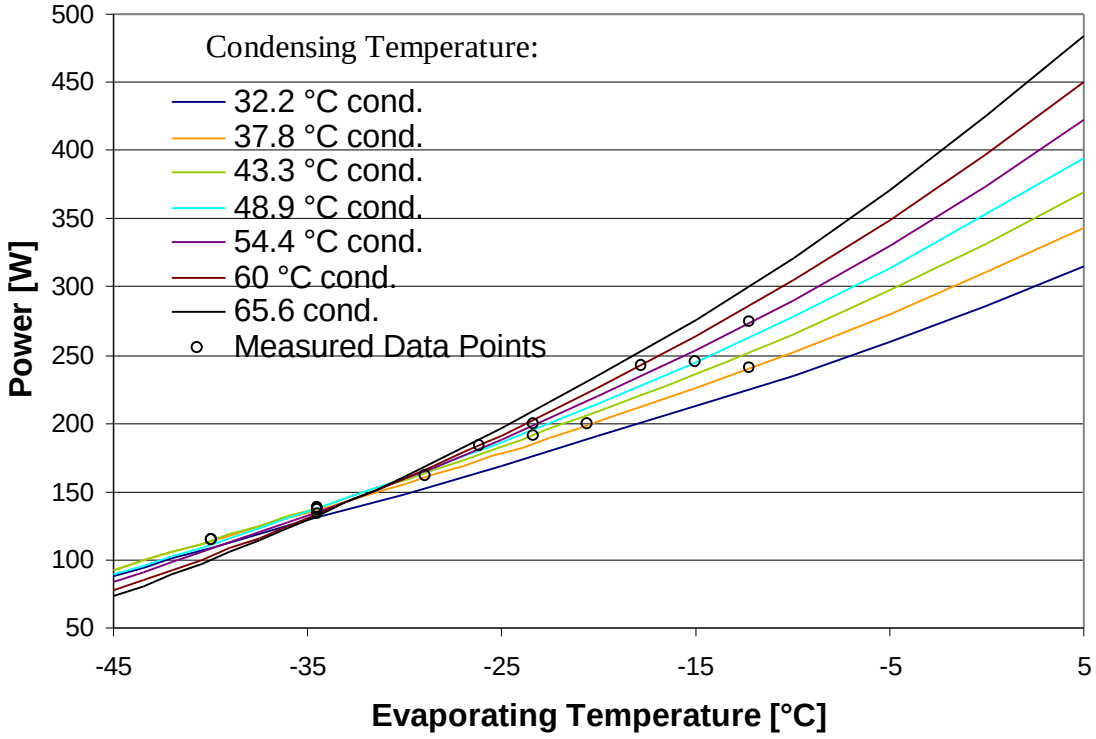
Power [W]
500
450
400
350
300
250
200
150
100
50
Condensing Temperature:
32.2 °C cond.
37.8 °C cond.
43.3 °C cond.
48.9 °C cond.
54.4 °C cond.
60 °C cond.
65.6 cond.
Measured Data Points
-45
-35
-25
-15
-5
5
Evaporating Temperature [°C]

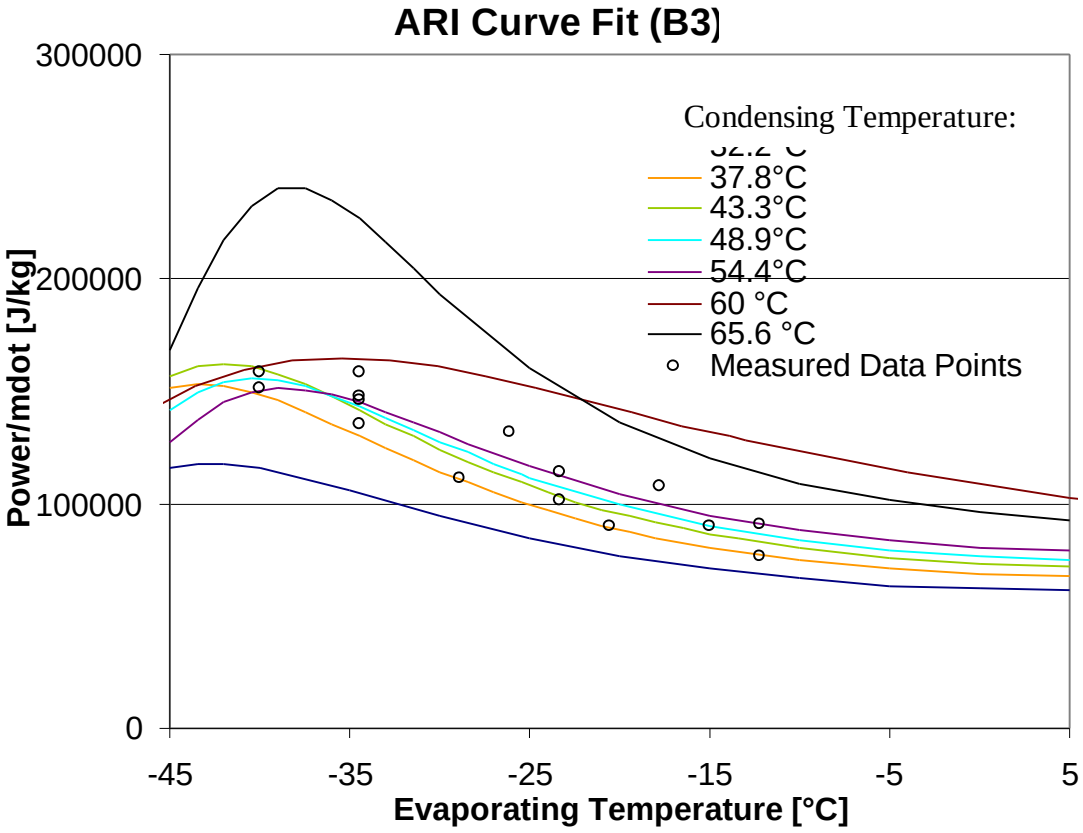
ARI Curve Fit (B3)
300000
200000
100000
0
Power/mdot [J/kg]
-45
-35
-25
-15
-5
5
Evaporating Temperature [°C]
Condensing Temperature:
37.8°C
43.3°C
48.9°C
54.4°C
60 °C
65.6 °C
Measured Data Points

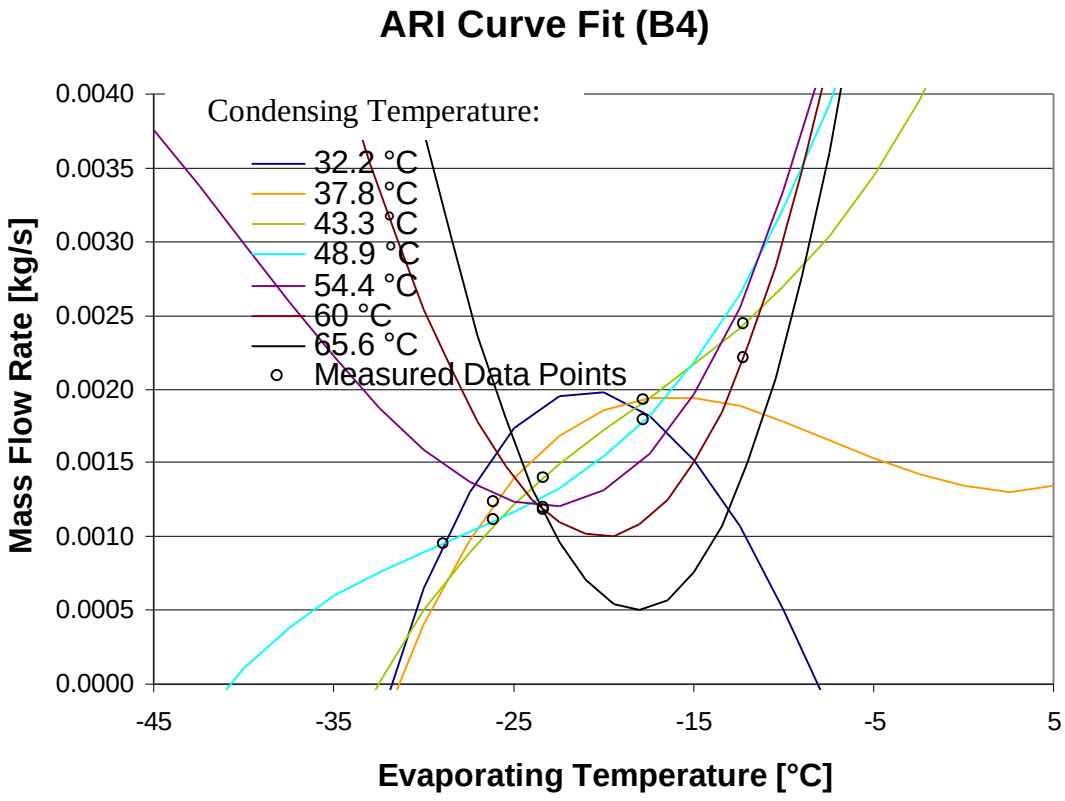
ARI Curve Fit (B4)
0.0040
0.0035
0.0030
0.0025
0.0020
0.0015
0.0010
0.0005
0.0000
Mass Flow Rate [kg/s]
-45
-35
-25
-15
-5
5
Evaporating Temperature [°C]
Condensing Temperature:
32.2 °C
37.8 °C
43.3 °C
48.9 °C
54.4 °C
60 °C
65.6 °C
Measured Data Points

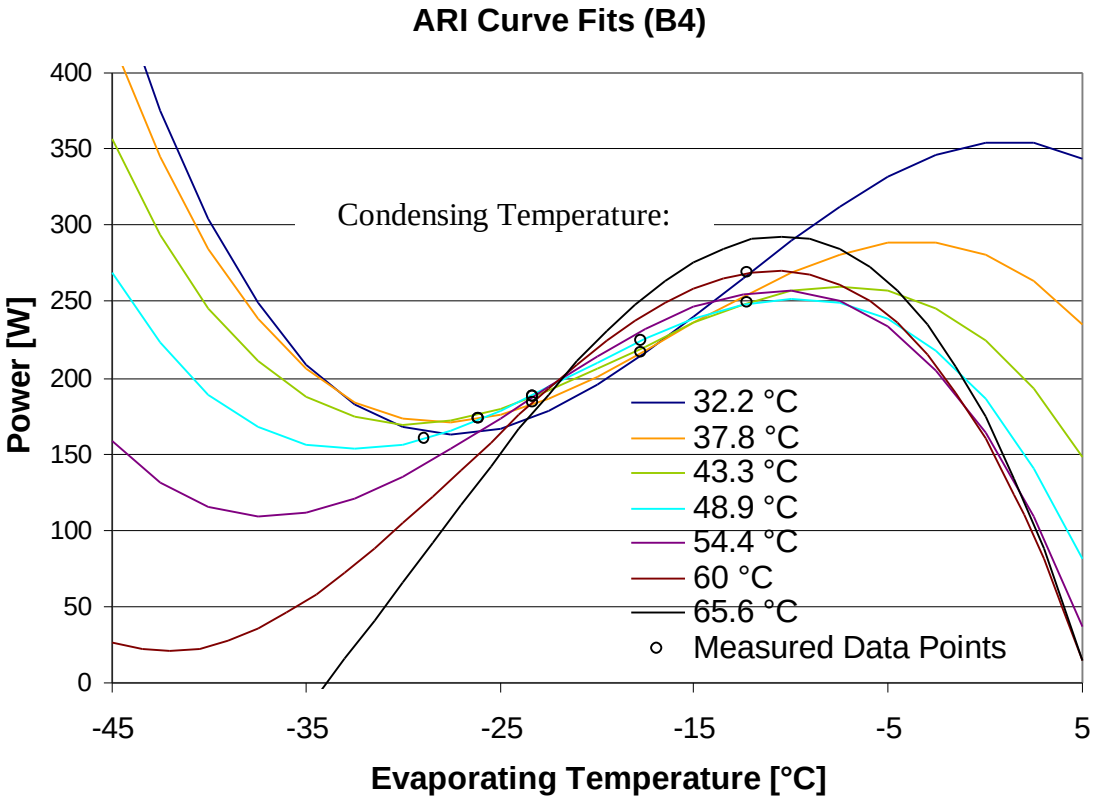
ARI Curve Fits (B4)
Power [W]
400
350
300
250
200
150
100
50
0
Condensing Temperature:
32.2 °C
37.8 °C
43.3 °C
48.9 °C
54.4 °C
60 °C
65.6 °C
Measured Data Points
-45
-35
-25
-15
-5
5
Evaporating Temperature [°C]

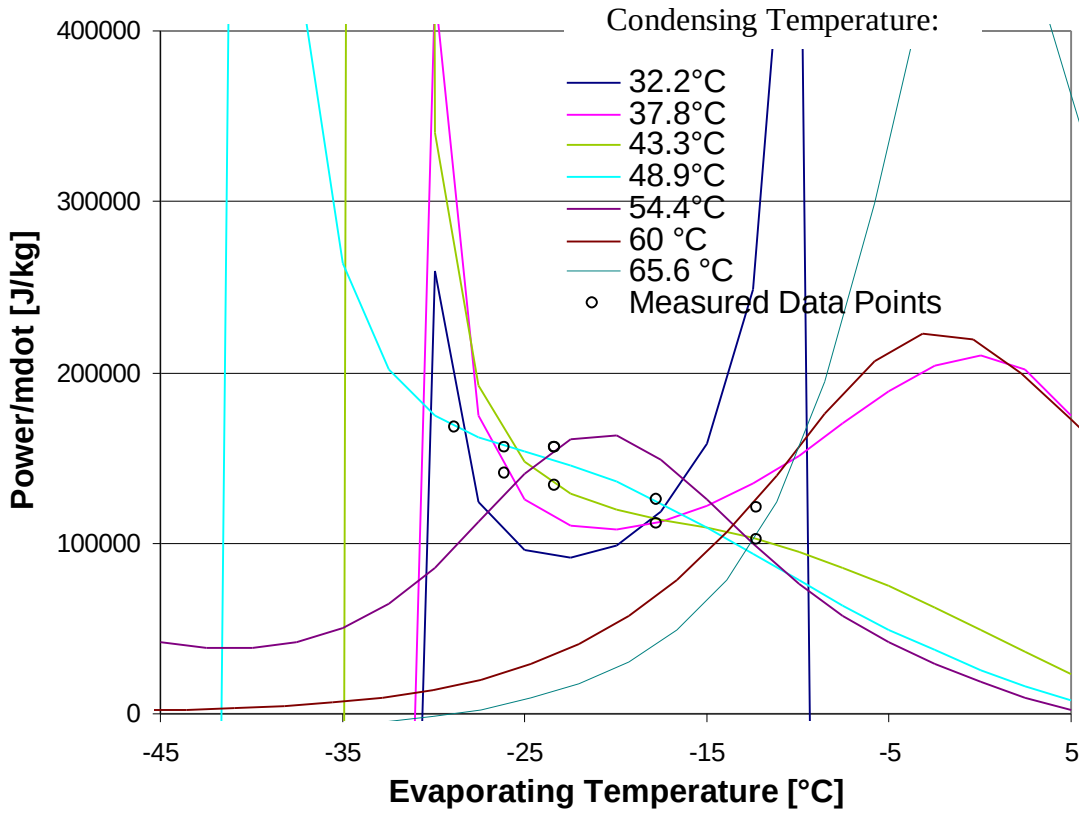
Power/mdot [J/kg]
400000
300000
200000
100000
0
Condensing Temperature:
32.2°C
37.8°C
43.3°C
48.9°C
54.4°C
60 °C
65.6 °C
Measured Data Points
-45
-35
-25
-15
-5
5
Evaporating Temperature [°C]

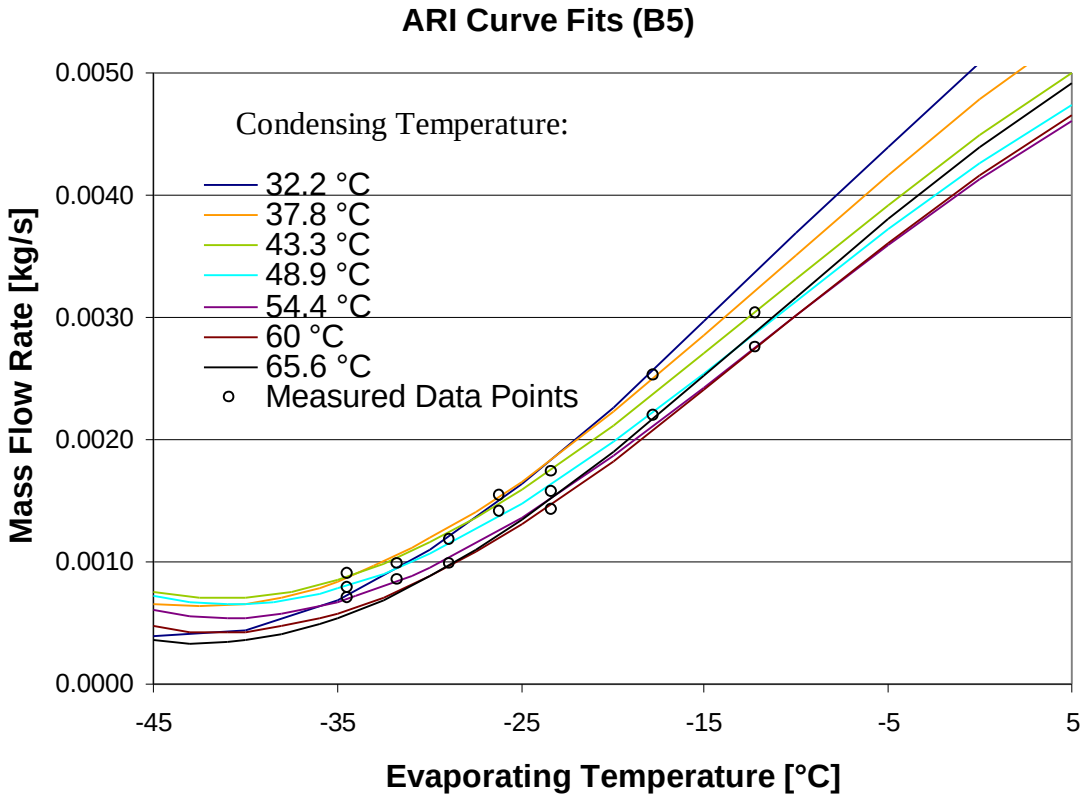
ARI Curve Fits (B5)
Mass Flow Rate [kg/s]
0.0050
0.0040
0.0030
0.0020
0.0010
0.0000
Condensing Temperature:
32.2 °C
37.8 °C
43.3 °C
48.9 °C
54.4 °C
60 °C
65.6 °C
Measured Data Points
-45
-35
-25
-15
-5
5
Evaporating Temperature [°C]

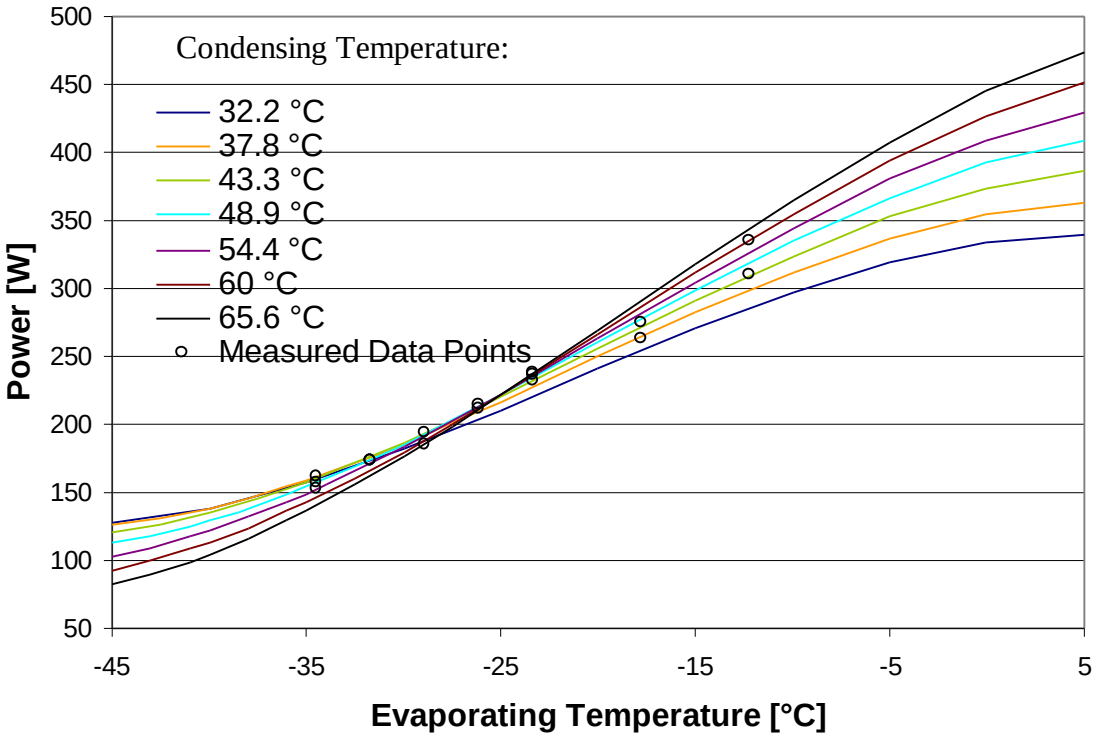
Power [W]
500
450
400
350
300
250
200
150
100
50
Condensing Temperature:
32.2 °C
37.8 °C
43.3 °C
48.9 °C
54.4 °C
60 °C
65.6 °C
Measured Data Points
-45
-35
-25
-15
-5
5
Evaporating Temperature [°C]

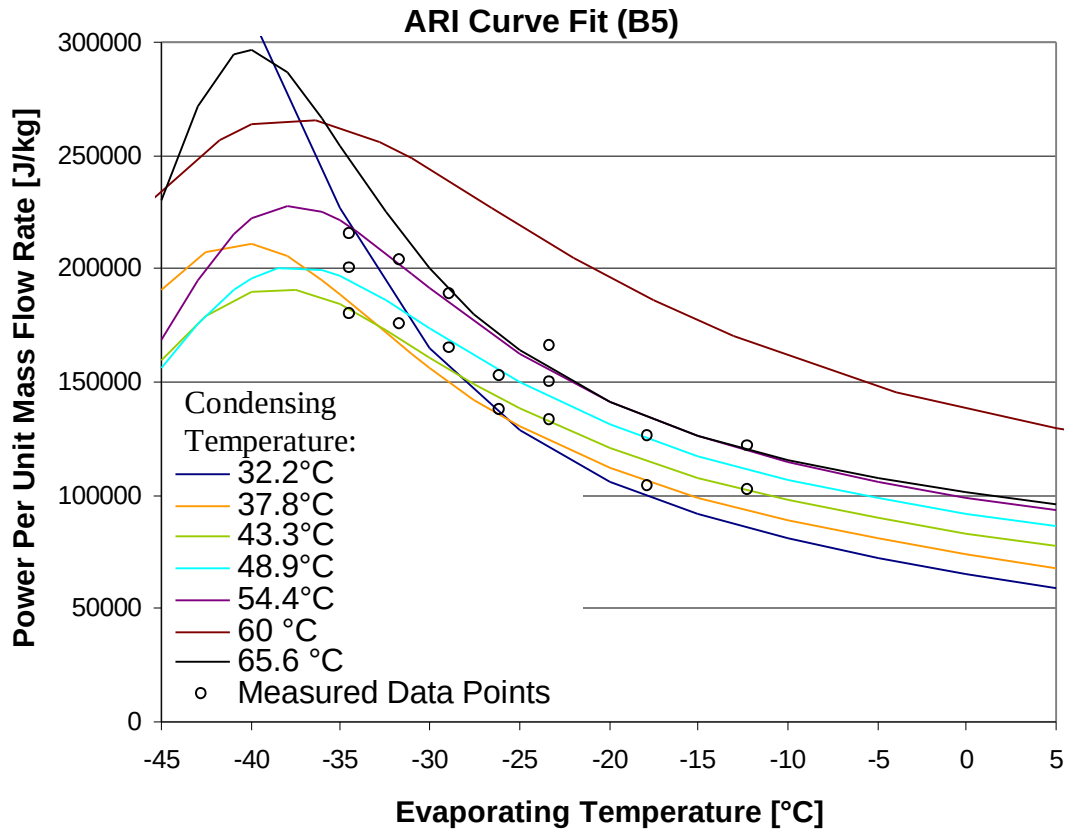
ARI Curve Fit (B5)
Power Per Unit Mass Flow Rate [J/kg]
300000
250000
200000
150000
100000
50000
0
-45
-40
-35
-30
-25
-20
-15
-10
-5
0
5
Evaporating Temperature [°C]
Condensing Temperature:
32.2°C
37.8°C
43.3°C
48.9°C
54.4°C
60 °C
65.6 °C
Measured Data Points

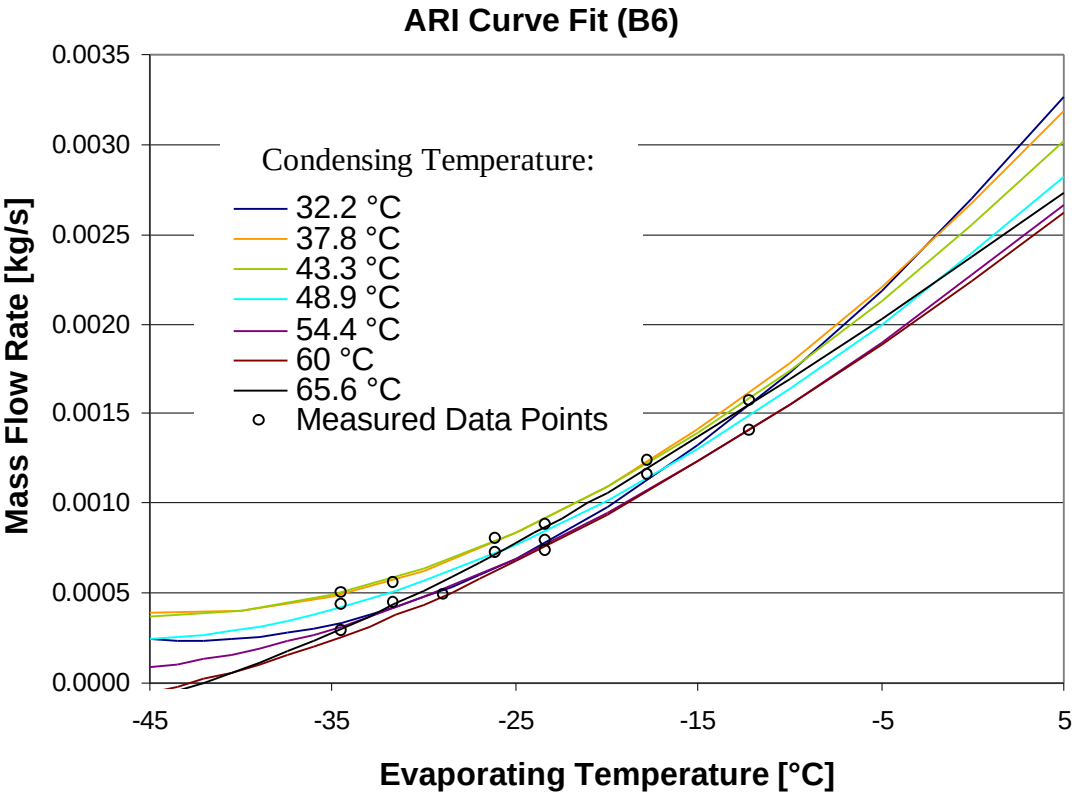
ARI Curve Fit (B6)
Mass Flow Rate [kg/s]
0.0035
0.0030
0.0025
0.0020
0.0015
0.0010
0.0005
0.0000
-45
-35
-25
-15
-5
5
Evaporating Temperature [°C]
Condensing Temperature:
32.2 °C
37.8 °C
43.3 °C
48.9 °C
54.4 °C
60 °C
65.6 °C
Measured Data Points

ARI Curve Fits (B6)

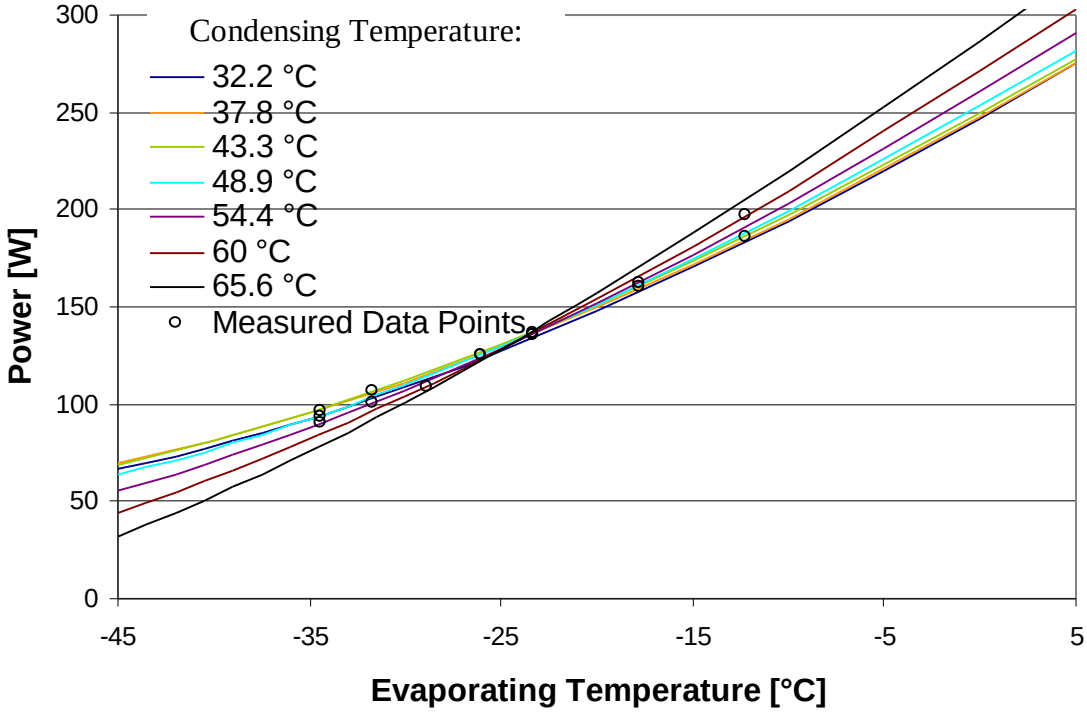

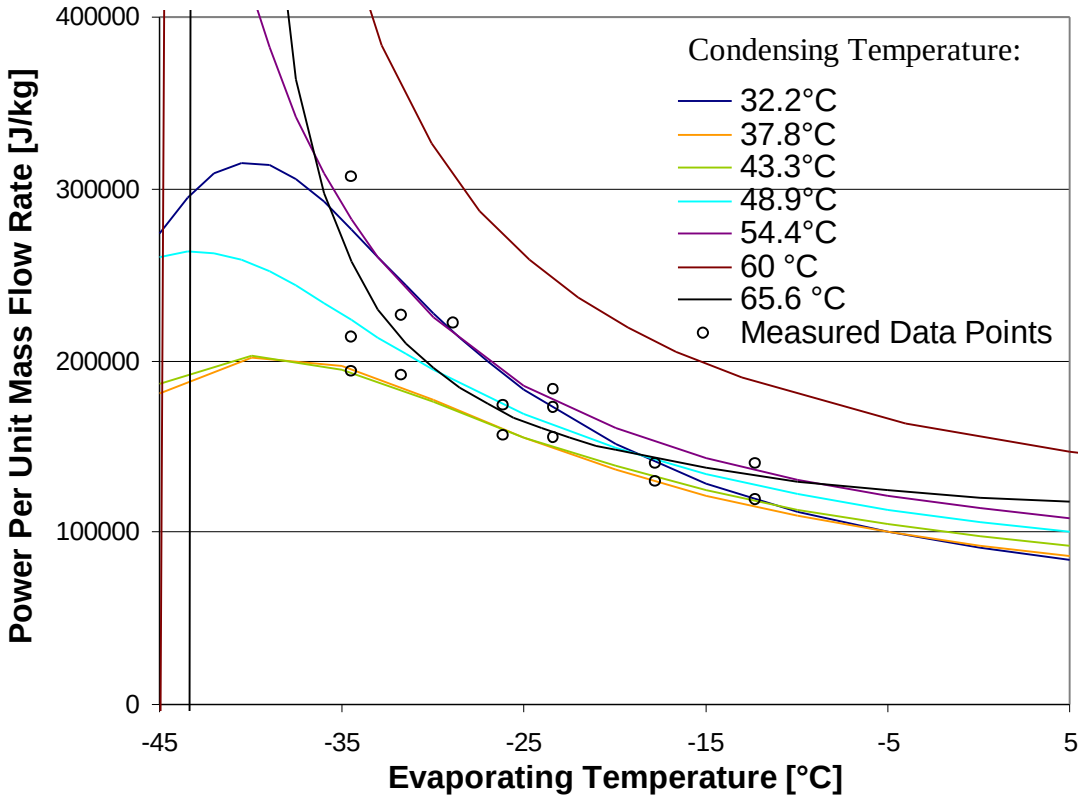

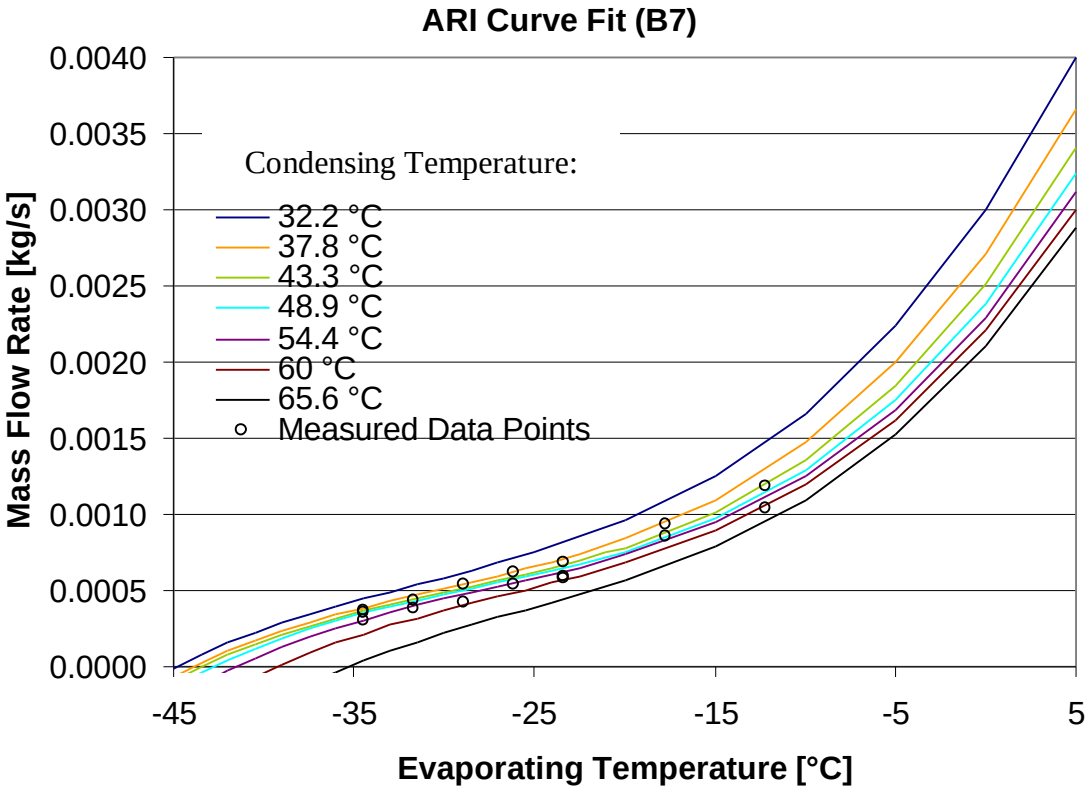
ARI Curve Fit (B7)
Mass Flow Rate [kg/s]
0.0040
0.0035
0.0030
0.0025
0.0020
0.0015
0.0010
0.0005
0.0000
Condensing Temperature:
32.2 °C
37.8 °C
43.3 °C
48.9 °C
54.4 °C
60 °C
65.6 °C
Measured Data Points
-45
-35
-25
-15
-5
5
Evaporating Temperature [°C]

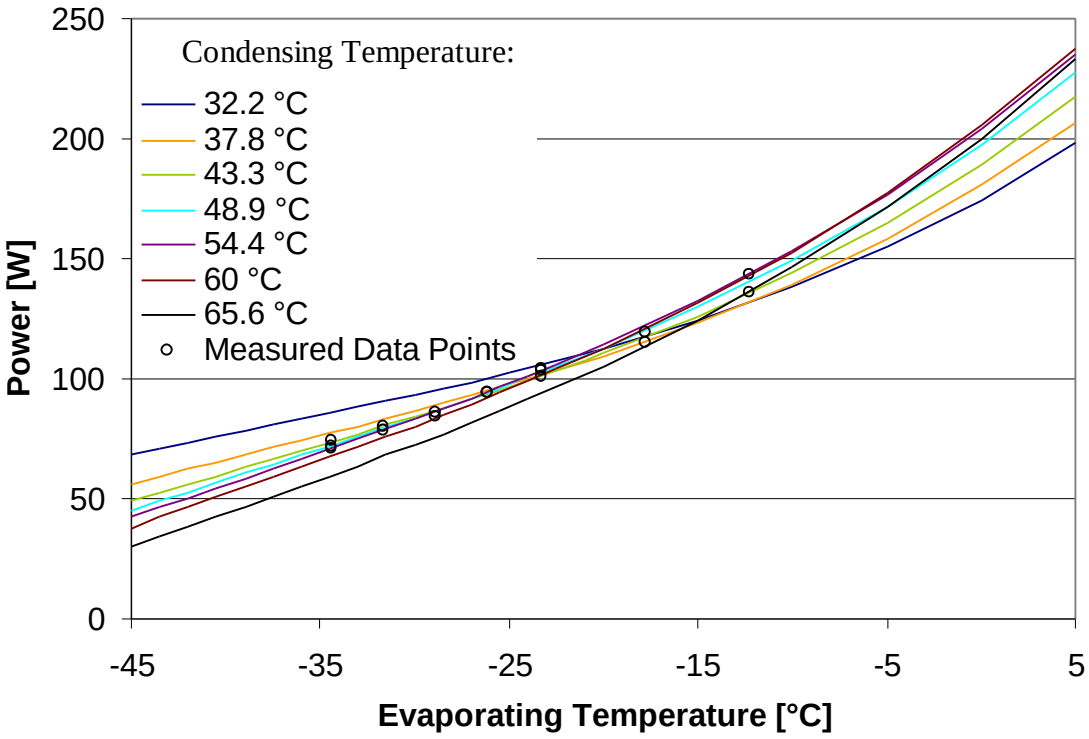
Power [W]
250
200
150
100
50
0
Condensing Temperature:
32.2 °C
37.8 °C
43.3 °C
48.9 °C
54.4 °C
60 °C
65.6 °C
Measured Data Points
-45
-35
-25
-15
-5
5
Evaporating Temperature [°C]

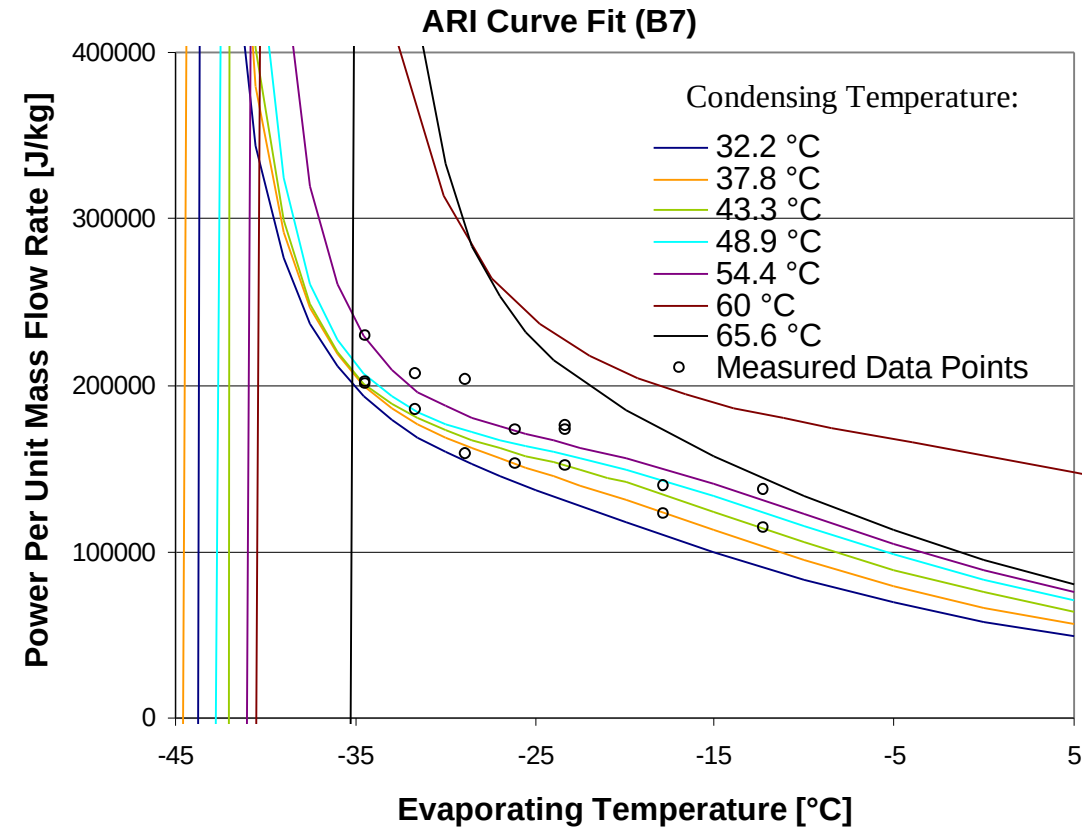
ARI Curve Fit (B7)
Power Per Unit Mass Flow Rate [J/kg]
400000
300000
200000
100000
0
-45
-35
-25
-15
-5
5
Evaporating Temperature [°C]
Condensing Temperature:
32.2 °C
37.8 °C
43.3 °C
48.9 °C
54.4 °C
60 °C
65.6 °C
Measured Data Points

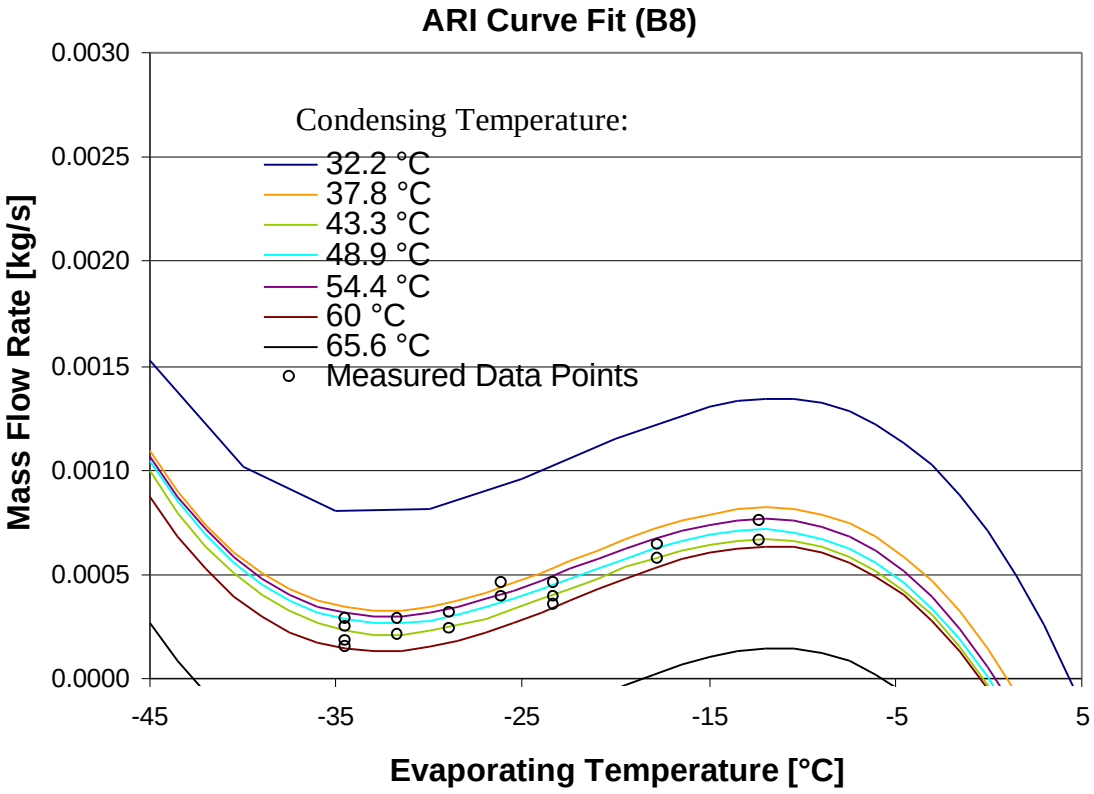
ARI Curve Fit (B8)
Mass Flow Rate [kg/s]
0.0030
0.0025
0.0020
0.0015
0.0010
0.0005
0.0000
-45
-35
-25
-15
-5
5
Evaporating Temperature [°C]
Condensing Temperature:
32.2 °C
37.8 °C
43.3 °C
48.9 °C
54.4 °C
60 °C
65.6 °C
Measured Data Points

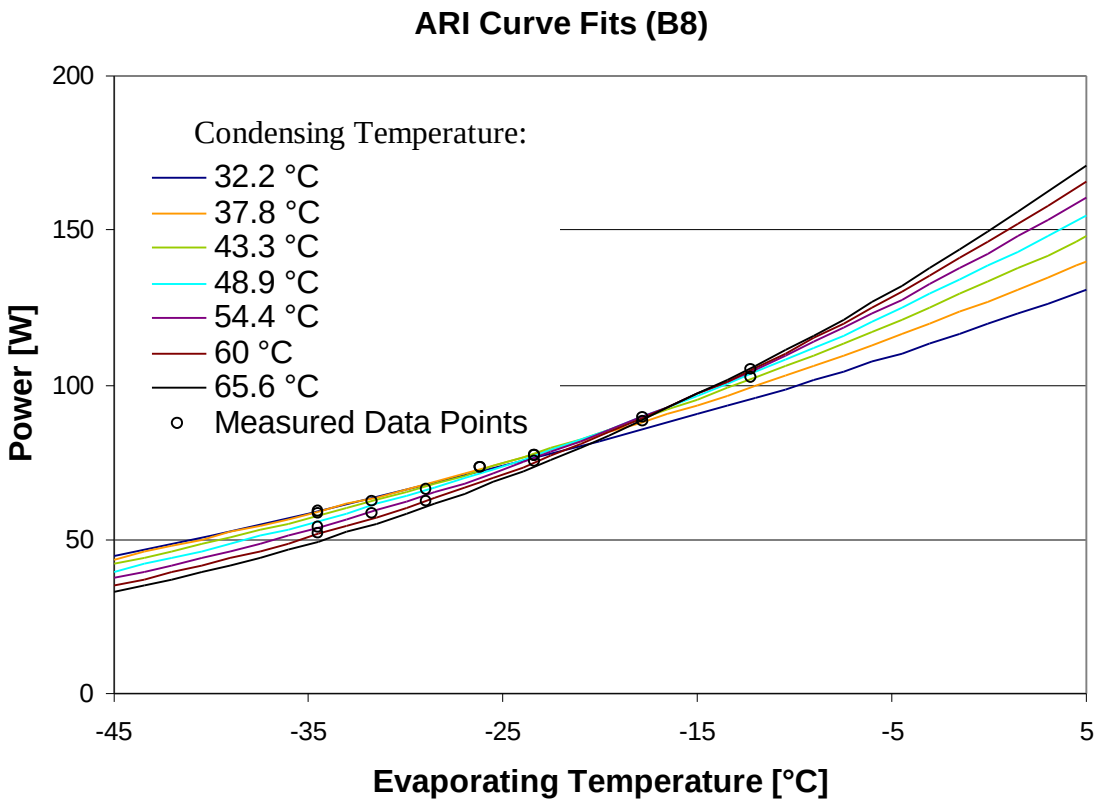
ARI Curve Fits (B8)
Condensing Temperature:
32.2 °C
37.8 °C
43.3 °C
48.9 °C
54.4 °C
60 °C
65.6 °C
Measured Data Points
Power [W]
200
150
100
50
0
-45
-35
-25
-15
-5
5
Evaporating Temperature [°C]

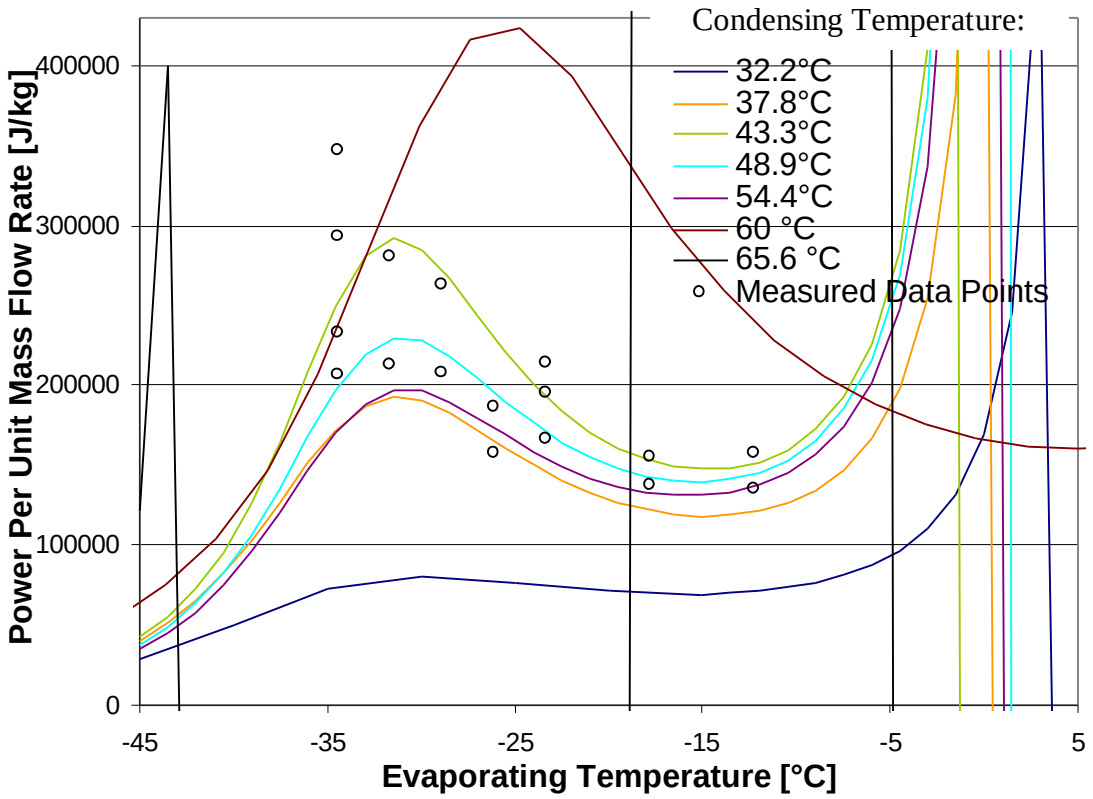
Condensing Temperature:
32.2°C
37.8°C
43.3°C
48.9°C
54.4°C
60 °C
65.6 °C
Measured Data Points
Power Per Unit Mass Flow Rate [J/kg]
400000
300000
200000
100000
0
-45
-35
-25
-15
-5
5
Evaporating Temperature [°C]

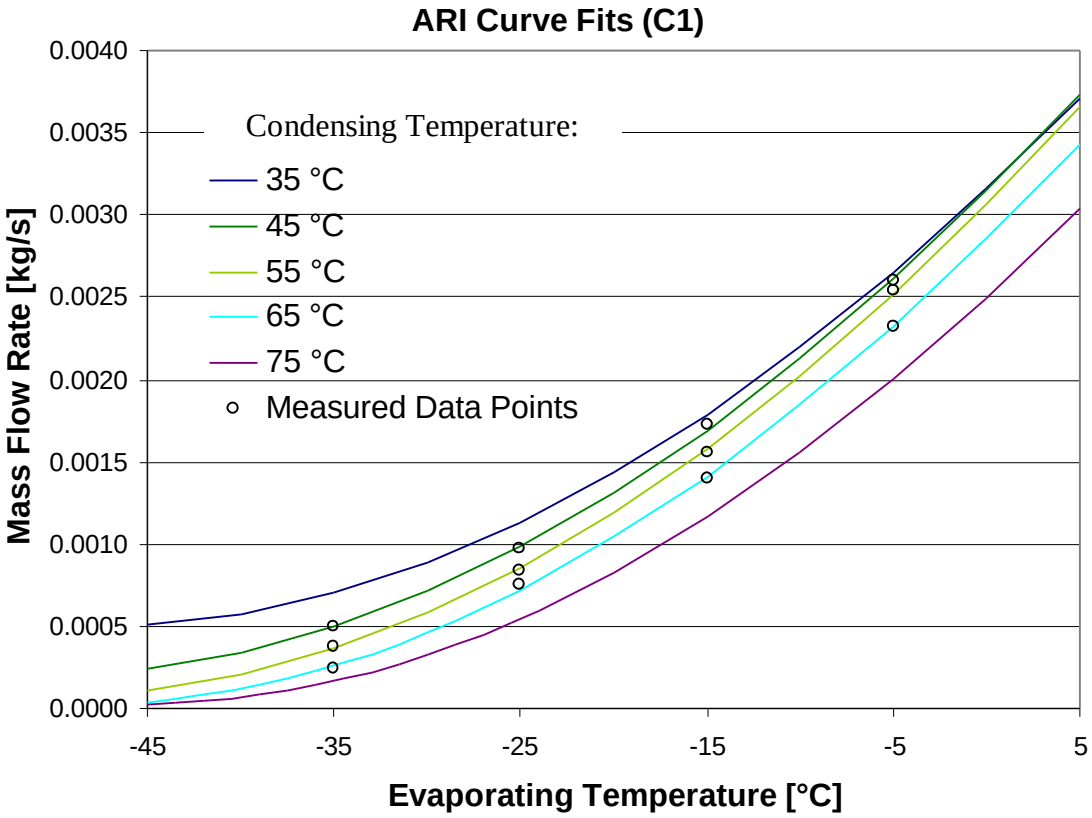
ARI Curve Fits (C1)
Mass Flow Rate [kg/s]
0.0040
0.0035
0.0030
0.0025
0.0020
0.0015
0.0010
0.0005
0.0000
Condensing Temperature:
35 °C
45 °C
55 °C
65 °C
75 °C
Measured Data Points
-45
-35
-25
-15
-5
5
Evaporating Temperature [°C]

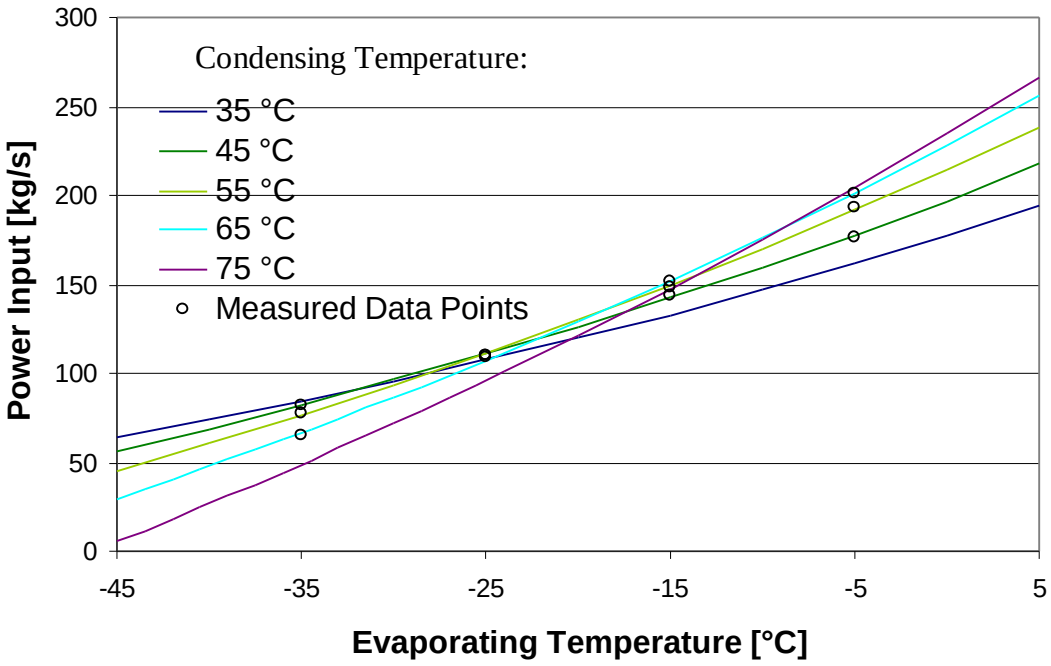
Power Input [kg/s]
300
250
200
150
100
50
0
Condensing Temperature:
35 °C
45 °C
55 °C
65 °C
75 °C
Measured Data Points
-45
-35
-25
-15
-5
5
Evaporating Temperature [°C]

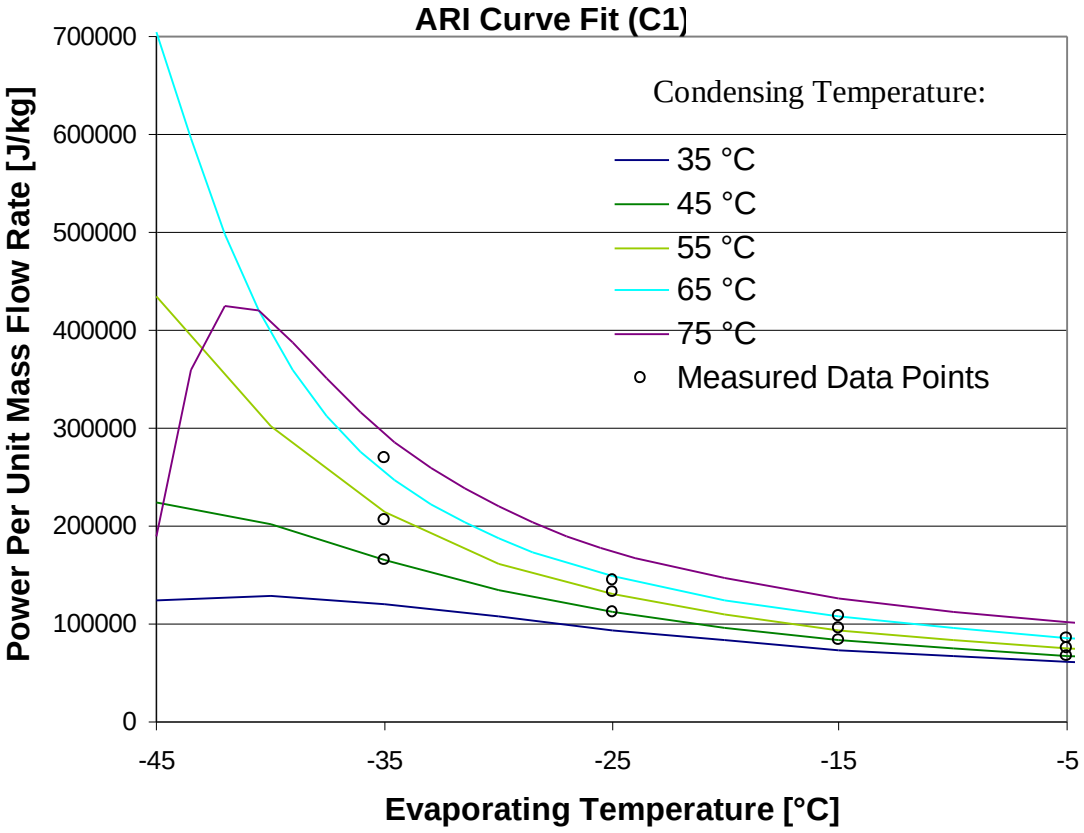
ARI Curve Fit (C1)
Power Per Unit Mass Flow Rate [J/kg]
700000
600000
500000
400000
300000
200000
100000
0
Condensing Temperature:
35 °C
45 °C
55 °C
65 °C
75 °C
Measured Data Points
-45
-35
-25
-15
-5
Evaporating Temperature [°C]

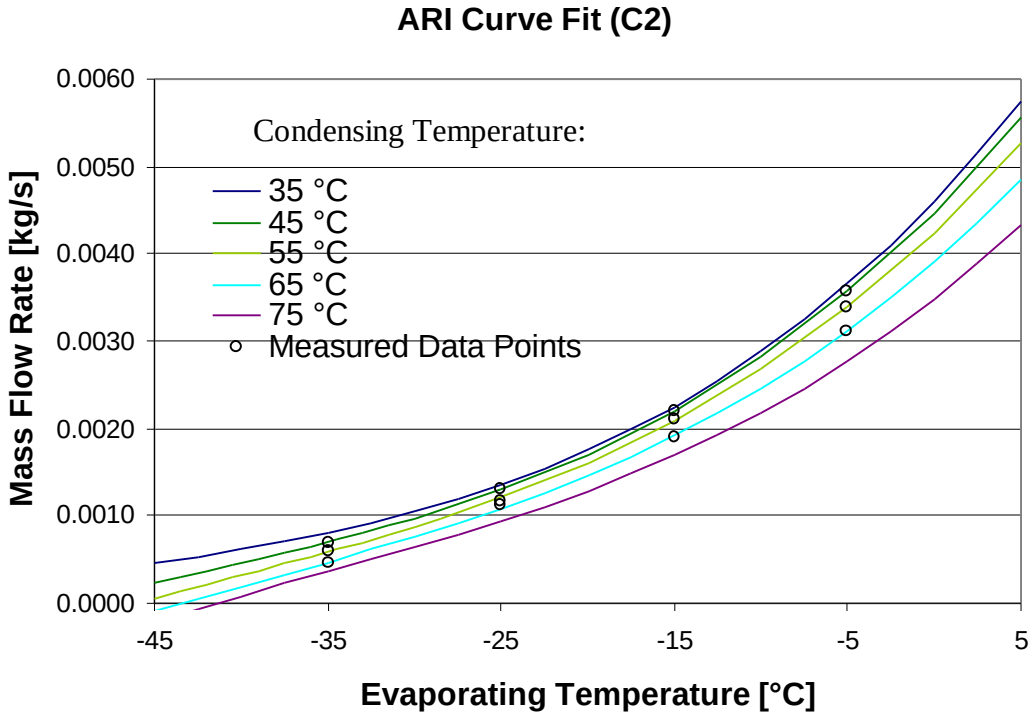
ARI Curve Fit (C2)
Mass Flow Rate [kg/s]
0.0060
0.0050
0.0040
0.0030
0.0020
0.0010
0.0000
Condensing Temperature:
35 °C
45 °C
55 °C
65 °C
75 °C
Measured Data Points
-45
-35
-25
-15
-5
5
Evaporating Temperature [°C]

ARI Curve Fits (C2)

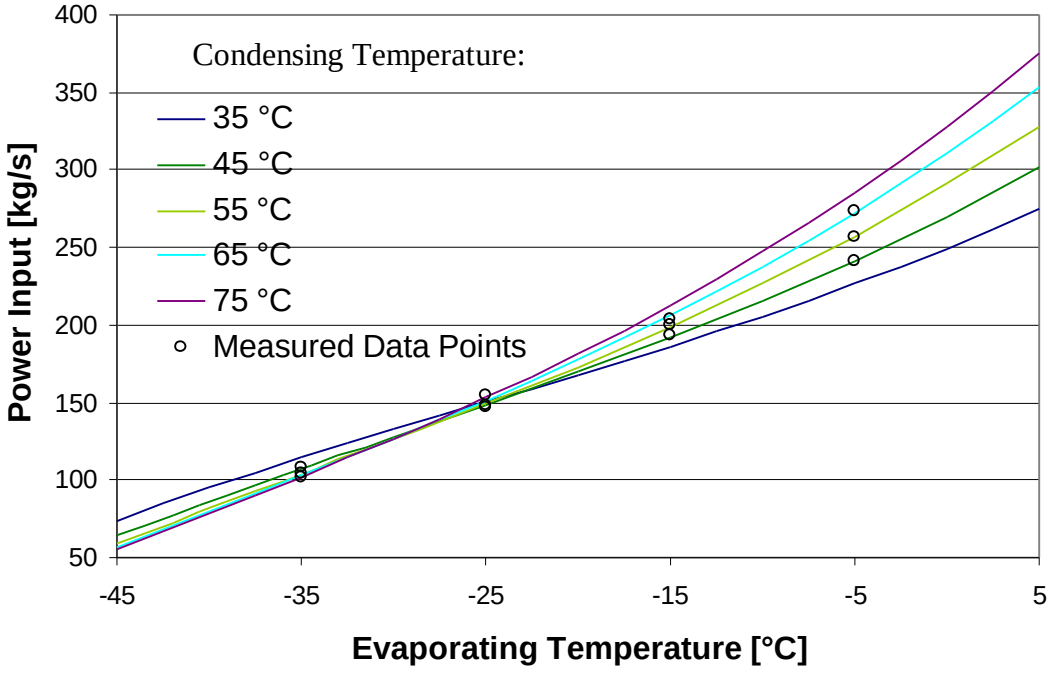

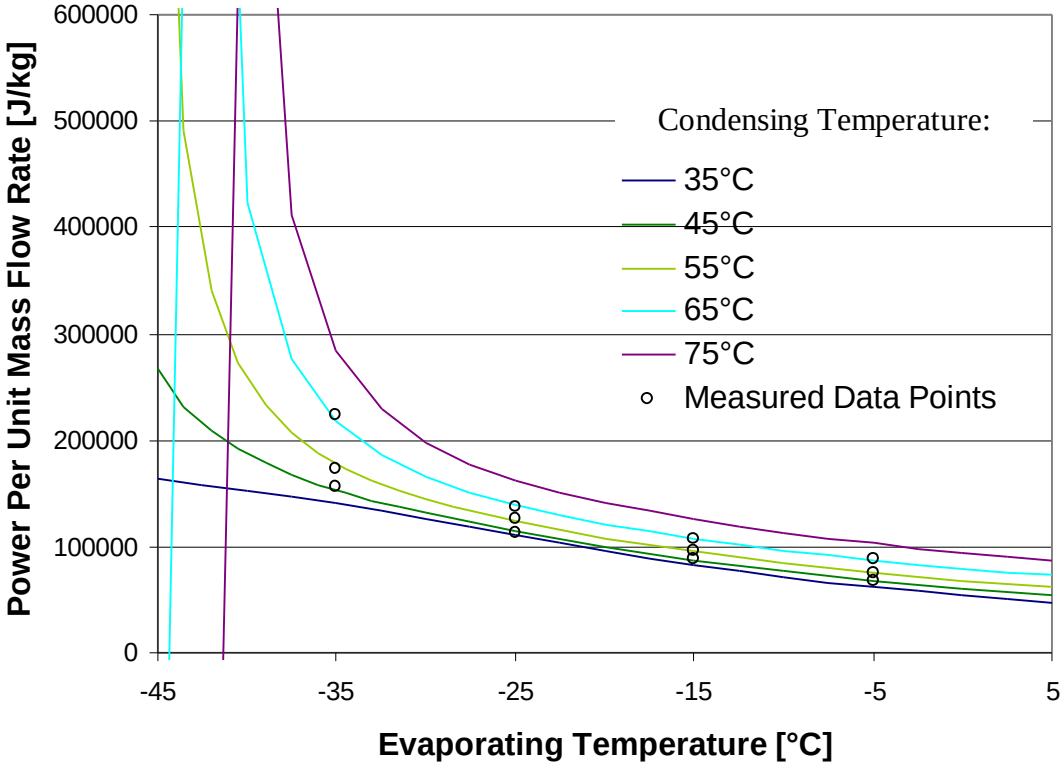

Appendix C: Mass Flow Rate Maps

The compressor maps shown in this appendix have been generated using the constant suction pressure drop model. The two parameters C and Δp are shown for each data set as well as a map that has been extrapolated two higher and lower condensing and evaporating temperatures. The map also shows the experimental data used to generate the map. Below each map is a table that contains the mean weighted and the relative errors between the model and the experimental data for each data point.

The ambient, compressor suction and liquid line temperature is 32.2 °C (90°F) for all maps. The displacement volume and motor speed for each compressor model is also shown.

The highest curve on each map is for the lowest condensing temperature. The lower curves represent the other condensing temperatures in ascending order.

Mass Flow Rate Model (A1a)

Model parameters: C = 0.033, Δp = 0.014, V = 5.686 cm^3 (0.347 in^3), RPM = 3500

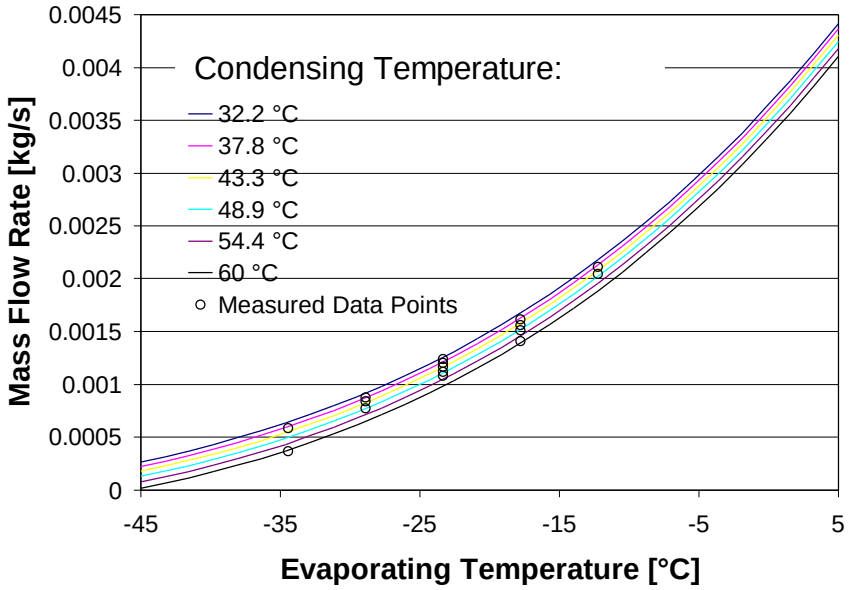

T_{evap} [°C]	T_{cond} [°C]	Mean Weighted Error [%]	Relative Error [%]
-12.2	37.8	1.2%	0.7%
-12.2	43.3	2.6%	1.5%
-17.8	37.8	-0.6%	-0.5%
-17.8	43.3	0.1%	0.1%
-17.8	48.9	0.2%	0.1%
-17.8	54.4	3.7%	3.2%
-23.3	37.8	-2.1%	-2.0%
-23.3	40.6	-1.1%	-1.2%
-23.3	43.3	-1.0%	-1.1%
-23.3	48.9	-2.8%	-3.0%
-23.3	54.4	-3.4%	-3.8%
-28.9	37.8	-1.4%	-1.9%
-28.9	43.3	-2.7%	-3.9%
-28.9	48.9	-1.3%	-2.1%
-34.4	37.8	1.5%	3.1%
-34.4	54.4	5.6%	18.8%
Average:		2.4%	5.2%

Mass Flow Rate Model (A1b)

Model parameters: C = 0.029, Δp = 0.044, V = 5.686 cm^3 (0.347 in^3), RPM = 3500

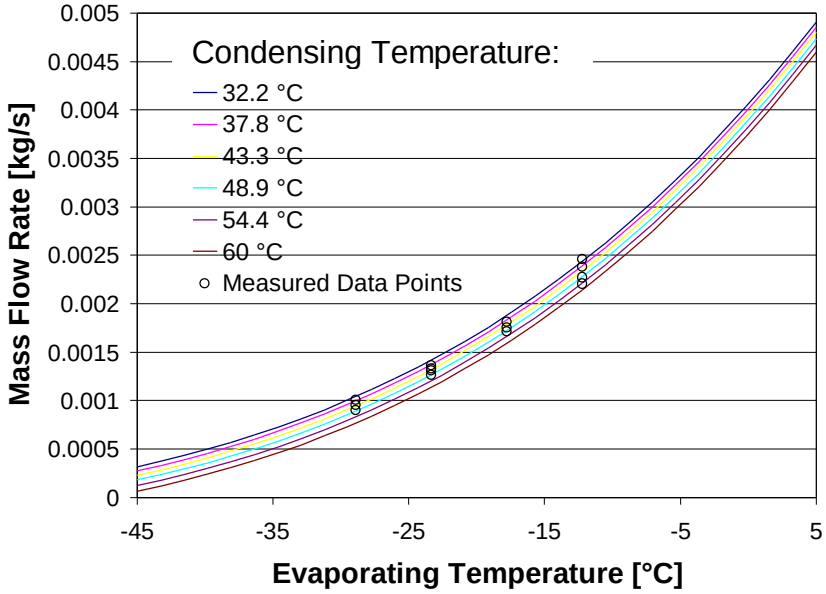

T_{evap} [°C]	T_{cond} [°C]	Mean Weighted Error [%]	Relative Error [%]
-12.2	37.8	-0.7%	-0.4%
-17.8	37.8	-0.9%	-0.8%
-23.3	37.8	0.0%	0.0%
-28.9	37.8	-0.1%	-0.1%
-23.3	40.6	0.0%	0.0%
-12.2	43.3	1.2%	0.8%
-17.8	43.3	0.0%	0.0%
-23.3	43.3	0.0%	0.0%
-28.9	43.3	0.5%	0.8%
-12.2	48.9	0.9%	0.6%
-17.8	48.9	-0.9%	-0.8%
-23.3	48.9	0.2%	0.3%
-28.9	48.9	1.0%	1.7%
-23.3	54.4	-1.1%	-1.4%
Average:		0.7%	0.8%

Mass Flow Rate Model (A2)

Model parameters: C = 0.029, Δp = 0.017, V = 6.997 cm^3 (0.427 in^3), RPM = 3500

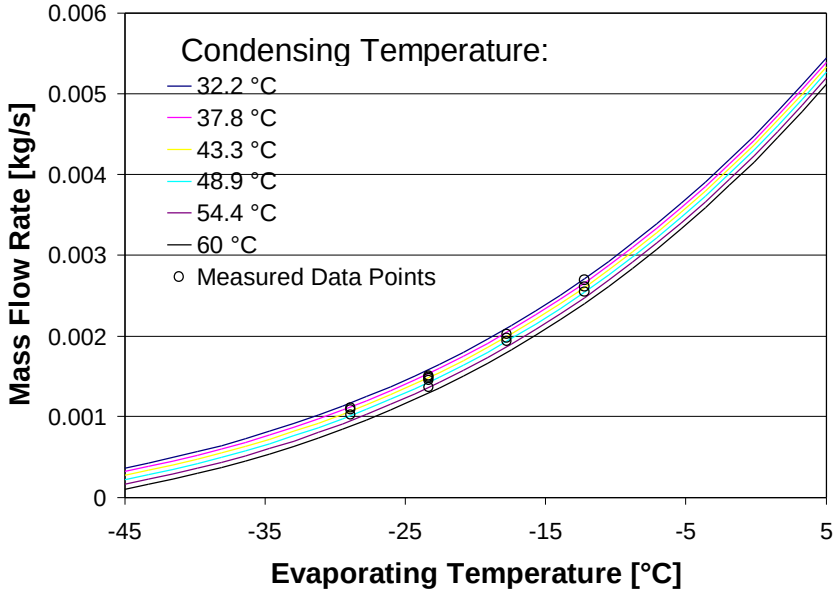

T_{evap} [°C]	T_{cond} [°C]	Mean Weighted Error [%]	Relative Error [%]
-12.2	37.8	-1.8%	-1.2%
-17.8	37.8	1.4%	1.2%
-23.3	37.8	1.8%	2.0%
-28.9	37.8	0.8%	1.2%
-23.3	40.6	1.2%	1.4%
-12.2	43.3	-0.4%	-0.3%
-17.8	43.3	1.0%	0.8%
-23.3	43.3	0.5%	0.6%
-28.9	43.3	-0.8%	-1.3%
-12.2	48.9	-0.2%	-0.2%
-17.8	48.9	-0.4%	-0.3%
-23.3	48.9	-1.3%	-1.6%
-28.9	48.9	-0.5%	-0.8%
-23.3	54.4	-0.3%	-0.4%
Average:		1.0%	1.1%

Mass Flow Rate Model (A3)

Model parameters: C = 0.031, Δp = 0.0, V = 6.211cm^3 (0.379 in^3), RPM=3500

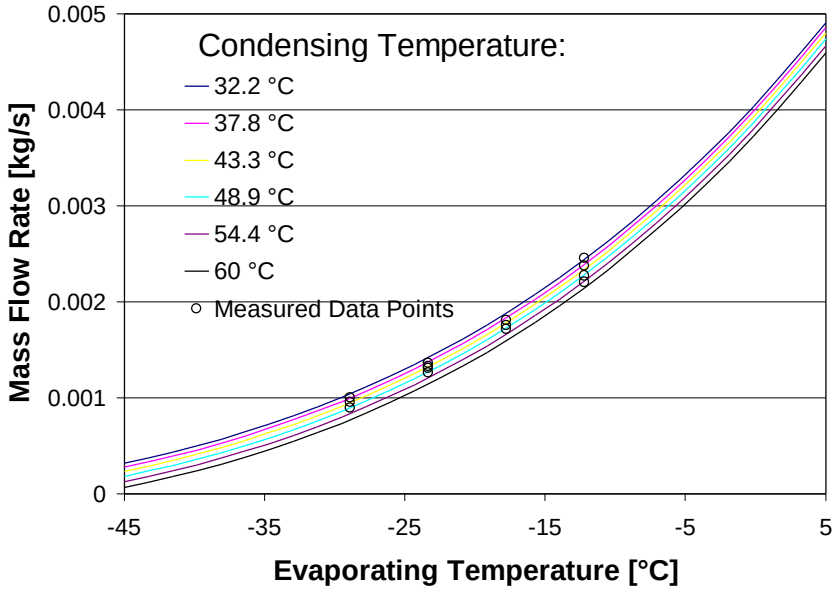

T_{evap} [°C]	T_{cond} [°C]	Mean Weighted Error [%]	Relative Error [%]
-12.2	37.8	-4.1%	-2.7%
-17.8	37.8	1.3%	1.2%
-23.3	37.8	0.7%	0.8%
-28.9	37.8	-0.5%	-0.8%
-23.3	40.6	1.1%	1.4%
-12.2	43.3	-2.5%	-1.7%
-17.8	43.3	1.6%	1.4%
-23.3	43.3	0.8%	1.0%
-28.9	43.3	-0.5%	-0.8%
-12.2	48.9	0.4%	0.3%
-17.8	48.9	0.6%	0.5%
-23.3	48.9	0.2%	0.2%
-28.9	48.9	-0.3%	-0.5%
-12.2	54.4	0.5%	0.4%
Average:		1.5%	1.2%

Mass Flow Rate Model (A4)

Model parameters: C = 0.029, Δp = 0.047, V = 6.997 cm^3 (0.427 in^3), RPM = 3500

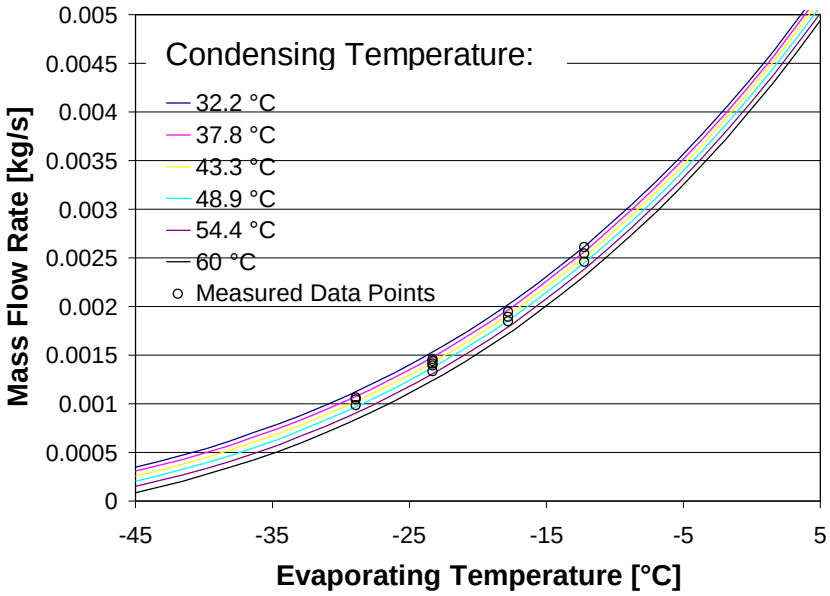

T_{evap} [°C]	T_{cond} [°C]	Mean Weighted Error [%]	Relative Error [%]
-12.2	37.8	-2.2%	-1.4%
-17.8	37.8	1.9%	1.6%
-23.3	37.8	1.3%	1.5%
-28.9	37.8	1.0%	1.6%
-23.3	40.6	0.9%	1.1%
-12.2	43.3	-1.4%	-1.0%
-17.8	43.3	1.7%	1.5%
-23.3	43.3	1.2%	1.4%
-28.9	43.3	-0.9%	-1.4%
-12.2	48.9	-0.1%	-0.1%
-17.8	48.9	1.0%	0.9%
-23.3	48.9	-1.4%	-1.6%
-28.9	48.9	-0.6%	-1.1%
-23.3	54.4	-1.4%	-1.7%
Average:		1.3%	1.3%

Mass Flow Rate Model (A5)

Model parameters: C = 0.024, Δp = 0.141, V = 7.751 cm^3 (0.473 in^3), RPM=3500

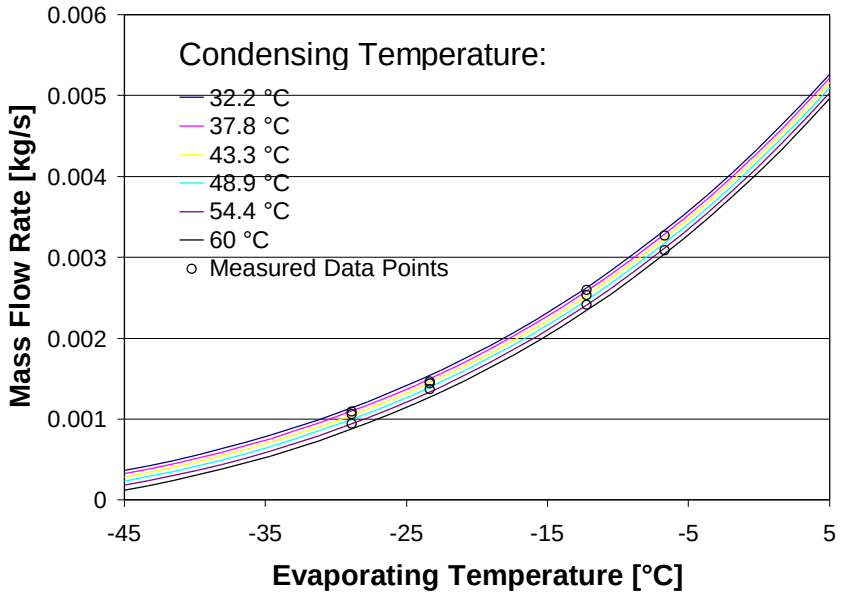

T_{evap} [°C]	T_{cond} [°C]	Mean Weighted Error [%]	Relative Error [%]
-12.2	37.8	-0.7%	-0.5%
-23.3	37.8	1.8%	2.4%
-28.9	37.8	0.4%	0.6%
-6.67	43.3	-1.6%	-0.9%
-12.2	43.3	-0.1%	-0.1%
-23.3	43.3	0.5%	0.7%
-28.9	43.3	-0.5%	-0.9%
-6.67	54.4	1.9%	1.2%
-12.2	54.4	-0.1%	-0.1%
-23.3	54.4	-1.5%	-2.1%
-28.9	54.4	-0.2%	-0.3%
Average:		1.1%	1.2%

Mass Flow Rate Model (A6a)

Model parameters: C = 0.020, Δp = 0.093, V = 6.57 cm^3 (0.4009 in^3), RPM = 3500

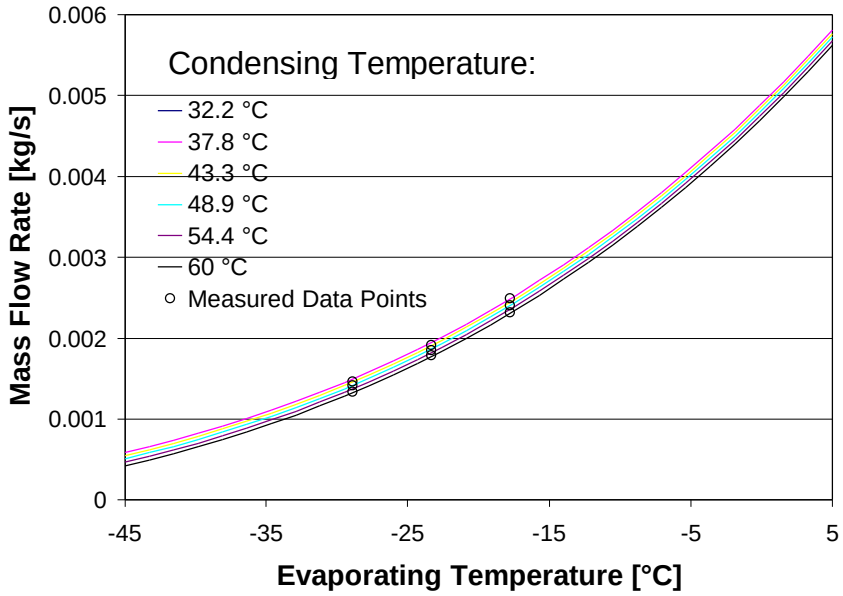

T_{evap} [°C]	T_{cond} [°C]	Mean Weighted Error [%]	Relative Error [%]
-17.8	54.4	3.1%	2.5%
-17.8	48.9	0.9%	0.7%
-17.8	43.3	-1.6%	-1.2%
-23.3	54.4	0.7%	0.7%
-23.3	48.9	-0.3%	-0.3%
-23.3	43.3	-1.4%	-1.4%
-28.9	54.4	0.4%	0.6%
-28.9	48.9	-1.2%	-1.6%
-28.9	43.3	-1.8%	-2.3%
Average:		1.5%	1.5%

Mass Flow Rate Model (A6b)

Model parameters: C = 0.028, Δp = 0.153, V = 6.57 cm^3 (0.4009 in^3), RPM = 3500

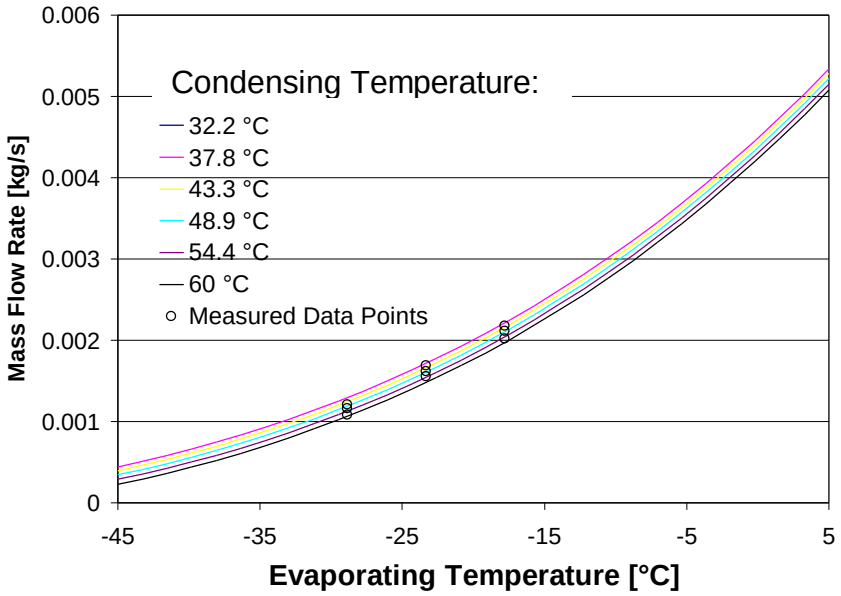

T_{evap} [°C]	T_{cond} [°C]	Mean Weighted Error [%]	Relative Error [%]
-17.8	54.4	2.9%	2.3%
-17.8	48.9	0.6%	0.5%
-17.8	43.3	0.1%	0.1%
-23.3	54.4	-1.5%	-1.5%
-23.3	48.9	-1.6%	-1.6%
-23.3	43.3	-2.8%	-2.7%
-28.9	54.4	1.1%	1.6%
-28.9	48.9	0.2%	0.3%
-28.9	43.3	0.4%	0.5%
Average:		1.6%	1.5%

Mass Flow Rate Model (B1)

Model parameters: C = 0.026, Δp = 0.025, V = 5.654 cm^3 (0.345 in^3), RPM = 3550

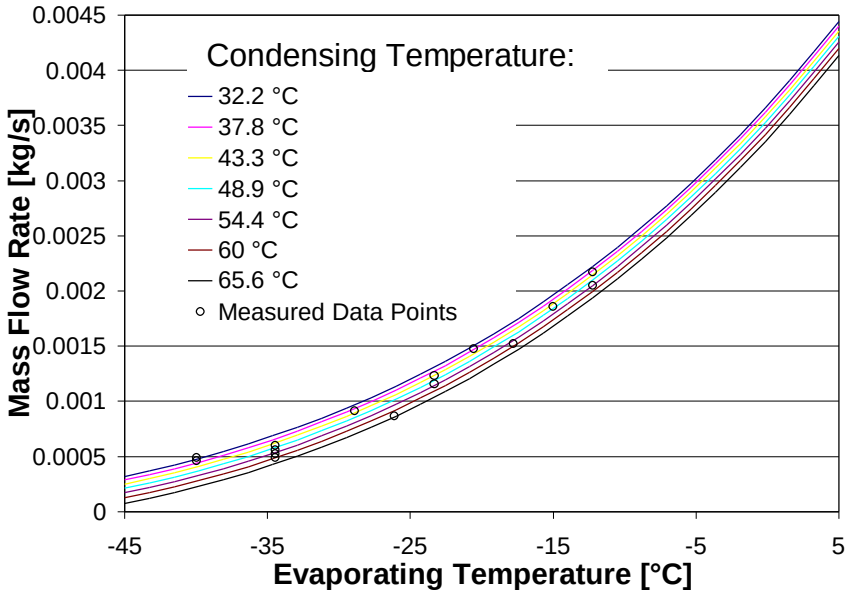

T_{evap} [°C]	T_{cond} [°C]	Mean Weighted Error [%]	Relative Error [%]
-40.0	37.8	-4.5%	-10.0%
-28.9	37.8	2.4%	2.9%
-20.6	37.8	-0.7%	-0.5%
-12.2	37.8	1.3%	0.7%
-40.0	43.3	-4.9%	-11.7%
-34.4	43.3	2.0%	3.7%
-23.3	43.3	0.0%	0.0%
-34.4	48.9	2.2%	4.3%
-15.0	48.9	-1.9%	-1.1%
-34.4	54.4	1.0%	2.0%
-23.3	54.4	-1.1%	-1.0%
-12.2	54.4	0.0%	0.0%
-34.4	60.0	-0.4%	-0.9%
-26.1	60.0	4.7%	6.0%
-17.8	60.0	-1.8%	-1.3%
Average:		2.5%	4.6%

Mass Flow Rate Model (B2)

Model parameters: C = 0.015, Δp = 0.058, V = 7.276 cm^3 (0.444 in^3), RPM = 3550

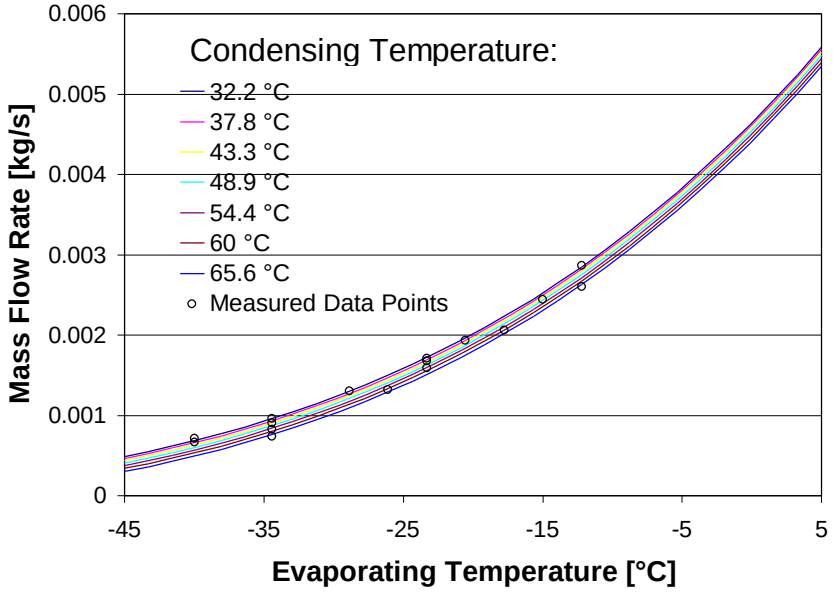

T_{evap} [°C]	T_{cond} [°C]	Mean Weighted Error [%]	Relative Error [%]
-40.0	37.8	-3.5%	-7.4%
-28.9	37.8	-2.1%	-2.5%
-23.3	37.8	-1.5%	-1.3%
-20.6	37.8	-0.1%	-0.1%
-12.2	37.8	-2.8%	-1.5%
-40.0	43.3	-2.1%	-4.8%
-34.4	43.3	-3.9%	-6.2%
-23.3	43.3	-1.1%	-1.0%
-34.4	48.9	-2.2%	-3.6%
-15.0	48.9	-0.7%	-0.4%
-34.4	54.4	0.8%	1.5%
-23.3	54.4	0.2%	0.2%
-12.2	54.4	7.5%	4.4%
-34.4	60.0	4.3%	8.9%
-26.1	60.0	0.8%	0.9%
-17.8	60.0	0.2%	0.1%

Average:	2.8%	3.9%

Mass Flow Rate Model (B3)

Model parameters: C = 0.017, Δp = 0.077, V = 8.374 cm^3 (0.511 in^3), RPM = 3550

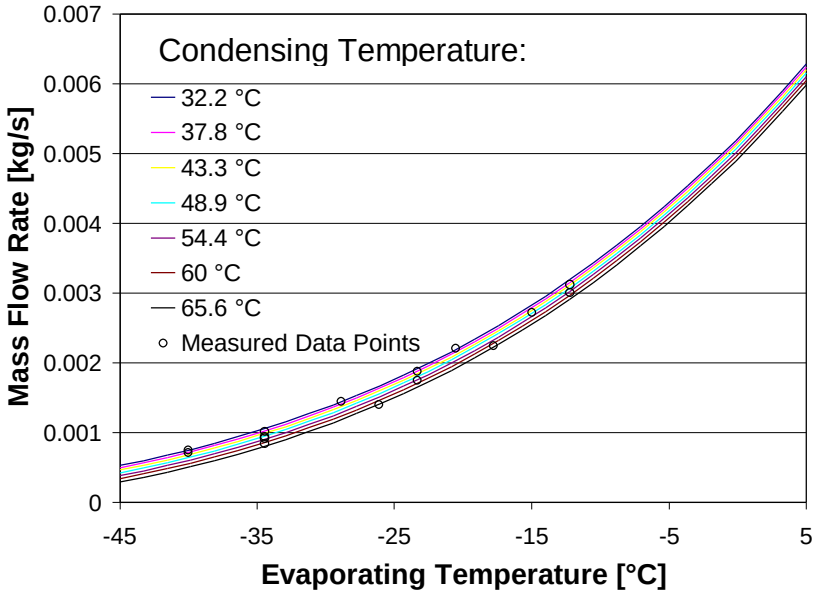

T_{evap} [°C]	T_{cond} [°C]	Mean Weighted Error [%]	Relative Error [%]
-40.0	37.8	-2.1%	-4.6%
-28.9	37.8	-2.1%	-2.5%
-20.6	37.8	-3.3%	-2.5%
-12.2	37.8	2.2%	1.2%
-40.0	43.3	-2.0%	-4.6%
-34.4	43.3	-1.6%	-2.7%
-23.3	43.3	-1.9%	-1.7%
-34.4	48.9	0.4%	0.7%
-15.0	48.9	-1.0%	-0.6%
-34.4	54.4	-0.8%	-1.4%
-23.3	54.4	0.2%	0.2%
-12.2	54.4	0.9%	0.5%
-34.4	60.0	1.2%	2.4%
-26.1	60.0	3.6%	4.2%
-17.8	60.0	2.0%	1.5%

Average:	1.9%	2.5%

Mass Flow Rate Model (B4)

Model parameters: C = 0.027, Δp = 0.192, V = 8.095 cm^3 (0.494 in^3), RPM = 3525

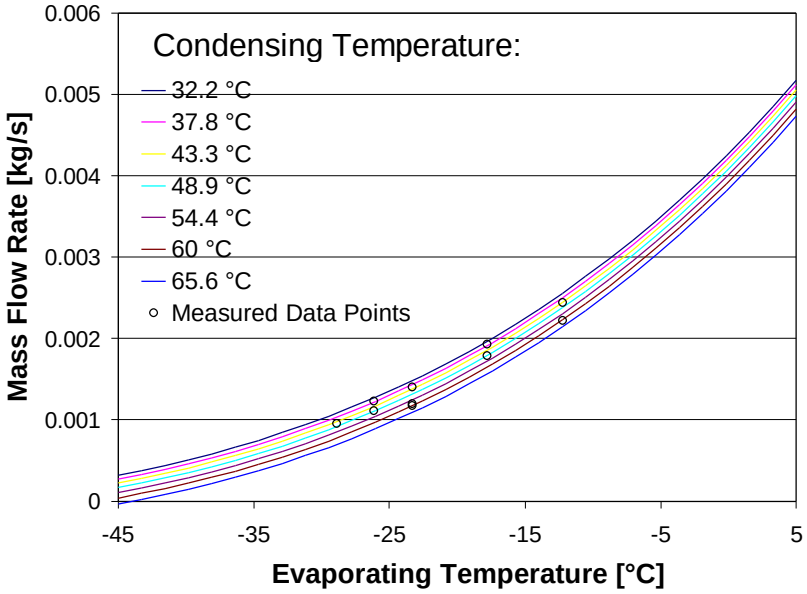

T_{evap} [°C]	T_{cond} [°C]	Mean Weighted Error [%]	Relative Error [%]
-26.1	37.8	-0.4%	-0.5%
-17.8	37.8	-1.0%	-0.8%
-23.3	43.3	-1.7%	-1.8%
-12.2	43.3	0.4%	0.2%
-28.9	48.9	-2.3%	-3.8%
-26.1	48.9	-0.1%	-0.1%
-17.8	48.9	0.4%	0.3%
-23.3	54.4	2.9%	3.7%
-23.3	60.0	-0.2%	-0.3%
-12.2	60.0	0.9%	0.7%
Average:		1.4%	1.8%

Mass Flow Rate Model (B5)

Model parameters: C = 0.029, Δp = 0.129, V = 9.406 cm^3 (0.574 in^3), RPM = 3525

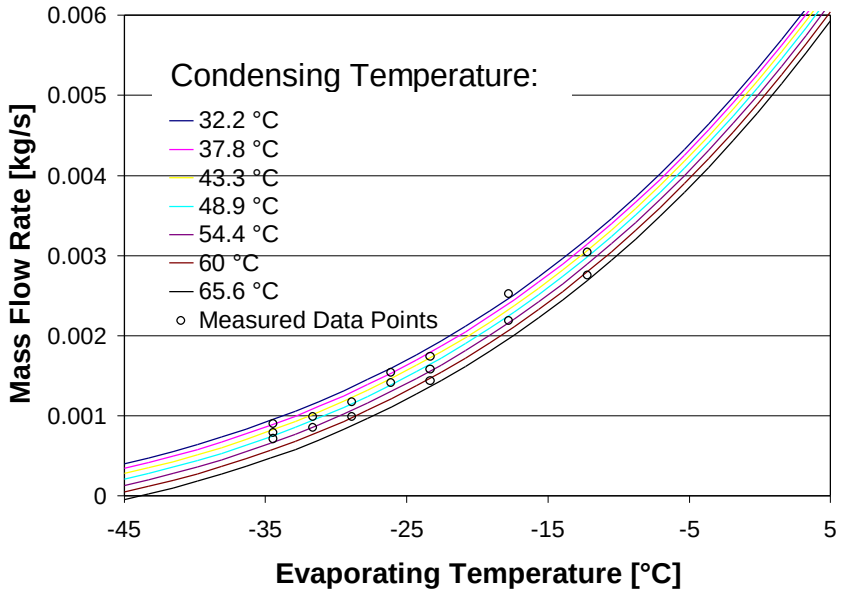

T_{evap} [°C]	T_{cond} [°C]	Mean Weighted Error [%]	Relative Error [%]
-34.4	37.8	-0.7%	-1.1%
-26.1	37.8	-0.4%	-0.4%
-17.8	37.8	-7.9%	-4.8%
-31.7	43.3	1.8%	2.8%
-23.3	43.3	-1.0%	-0.9%
-12.2	43.3	1.9%	0.9%
-34.4	48.9	-2.6%	-5.0%
-28.9	48.9	-1.6%	-2.1%
-26.1	48.9	-1.7%	-1.9%
-17.8	48.9	4.1%	2.9%
-34.4	54.4	-2.7%	-5.8%
-31.7	54.4	0.5%	0.9%
-23.3	54.4	-1.1%	-1.1%
-28.9	57.2	2.3%	3.6%
-23.3	60	2.2%	2.3%
-12.2	60	3.2%	1.8%

Average:	2.8%	2.9%

Mass Flow Rate Model (B6)

Model parameters: C = 0.025, Δp = 0.236,V = 5.588 cm^3 (0.341 in^3), RPM = 3475

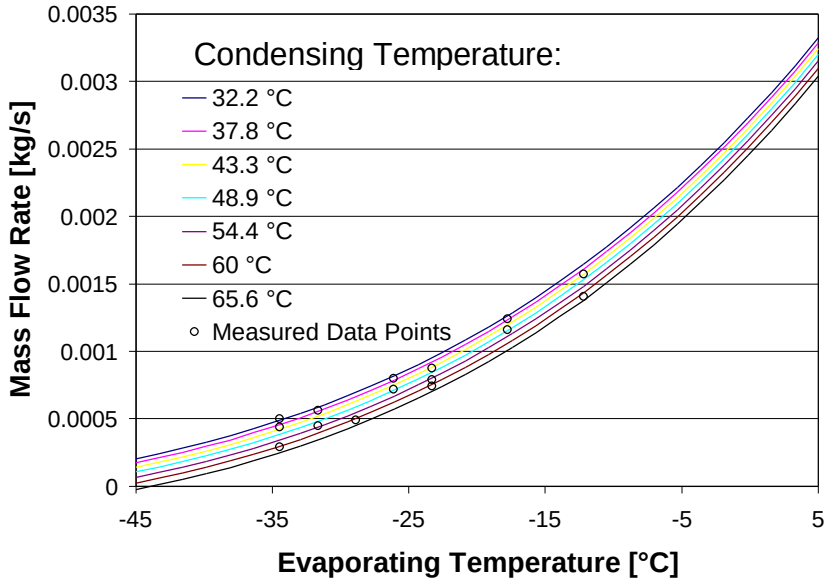

T_{evap} [°C]	T_{cond} [°C]	Mean Weighted Error [%]	Relative Error [%]
-34.4	37.8	-5.2%	-8.4%
-26.1	37.8	-1.9%	-1.9%
-17.8	37.8	-0.9%	-0.6%
-31.7	43.3	-4.8%	-6.8%
-23.3	43.3	0.9%	0.8%
-12.2	43.3	0.1%	0.1%
-34.4	48.9	-6.2%	-11.4%
-26.1	48.9	-1.0%	-1.2%
-17.8	48.9	-0.4%	-0.3%
-34.4	54.4	6.4%	17.6%
-31.7	54.4	-0.6%	-1.1%
-23.3	54.4	1.4%	1.4%
-28.9	60.0	1.4%	2.2%
-23.3	60.0	1.6%	1.7%
-12.2	60.0	3.6%	2.1%
Average:		3.2%	6.2%

Mass Flow Rate Model (B7)

Model parameters: C = 0.017, Δp = 0.241, V = 3.998 cm^3 (0.244 in^3), RPM = 3475

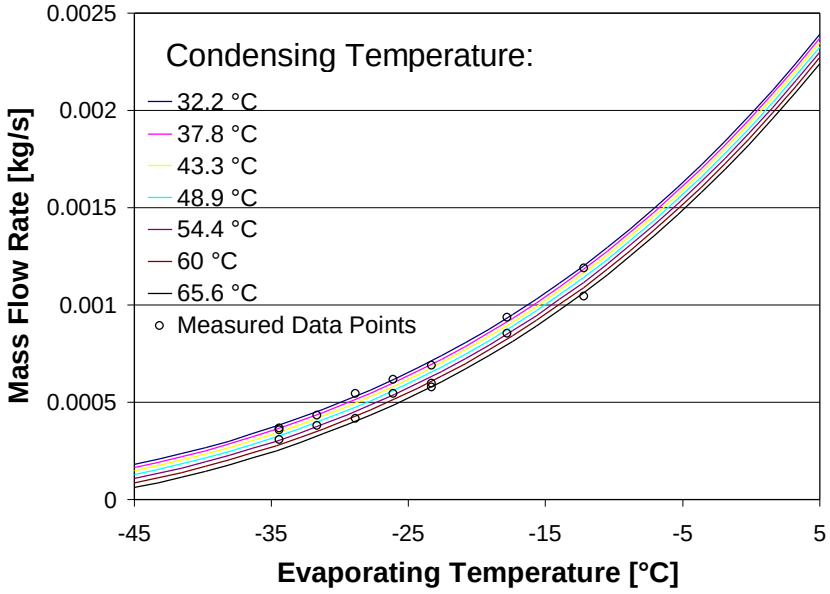

T_{evap} [°C]	T_{cond} [°C]	Mean Weighted Error [%]	Relative Error [%]
-26.1	37.8	-3.0%	-3.0%
-17.8	37.8	-3.3%	-2.1%
-34.4	43.3	-3.2%	-5.4%
-31.7	43.3	-2.6%	-3.7%
-23.3	43.3	-2.2%	-2.0%
-12.2	43.3	-4.0%	-2.1%
-34.4	48.9	-4.6%	-7.9%
-28.9	48.9	-11.2%	-12.7%
-26.1	48.9	2.7%	3.0%
-17.8	48.9	3.6%	2.6%
-34.4	54.4	-0.4%	-0.7%
-31.7	54.4	-0.5%	-0.8%
-23.3	54.4	5.6%	5.8%
-28.9	60.0	2.1%	3.1%
-23.3	60.0	4.8%	5.1%
-12.2	60.0	7.5%	4.4%
Average:		4.6%	5.0%

Mass Flow Rate Model (B8)

Model parameters: C = 0.0218, Δp = 0.293, V = 2.95 cm^3 (0.18 in^3), RPM = 3500

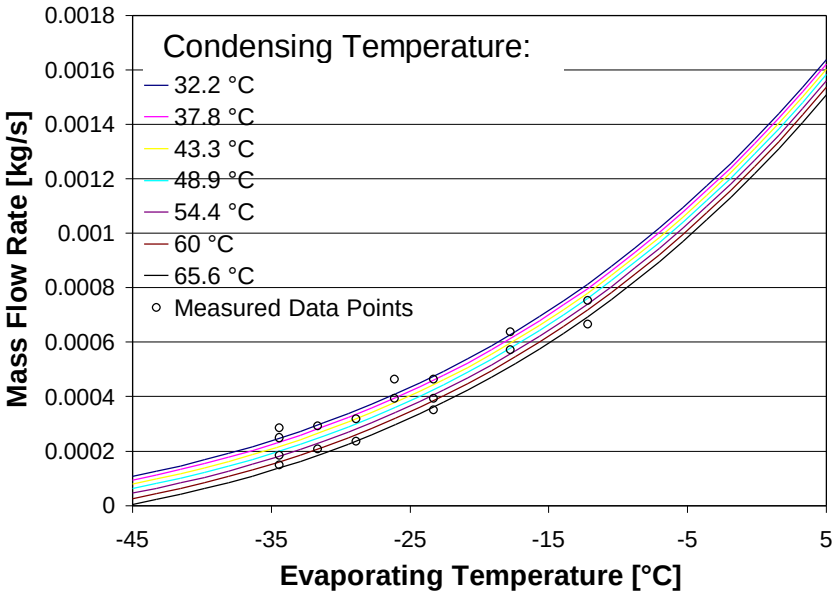

T_{evap} [°C]	T_{cond} [°C]	Mean Weighted Error [%]	Relative Error [%]
-34.4	37.8	-13.4%	-18.3%
-26.1	37.8	-17.7%	-14.9%
-17.8	37.8	-6.3%	-3.8%
-34.4	43.3	-8.0%	-12.5%
-31.7	43.3	-6.8%	-9.0%
-23.3	43.3	-4.9%	-4.2%
-12.2	43.3	7.1%	3.6%
-28.9	48.9	-4.4%	-5.4%
-26.1	48.9	-8.3%	-8.2%
-17.8	48.9	1.4%	1.0%
-34.4	54.4	-0.7%	-1.5%
-31.7	54.4	5.6%	10.6%
-23.3	54.4	3.1%	3.1%
-34.4	60.0	2.8%	7.1%
-28.9	60.0	6.3%	10.4%
-23.3	60.0	8.6%	9.5%

-12.2	60.0	13.7%	8.0%
Average:		8.2	9.0

Mass Flow Rate Model (B9a)

Model parameters: C = 0.028, Δp = 0.215, V = 8.095 cm^3 (0.494 in^3), RPM = 3500

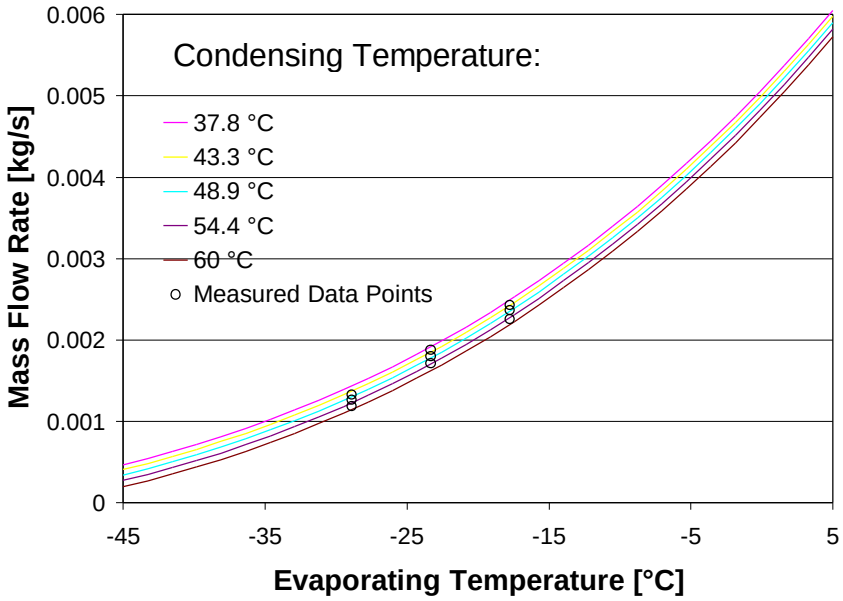

T_{evap} [°C]	T_{cond} [°C]	Mean Weighted Error [%]	Relative Error [%]
-17.8	54.4	2.3%	1.8%
-17.8	48.9	0.3%	0.2%
-17.8	43.3	0.7%	0.5%
-23.3	54.4	-1.6%	-1.7%
-23.3	48.9	-2.3%	-2.3%
-23.3	43.3	-2.6%	-2.5%
-28.9	54.4	0.8%	1.2%
-28.9	48.9	0.7%	1.0%
-28.9	43.3	1.6%	2.2%
Average:		1.6%	1.7%

Mass Flow Rate Model (B9b)

Model parameters: C = 0.023, Δp = 0.202, V = 8.095 cm^3 (0.494 in^3), RPM = 3500

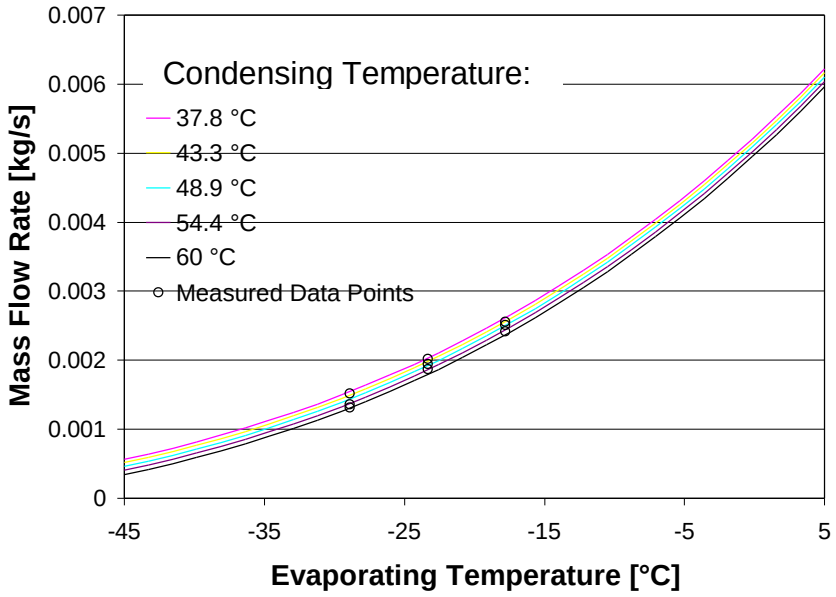

T_{evap} [°C]	T_{cond} [°C]	Mean Weighted Error [%]	Relative Error [%]
-17.8	54.4	2.1%	1.6%
-17.8	48.9	0.9%	0.7%
-17.8	43.3	1.3%	1.0%
-23.3	54.4	-1.4%	-1.5%
-23.3	48.9	-2.0%	-2.0%
-23.3	43.3	-3.0%	-2.9%
-28.9	54.4	1.7%	2.5%
-28.9	48.9	2.3%	3.3%
-28.9	43.3	-2.6%	-3.4%
Average:		2.0%	2.3%

Mass Flow Rate Model (B9c)

Model parameters: C = 0.026, Δp = 0.184, V = 8.095 cm^3 (0.494 in^3), RPM = 3500

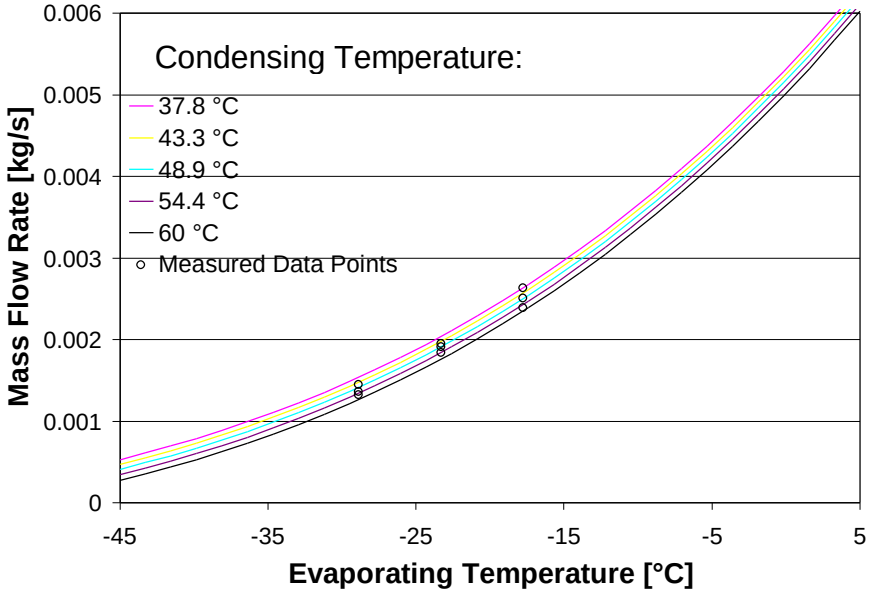

T_{evap} [°C]	T_{cond} [°C]	Mean Weighted Error [%]	Relative Error [%]
-17.8	54.4	2.9%	2.4%
-17.8	48.9	1.0%	0.7%
-17.8	43.3	-2.1%	-1.5%
-23.3	54.4	-1.3%	-1.4%
-23.3	48.9	-1.4%	-1.4%
-23.3	43.3	0.0%	0.0%
-28.9	54.4	-0.8%	-1.2%
-28.9	48.9	1.0%	1.4%
-28.9	43.3	0.4%	0.5%
Average:		1.5%	1.3%

Mass Flow Rate Model (C1)

Model parameters: C = 0.032, Δp = 0.075, V= = 5.57 cm^3 (0.3399 in^3), RPM = 3500

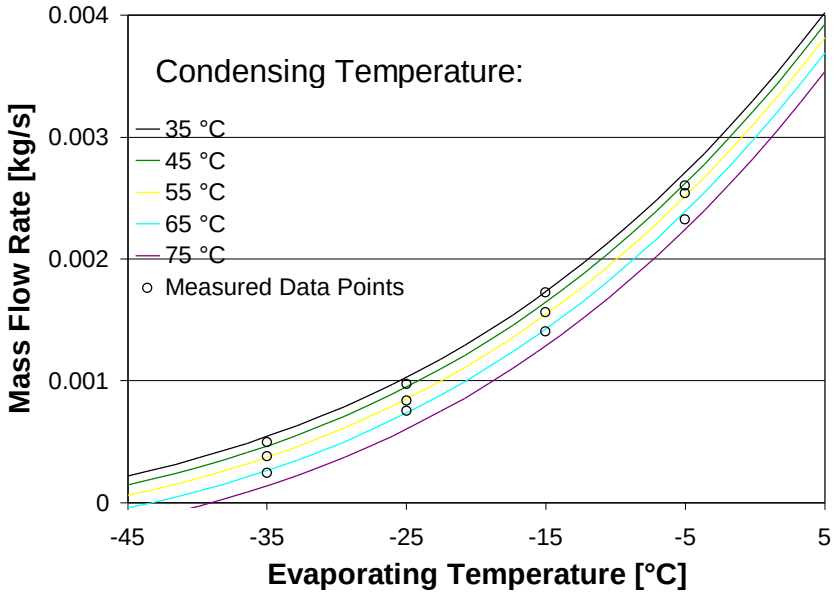

T_{evap} [°C]	T_{cond} [°C]	Mean Weighted Error [%]	Relative Error [%]
-35	45	-2.2%	-5.9%
-25	45	-1.9%	-2.5%
-15	45	-6.0%	-4.6%
-5	45	1.5%	0.8%
-35	55	-0.5%	-1.8%
-25	55	1.1%	1.7%
-15	55	-1.3%	-1.1%
-5	55	-1.7%	-0.9%
-35	65	1.6%	8.6%
-25	65	-1.3%	-2.3%
-15	65	1.7%	1.6%
-5	65	5.1%	2.9%
Average:		2.7%	3.7%

Mass Flow Rate Model (C2)

Model parameters: C = 0.028, Δp = 0.061, V = 7.16 cm^3 (0.4369 in^3), RPM = 3500

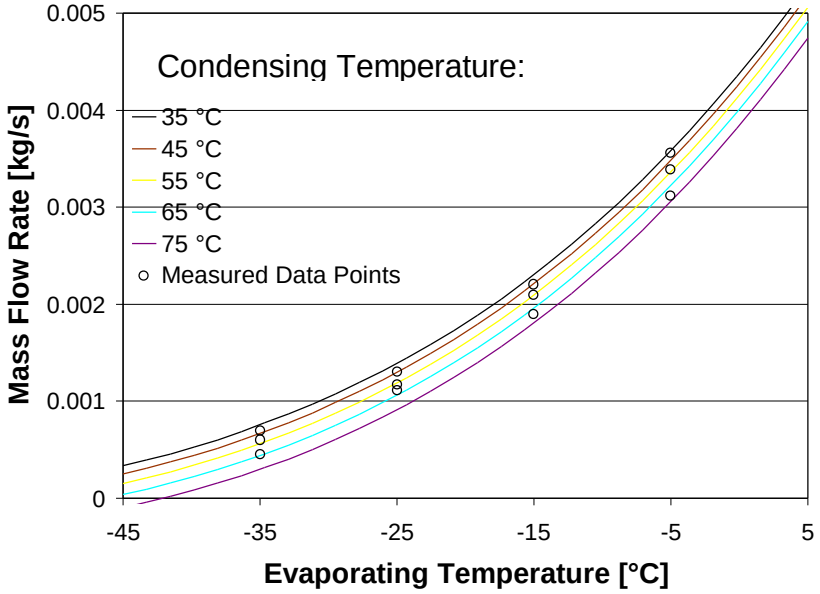

T_{evap} [°C]	T_{cond} [°C]	Mean Weighted Error [%]	Relative Error [%]
-35	45	-1.4%	-3.6%
-25	45	-0.3%	-0.5%
-15	45	0.3%	0.3%
-5	45	-4.5%	-2.3%
-35	55	-2.1%	-6.3%
-25	55	1.0%	1.5%
-15	55	0.0%	0.0%
-5	55	-1.6%	-0.8%
-35	65	-0.7%	-2.9%
-25	65	-2.9%	-4.7%
-15	65	3.5%	3.3%
-5	65	5.7%	3.3%
Average:		2.6%	3.1%

Appendix D: Power Maps

This appendix contains the power models for all sets of testing data. The plot shows the exponential combined efficiency model extrapolated to higher and lower evaporating temperatures than were represented in the data as well as the experimental data itself. The model parameters have been determined using all measured data points. In the table below the plot, the mean weighted and relative errors between the two models and the experimental data is recorded for each measured data point.

In addition, the curve fit parameters for both models are shown as well as the range of the combined efficiency that occurs in the experimental data.

For fitting the power model parameters, the mass flow rate calculated with the constant percentage pressure drop model has been used.

The curves for the different condensing temperatures are in consecutive order. The highest condensing temperature curve is the highest one for high evaporating temperatures and the lowest one for low evaporating temperatures.

Power Model (A1a)

Model parameters: inverse proportional: a = 0.738, b = -17.08
exponential: d = 0.664, e = -0.620, f = -0.0185
Combined efficiency ranges from 0.49 to 0.64

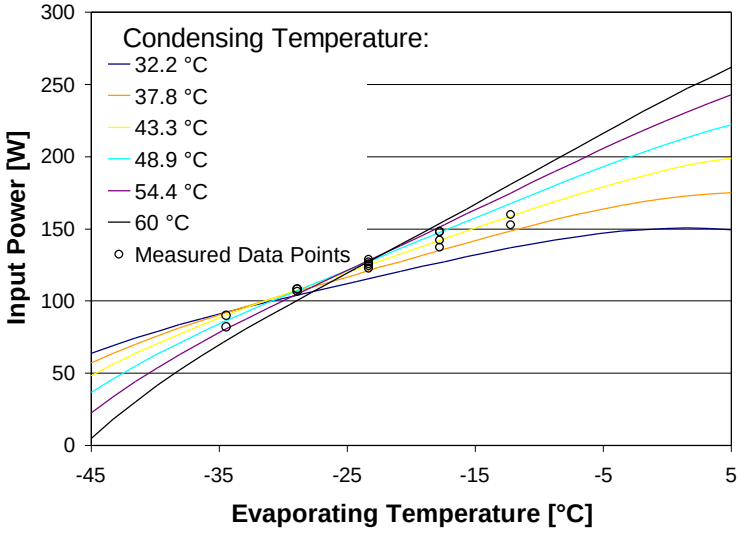

		Inverse Proportional		Exponential	
T_{evap} [°C]	T_{cond} [°C]	Mean Weighted Error [%]	Relative Error [%]	Mean Weighted Error [%]	Relative Error [%]
-12.2	37.8	-2.2%	-1.8%	-1.9%	-1.6%
-12.2	43.3	0.2%	0.1%	0.6%	0.4%
-17.8	37.8	-1.2%	-1.1%	-1.4%	-1.3%
-17.8	43.3	0.3%	0.3%	0.1%	0.1%
-17.8	48.9	0.4%	0.3%	0.2%	0.2%
-17.8	54.4	3.5%	3.0%	3.3%	2.8%
-23.3	37.8	-0.1%	-0.1%	-0.2%	-0.2%
-23.3	40.6	0.0%	0.0%	-0.1%	-0.1%
-23.3	43.3	0.1%	0.1%	0.0%	0.0%
-23.3	48.9	-0.1%	-0.1%	-0.2%	-0.2%
-23.3	54.4	-0.2%	-0.2%	-0.3%	-0.3%
-28.9	37.8	-0.2%	-0.3%	0.1%	0.1%
-28.9	43.3	-0.9%	-1.0%	-0.6%	-0.6%
-28.9	48.9	-1.1%	-1.3%	-0.8%	-0.9%
-34.4	37.8	2.3%	3.2%	2.2%	3.1%
-34.4	54.4	-1.6%	-2.4%	-1.7%	-2.6%
Average:		**1.3%**	**1.4%**	**1.3%**	**1.4%**

Power Model (A1b)

Model parameters: inverse proportional: a = 0.694, b = -14.58
exponential: d = 0.624, e = -0.703, f = -0.0223
Combined efficiency ranges from 0.52 to 0.62

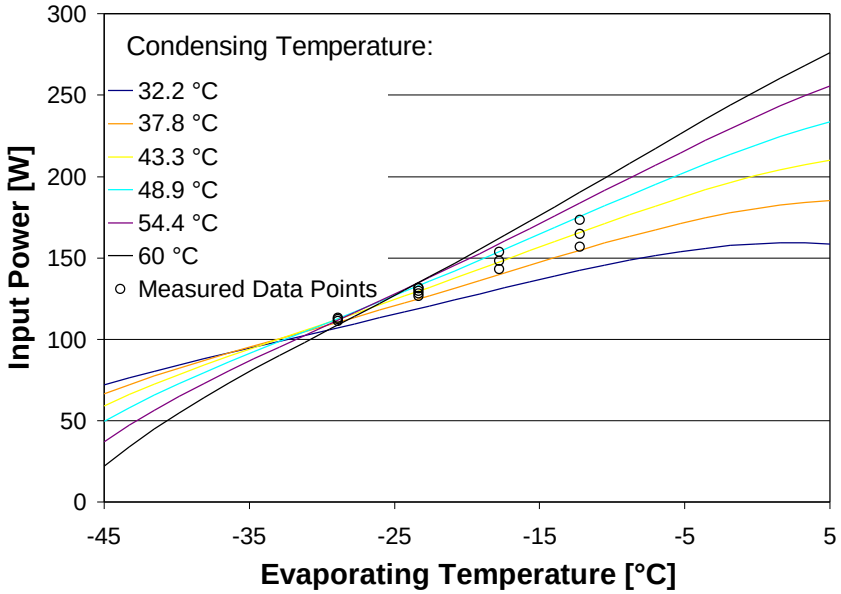

		Inverse Proportional		Exponential	
T_{evap} [°C]	T_{cond} [°C]	Mean Weighted Error [%]	Relative Error [%]	Mean Weighted Error [%]	Relative Error [%]
-12.2	37.8	-1.8%	-1.6%	-1.3%	-1.1%
-17.8	37.8	-1.7%	-1.6%	-2.0%	-2.0%
-23.3	37.8	-0.3%	-0.3%	-0.7%	-0.7%
-28.9	37.8	-0.4%	-0.5%	0.0%	0.0%
-23.3	40.6	0.1%	0.1%	-0.3%	-0.3%
-12.2	43.3	0.4%	0.3%	0.9%	0.7%
-17.8	43.3	0.1%	0.1%	-0.4%	-0.3%
-23.3	43.3	0.6%	0.6%	0.2%	0.2%
-28.9	43.3	-0.4%	-0.5%	0.1%	0.1%
-12.2	48.9	0.7%	0.5%	1.2%	1.0%
-17.8	48.9	0.4%	0.3%	-0.1%	-0.1%
-23.3	48.9	1.2%	1.2%	0.7%	0.8%
-28.9	48.9	-1.1%	-1.3%	-0.7%	-0.8%
-23.3	54.4	2.2%	2.3%	1.8%	1.9%
Average:		**1.0%**	**1.0%**	**1.0%**	**0.9%**

Power Model (A2)

Model parameters: inverse proportional: a = 0.652, b = -13.33
exponential: d = 0.586, e = -0.709, f = -0.0235
Combined efficiency ranges from 0.50 to 0.59

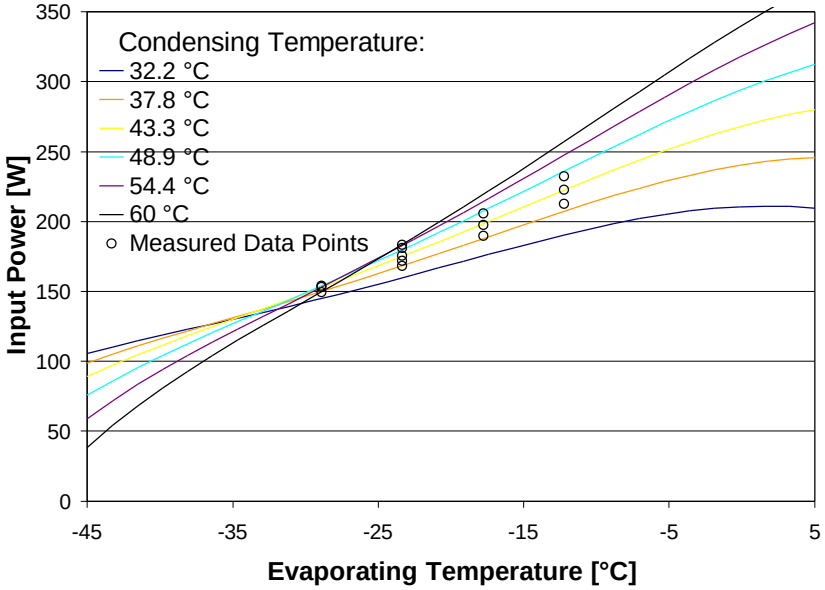

		Inverse Proportional		Exponential	
T_{evap} [°C]	T_{cond} [°C]	Mean Weighted Error [%]	Relative Error [%]	Mean Weighted Error [%]	Relative Error [%]
-12.2	37.8	-3.3%	-2.9%	-2.8%	-2.4%
-17.8	37.8	-0.5%	-0.5%	-1.0%	-0.9%
-23.3	37.8	0.5%	0.6%	0.1%	0.1%
-28.9	37.8	-0.4%	-0.5%	0.2%	0.3%
-23.3	40.6	0.5%	0.6%	0.1%	0.1%
-12.2	43.3	-0.5%	-0.4%	0.1%	0.1%
-17.8	43.3	1.0%	1.0%	0.5%	0.5%
-23.3	43.3	0.3%	0.3%	-0.1%	-0.1%
-28.9	43.3	-0.8%	-0.9%	-0.2%	-0.2%
-12.2	48.9	1.4%	1.1%	2.0%	1.6%
-17.8	48.9	1.6%	1.4%	1.1%	1.0%
-23.3	48.9	-0.2%	-0.2%	-0.6%	-0.6%
-28.9	48.9	-0.5%	-0.6%	0.1%	0.1%
-23.3	54.4	0.4%	0.4%	-0.1%	-0.1%
Average:		**1.2%**	**1.0%**	**1.0%**	**0.9%**

Power Model (A3)

Model parameters: inverse proportional: a = 0.724, b = -14.97
exponential: d = 0.657, e = -0.595, f = -0.0197
Combined efficiency ranges from 0.55 to 0.65

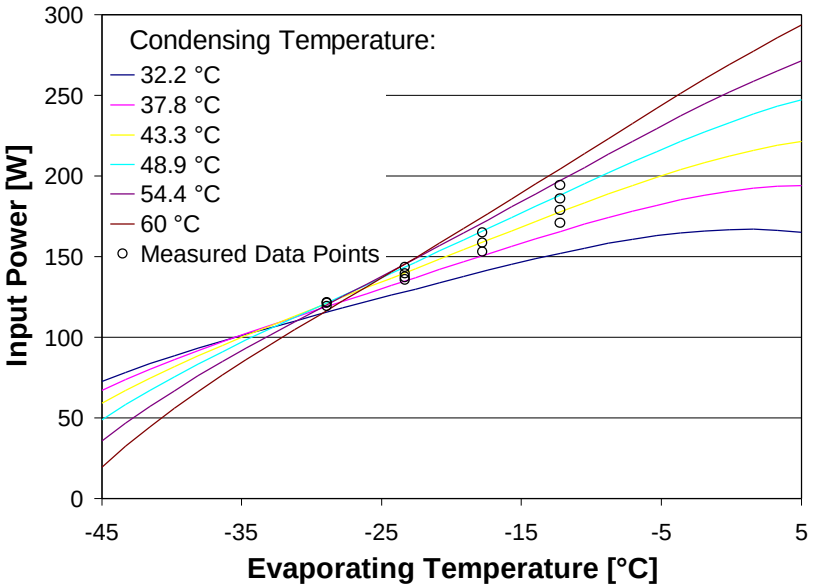

		Inverse Proportional		Exponential	
T_{evap} [°C]	T_{cond} [°C]	Mean Weighted Error [%]	Relative Error [%]	Mean Weighted Error [%]	Relative Error [%]
-12.2	37.8	-3.6%	-3.2%	-3.4%	-3.0%
-17.8	37.8	-1.3%	-1.2%	-1.6%	-1.6%
-23.3	37.8	-0.3%	-0.3%	-0.5%	-0.5%
-28.9	37.8	-0.3%	-0.3%	0.0%	0.0%
-23.3	40.6	0.5%	0.6%	0.3%	0.3%
-12.2	43.3	-0.9%	-0.7%	-0.6%	-0.5%
-17.8	43.3	0.7%	0.7%	0.4%	0.4%
-23.3	43.3	0.5%	0.6%	0.3%	0.4%
-28.9	43.3	-0.4%	-0.5%	-0.1%	-0.2%
-12.2	48.9	1.3%	1.1%	1.6%	1.3%
-17.8	48.9	1.1%	1.0%	0.7%	0.7%
-23.3	48.9	0.4%	0.4%	0.1%	0.1%
-28.9	48.9	-0.2%	-0.2%	0.1%	0.1%
-12.2	54.4	1.7%	1.3%	2.0%	1.5%
Average:		**1.3%**	**1.1%**	**1.2%**	**1.1%**

Power Model (A4)

Model parameters: inverse proportional: a = 0.685, b = -11.59
exponential: d = 0.619, e = -1.646, f = -0.035
Combined efficiency ranges from 0.54 to 0.63

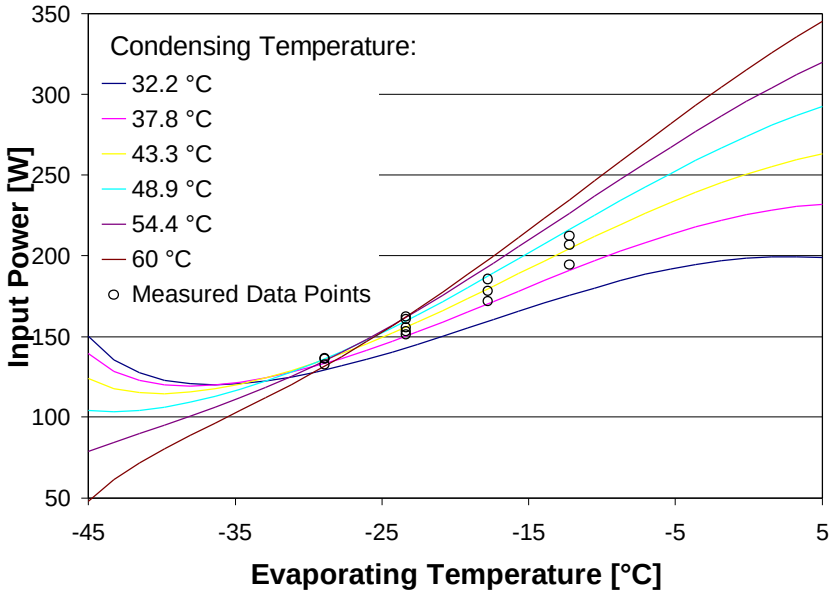

		Inverse Proportional		Exponential	
T_{evap} [°C]	T_{cond} [°C]	Mean Weighted Error [%]	Relative Error [%]	Mean Weighted Error [%]	Relative Error [%]
-17.8	37.8	-0.2%	-0.2%	-0.8%	-0.8%
-23.3	37.8	0.4%	0.5%	-0.5%	-0.5%
-28.9	37.8	-0.6%	-0.8%	0.6%	0.8%
-23.3	40.6	0.8%	0.9%	-0.1%	-0.1%
-12.2	43.3	-2.4%	-1.9%	-1.4%	-1.1%
-17.8	43.3	1.6%	1.5%	0.9%	0.8%
-23.3	43.3	1.3%	1.4%	0.4%	0.4%
-28.9	43.3	-1.7%	-2.1%	-0.5%	-0.6%
-12.2	48.9	1.4%	1.1%	2.5%	2.0%
-17.8	48.9	1.9%	1.7%	1.2%	1.1%
-23.3	48.9	0.4%	0.4%	-0.5%	-0.5%
-28.9	48.9	-1.1%	-1.4%	0.1%	0.1%
-23.3	54.4	0.8%	0.9%	-0.1%	-0.1%
Average:		**1.5%**	**1.4%**	**1.1%**	**0.9%**

Power Model (A5)

Model parameters: inverse proportional: a = 0.684, b = -13.37
exponential: d = 0.639, e = -0.371, f = -0.0142
Combined efficiency ranges from 0.53 to 0.64

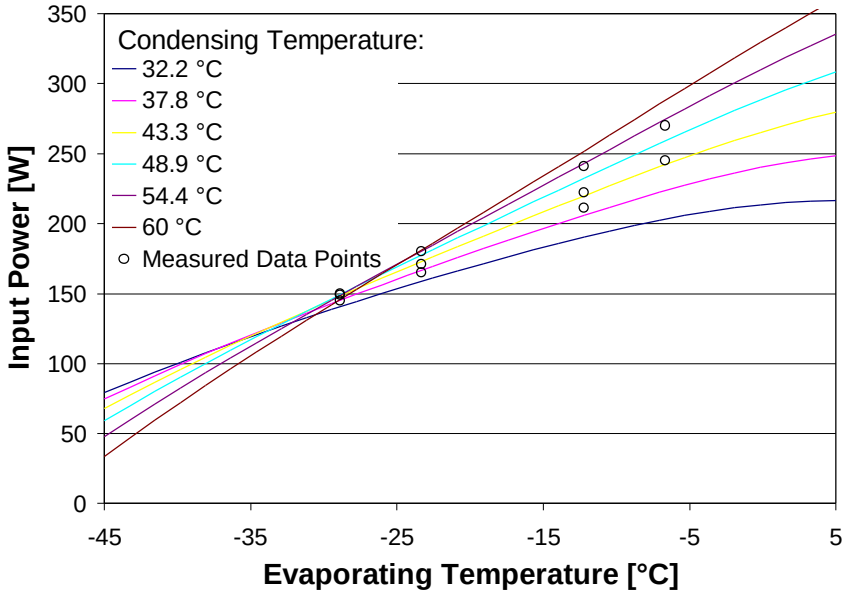

		Inverse Proportional		Exponential	
T_{evap} [°C]	T_{cond} [°C]	Mean Weighted Error [%]	Relative Error [%]	Mean Weighted Error [%]	Relative Error [%]
-12.2	37.8	-2.4%	-2.2%	-2.6%	-2.4%
-23.3	37.8	0.7%	0.8%	0.8%	0.9%
-28.9	37.8	0.3%	0.3%	0.2%	0.2%
-6.67	43.3	-1.5%	-1.2%	-1.4%	-1.1%
-12.2	43.3	-0.9%	-0.8%	-1.0%	-0.9%
-23.3	43.3	0.8%	0.9%	1.0%	1.1%
-28.9	43.3	-0.3%	-0.4%	-0.4%	-0.5%
-6.67	54.4	2.2%	1.6%	2.3%	1.7%
-12.2	54.4	1.3%	1.0%	1.1%	0.9%
-23.3	54.4	0.1%	0.1%	0.2%	0.2%
-28.9	54.4	-0.6%	-0.8%	-0.7%	-0.9%
Average:		**1.2%**	**1.1%**	**1.3%**	**1.2%**

Power Model (A6a)

Model parameters: inverse proportional: a = 0.665, b = -10.27
exponential: d = 0.619, e = -0.3885, f = -0.0192
Combined efficiency ranges from 0.57 to 0.61

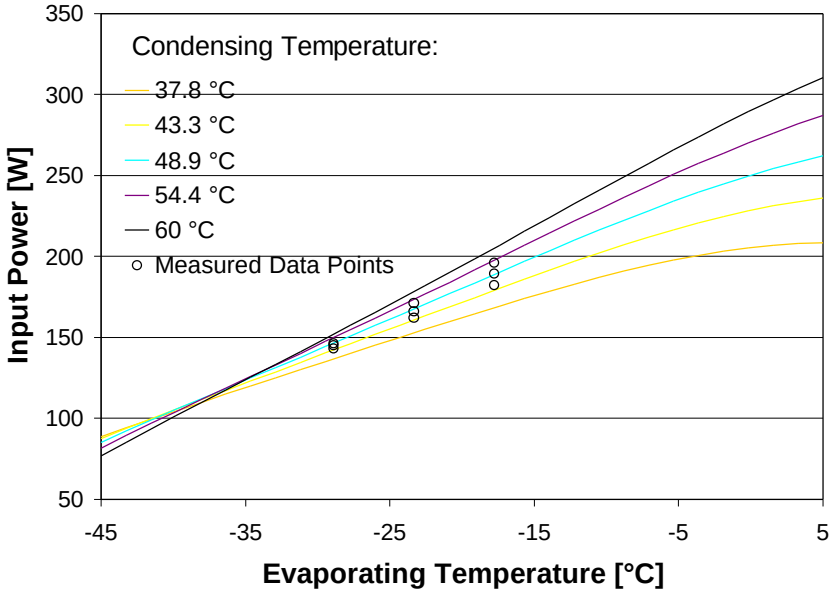

		Inverse Proportional		Exponential	
T_{evap} [°C]	T_{cond} [°C]	Mean Weighted Error [%]	Relative Error [%]	Mean Weighted Error [%]	Relative Error [%]
-17.8	54.4	1.2%	1.0%	1.3%	1.1%
-17.8	48.9	-0.1%	-0.1%	0.0%	0.0%
-17.8	43.3	-1.5%	-1.4%	-1.4%	-1.3%
-23.3	54.4	1.0%	0.9%	0.8%	0.8%
-23.3	48.9	0.5%	0.5%	0.4%	0.4%
-23.3	43.3	-1.1%	-1.2%	-1.3%	-1.3%
-28.9	54.4	1.2%	1.4%	1.3%	1.4%
-28.9	48.9	-0.1%	-0.1%	0.0%	0.0%
-28.9	43.3	-1.4%	-1.6%	-1.3%	-1.5%
Average:		**1.0%**	**1.0%**	**1.0%**	**1.0%**

Power Model (A6b)

Model parameters: inverse proportional: a = 0.656, b = -16.38
exponential: d = 0.567, e = -1.335, f = -0.0282
Combined efficiency ranges from 0.50 to 0.56

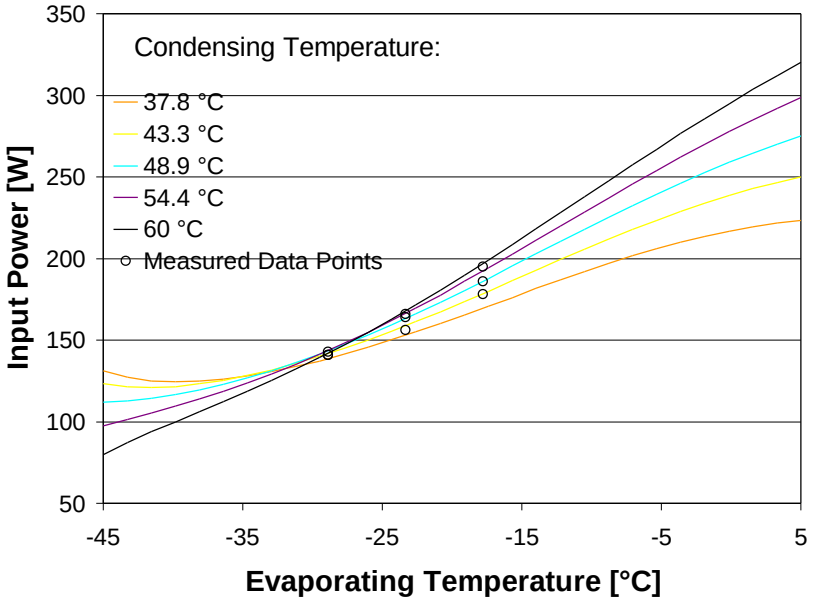

		Inverse Proportional		Exponential	
T_{evap} [°C]	T_{cond} [°C]	Mean Weighted Error [%]	Relative Error [%]	Mean Weighted Error [%]	Relative Error [%]
-17.8	54.4	-1.5%	-1.3%	-1.1%	-0.9%
-17.8	48.9	0.0%	0.0%	0.4%	0.3%
-17.8	43.3	0.5%	0.4%	0.8%	0.7%
-23.3	54.4	0.4%	0.4%	-0.4%	-0.4%
-23.3	48.9	-0.2%	-0.2%	-0.9%	-0.9%
-23.3	43.3	2.0%	2.1%	1.3%	1.3%
-28.9	54.4	0.4%	0.4%	0.7%	0.8%
-28.9	48.9	-0.9%	-1.0%	-0.5%	-0.6%
-28.9	43.3	-0.5%	-0.6%	-0.2%	-0.2%
Average:		**0.9%**	**0.9%**	**0.8%**	**0.8**

Power Model (B1)

Model parameters: inverse proportional: a = 0.766, b = -16.01
exponential: d = 0.680, e = -0.826, f = -0.025
Combined efficiency ranges from 0.60 to 0.68

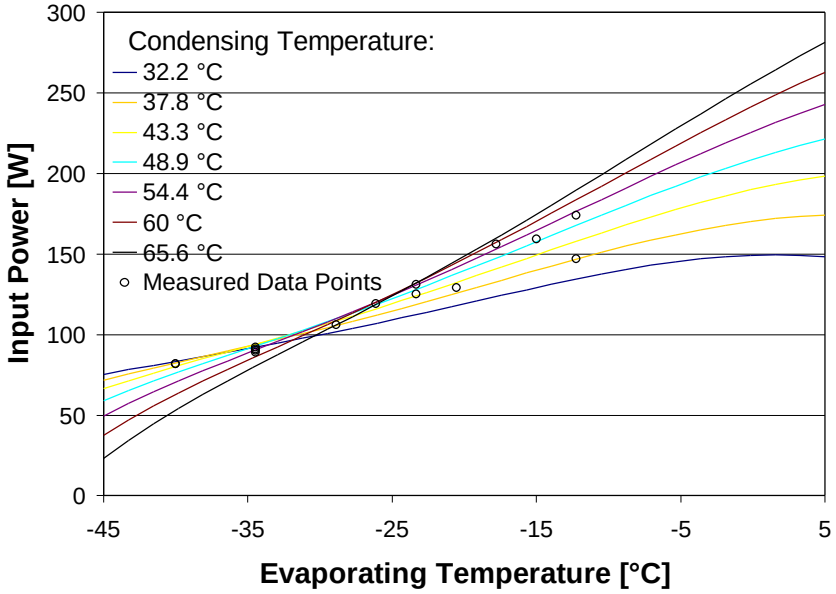

		Inverse Proportional		Exponential	
T_{evap} [°C]	T_{cond} [°C]	Mean Weighted Error [%]	Relative Error [%]	Mean Weighted Error [%]	Relative Error [%]
-40	37.8	0.0%	0.0%	0.5%	0.7%
-28.9	37.8	0.5%	0.6%	-0.2%	-0.2%
-20.6	37.8	-1.9%	-1.8%	-2.8%	-2.6%
-12.2	37.8	-1.5%	-1.2%	-0.3%	-0.2%
-40	43.3	-2.0%	-2.8%	-1.5%	-2.2%
-34.4	43.3	1.6%	2.1%	1.8%	2.3%
-23.3	43.3	0.3%	0.2%	-0.8%	-0.8%
-34.4	48.9	1.6%	2.1%	1.8%	2.3%
-15	48.9	-1.7%	-1.3%	-1.3%	-0.9%
-34.4	54.4	0.3%	0.4%	0.5%	0.6%
-23.3	54.4	0.9%	0.8%	-0.3%	-0.2%
-12.2	54.4	0.4%	0.3%	1.9%	1.3%
-34.4	60	-2.4%	-3.1%	-2.2%	-2.9%
-26.1	60	2.2%	2.2%	1.1%	1.1%
-17.8	60	1.4%	1.1%	1.0%	0.8%
Average:		**1.5%**	**1.6%**	**1.4%**	**1.6%**

Power Model (B2)

Model parameters: inverse proportional: a = 0.714, b = -8.47
exponential: d = 0.666, e = -0.506, f = -0.0278
Combined efficiency ranges from 0.53 to 0.68

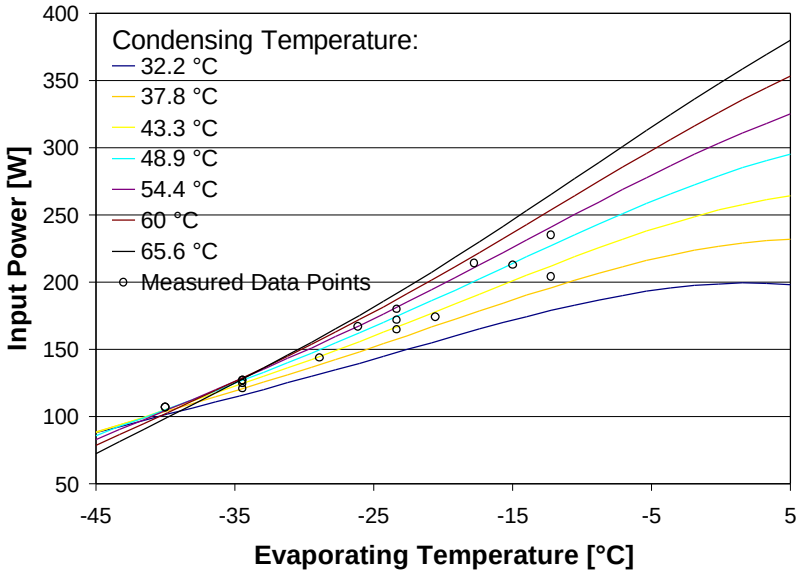

		Inverse Proportional		Exponential	
T_{evap} [°C]	T_{cond} [°C]	Mean Weighted Error [%]	Relative Error [%]	Mean Weighted Error [%]	Relative Error [%]
-40	37.8	-2.4%	-3.6%	-1.9%	-2.8%
-28.9	37.8	-2.5%	-2.8%	-3.1%	-3.5%
-23.3	37.8	-3.7%	-3.6%	-4.3%	-4.2%
-20.6	37.8	-3.3%	-3.1%	-3.8%	-3.6%
-12.2	37.8	-5.7%	-4.5%	-4.7%	-3.7%
-40	43.3	-1.6%	-2.4%	-1.0%	-1.5%
-34.4	43.3	-1.5%	-1.9%	-1.4%	-1.8%
-23.3	43.3	-2.4%	-2.3%	-3.2%	-3.0%
-34.4	48.9	0.2%	0.2%	0.2%	0.2%
-15	48.9	0.4%	0.3%	0.8%	0.6%
-34.4	54.4	2.4%	3.0%	2.4%	3.0%
-23.3	54.4	1.9%	1.7%	1.1%	1.0%
-12.2	54.4	2.8%	1.9%	4.0%	2.8%
-34.4	60	5.0%	6.7%	5.1%	6.8%
-26.1	60	4.0%	3.8%	3.2%	3.1%
-17.8	60	4.0%	3.0%	3.8%	2.9%
Average:		**3.1%**	**3.2%**	**3.1%**	**3.2%**

Power Model (B3)

Model parameters: inverse proportional: a = 0.687, b = -6.091
exponential: d = 0.647, e = -1.096, f = -0.0467
Combined efficiency ranges from 0.54 to 0.67

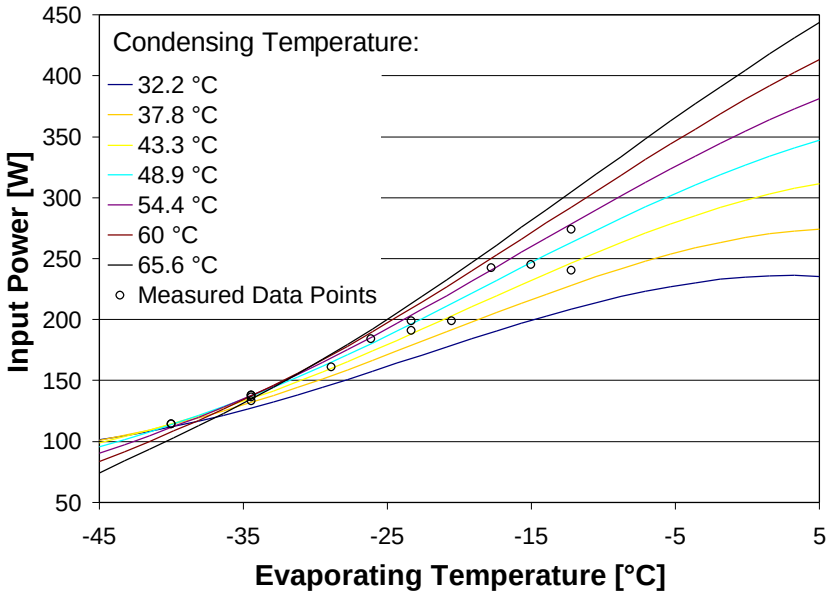

		Inverse Proportional		Exponential	
T_{evap} [°C]	T_{cond} [°C]	Mean Weighted Error [%]	Relative Error [%]	Mean Weighted Error [%]	Relative Error [%]
-40	37.8	-2.5%	-3.9%	-0.2%	-0.4%
-28.9	37.8	-2.4%	-2.7%	-3.9%	-4.4%
-20.6	37.8	-3.5%	-3.2%	-4.2%	-3.8%
-12.2	37.8	-7.9%	-6.0%	-6.5%	-4.9%
-40	43.3	-2.2%	-3.4%	0.1%	0.2%
-34.4	43.3	-1.2%	-1.5%	-1.7%	-2.2%
-23.3	43.3	-0.3%	-0.3%	-1.6%	-1.5%
-34.4	48.9	-0.1%	-0.1%	-0.6%	-0.7%
-15	48.9	0.1%	0.1%	0.9%	0.7%
-34.4	54.4	1.4%	1.9%	0.9%	1.2%
-23.3	54.4	3.8%	3.4%	2.4%	2.2%
-12.2	54.4	0.8%	0.5%	2.5%	1.6%
-34.4	60	2.7%	3.6%	2.2%	2.9%
-26.1	60	4.7%	4.6%	3.0%	2.9%
-17.8	60	4.5%	3.3%	4.5%	3.3%
Average:		**3.3%**	**3.1%**	**2.9%**	**2.6%**

Power Model (B4)

Model parameters: inverse proportional: a = 0.616, b = -12.06
exponential: d = 0.559, e = -0.574, f = -0.0219
Combined efficiency ranges from 0.46 to 0.56

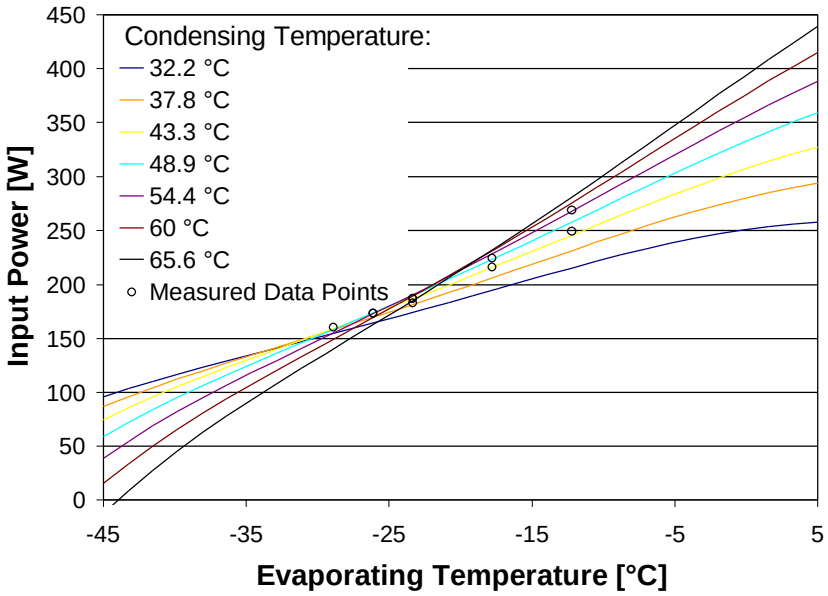

		Inverse Proportional		Exponential	
T_{evap} [°C]	T_{cond} [°C]	Mean Weighted Error [%]	Relative Error [%]	Mean Weighted Error [%]	Relative Error [%]
-26.1	37.8	-1.8%	-2.1%	-1.7%	-2.0%
-17.8	37.8	-4.5%	-4.2%	-4.9%	-4.6%
-23.3	43.3	0.1%	0.2%	-0.1%	-0.1%
-12.2	43.3	-2.1%	-1.7%	-1.7%	-1.4%
-28.9	48.9	-1.3%	-1.7%	-0.8%	-1.0%
-26.1	48.9	0.4%	0.5%	0.5%	0.6%
-17.8	48.9	0.0%	0.0%	-0.4%	-0.4%
-23.3	54.4	2.2%	2.4%	1.9%	2.1%
-23.3	60.0	3.4%	3.8%	3.2%	3.5%
-12.2	60.0	2.9%	2.2%	3.3%	2.5%
Average:		**2.3%**	**2.3%**	**2.3%**	**2.3%**

Power Model (B5)

Model parameters: inverse proportional: a = 0.597, b = -11.53
exponential: d = 0.540, e = -0.516, f = -0.0221
Combined efficiency ranges from 0.41 to 0.54

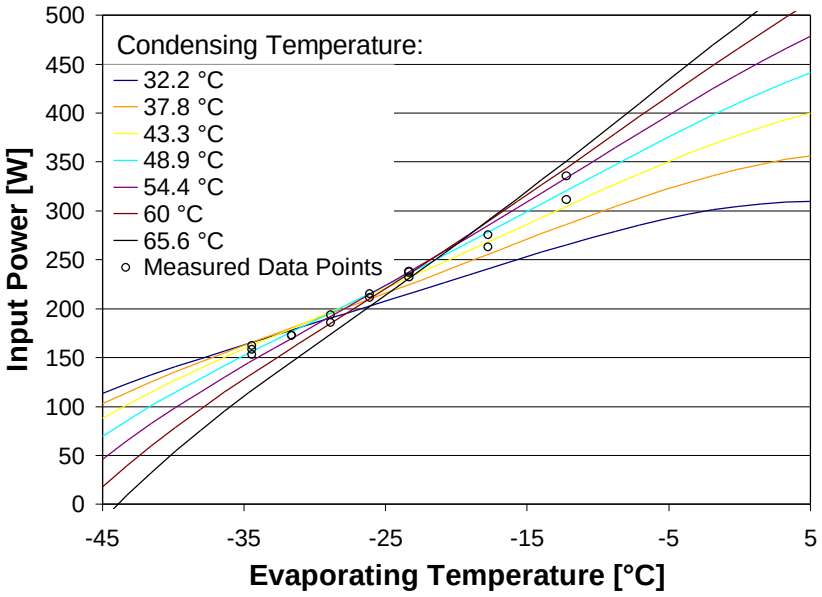

		Inverse Proportional		Exponential	
T_{evap} [°C]	T_{cond} [°C]	Mean Weighted Error [%]	Relative Error [%]	Mean Weighted Error [%]	Relative Error [%]
-34.4	37.8	1.2%	1.6%	1.6%	2.2%
-26.1	37.8	-0.4%	-0.4%	-0.8%	-0.8%
-17.8	37.8	-3.0%	-2.5%	-3.4%	-2.9%
-31.7	43.3	2.8%	3.6%	3.0%	3.9%
-23.3	43.3	0.5%	0.5%	-0.1%	-0.1%
-12.2	43.3	-3.7%	-2.6%	-2.9%	-2.0%
-34.4	48.9	-1.2%	-1.7%	-0.9%	-1.2%
-28.9	48.9	1.0%	1.1%	0.9%	1.0%
-26.1	48.9	0.8%	0.8%	0.4%	0.4%
-17.8	48.9	1.4%	1.1%	1.0%	0.8%
-34.4	54.4	-3.3%	-4.7%	-3.0%	-4.2%
-31.7	54.4	-1.8%	-2.3%	-1.6%	-2.0%
-23.3	54.4	0.8%	0.8%	0.2%	0.2%
-28.9	57.2	1.4%	1.6%	1.3%	1.6%
-23.3	60	-0.4%	-0.3%	-1.0%	-0.9%
-12.2	60	3.0%	1.9%	3.9%	2.5%
Average:		**2.0%**	**2.1%**	**2.0%**	**2.1%**

Power Model (B6)

Model parameters: inverse proportional: a = 0.5624, b = -11.68
exponential: d = 0.500, e = -0.648, f = -0.0256
Combined efficiency ranges from 0.38 to 0.51

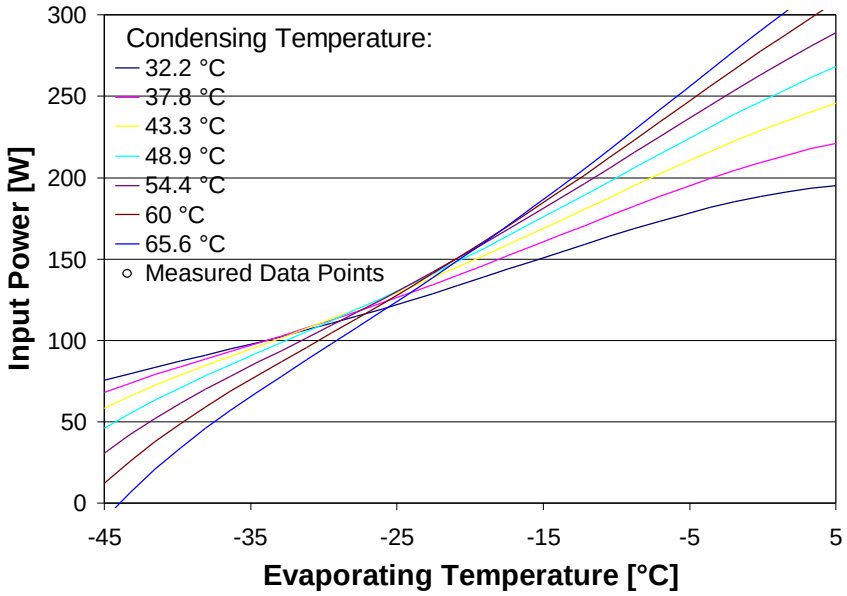

		Inverse Proportional		Exponential	
T_{evap} [°C]	T_{cond} [°C]	Mean Weighted Error [%]	Relative Error [%]	Mean Weighted Error [%]	Relative Error [%]
-34.4	37.8	0.8%	1.1%	1.7%	2.3%
-26.1	37.8	-0.2%	-0.2%	-1.0%	-1.0%
-17.8	37.8	-5.9%	-4.8%	-6.4%	-5.2%
-31.7	43.3	-0.6%	-0.7%	-0.4%	-0.5%
-23.3	43.3	1.2%	1.2%	0.2%	0.2%
-12.2	43.3	-4.6%	-3.2%	-3.2%	-2.3%
-34.4	48.9	-0.6%	-0.8%	0.3%	0.4%
-26.1	48.9	2.1%	2.2%	1.2%	1.3%
-17.8	48.9	1.7%	1.4%	1.2%	1.0%
-34.4	54.4	-2.6%	-3.8%	-1.8%	-2.7%
-31.7	54.4	-0.8%	-1.1%	-0.6%	-0.8%
-23.3	54.4	3.0%	2.9%	1.9%	1.8%
-28.9	60.0	-0.1%	-0.1%	-0.5%	-0.6%
-23.3	60.0	2.4%	2.4%	1.4%	1.3%
-12.2	60.0	3.1%	2.0%	4.7%	3.1%
Average:		**2.6%**	**2.3%**	**2.4%**	**2.1%**

Power Model (B7)

Model parameters: inverse proportional: a = 0.558, b = -8.96
exponential: d = 0.510, e = -0.501, f = -0.0257
Combined efficiency ranges from 0.42 to 0.53

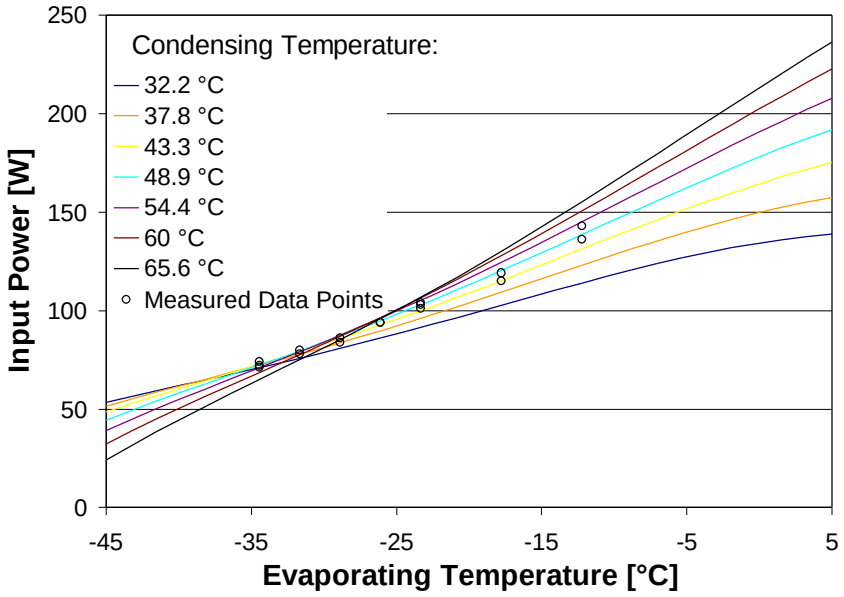

		Inverse Proportional		Exponential	
T_{evap} [°C]	T_{cond} [°C]	Mean Weighted Error [%]	Relative Error [%]	Mean Weighted Error [%]	Relative Error [%]
-26.1	37.8	-4.2%	-4.3%	-4.8%	-4.9%
-17.8	37.8	-6.2%	-5.2%	-6.4%	-5.4%
-34.4	43.3	-2.1%	-2.7%	-1.4%	-1.9%
-31.7	43.3	-1.2%	-1.5%	-1.1%	-1.3%
-23.3	43.3	-3.8%	-3.6%	-4.6%	-4.3%
-12.2	43.3	-6.8%	-4.9%	-5.7%	-4.0%
-34.4	48.9	-0.4%	-0.5%	0.3%	0.4%
-28.9	48.9	1.2%	1.4%	0.9%	1.1%
-26.1	48.9	1.3%	1.3%	0.7%	0.7%
-17.8	48.9	1.1%	0.9%	0.8%	0.7%
-34.4	54.4	-0.7%	-1.0%	-0.1%	-0.1%
-31.7	54.4	0.9%	1.2%	1.1%	1.4%
-23.3	54.4	2.9%	2.7%	2.1%	1.9%
-28.9	60.0	3.3%	3.8%	3.0%	3.5%
-23.3	60.0	6.4%	6.1%	5.6%	5.3%
-12.2	60.0	6.1%	4.1%	7.3%	5.0%
Average:		**3.7%**	**3.3%**	**3.7%**	**3.2%**

Power Model (B8)

Model parameters: inverse proportional: a = 0.553, b = -14.51
exponential: d = 0.481, e = -0.633, f = -0.0218
Combined efficiency ranges from 0.32 to 0.49

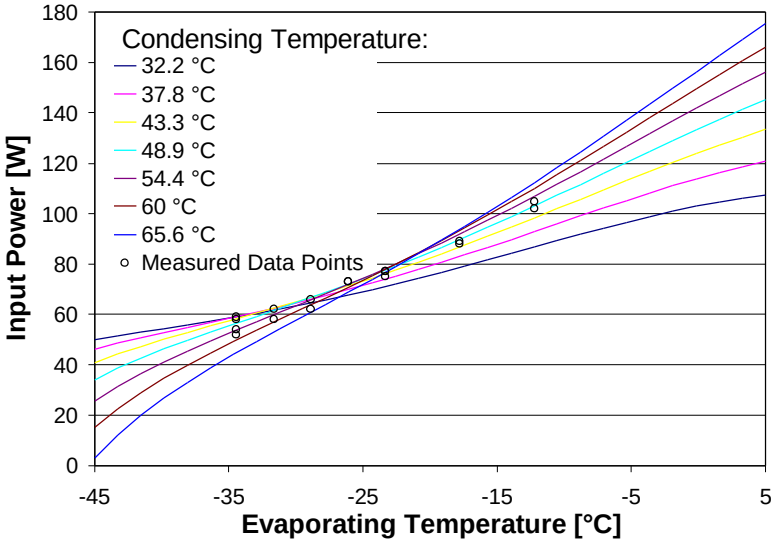

		Inverse Proportional		Exponential	
T_{evap} [°C]	T_{cond} [°C]	Mean Weighted Error [%]	Relative Error [%]	Mean Weighted Error [%]	Relative Error [%]
-34.4	37.8	-0.3%	-0.4%	0.1%	0.1%
-26.1	37.8	-3.8%	-3.8%	-4.3%	-4.3%
-17.8	37.8	-6.5%	-5.3%	-6.9%	-5.6%
-34.4	43.3	0.0%	0.0%	0.4%	0.5%
-31.7	43.3	0.4%	0.5%	0.6%	0.7%
-23.3	43.3	-0.4%	-0.3%	-1.1%	-1.1%
-12.2	43.3	-6.3%	-4.4%	-5.1%	-3.6%
-28.9	48.9	1.1%	1.2%	0.9%	1.0%
-26.1	48.9	-0.8%	-0.8%	-1.4%	-1.4%
-17.8	48.9	1.5%	1.2%	1.0%	0.8%
-34.4	54.4	-0.8%	-1.0%	-0.4%	-0.5%
-31.7	54.4	2.2%	2.7%	2.4%	2.9%
-23.3	54.4	2.5%	2.3%	1.7%	1.6%
-34.4	60.0	-3.4%	-4.7%	-3.0%	-4.2%
-28.9	60.0	2.6%	3.0%	2.4%	2.8%
-23.3	60.0	4.9%	4.7%	4.1%	3.9%
-12.2	60.0	5.7%	3.9%	7.0%	4.9%
Average:		**3.3%**	**3.0%**	**3.3%**	**2.9%**

Power Model (B9a)

Model parameters: inverse proportional: a = 0.609, b = -16.06
exponential: d = 0.750, e = -0.425, f = -0.036
Combined efficiency ranges from 0.46 to 0.51

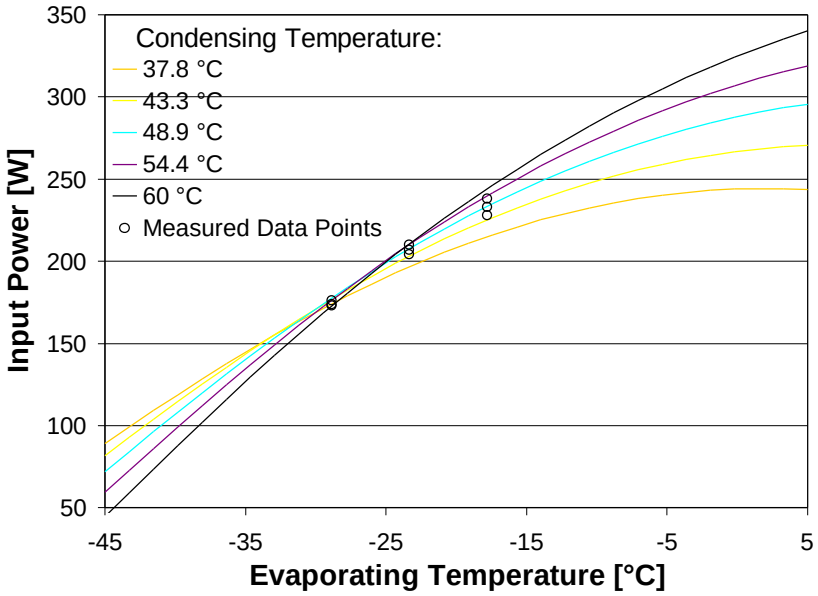

		Inverse Proportional		Exponential	
T_{evap} [°C]	T_{cond} [°C]	Mean Weighted Error [%]	Relative Error [%]	Mean Weighted Error [%]	Relative Error [%]
-17.8	54.4	1.7%	1.5%	1.3%	1.1%
-17.8	48.9	1.0%	0.9%	0.6%	0.5%
-17.8	43.3	-0.7%	-0.6%	-1.1%	-1.0%
-23.3	54.4	-1.4%	-1.3%	-0.6%	-0.6%
-23.3	48.9	-1.0%	-1.0%	-0.3%	-0.3%
-23.3	43.3	-1.7%	-1.7%	-1.0%	-1.0%
-28.9	54.4	0.1%	0.2%	-0.2%	-0.2%
-28.9	48.9	-0.1%	-0.1%	-0.4%	-0.5%
-28.9	43.3	1.9%	2.2%	1.6%	1.8%
Average:		**1.2%**	**1.2%**	**0.9%**	**0.9%**

Power Model (B9b)

Model parameters: inverse proportional: a = 0.589, b = -10.68
exponential: d = 0.780, e = -0.370, f = -0.00227
Combined efficiency ranges from 0.49 to 0.54

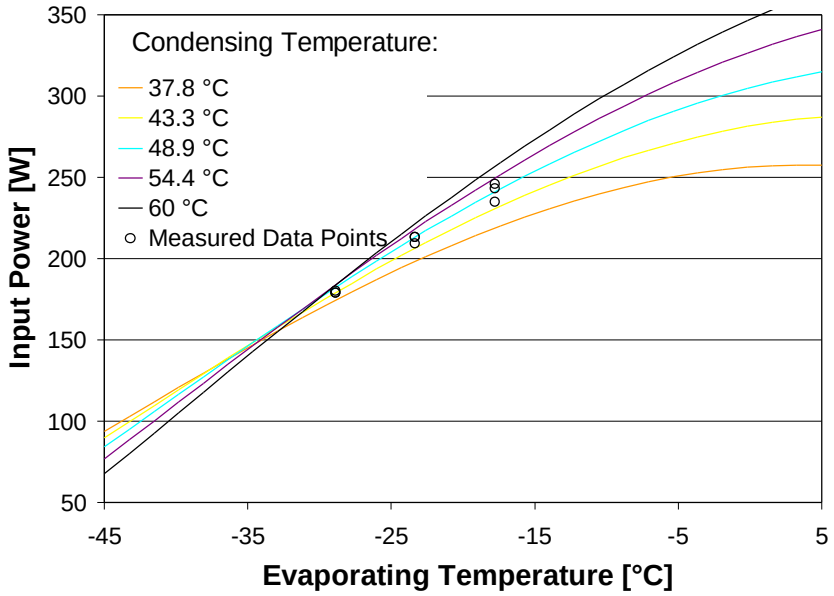

		Inverse Proportional		Exponential	
T_{evap} [°C]	T_{cond} [°C]	Mean Weighted Error [%]	Relative Error [%]	Mean Weighted Error [%]	Relative Error [%]
-17.8	54.4	2.6%	2.2%	2.3%	2.0%
-17.8	48.9	-0.3%	-0.3%	-0.6%	-0.5%
-17.8	43.3	-1.5%	-1.3%	-1.7%	-1.5%
-23.3	54.4	1.3%	1.3%	1.9%	1.8%
-23.3	48.9	-1.0%	-1.0%	-0.5%	-0.5%
-23.3	43.3	-2.2%	-2.2%	-1.7%	-1.7%
-28.9	54.4	1.3%	1.6%	1.1%	1.3%
-28.9	48.9	0.7%	0.8%	0.5%	0.6%
-28.9	43.3	-1.2%	-1.4%	-1.4%	-1.7%
Average:		**1.5%**	**1.5%**	**1.4%**	**1.4%**

Power Model (B9c)

Model parameters: inverse proportional: a = 0.617, b = -12.1
exponential: d = 0.562, e = -0.459, f = -0.0192
Combined efficiency ranges from 0.49 to 0.55

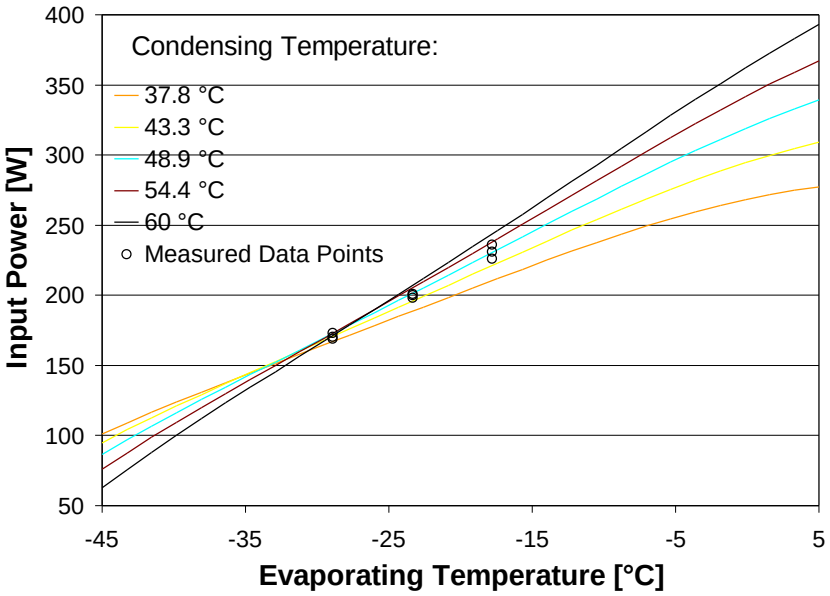

		Inverse Proportional		Exponential	
T_{evap} [°C]	T_{cond} [°C]	Mean Weighted Error [%]	Relative Error [%]	Mean Weighted Error [%]	Relative Error [%]
-17.8	54.4	1.5%	1.3%	1.6%	1.4%
-17.8	48.9	0.1%	0.1%	0.2%	0.2%
-17.8	43.3	-2.0%	-1.8%	-1.9%	-1.7%
-23.3	54.4	1.6%	1.6%	1.4%	1.4%
-23.3	48.9	0.2%	0.3%	0.1%	0.1%
-23.3	43.3	-1.4%	-1.4%	-1.5%	-1.6%
-28.9	54.4	-1.2%	-1.4%	-1.1%	-1.3%
-28.9	48.9	0.3%	0.4%	0.4%	0.5%
-28.9	43.3	0.6%	0.8%	0.7%	0.9%
Average:		**1.2%**	**1.2%**	**1.2%**	**1.2%**

Power Model (C1)

Model parameters: inverse proportional: a = 0.767, b = -20.41
exponential: d = 0.678, e = -1.071, f = -0.02315
Combined efficiency ranges from 0.40 to 0.69

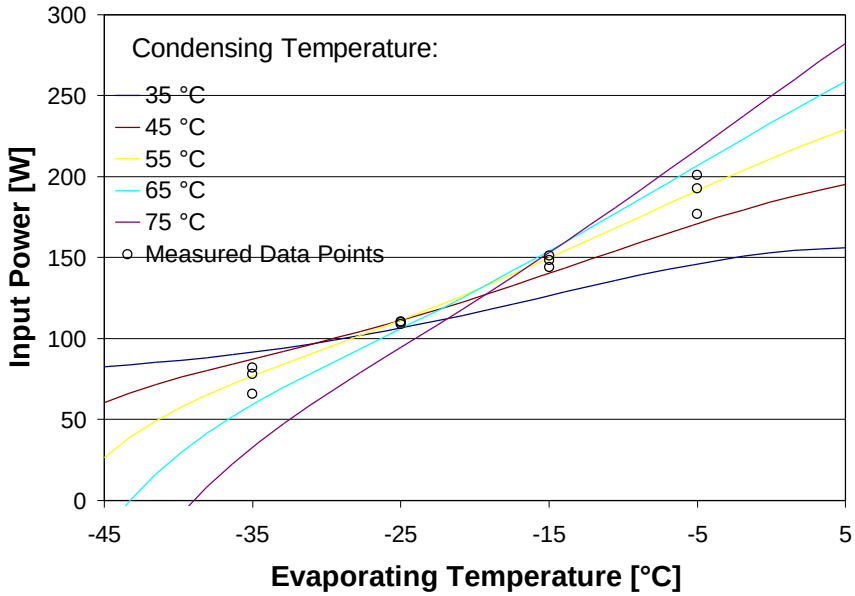

		Inverse Proportional		Exponential	
T_{evap} [°C]	T_{cond} [°C]	Mean Weighted Error [%]	Relative Error [%]	Mean Weighted Error [%]	Relative Error [%]
-35	45	2.4%	3.7%	4.2%	6.5%
-25	45	2.8%	3.2%	1.0%	1.2%
-15	45	-1.1%	-1.0%	-3.0%	-2.6%
-5	45	-6.5%	-4.6%	-4.6%	-3.3%
-35	55	-2.4%	-3.9%	-0.8%	-1.4%
-25	55	2.6%	3.0%	0.9%	1.0%
-15	55	2.9%	2.5%	0.9%	0.7%
-5	55	-3.1%	-2.0%	-1.0%	-0.7%
-35	65	-6.3%	-12.1%	-5.1%	-9.7%
-25	65	-0.6%	-0.6%	-2.2%	-2.6%
-15	65	4.4%	3.6%	2.3%	1.9%
-5	65	2.4%	1.5%	4.6%	2.9%
Average:		**3.6%**	**4.5%**	**3.0%**	**3.9%**

Power Model (C2)

Model parameters: inverse proportional: a = 0.740, b = -16.25
exponential: d = 0.666, e = -1.026, f = -0.0264
Combined efficiency ranges from 0.43 to 0.68

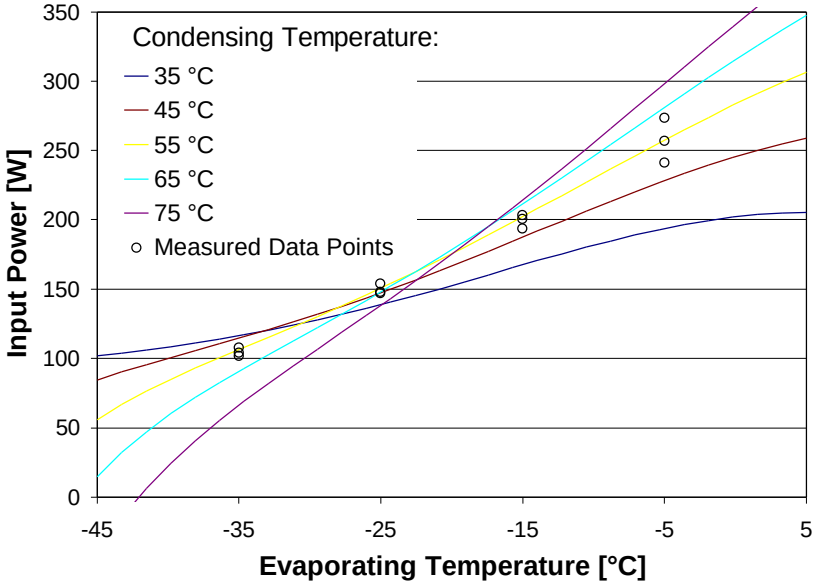

		Inverse Proportional		Exponential	
T_{evap} [°C]	T_{cond} [°C]	Mean Weighted Error [%]	Relative Error [%]	Mean Weighted Error [%]	Relative Error [%]
-35	45	2.4%	4.0%	3.9%	6.4%
-25	45	2.5%	3.0%	0.3%	0.4%
-15	45	-1.5%	-1.3%	-3.4%	-3.1%
-5	45	-8.7%	-6.4%	-7.2%	-5.3%
-35	55	-0.5%	-0.8%	1.3%	2.2%
-25	55	3.5%	4.2%	1.5%	1.8%
-15	55	2.9%	2.5%	1.0%	0.9%
-5	55	-1.4%	-1.0%	0.5%	0.3%
-35	65	-8.2%	-14.3%	-6.1%	-10.7%
-25	65	-1.8%	-2.1%	-3.4%	-3.9%
-15	65	6.2%	5.4%	4.4%	3.9%
-5	65	2.0%	1.3%	4.2%	2.7%
Average:		**4.3%**	**5.3%**	**3.8%**	**4.5%**

Appendix E: EES Programs

This appendix contains the two EES files that have been used to perform the non-linear least squares curve fits required to determine the parameters of the models.

The first program calculates the model parameters of the mass flow rate model and writes the calculated mass flow rate values in a lookup table. This lookup table is read by the second program that determines the parameters for the power model.

The program uses the constant percentage suction pressure drop model with two parameters (C and Δp) and alternatively the exponential (d, e, and f) or the inverse proportional (a and b) model for power.

"!Mass Flow Rate"

"This program performs a least squares curve fit of the constant percentage suction pressure drop model for mass flow rate to measured calorimeter data. The program reads measured from a lookup table. Operating conditions can be entered in terms of temperatures or pressures in degrees Celsius or Fahrenheit or in psi. The calculated mass flow rate has to be in kg/s. The ambient temperature is set equal to 32.2 C (90 F). Either mass flow rate or refrigeration capacity can be entered as measured data."

"Function that converts Fahrenheit temperature to Celsius temperatures"

```
FUNCTION CONTEMP(t)
CONTEMP:=(T-32)/1.8
END
```

"Function to look up measured mass flow rate or capacity"

```
Function m_dot_meas( m_cap,line,RUnits,p_evap,p_cond,Refr$,table$)
IF (m_cap <0) THEN
m_dot_meas=lookup( table$,line,'m_dot')*if(RUnits,0,convert(lbm/hr,kg/s),1,co
nvert(kg/hr,kg/s))
ELSE
m_dot_meas=lookup( table$,line,'Capacity')*convert(Btu/hr,
kW)/(enthalpy(Refr$,p=p_evap,T=contemp(90))-
enthalpy(Refr$,p=p_cond,T=contemp(90)))
ENDIF
END
```

"Evaporating Pressure"

```
FUNCTION PevapFunction(Refr$, Table$, T_evap, p,line)
IF (p<0) THEN
    PevapFunction=pressure(Refr$,T=T_evap,x=1)
    ELSE
    PevapFunction=LOOKUP(table$,line,'p_3_eng')*CONVERT( psi,kPa)
ENDIF
END
```

"Condensing Pressure"

```
FUNCTION PcondFunction(Refr$, Table$, T_cond, p,line)
IF (p<0) THEN
    PcondFunction=pressure(Refr$,T=T_cond,x=1)
    ELSE
    PcondFunction=LOOKUP(table$,line,'p_4_eng')*CONVERT( psi,kPa)
ENDIF
END
```

"Evaporating Temperature"

```
FUNCTION TevapFunction(Refr$, Table$, line, T,p_evap)
IF (T<0) THEN
    TevapFunction=temperature(Refr$,p=p_evap,x=1)
    ELSE
    IF (T>0) THEN
        TevapFunction=contemp(LOOKUP( table$,line,'T_evap_eng'))
        ELSE
        TevapFunction=LOOKUP(table$,line,'T_evap')
    ENDIF
ENDIF
END

"Condensing Temperature"
FUNCTION TcondFunction(Refr$, Table$, line, T,p_cond)
IF (T<0) THEN
    TcondFunction=temperature(Refr$,p=p_cond,x=1)
    ELSE
    IF (T>0) THEN
        TcondFunction=contemp(LOOKUP( table$,line,'T_cond_eng'))
        ELSE
        TcondFunction=LOOKUP(table$,line,'T_cond')
    ENDIF
ENDIF
END

FUNCTION CalculatedMassFlow(start, stop,RelativeError)
$common  m_dot_calc[1..20]
  i:=start-1
  repeat
    i:=i+1
    mdot:=m_dot_calc[ i]
    Lookup(i,1):=m_dot_calc[i]
  until (i>=stop)
    CalculatedMassFlow:=1
END

Calculated=CalculatedMassFlow(start, stop,RelativeError)+NRMS_massflow

start=1

"Data Flags"
Eng=-1
SI=1
mdot=-1
Cap=1
```

```
p_lookup=1
p_calculate=-1
T_lookupF=1
T_lookupC=0
T_calculate=-1

"Lookup Measured Data"
table$='c:\data\CalorimeterData.lkt'  ;stop=11    ; Refr$='R134a';
RUnits=Eng;   m_cap=Cap;   p=p_calculate;     T=T_lookupF

Duplicate line=start,stop
"Model equation"
m_dot_calc[line]=(1+C-
C*(p_discharge[line]/p_suction[line])^(1/n[line]))*V[line]*RPM[line]/60/v_suctio
n[line]

"Volumetric Efficiences"
m_dot_calc[line]/(V[line]*RPM[line]/60/v_suction[line])=eta_v_calc[line]
m_dot_meas[line]/(V[line]*RPM[line]/60/v_suction[line])=eta_v_meas[line]


"Pressures and Temperatures"
p_evap[line]=PevapFunction(Refr$, Table$, T_evap[line], p,line)
p_cond[line]=PcondFunction(Refr$, Table$, T_cond[line], p,line)
T_suction[line]=contemp(90)+DELTAT_suction
T_evap[line]=TevapFunction(Refr$, Table$, line, T,p_evap[line])
T_cond[line]=TcondFunction(Refr$, Table$, line, T,p_cond[line])
p_suction[line]=p_evap[line]*(1-p_L)
p_discharge[line]=p_cond[line]*(1+p_H)
PR[line]=p_discharge[line]/p_suction[line]

"Ideal Gas Law:" p_suction[line]*v_suction[line]=R*(T_suction[line]+273.15)

"Mass Flow Rate OR Capacity"
m_dot_meas[line]=m_dot_meas(m_cap,line,RUnits,p_evap[line],p_cond[line],
Refr$,table$)

RPM[line]=lookup(table$,line,'Speed')
V[line]=lookup(table$,line,'Volume')*if(RUnits,0,convert(in^3,m^3),1,convert(c
m^3,m^3))
Power_meas[line]=lookup(table$,line,'Power')

"Errors"
(m_dot_calc[line]-m_dot_meas[line])=DELTAm_dot[line]
MeanWeightedError_mdot[line]=DELTAm_dot[line]/m_dot_bar
```

```
RelativeError_mdot[line]=DELTAm_dot[line]/m_dot_meas[line]

"k"
c_p[line]=SPECHEAT(R134a,T=T_suction[line],P=P_suction[line])
c_v[line]=c_p[line]-R
k[line]=c_p[line]/c_v[line]
k[line]=n[line]

end
"Gas Constant"
R=8.314/MOLARMASS(Refr$)

"Root Mean Squares"
MeanWeightedError_mdot=SQRT(SUM(MeanWeightedError_mdot[line]^2,lin
e=start,stop)/(stop-start+1))
m_dot_bar=SUM(m_dot_meas[line],line=start,stop)/(stop-start+1)
RelativeError_mdot=SQRT(SUM(RelativeError_mdot[line]^2,line=start,stop)/(
stop-start+1))

"Model parmeters"
DELTAT_suction=0
p_H=0
$SAVELOOKUP c:\data\calcMdot.lkt
```

"!Power Model"

"This program performs a least squares curve fit of the exponential power model to measured calorimeter data. The inverse proportional equation is commented out and can be use instead of the exponential one. The program reads measured data and previously calculated mass flow rate data from a lookup table. Operating conditions can be entered in terms of temperatures or pressures in degrees Celsius or Fahrenheit or in psi. The calculated mass flow rate has to be in kg/s. The ambient temperature is set equal to 32.2 C (90 F)"

```
      "Function that converts Fahrenheit temperature to Celsius temperatures"
FUNCTION CONTEMP(t)
CONTEMP:=(T-32)/1.8
END

"Function to look up measured mass flow rate or capacity"
Function m_dot_meas( m_cap,line,RUnits,p_evap,p_cond,Refr$,table$)
IF (m_cap <0) THEN
m_dot_meas=lookup( table$,line,'m_dot')*if(RUnits,0,convert(lbm/hr,kg/s),1,co
nvert(kg/hr,kg/s))
ELSE
m_dot_meas=lookup( table$,line,'Capacity')*convert(Btu/hr,
kW)/(enthalpy(Refr$,p=p_evap,T=contemp(90))-
enthalpy(Refr$,p=p_cond,T=contemp(90)))
ENDIF
END

"Evaporating Pressure"
FUNCTION PevapFunction(Refr$, Table$, T_evap, p,line)
IF (p<0) THEN
    PevapFunction=pressure(Refr$,T=T_evap,x=1)
    ELSE
    PevapFunction=LOOKUP(table$,line,'p_3_eng')*CONVERT( psi,kPa)
ENDIF
END

"Condensing Pressure"
FUNCTION PcondFunction(Refr$, Table$, T_cond, p,line)
IF (p<0) THEN
    PcondFunction=pressure(Refr$,T=T_cond,x=1)
    ELSE
    PcondFunction=LOOKUP(table$,line,'p_4_eng')*CONVERT( psi,kPa)
ENDIF
END
"Evaporating Temperature"
```

```
FUNCTION TevapFunction(Refr$, Table$, line, T,p_evap)
IF (T<0) THEN
    TevapFunction=temperature(Refr$,p=p_evap,x=1)
    ELSE
    IF (T>0) THEN
        TevapFunction=contemp(LOOKUP( table$,line,'T_evap_eng'))
        ELSE
        TevapFunction=LOOKUP(table$,line,'T_evap')
    ENDIF
ENDIF
END

"Condensing Temperature"
FUNCTION TcondFunction(Refr$, Table$, line, T,p_cond)
IF (T<0) THEN
    TcondFunction=temperature(Refr$,p=p_cond,x=1)
    ELSE
    IF (T>0) THEN
        TcondFunction=contemp(LOOKUP( table$,line,'T_cond_eng'))
        ELSE
        TcondFunction=LOOKUP(table$,line,'T_cond')
    ENDIF
ENDIF
END

start=1

"Data Flags"
Eng=-1
SI=1
mdot=-1
Cap=1
p_lookup=1
p_calculate=-1
T_lookupF=1
T_lookupC=0
T_calculate=-1

"Lookup Measured Data"
table$='c:\data\CalorimeterData.lkt'      ;stop=9  ;Refr$='R134a';
Runits=Eng;    m_cap=mdot;       p=p_lookup;      T = T_calculate  ;
p_L=0.1527

Duplicate line=start,stop
"Model equation"
```

```
P\mdot_calc[line]*eta[line]=n[line]/(n[line]-
1)*p_suction[line]*1000*v_suction[line]*((p_discharge[line]/p_suction[line])^((n
[line]-1)/n[line])-1)
P\mdot_calc[line]*m_dot_meas[line]=Power_calc[line]
{eta[line]=a+b/p_evap[line]      }
eta[line]=d+e*exp(f*p_evap[line])

"Efficiences"
eta_meas[line]=(n[line]/(n[line]-1) *p_suction[line]*1000*v_suction[line]*
((p_discharge[line]/p_suction[line])^((n[line]-1)/n[line])-
1))/(Power_meas[line]/m_dot_meas[line])

"Pressures and Temperatures"
p_evap[line]=PevapFunction(Refr$, Table$, T_evap[line], p,line)
p_cond[line]=PcondFunction(Refr$, Table$, T_cond[line], p,line)
T_suction[line]=contemp(90)+DELTAT_suction
T_evap[line]=TevapFunction(Refr$, Table$, line, T,p_evap[line])
T_cond[line]=TcondFunction(Refr$, Table$, line, T,p_cond[line])
p_suction[line]=p_evap[line]*(1-p_L)
p_discharge[line]=p_cond[line]*(1+p_H)
PR[line]=p_discharge[line]/p_suction[line]

"Ideal Gas Law:" p_suction[line]*v_suction[line]=R*(T_suction[line]+273.15)

"Lookup Calculated Mass Flow Rate"
m_dot_meas[line]=lookup('c:\data\calcmdot.lkt',line,1)

"Lookup Compressor Data"
RPM[line]=lookup(table$,line,'Speed')
V[line]=lookup(table$,line,'Volume')*if(RUnits,0,convert(in^3,m^3),1,convert(c
m^3,m^3))
Power_meas[line]=lookup(table$,line,'Power')

"Errors"
(Power_calc[line]-Power_meas[line])=DELTAPower[line]
RelativeError_Power[line]=(DELTAPower[line])/Power_meas[line]
MeanWeightedError_Power[line]=DELTAPower[line]/Power_bar

"k"
c_p[line]=SPECHEAT(R134a,T=T_suction[line],P=P_suction[line])
c_v[line]=c_p[line]-R
k[line]=c_p[line]/c_v[line]
k[line]=n[line]
end
```

"Gas Constant"
R=8.314/MOLARMASS(Refr$)

"Root Mean Squares"
MeanWeightedError=SQRT(SUM(MeanWeightedError_Power[line]^2,line=start,stop)/(stop-start+1))
Power_bar=SUM(Power_meas[line],line=start,stop)/(stop-start+1)
RelativeError=SQRT(Sum(RelativeError_Power[line]^2,line=start,stop)/(stop-start+1))

"Model parmeters"
DELTAT_suction=0
p_H=0

References

Air-Conditioning and Refrigeration Institute (1991): Standard 540-91 "A method for presentation of compressor performance data".

Association of Home Appliance Manufacturers (AHAM, 1993): AHAM Guide to the National Appliance Energy Conservation Act, Washington D.C., http://www.aham.org/mfrs/govt/effic/naecagd.pdf

BAEHR, Hans Dieter (1992): Thermodynamik, Springer-Verlag, Berlin, 8th edition.

BROK, S.W.; TOUBER, S.;VAN DER MEER, J.S. (1980): Modeling of Cylinder Heat Transfer – Large Effort, Little Effect? Proceedings of the 1980 International Compressor Conference, Purdue University, West Lafayette, Indiana, pp. 43-50.

BROWNE, Matthew W.; BANSAL, Pradeep K. (1998): Challenges in Modeling Vapor-Compression Liquid Chillers, ASHRAE Transaction 1998, Vol. 104, part 1A, pp. 474-186.

BULLARD, Clark (1998): Personal conversation, experimental data.

CAVALLINI, A.; DORETTI, L.; LONGO, G.A.; ROSETTO, L.; BELLA, B.; ZANNERIO, A. (1996): Thermal Analysis of a Hermetic Reciprocating Compressor, Proceedings of the 1996 International Compressor Conference, Purdue University, West Lafayette, Indiana, pp. 535-540.

ÇENGEL, Yunus A.; BOLES, Michael A. (1994): Thermodynamics. An Engineering Approach, McGraw-Hill, Inc., New York, 2nd edition.

CHLUMSKÝ, Vladimír (1965): Reciprocating and Rotary Compressors, SNTL Publishers of Technical Literature, Prague.

DABIRI, A.E.; RICE C.K. (1981): A Compressor Simulation Model With Corrections for the Level of Suction Gas Superheat, ASHRAE Transaction 1981, Vol. 87, Part 2, pp. 771-780.

Engineering Equation Solver (EES, 1999): Software, F-Chart Software, Middleton, WI.

Environmental Protection Agency (EPA) (1993): EPA Refrigerator Analysis (ERA), Software, Report EPA-430R-93-007.

ESCANES, F.; PÉREZ-SEGARRA, C.D.; RIGOLA, J.; SERRA, J.M.; PONS, J.; ESCRIBÀ, M.; JORNET, M. (1996): Numerical Simulation of Hermetic Reciprocating Compressors. Recent Improvements and Experimental Validation, Proceedings of the 1996 International Compressor Conference, Purdue University, West Lafayette, Indiana, pp. 193-198.

FAGOTTI, Fabian; TODESCAT, Márcio Luiz; FERREIRA Rogério Tadeu da Silva; PRATA, Álvaro Toubes (1994): Heat Transfer Modeling in a Reciprocating Compressor, Proceedings of the 1994 International Compressor Conference, Purdue University, West Lafayette, Indiana, pp. 605-610.

FOX, Robert W.; McDonald, Alan T. (1992): Introduction to Fluid Mechanics, John Wiley & Sons, Inc., New York, 4th edition.

FRÖHLICH, F (1961): Kolbenverdichter, Springer Verlag, Berlin.

HABERSCHILL, P.; BORG, S.; MONDOT, M.; LALLEMAND, M. (1994): Hermetic Compressor Models Determination of Parameters From a Minimum Number of

Tests, Proceedings of the 1994 International Compressor Conference, Purdue University, West Lafayette, Indiana, pp. 133-138.

HAHNE Erich (1993): Technische Thermodynamik, Addison-Wesley Publishing Company, Bonn, 2nd edition.

HAIDER, Imam; LAVANNIS, Mahesh; RADERMACHER, Reinhard (1997): Investigations of the EPA Refrigerator Analysis (ERA) Software: Compressor Map and Ambient Temperature Effects, ASHRAE Transactions 1997, Vol. 103, Part 1, pp. 608-618.

HILLER, Dr. Carl C.; GLICKSMAN, Dr. Leon R. (1976): Detailed Modeling and Computer Simulation of Reciprocating Refrigeration Compressors, Proceedings of the 1976 International Compressor Conference, Purdue University, West Lafayette, Indiana, pp. 12-17.

INCROPERA, Frank. P.; DE WITT, David. P.(1996): Introduction to Heat Transfer, John Wiley & Sons, New York, 3rd edition.

KENT, Richard G. (1974): Application of Basic Thermodynamics to Compressor Cycle Analysis, Proceedings of the 1974 International Compressor Conference, Purdue University, West Lafayette, Indiana, pp.291-296.

LEE, Sukhyung (1983): First Law Analysis of Unsteady Processes with Application to a Charging Process and a Reciprocating Compressor, MS Thesis, The Ohio State University.

MACLAREN, J.F.T.; TRAMSHEK, A.B.; PASTRANA, O.F. (1976): A Study of Boundary Conditions Encountered in Reciprocating Compressor Systems,

Proceedings of the 1976 International Compressor Conference, Purdue University, West Lafayette, Indiana, pp. 33-41.

MARRIOTT, Lee Water (1973): Control of a Refrigeration Compressor Calorimeter of Minimum Testing Time, Ph.D. Thesis, University of Michigan.

MORAN, Michael J.; SHAPIRO, Howard N. (1993): Fundamentals of Engineering Thermodynamics, John Wiley & Sons, New York, 2nd edition.

NG, E.H.; TRAMSHEK, A.B.; MACLAREN, J.F.T. (1980): Computer Simulation of a Reciprocating Compressor Using a Real Gas Equation of State, Proceedings of the 1980 International Compressor Conference, Purdue University, West Lafayette, Indiana, pp. 33-42.

PÉREZ-SEGARRA, C.D.; ESCANES, F.; OLIVA, A. (1994): Numerical Study of the Thermal and Fluid-dynamic Behaviour of Reciprocating Compressors (1994), Proceedings of the 1994 International Compressor Conference, Purdue University, West Lafayette, Indiana, pp. 145-150.

POPOVIC, Predrag and SHAPIRO, Howard N. (1995): A Semi-empirical Method for Modeling a Reciprocating Compressor in Refrigeration Systems, ASHRAE Transactions 1995, Vol. 101, Part 2, pp. 367-382.

PRAKASH, Rajendra; SINGH, Rajendra (1974): Mathematical Modeling and Simulation of Refrigerating Compressors, Proceedings of the 1974 International Compressor Conference, Purdue University, West Lafayette, Indiana, pp. 274-285.

RASMUSSEN, Bjarne Dindler (1997): Variable Speed Hermetic Reciprocating Compressors for Domestic Refrigerators. Ph.D. Thesis, Technical University of Denmark.

RECHTENWALD, Gerald William (1984): Numerical Modeling of the Flow and Heat Transfer in the Cylinder of a Reciprocating Compressor, MS Thesis, University of Minnesota.

RECHTENWALD, Gerald William: A Study of Heat Transfer Between the Walls and Gas Inside the Cylinder of a Reciprocating Compressor, Ph.D. Thesis, University of Minnesota, 1989.

RÖTTGER, Dr.-Ing. W.; KRUSE, D.-Ing. (1976): Analysis of the Working Cycle of Single-stage Refrigeration Compressors Using Digital Computers, Proceedings of the 1976 International Compressor Conference, Purdue University, West Lafayette, Indiana, pp. 18-24.

RIGOLA, J.; PÉREZ-SEGARRA, C.D.; OLIVA, A.; SERRA, J.M.; PONS, J.; ESCRIBÀ, M.; JORNET, M. (1996): Parametric Study of Hermetic Reciprocating Compressors, Heat Transfer Modeling in a Reciprocating Compressor, Proceedings of the 1996 International Compressor Conference, Purdue University, West Lafayette, Indiana, pp. 529-534.

THRELKELD, J.L. (1962): Thermal Environmental Engineering, Prentice-Hall, Englewood Cliffs, NJ.

TODESCAT, Márcio Luiz; FAGOTTI, Fabian; PRATA, Álvaro Toubes; FERREIRA, Rogério Tadeu da Silva (1992): Thermal Energy Analysis in Reciprocating

Hermetic Compressors, Proceedings of the 1992 International Compressor Conference, Purdue University, West Lafayette, Indiana,. pp. 1419-1428.